UNIVERSIDAD NACIONAL AUTÓNOMA DE MÉXICO
DOCTORADO EN CIENCIAS BIOMÉDICAS INSTITUTO DE INVESTIGACIONES BIOMÉDICAS

CURSO TEMPORAL DE LOS MECANISMOS INVOLUCRADOS EN LA TRANSICIÓN DE LA LESION RENAL AGUDA A LA ENFERMEDAD RENAL CRÓNICA EN ROEDORES: DIAGNÓSTICO Y EPIGENÉTICA

TESIS
QUE PARA OPTAR POR EL GRADO DE DOCTOR EN CIENCIAS

PRESENTA

ANDREA SÁNCHEZ NAVARRO

DIRECTOR DE TESIS

DRA. NORMA ARACELI BOBADILLA SANDOVAL
Instituto de Investigaciones Biomédicas

COMITÉ TUTOR

DRA. MARCIA HIRIART URDANIVIA
Instituto de Fisiología Celular

DR. FÉLIX RECILLAS TARGA
Instituto de Fisiología Celular

CIUDAD DE MÉXICO, AGOSTO DE 2021

PDCB/AOR/IIB/012/2021

Lic. Diana González Nieto
Directora de Certificación y Control Documental
Dirección General de Administración Escolar, UNAM
P r e s e n t e.

Nos permitimos informarle que el Comité Académico de Doctorado en Ciencias Biomédicas, en su reunión 494 del 04 de agosto del 2021, designó el siguiente jurado para examen de grado **DOCTORA EN CIENCIAS** de **Sánchez Navarro Andrea,** con número de cuenta **413006660,** con la tesis titulada: **"Curso temporal de los mecanismos involucrados en la transición de la lesión renal aguda a la enfermedad renal crónica (ERC) en roedores: diagnóstico y epigenética"**, dirigida por la Dra. Norma Araceli Bobadilla Sandoval.

Presidente:	Dra. María Eugenia Gonsebatt Bonaparte
Secretario:	Dra. Norma Araceli Bobadilla Sandoval
Vocal:	Dr. Víctor Julián Valdés Rodríguez
Vocal:	Dr. Julio César Carrero Sánchez
Vocal:	Dr. José Pedraza Chaverri

A t e n t a m e n t e
"POR MI RAZA HABLARÁ EL ESPÍRITU"
Ciudad Universitaria, Cd. Mx., a 09 de agosto de 2021

DRA. AUREA OROZCO RIVAS
COORDINADORA

DOCTORADO EN CIENCIAS BIOMÉDICAS
COORDINACIÓN

AOR/aap

RECONOCIMIENTOS

Este trabajo se realizó bajo la tutoría de la Dra. Norma A. Bobadilla Sandoval, en la Unidad de Fisiología Molecular del departamento de Medicina Genómica y Toxicología ambiental del Instituto de Investigaciones Biomédicas sede periférica en el Instituto Nacional de Ciencias Médicas y Nutrición Salvador Zubirán. El trabajo se efectúo entre Julio de 2016 y Julio de 2021.

El estudio fue realizado con el apoyo financiero de los proyectos de CONACyT: 235855, 235964, 272390, y A1-S-8715 por la DGAPA-PAPIIT-UNAM: IN223915 y IN201619 otorgados a la Dra. Norma A. Bobadilla Sandoval.

Durante mis estudios de doctorado recibí una beca otorgada por el CONACyT con el número 607517.

Agradezco la asesoría técnica de la QFB Rosalba Pérez Villalva durante la realización de este trabajo.

Agradezco al Programa de Doctorado en Ciencias Biomédicas del Instituto de Investigaciones Biomédicas y al Instituto Nacional de Ciencias Médicas y Nutrición Salvador Zubirán por todas las facilidades que se me otorgaron durante la realización de este proyecto.

Se reconoce el apoyo técnico del personal del bioterio del Instituto Nacional de Ciencias Médicas y Nutrición Salvador Zubirán, en particular M.V.Z Mariela Contreras.

Agradezco a la Universidad Nacional Autónoma de México por ayudarme a alcanzar esta meta.

AGRADECIMIENTOS

A **Norma Bobadilla**: por el apoyo y confianza que me ha brindado como alumna, y que me ha llevado a crecer como persona, así como el cariño y amistad. Gracias.

A mis padres: **Gabriela y Pedro**, que han sido un gran ejemplo y que me han brindado su amor incondicional, enseñándome a no dejarme rendir. Los amo.

A mis hermanas: **Brenda y Gaby** por creer en mí, cuidarme, ser mis amigas y confidentes, y siempre alentarme cuando lo necesito. Sé que siempre estamos para apoyarnos.

A **Rosy**: Gracias, porque además de ser el mejor apoyo en el laboratorio, me brindo su amistad, cariño y tiempo.

A **Adrián**: por ser mi fiel compañero en las buenas y en las malas, mi conciencia cuando lo necesito y mi apoyo incondicional. Y por dejarme formar parte de su vida. Gracias.

A mis amigos **Jonatán**, **Dominique, Nadyeli**: por los momentos compartidos, las horas de diversión y ayudarme a crear bellos momentos.

A mis compañeros de laboratorio y del departamento de Nefrología: **Miguel, Toñito, Isaac, Adriancito, Rebe, Luis, Héctor ("elh"), Germán** y a todos los que pasaron por el laboratorio, porque cada uno de ustedes contribuyeron a mi crecimiento profesional y personal.

Al **Dr. Gerardo Gamba** por sus aportaciones durante la realización del proyecto.

INDICE

ABREVIATURAS

TFG	Tasa de filtrado glomerular
LRA	Lesión Renal Aguda
KDIGO	Kidney Disease: Improving Global Outcomes
CrS	Creatinina sérica
CrU	Creatinina urinaria
ERC	Enfermedad Renal Crónica
AKIN	Acute Kidney Injury Network
HIF-1α	Factor Inducible por Hipoxia 1 α
MAP cinasas	Proteína quinasas activadas por mitógenos o Mitogen - Activated Protein Kinases
I/R	Isquemia/reperfusión
TGF-β	Factor de crecimiento transformante-β
RASAL1	RAS Protein Activator Like 1
Shh	Shh Sonic hedgehog
ENSANUT	Encuesta en Salud y Nutrición
OMS	Organización Mundial de la Salud
HDL	Lipoproteína de baja densidad
ORG	Glomerulopatía relacionada a la obesidad
GSFS	Glomeruloesclerosis focal y segmentaria
SAOS	Síndrome de apnea obstructiva del sueño
NGAL	Gelatinasa de neutrófilos asociada a lipocalina 2
Kim-1	Molécula de daño renal 1

IL-18	Interleucina 18
NAG	N-acetil-beta-glucosaminidasa
L-FABP	Proteína de unión a ácidos grasos de hígado
TIMP-2	Inhibidor tisular de las metaloproteinasas 2
Hsp72	Proteína de choque térmico 72
TNF-α,	Factor de necrosis tumoral alfa
IL-6	interleucina 6
MCP-1	Proteína quimio atrayente de monocitos
HDAC	Desacetilasa de histonas
MHFD	Dieta moderadamente alta en grasas
RE	Retículo Endoplásmico
VEGF	Factor de crecimiento vascular y endotelial
IL-10	Interleucina 10
VAA	vasculitis asociada a ANCA
NL	Nefritis lúpica proliferativa de clases III y IV
FSR	Flujo sanguíneo renal
ERCT	Enfermedad renal crónica terminal
H_2O_2	Peroxido de hidrogeno
Sham	Operación simulada
UNx	Nefrectomía derecha
IR + UNx	UNx más isquemia renal
LPS	Lipopolisacaridos

REACTIVOS Y EQUIPOS

QuantiChrom	-Creatinine Assay Kit (DICT-500).
Gould, Puerto Rico	-Transductor de presión (Modelo p23 db)
Transonic, Ithaca, NY	-Sonda de ultrasonido (1RB)
Roche	-Amplex Red Hydrogen Peroxide/ Peroxidase Assay
Invitrogen	-TRIZoL
SIGMA	-DNTP
	-Proteínasa K
	-RNAasa A
	-SDS- Sodium dodecyl sulfate
	-TCA- Ácido tricloroacético
	-PAS- Ácido periódico de Schiff
Applied Biosystems	-Sondas TaqMan
	-rRNA 18S eucariota (Rn03928990_g1, No. Cat. 4319413E)
	-Termociclador en tiempo real ABI 7300 Prism o QuantStuido5
Life Technologies	-Transcriptasa reversa (MMLV)
	-Hexámeros al azar
	-Lipofectamine 2000
Millipore	-PVDF-Membrana de difloruro de polivinilo
	-Kit de quimioluminiscencia comercial (WBKLS0500)
BioRad	-Agente bloqueante
	- Transblot (SD cell)
	-Ensayo de proteínas de Lowry (5000113 y 5000114)
ENZO	-Anticuerpo HSP72
Santa Cruz	-Anti-mouse IgG (sc-2031)
	-Anti-serpinA3K (55480-1-AP)
	-Anti-conejo IgG (sc-2004)
	-Anti-Sirt7 (sc365344)
	-Anti-Sirt3 (sc-365175)

	-Anti-IL-6 (sc57315)
Abcam	-Anti-β-actina/HRP [AC-15] (ab49900)
Zymo Research	-Kit de metilación de DNA 5-mC
Promega	-Vector pGEM-T Easy
Gardner, PA, EE. UU.	-Dieta de control, Zeigler Rodent RQ 22–5
Echo Medical Systems, Houston, TX	-Resonador magnético
Beckman Coulter, Fullerton, CA, EE. UU.	-Analizador automático SynchronCX
Bio SB	-Bloqueador de fondo inmunoDNA (BSB 0107) -Sustrato de peroxidasa DAB, (BSB 0009).
Biocare medical	-Anticuerpo secundario de cabra en roedor-HRP, (MM620)
Raybiotech Inc	-Kit ELISA de serpinA3 (ELH-SerpinA3) -Kit ELISA TNF-α (ELM-TNFa-2)
New England Biolabs	-DNA polimerasa de alta fidelidad Phusion -Células HEK293 (ATCC CRL-1573) -PNGAasa F
Exocell	-Kit de ELISA de albuminuria
Boster	-Anticuerpo KiM-1 (No. Cat. PA1632)

RESUMEN

Los estudios clínicos, epidemiológicos y experimentales han demostrado que lesión renal aguda (LRA) es un factor de riesgo independiente para el desarrollo de enfermedad renal crónica (ERC) y enfermedad renal en etapa terminal (ERT). En esta transición, la severidad y duración del insulto inicial es proporcional al riesgo de ERC y la edad es otro factor preponderante.

La ERC ha aumentado en las últimas dos décadas y diagnosticar a los pacientes en fases tempranas de esta enfermedad es difícil, y es aún más difícil predecir la transición de LRA a la ERC. Además, la única forma de saber si un paciente presenta fibrosis y daño estructural es a través de una biopsia renal, que es poco común en la práctica clínica por los riesgos que conlleva.

Hemos demostrado previamente que un episodio de LRA inducido por isquemia / reperfusión renal (IR) bilateral moderada o grave en ratas macho es suficiente para inducir la progresión a ERC después de nueve meses. Sin embargo, los mecanismos involucrados en la transición de LRA a ERC son muy poco conocidos, y aún menos conocidos son las alteraciones que ocurren temporalmente a lo largo de dicha transición. Por lo tanto, es relevante comprender mejor los mecanismos que desencadenan la transición de LRA a ERC, así como establecer una comprensión temporal de los mecanismos fisiopatológicos a lo largo de la transición, lo que no solo nos permitirá comprender este proceso sino también proponer tratamientos efectivos durante el transcurso del tiempo de la enfermedad. Aunado a ello, sabemos que México ocupa uno de los primeros lugares en obesidad y síndrome metabólico a nivel mundial, es por ello, que parte de este trabajo se centro

en estudiar los mecanismos iniciales que promueven la progresión a ERC utilizando un modelo de obesidad.

En este estudio, utilizamos el modelo de IR renal unilateral más nefrectomía contralateral, que nos permitió inducir ERC después de cuatro meses. Descubrimos que la hemodinámica renal anormal redujo la señalización de HIF-1, aumentó el estrés oxidativo y afectó la metilación global del ADN en la fase temprana de la transición de LRA a ERC. También demostramos que la reducción de la señalización de Factor Inducible por Hipoxia 1 α (HIF-1 α) / Factor de crecimiento vascular (Vegfa) se vio afectada por la hipermetilación del ADN del promotor del gen Vegfa, contribuyendo a la transición de LRA a ERC.

Finalmente, usamos el mismo modelo para la búsqueda de biomarcadores renales no invasivos para la detección oportuna del daño renal, encontrando que la serpinA3K es un biomarcador oportuno y eficiente para la detección de la transición de ERC, ERC de distintas etiologías, y la LRA; además, actualmente tenemos la solicitud de patente. Dentro de las alteraciones epigenéticas evaluamos el papel de la desacetilasa de histonas, sirt7 en el daño renal, encontrando que la deficiencia de esta enzima previene el desarrollo de inflamación en respuesta a la LRA.

Los resultados del presente trabajo contribuyen de manera importante al entendimiento de la fisiopatología de la ERC desde diferentes aspectos: moleculares, temporales, epigenéticos y de diagnóstico, lo cual ayudará a la búsqueda de tratamientos efectivos para evitar y retrasar está enfermedad.

1 INTRODUCCIÓN

1.1 Anatomía y Fisiología Renal

La homeostasis es un proceso de balance dentro de los organismos, en donde están involucrados procesos de entrada y salida de nutrientes, así como, la eliminación de desechos. Uno de los sistemas que se encarga de la eliminación de los desechos es el sistema urinario, ya que es capaz de filtrar toda la sangre del organismo y de esa manera eliminar selectivamente los desechos, así como reabsorber nutrientes (1).

El sistema urinario está compuesto por dos riñones con su respectivo uréter, la vejiga y uretra. Todos estos componentes llevan en conjunto a la eliminación de los desechos a través de la orina, pero es en el riñón en donde se llevan a cabo los procesos de filtración, secreción y eliminación de los componentes metabólicos.

En humanos, los riñones se encuentran ubicados en la parte posterior del peritoneo, entre la doceava vértebra torácica y tercera vértebra lumbar. Tienen un peso de entre 125-170 g en hombres y de 115-155 g en las mujeres, representando solo el 0.5% del peso del organismo. Son órganos que presentan una clara organización entre las células endoteliales y las células epiteliales, que lo hace competente para desempeñar sus funciones. Entre estas funciones está la filtración del plasma sanguíneo, la regulación del balance de hídrico, electrolítico y ácido-base. También los riñones cumplen un papel muy importante en la regulación de la eritropoyesis (generación de células sanguíneas) y en la regulación del calcio, al producir hormonas como eritropoyetina y vitamina D, respectivamente (1).

La anatomía de los riñones está en estrecha relación con su función, debido a que, cuenta con glomérulos y un área extensa de tubos de epitelio renal que le permiten realizar de forma correcta la filtración, la secreción y la reabsorción de iones y sustancias. El primer paso es la filtración del plasma sanguíneo. Luego para modificar el ultrafiltrado glomerular cuenta con una vasta cantidad de capilares que permiten llevar a cabo la reabsorción o secreción a lo largo de su paso por los túbulos renales (2).

A simple vista en un corte transversal pueden apreciarse dos zonas en el riñón; en la parte externa se encuentra la corteza renal, que es donde se encuentran los glomérulos y hacia el centro se ubica la médula renal. Dentro de la médula se encuentran entre 8-18 pirámides renales que desembocan hacia los cálices menores en donde fluye la orina hacia el seno renal, para posteriormente ser eliminada. (1,2)

La unidad funcional del riñón es la nefrona, cada riñón presenta entre 800,000 a 1, 200,000 nefronas. Las nefronas están formadas por un penacho capilar llamado glomérulo y una serie de túbulos epiteliales que están divididos en túbulo proximal, asa de Henle, túbulo distal y túbulo colector. Cada uno de estos segmentos presenta una enorme selectividad al paso de iones y metabolitos a través de sus membranas, esto es importante para que los procesos de reabsorción y secreción se lleven a cabo de forma óptima (2).

La función renal comienza con la filtración del plasma sanguíneo a través de glomérulo generando un ultrafiltrado libre de proteínas, posteriormente al pasar por las distintas zonas de los túbulos renales, se van reabsorbiendo iones y sustancias como glucosa y al mismo tiempo se secretan otros desechos que no fueron filtrados

al inicio. Al final, tenemos un concentrado de desechos llamado orina que se excretará a través del túbulo colector. Al volumen de filtrado que se genera por unidad de tiempo se le llama Tasa de Filtrado Glomerular (TFG), la cual es de unos 180 litros al día. Es por esta razón que el riñón recibe aproximadamente el 20% del gasto cardiaco, esto indica lo metabólicamente activo que es este órgano, es por ello por lo que incluso períodos leves de hipoxia son capaces de generar un gran daño (1, 2, 3).

1.2 Lesión Renal Aguda (LRA)

Dentro de las entidades fisiopatologías del tejido renal se encuentra la LRA. Esta enfermedad se caracteriza por la caída abrupta y transitoria del flujo sanguíneo renal, lo que ocasiona una reducción de la función y el consecuente daño endotelial y epitelial por hipoxia (4, 5). Se conoce que la LRA afecta al 15% de los pacientes hospitalizados, siendo la mayor la incidencia en los pacientes en terapia intensiva que es entre el 30 al 60% y con una tasa de mortalidad de alrededor del 40% (6). En la clínica este fenómeno se puede presentar por diversas causas, como es la sepsis, el uso de medicamentos nefrotóxicos o medios de contraste, la hipovolemia generada por hemorragias, deshidratación o por una disminución en la presión arterial y cirugías mayores (5, 6, 7, 8), lo que trae como consecuencia que ocurran procesos de isquemia/reperfusión (IR). La isquemia causa un proceso de hipoxia, que puede llevar a la muerte de las células epiteliales proximales por apoptosis y necrosis, ya que el oxígeno es indispensable para la fisiología de estas células. Aunado a este fenómeno, el proceso de reperfusión incrementa la generación de

especies reactivas, generando daño oxidante en macromoléculas, como, los ácidos nucleicos, las proteínas y los lípidos (4, 5, 8).

Hace varios años no existían consensos de la definición clínica de LRA, en las últimas décadas se han establecido algunos parámetros clínicos para unificar la definición estándar de LRA y la ERC mediante las guías Kidney Disease: Improving Global Outcomes (KDIGO) (9).

La LRA implica la reducción de la función renal, que se determina por un aumento de la concentración de creatinina sérica de ≥0,3 mg/dl durante 48 h o aumento de ≥1.5 veces en los últimos 7 días, o diuresis <0,5 ml/kg/h durante 6 h. La LRA se clasifican en tres grados de severidad las cuales en las guías KDIGO se definen por el aumento de la creatinina sérica con referencia a los valores basales: Red de Lesión Renal Aguda (por sus siglas en inglés, Acute Kidney Injury Network (AKIN)) I con un aumento CrS ≥0.3mg/d o 1.3-1.9 veces del basal, AKIN II 2-2.9 veces del basal y AKIN III 3 veces del basal o porque se inicie la terapia de remplazo renal (9). Desafortunadamente estos cambios ocurren 48 h después de haber ocurrido la LRA, además no siempre es factible conocer los valores basales de referencia del paciente. Esto trae como consecuencia que la incidencia de LRA no haya disminuido en los últimos 40 años. (6, 8). Por lo tanto, la LRA constituye un serio problema de salud pública alrededor del mundo, generando costos de hasta 9 mil millones de dólares para el sistema de salud norteamericano (6). En la actualidad, la búsqueda de biomarcadores tempranos para la detección de la LRA (10, 11), así como, la generación de estrategias terapéuticas que sean capaces de prevenir el desarrollo de un episodio de LRA resulta indispensable.

1.3 Mecanismos responsables de la LRA

En la actualidad se tiene noción de algunos de los mecanismos involucrados en la LRA, sin embargo, no se ha terminado de entender a esta entidad del todo. Se conoce que durante la LRA hay un ambiente de hipoxia, que lleva a la muerte celular, principalmente del epitelio tubular, tanto por apoptosis que es una muerte celular programada, como por necrosis, muerte celular que promueve la liberación del material celular. Ambos mecanismos generan una pérdida importante de epitelio tubular renal, que se desprende y las células epiteliales se pueden encontrar en la orina de los pacientes con este tipo de lesión. Se ha demostrado que las células epiteliales más dañadas son las del túbulo proximal, específicamente, los segmentos S2 y S3 (4, 5, 8, 12).

Después de un episodio de LRA, ocurre una cascada de eventos, como pérdida del borde en cepillo, alteraciones de la polaridad celular, aumento del estrés oxidativo y disfunción mitocondrial de las células epiteliales tubulares proximales (4, 5, 7, 8, 12). Estos procesos también se acompañan de inflamación e infiltración de macrófagos (13, 14, 15). Aunque el epitelio tubular tiene capacidad de regeneración (12), el epitelio lesionado ya no es el mismo. Una subpoblación de células tubulares desdiferenciadas y en proliferación que se recuperan del daño renal agudo sufren una detención del ciclo celular y no pueden volver a diferenciarse, lo que lleva a una atrofia tubular; todos estos eventos contribuyen en gran medida a la fibrosis tubulointersticial que se observa a largo plazo (12, 18).

En consecuencia, se produce una reparación inadecuada (16-19), donde hay infiltración persistente de macrófagos (13, 14, 15), disociación de pericitos de los capilares tubulares (19) y arresto de algunas células tubulares en la fase G2 / M

(20), lo que conduce a la fibrosis progresiva (18, 20-22). Se han dilucidado algunos mecanismos implicados, como la transdiferenciación de pericitos en miofibroblastos (19,22), la proliferación descontrolada de células epiteliales (22), la aparición de un fenotipo anormal del túbulo proximal (23, 24), la producción excesiva de TGFβ tanto por el epitelio tubular (18), como por los miofibroblastos locales (24,25), acumulación de proteínas de la matriz extracelular (26,27), la pérdida de la microvasculatura,proceso denominado rarefacción vascular (28-30), hipoxia crónica (30,31) y estrés crónico del retículo endoplásmico (32).

Durante la LRA, las células de este segmento sufren cambio de su polaridad, debido a que, la bomba $Na^{+}K^{+}$ATPasa, que normalmente se encuentra en el lado basolateral se relocaliza al lado apical, así como, cambios en el citoesqueleto que producen la pérdida del borde en cepillo, una estructura especializada que presenta este tipo epitelial. Los dos procesos antes mencionados se relacionan con una disminución en la capacidad de reabsorción del epitelio. Otro componente que sufre daño durante este proceso es la microcirculación, que no es capaz de responder a la hipoxia llevando a la rarefacción vascular (17, 28-30, 34). En la Figura 1 se esquematiza algunos de los procesos celulares que se alteran durante la LRA.

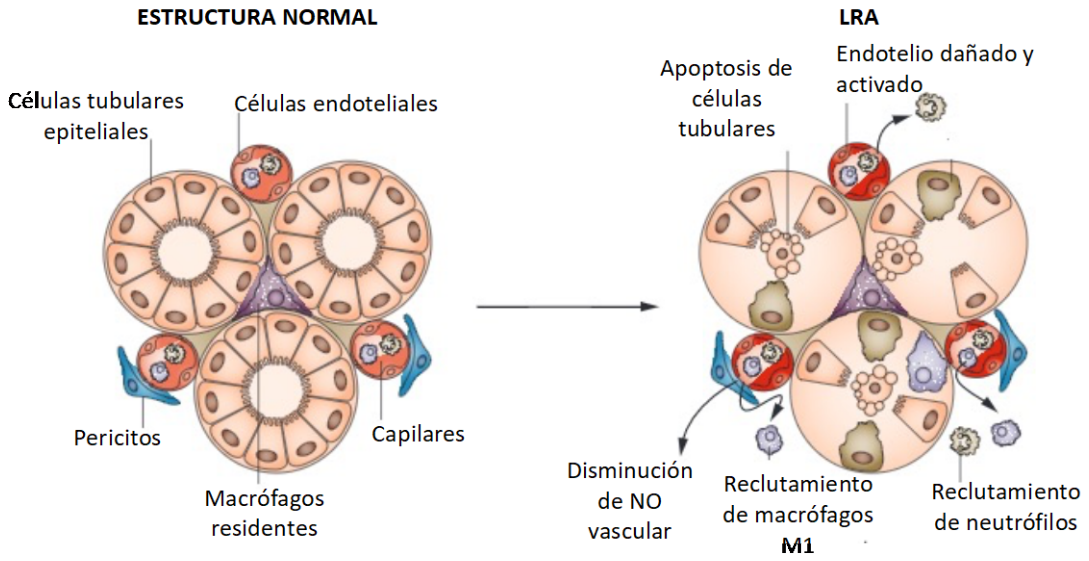

Figura 1. Efectos de un episodio de LRA en el riñón, responsables de causar el daño. Modificada de Ref.17.

Aunque se han dilucidado algunos mecanismos, muchos otros permanecen desconocidos y se sabe menos sobre los cambios temporales durante la progresión de la enfermedad renal crónica (ERC), como la hemodinámica renal, la lesión estructural, la señalización de HIF y las modificaciones epigenéticas.

1.4 Enfermedad Renal Crónica

La ERC se caracteriza por la pérdida progresiva de las nefronas y de la función renal, lo que puede resultar a largo plazo en la pérdida de la función renal completamente, momento en el cual, la única forma de que el paciente sobreviva es con terapias de remplazo renal, como diálisis peritoneal y hemodiálisis, o bien el trasplante renal. Ambas posibilidades terapéuticas generan enormes costos a los sistemas de salud. En las últimas dos décadas, la incidencia de la ERC ha aumentado más de tres veces y es un síndrome que en la actualidad tiene importantes implicaciones para la salud de las poblaciones y la sostenibilidad económica de los sistemas de salud en todo el mundo (33-36).

Las guías KDIGO definen la ERC como la disminución de TFG <60mL/min/1.73m^2 persistente por >3 meses y se clasifica de acuerdo con la causa específica (37), en combinación con la estratificación de la gravedad según la TFG y los niveles de albuminuria (9). Para hacer la evaluación de TFG se toma la elevación de la creatinina sérica por >3 meses, además se toma en cuenta anormalidades en el sedimento urinario, estudio de imagen o histología (37). La desventaja de estas evaluaciones es que detecta a la enfermedad de manera tardía y en el caso de los estudios histológicos, son invasivos, lo que conlleva a un riesgo mayor para el paciente y dependiendo del área donde se tome la muestra, puede no dar información certera. Por estas razones, se están haciendo esfuerzos para identificar nuevos biomarcadores que además no sean invasivos. Retomaremos este concepto más adelante.

1.5 Transición de la LRA a ERC

Durante mucho tiempo se especuló que los pacientes que sobrevivían a un episodio de LRA no tenían ninguna repercusión posterior y que el epitelio era capaz de regenerarse y regresar a su funcionamiento normal. Sin embargo, estudios clínicos y modelos experimentales recientes han demostrado que la LRA es un factor de riesgo independiente para desarrollar ERC (16, 17, 34).

Resulta evidente que cada vez existe mayor conocimiento sobre los mecanismos involucrados en un evento de LRA, sin embargo, como se comentó la LRA se ha convertido en un reto aún mayor, debido al riesgo inminente que tiene el paciente de desarrollar ERC en un futuro no lejano. A pesar de que el tejido renal tiene la habilidad de recuperarse del daño celular letal o subletal, lo cual se observa

de manera funcional cuando los pacientes son egresados de la hospitalización con cifras de creatinina en parámetros normales, los procesos celulares del endotelio y del túbulo renal no se recuperan totalmente, lo que condicionan al desarrollo de disfunción renal progresiva, Figura 2 (36).

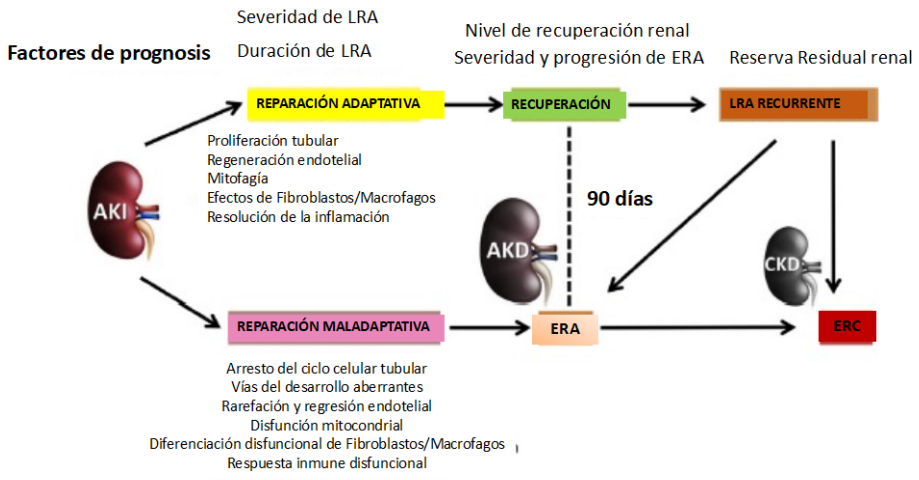

Figura 2. Patobiología de la reparación ineficiente que lleva de LRA a ERC. Modificado de Ref. 36

En los últimos años se han propuesto varias teorías tratando de explicar como un episodio de LRA puede conducir al desarrollo de ERC dentro las que destacan: ciclos de daño/reparación/regeneración continuos a lo largo del tiempo (5, 12), rarefacción de los capilares peri-tubulares con el desarrollo subsecuente de hipoxia crónica (27-30) y la activación de las vías de señalización en donde están involucrados factores como HIF-1α, MAP cinasas, y citocinas pro-fibróticas y pro-inflamatorias (31, 39). También se ha mostrado que después de la isquemia/ reperfusión (I/R) no solo no hay proliferación de las células endoteliales, sino que se presenta una transición del endotelio a mesénquima. Es decir, la disminución en la densidad vascular que ocurre después de la LRA resulta en parte por la transición fenotípica que sufren las células epiteliales que se combina con la capacidad impedida de regeneración (20, 22). Además, Conger et al. mostraron que el riñón

post-isquémico pierde la capacidad de autorregular adecuadamente el flujo sanguíneo renal. Estas condiciones en conjunto perpetúan los ciclos continuos de daño por hipoxia e inflamación que eventualmente conducen al desarrollo de ERC (34). Aunque es esencial que las células tubulares proliferen para restablecer la estructura tubular normal, dos estudios recientes sugieren que las células epiteliales de los túbulos renales también juegan un papel crítico en el desarrollo de la fibrosis túbulo intersticial característica de la ERC, a través de inducir un arresto en el ciclo celular y modificaciones epigenéticas (101). Yang L. et al. demostraron que después de daño renal por I/R o por nefrotóxicos o por obstrucción uretral, las células epiteliales sufren un arresto en el ciclo celular en la fase G2/M, lo que resulta en un fenotipo que facilita la producción de factores pro-fibróticos, como TGF-β, Esto se debe a que en las células del túbulo proximal que se encuentran arrestadas, la cinasa JNK se activa y sobre-regula la producción de citocinas pro-inflamatorias (20). Además, Bechtel W et al. infirieron que el mantenimiento de la fibrosis puede representar que los fibroblastos activados no pueden regresar a su estado basal debido a que sufren alteraciones únicas en la metilación de los fibroblastos. De hecho, estos autores identificaron 12 genes candidatos para ser regulados por metilación, pero demostraron que la metilación en el gen RASAL1 por la metiltransferasa Dnmt1.5, es esencial para la activación crónica de los fibroblastos. Este estudio mostró que los cambios epigenéticos toman lugar en la progresión de la ERC (40). Además, en otros estudios recientes se ha demostrado que la activación aberrante de vías implicadas en el desarrollo embrionario como Wnt/β-catenina, Shh y Snail contribuyen al cambió en el fenotipo de las células tubulares y al desarrollo de fibrosis (41-43). La Figura 3 esquematiza los mecanismos conocidos de la transición de LRA a ERC.

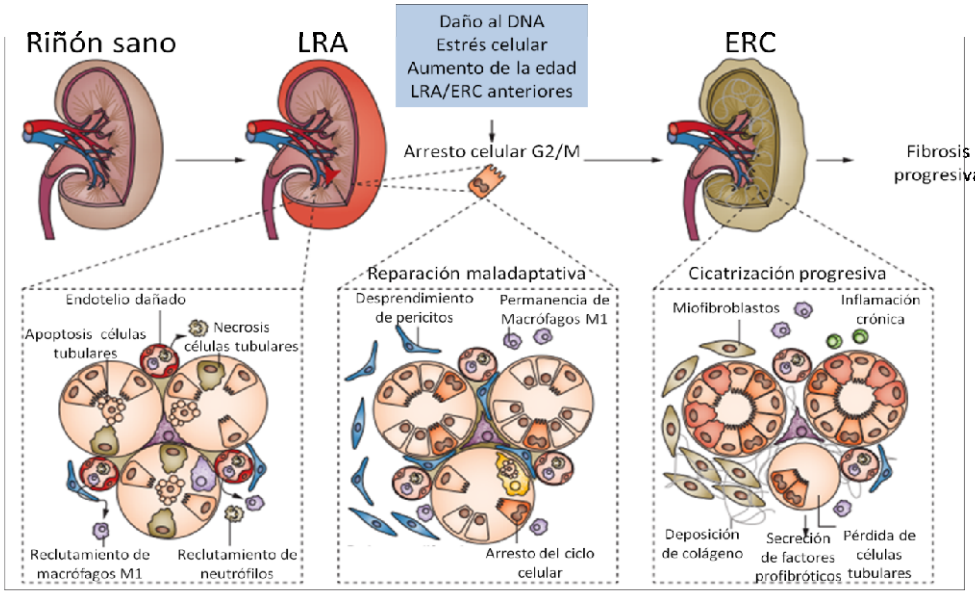

Figura 3. Transición de LRA a ERC. La inflamación crónica, muerte celular y desarrollo de fibrosis. Modificada de Ref. 17.

Previamente, demostramos que un episodio de LRA inducida por I/R bilateral moderada o grave en ratas macho es suficiente para inducir la progresión de la ERC después de nueve meses (26). Curiosamente, esta transición no se observó en ratas hembra, a pesar de una magnitud similar de LRA a las de las ratas macho. La única diferencia en la fase inicial posterior a la isquemia fue que las hembras no mostraron estrés oxidante, lo que sugiere un papel fundamental de la generación de ROS en esta transición (21).

Debido a que la ERC se desarrolló después de nueve meses, surge la necesidad de tener un modelo que resulte eficiente, en cuanto a tiempo y costos, y que permita estudiar los procesos involucrados en la transición de LRA a ERC en periodos de tiempo más cortos.

Algunos modelos que se han descrito que logran acelerar la ERC son los modelos de Nefrectomía 5/6 y la UUO (44-45). Sin embargo, ambos modelos resultan demasiado agresivos, y llevan a hipertensión y fibrosis severa, respectivamente, lo que no permiten evaluar mecanismos temporales de

progresión. La nefrectomía unilateral o uninefrectomía, es un modelo que reduce la masa renal en un 50%, lo que permite que el riñón remanente tenga un proceso de hipertrofia compensatoria, así como, un aumento en la tasa funcional y el flujo sanguíneo renal, capaces de mantener la función renal normal (44). Se considera que el riñón remanente, al tener una mayor actividad metabólica, es más susceptible a episodios de daño, y es *por ello, que sería interesante explorar este modelo para estudiar los mecanismos temporales de la transición de la LRA a ERC.*

1.6 Obesidad y daño renal

El aumento en la prevalencia de la obesidad es un problema de salud a nivel mundial, ya que, el exceso de tejido adiposo incrementa el riesgo de enfermedades cardiovasculares, diabetes y cáncer (46, 47). En una revisión sistemática publicada en el 2017, se estimó que 1.46 mil millones de adultos con sobrepeso en todo el mundo y de estos, 502 millones presentaban obesidad (48). De acuerdo con la Encuesta en Salud y Nutrición (ENSANUT) de 2016 en México, la prevalencia combinada de sobrepeso y obesidad estimada en adultos fue 72.5% y en edad escolar, la prevalencia combinada de sobrepeso y obesidad fue de 33.2% (49). Se ha estimado que para el 2025, la prevalencia mundial de obesidad aumentará de 11 a 18% en hombres y de 15 a 21% en mujeres, por lo que, existe una gran preocupación en los sistemas de salud (48).

Actualmente, se considera a la diabetes y a la hipertensión como las principales causas de ERC, asociadas ambas enfermedades con obesidad (50). Por lo que, algunos autores consideran que la ERC en pacientes obesos es ocasionada indirectamente a través de la influencia de factores de riesgo como el síndrome

metabólico; sin embargo, en otros estudios se sugiere una relación directa entre la obesidad y la ERC (51). Además, se tienen reconocidos dos fenotipos en la obesidad, uno con disfunción metabólica, y el otro sin disfunción metabólica, además de que se ha reportado la transición entre estas dos entidades en el transcurso del tiempo (52).

De acuerdo con la Organización Mundial de la Salud (OMS), el síndrome metabólico se define por la coexistencia de la resistencia a la insulina con al menos dos de las siguientes entidades fisiopatológicas: hipertensión arterial sistémica (≥ 140/90 mm Hg), dislipidemia manifestada como hipertrigliceridemia, con una concentración mayor a 150 mg/dL o lipoproteína de baja densidad (HDL) menor a 35 mg/dL en hombres o 39 mg/dL en mujeres, obesidad central o abdominal caracterizada por un índice de masa corporal (IMC) menor a 30 kg/kg/m^2, microalbuminuria con un índice albuminuria-creatinina de 30 mg/g o más, o una tasa de excreción urinaria de albúmina mayor a 20 µg/min. (52, 53).

Así mismo, un metaanálisis publicado en 2017 **identificó a la obesidad como un factor de riesgo independiente para el desarrollo de ERC**, con o sin la presencia de síndrome metabólico, siendo caracterizado por un riesgo aumentado de tener una TFG baja (<60 mL/min/1.73 m²) y albuminuria (48). Además, se ha identificado a la obesidad como un factor potencial de riesgo para el desarrollo de ERC terminal en pacientes con ERC (53).

Se han identificado diferentes vías fisiopatológicas por las que, la obesidad podría estar relacionada con el desarrollo de ERC. Una es la glomerulopatía relacionada a la obesidad (por sus siglas en inglés ORG), la cual está caracterizada por una disminución de la TFG y una disminución del flujo sanguíneo renal efectivo,

así como, disfunción e hipertrofia de los podocitos que se acompaña de una disminución en la densidad y número de estos, hipertensión e hipertrofia glomerular y el hallazgo histopatológico de glomerulomegalia, lo que conlleva a una forma secundaria adaptativa de glomeruloesclerosis focal y segmentaria (GSFS) a largo plazo (51). Se ha visto que, solo una proporción menor de los pacientes obesos presentan clínicamente ORG manifestada con proteinuria. Debido a la alta incidencia de obesidad en nuestra población y as su relación con la ECR,la búsqueda de biomarcadores para la detección oportuna de esta patología es crucial.

La obesidad es considerada un estado de inflamación crónica, además de que se asocia con diferentes condiciones patológicas como, la resistencia a la insulina, la lipotoxicidad generada en diferentes órganos, y el síndrome de apnea obstructiva del sueño (SAOS). Además, se conoce que una dieta rica en fructosa incrementa el estrés oxidante que propicia disfunción endotelial y un estado pro-inflamatorio (51).

Algunos de los mecanismos descritos se encuentran el Figura 4, en donde la hipertensión sistémica y la hipertensión glomerular ocasionan el engrosamiento de la membrana basal glomerular (MBG) y el daño de los podocitos (54). *Sin embargo poco se ha estudiado sobre el daño tubular en esta patología, y se desconoce, los mecanismos iniciadores clave para el desarrollo de daño renal inducido por* obesidad.

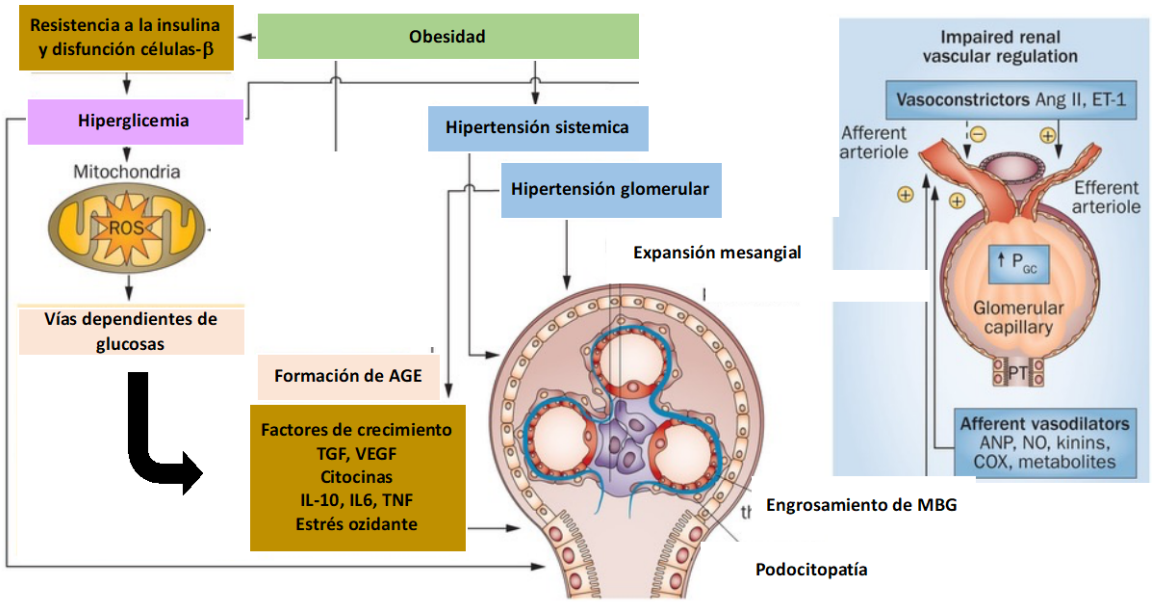

Figura 4. Daño renal inducido por obesidad. AGE- Productos avanzados de glicosilación, MBG-Membrana Basal glomerular. Modificado de Ref. 54

1.7 Biomarcadores de daño renal

Se conoce que la detección y el inicio temprano del tratamiento en LRA y su transición a ERC puede ayudar a un mejor pronóstico de estos pacientes. En la actualidad, aunque se han propuesto algunos biomarcadores de LRA, no se cuentan con estudios sólidos que apoyen a estos biomarcadores para el diagnóstico oportuno de la ERC. Estudios recientes han demostrado que la fibrosis tubulointersticial se presenta desde etapas tempranas de la enfermedad (21), por lo que, es importante identificar nuevos marcadores tempranos de la presencia de fibrosis renal como posibles biomarcadores de ERC.

Para el diagnóstico de LRA se han descrito múltiples biomarcadores que parecen prometedores como: la gelatinasa de neutrófilos asociada a lipocalina 2 (NGAL), la molécula de daño renal 1 (Kim-1), la interleucina 18 (IL-18), la N-acetil-

beta-glucosaminidasa (NAG), la proteína de unión a ácidos grasos de hígado (L-FABP), el inhibidor tisular de las metaloproteinasas 2 (TIMP-2) y la proteína de choque térmico 72 (Hsp72) (11, 55-61). Sin embargo, la mayoría han sido poco sensibles, por lo que se ha llegado a proponer el uso de un panel de varias de estas proteínas para aumentar la sensibilidad. Hsp72 fue descrita por nuestro grupo y ha mostrado ser sensible y específica para la detección de LRA en pacientes críticamente enfermos (61, 62). Definitivamente, cada biomarcador debe ser analizado en cada contexto de la LRA y muchos estudios alrededor del mundo exploran la efectividad de cada uno.

En el caso de la ERC, los biomarcadores que se utilizan para el diagnóstico son la presencia de albuminuria o la reducción de tasa de filtrado glomerular mediada por creatinina o cistatina C; es importante mencionar que estos bimarcadores se alteran cuando la enfermedad ha progresado y no se cuentan con biomarcadores efectivos para detectar a la ERC incipiente (11, 63, 64). Además, es necesario contar con un biomarcador que refleje el estado de fibrosis renal lo que evitaría el uso de métodos invasivos como la biopsia renal. Uno de los que se ha propuesto son los niveles plasmáticos de TGFβ, sin embargo, los resultados no son convincentes (65). En este sentido, el contar con un biomarcador temprano que pueda estratificar el grado de daño que ha sufrido el paciente y que además permita conocer la respuesta al tratamiento, permitirá ofrecer un tratamiento capaz de prevenir desenlaces no deseados, como la muerte del paciente o la progresión a ERC en estadios avanzados. Este concepto lo retomaremos más adelante.

1.8 Influencia de modificaciones epigenéticas en la enfermedad renal

Inicialmente se descubrió que algunos cambios hereditarios ocurrían sin alterar la secuencia del DNA, estos fueron llamados cambios epigenéticos.
Estos cambios ocurren por metilación del DNA o por metilación o acetilación de las histonas, proteínas que rodean a cada 146 pares de bases de DNA, estructura llamada cromatina. Estas modificaciones modifican la compactación de la cromatina y están relacionadas con la actividad transcripcional.

En los últimos años, las modificaciones epigenéticas ha tomado gran relevancia en el desarrollo de diversas patologías. Las enfermedades renales no son la excepción, pero para el caso de la LRA y la ERC poco se conoce al respecto. En el caso de enfermedades renales, las principales modificaciones epigenéticas que se han visto involucradas son: la metilación del DNA y de las histonas, la acetilación/desacetilación de las histonas y recientemente la influencia de los de los miRNAs en la expresión de proteínas (67-68). Se ha demostrado que la hipometilación en fibroblastos es capaz de conferirles un fenotipo profibrótico, lo que contribuye al desarrollo de fibrosis renal (40). Además, estudios recientes han sugerido que los procesos inflamatorios y de reparación, tienen un componente de regulación epigenética muy importante (69, 70). Se ha demostrado, por ejemplo, que cambios en la metilación de regiones promotoras de los genes de factor TNF-α, IL-6 y MCP-1 promueven la llegada de remodeladores de la cromatina como, Brahma-related gene-1 y Pol II, promoviendo la transcripción de estos genes en la LRA (70). También se sabe que los inhibidores de desacetilasas de histonas (HDAC), enzimas encargadas de añadir una pequeña molécula que se llama grupo acetilo, se han involucrado en la prevención de LRA. Sin embargo, se conoce muy

poco sobre la participación de las modificaciones epigenéticas en la transición de LRA a ERC.

Por lo tanto, resulta interesante conocer si hay procesos dinámicos en la metilación de DNA durante la transición de la LRA a ERC y conocer la expresión de uno o más genes que puedan modularse por metilación y que promuevan la transición.

1.9 Sirtuinas como orquestadoras de cambios epigenéticos

Las HDAC son enzimas que extraen grupos acetilo, de las proteínas histonas que se encuentran formando la cromatina. La eliminación del este grupo acetilo modula la forma en que las histonas se unen al DNA, con ello, pueden afectar su actividad (66). Existen cuatro tipos de desacetilasas de histonas que se han denominado Clase I, II, III y IV. Específicamente, las desacetilasas clase III, son conocidas como sirtuinas. La diferencia de está familia es que dependen del cofactor NAD+ para realizar su actividad enzimática, por lo que pueden censar el estado metabólico de la célula (71). Se han identificado siete tipos de sirtuinas, de la 1 a la 7, siendo la sirtuina 7 (Sirt7) la menos estudiada hasta ahora.

Las sirtuinas se han implicado en el desarrollo de diversas patologías humanas incluyendo: cáncer, diabetes tipo II, dislipidemias, enfermedades cardiovasculares o desordenes neurodegenerativos. Las Sirt6 y Sirt7 se encuentran canónicamente en el núcleo, las Sirt3–5 se localizan principalmente en la mitocondria y las Sirt1-2 se encuentran en el núcleo y en el citoplasma (71). La Sirt7 regula la homeostasis celular, ya que, participa en múltiples procesos celulares como la transcripción, la síntesis de ribosomas, la conformación de la cromatina y

la proliferación celular. La Sirt7 regula la expresión de genes, ya sea afectando de manera directa la transcripción de genes específicos, o bien por la desacetilación de la histona 3 en el residuo de lisina 18 (H3K18), que reprime la transcripción. Se ha reportado que la Sirt7 también funciona como un regulador vital para atenuar las condiciones de estrés, al activar moléculas de supervivencia celular. De acuerdo con esto, la sobreexpresión de Sirt7 en algunos tipos de cáncer se ha relacionado con mayor proliferación, sobrevida celular, así como, fibrosis cardiaca asociada a angiotensina II (71-73). En cambio, la depleción de Sirt7 se asocia con mayor daño al DNA, apoptosis, hepatoesteatosis crónica y ateroesclerosis.

Debido al amplio espectro de funciones que puede ejercer la Sirt7 se requieren estudiar su papel en cada condición fisiopatológica para descifrar los mecanismos involucrados (71). Algunos trabajos han reportado que el uso de los inhibidores de desacetilasas de histonas, es capaz de prevenir procesos fibróticos e inflamatorios (72). Sin embargo, también hay evidencia que indica que, la activación o sobreexpresión de Sirt1, Sirt3, Sirt5 y Sirt6 promueve protección frente a episodios de lesión renal aguda (LRA), en diferentes contextos patológicos (74-77)

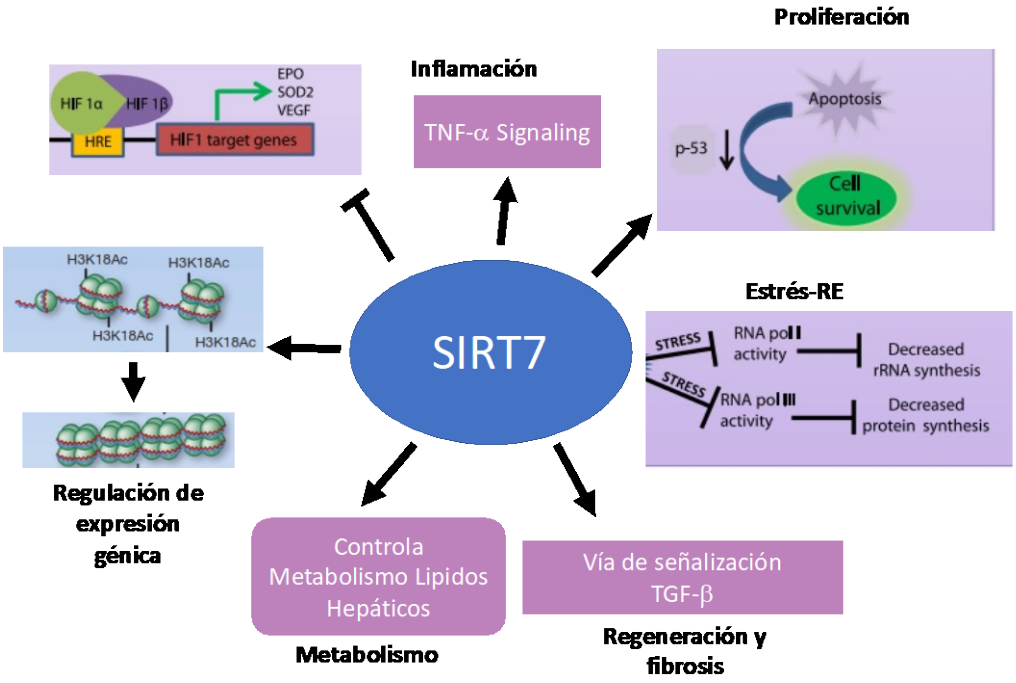

Figura 5. Papel de la sirtuin7. Modificado de Ref. 79 y Ref. 86.

Recientemente se mostró la relación que existe entre la Sirt7 con la respuesta a estrés inducido por hipoxia, mediante su interacción con las proteínas HIF-1α y HIF-2α. Esta interacción regula a la baja la cantidad de HIF-1α y HIF-2α., mediante su degradación independiente de la vía proteasomal o lisosomal, lo que, implica que la inhibición de Sirt7 puede ser crítica para la señalización adecuada frente a hipoxia (79). Además, estudios en ratones deficientes de la Sirt7 usando el modelo de esteatosis hepática, han demostrado que la Sirt7 es inducida en respuesta al estrés del retículo endoplásmico (RE) y se estabiliza en los promotores de proteínas ribosomales al interactuar con el factor Myc para silenciar la expresión de genes y aliviar el estrés-RE (85), además de su implicación en la regulación de procesos fibróticos e inflamatorios (80, 83-84, 86).

La Sirt7 ha cobrado relevancia en la respuesta inflamatoria en los últimos años. En contraste con el hallazgo de que la sobreexpresión de la Sirt1 promueve protección inhibiendo la inflamación, es la deficiencia de la Sirt7 la que parece

suprimir la respuesta inflamatoria. La Sirt7 juega un papel importante en la regulación de la exportación nuclear de NFkB, lo que fue puesto de manifiesto en el modelo de inducción de daño renal por cisplatino (80, 86), en dónde se demostró que los ratones deficientes de la Sirt7 presentaron menor concentración de citocinas proinflamatorias en comparación con los ratones silvestres, por lo que, la falta de Sirt7 confiere renoprotección en este escenario. También se ha demostrado que la deficiencia de la Sirt7 es suficiente para prevenir el hígado graso inducido por una dieta alta en grasa, al regular el metabolismo de lípidos mediante la degradación de factores como TR4, que promueven la acumulación de ácidos grasos y la síntesis de triglicéridos (84). En la figura 5 se esquematizan algunas de las funciones de la Sirt7. Sin embargo, *se desconoce el efecto de la Sirt7 en otros modelos de daño renal, y mucho menos se sabe si la ausencia de esta desacetilasa puede afectar la progresión a ERC.*

El presente proyecto fue diseñado para mejorar nuestro conocimiento sobre los mecanismos y contar con un método de diagnóstico oportuno de la ERC. Por lo tanto este proyecto abordó tres perspectiva diferentes, como se esquematiza en la Figura 6: 1) evaluando las vías de señalización que se encienden de manera temporal en el desarrollo de daño renal inducido por un episodio de LRA o por la obesidad, 2) buscando nuevos biomarcadores no invasivos para la detección oportuna del daño renal y 3) evaluando algunas alteraciones epigenéticas como: la metilación global del DNA, la metilación del promotor del gen del factor de crecimiento del endotelio vascular (VEGF por sus siglas en inglés) y la implicación de la deficiencia de la desacetilasa de histonas, sirt7 en el daño renal. Como se verá mas adelante, la mayoría de los resultados del proyecto han sido publicados en tres

artículos originales en revistas indizadas, también se publicó un artículo de revisión y estamos preparando dos manuscritos mas.

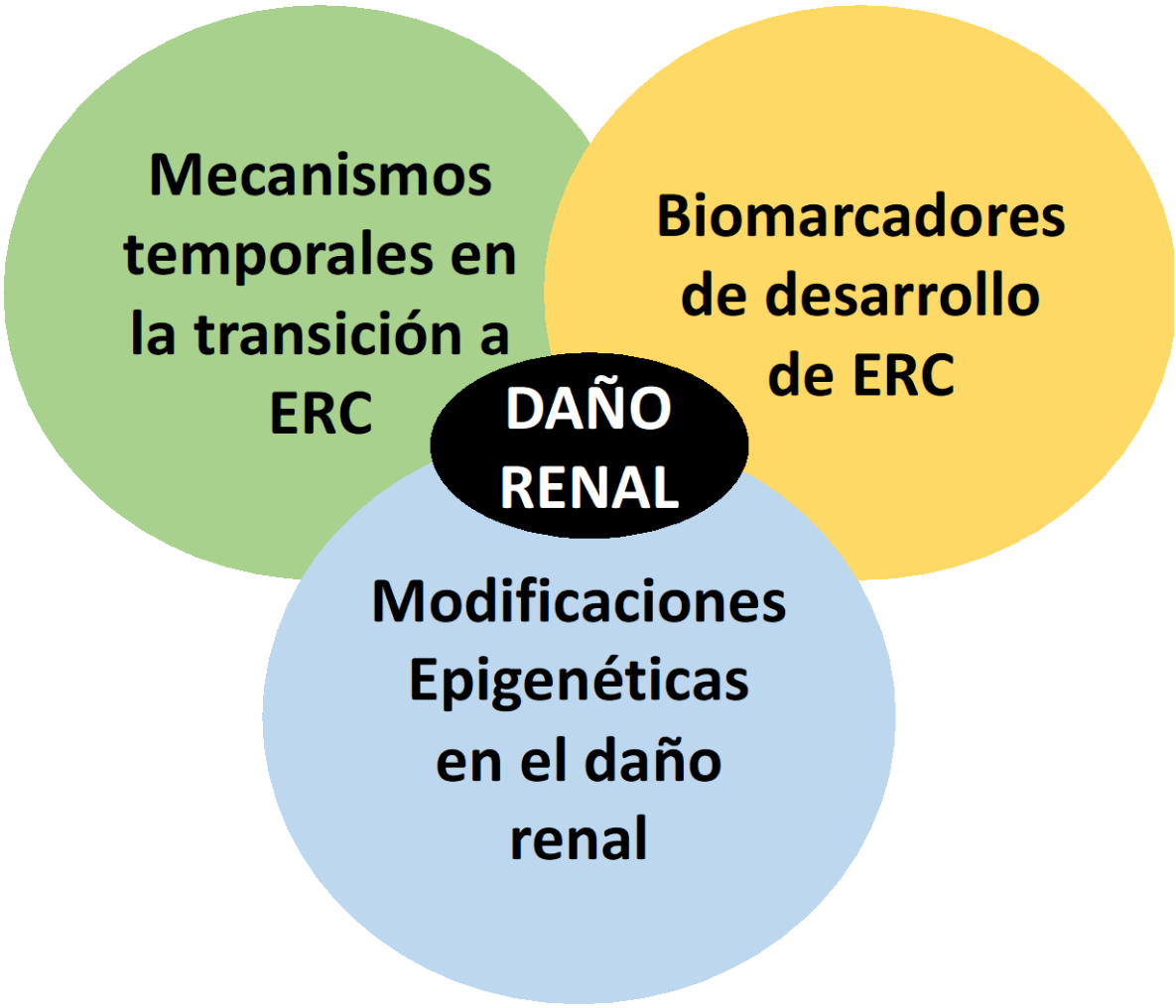

Figura 6. Esquema de los objetivos.

2. PLANTEAMIENTO DEL PROBLEMA

El daño renal es una patología compleja, en donde diversos mecanismos celulares juegan un papel importante. Sin embargo, no conocemos la temporalidad ni los mecanismos iniciales que llevan a desarrollo de daño renal. Aunado ha esto la mortalidad y morbilidad de la LRA no ha disminuido en los últimos años, acompañado con el aumento en la obesidad y síndrome metabólico en nuestro país, que esta directamente relacionada con un incremento en la nefropatía diabética y la ERC. Además, la mayoría de los modelos murinos de obesidad en los que se induce daño renal utilizan modelos usando una dieta que duplica la proporción ingesta de grasas en pacientes obesos. Por lo tanto, es crucial estudiar el impacto de una ingesta alta en grasas en la fisiología renal usando un modelo de obesidad común en humanos

Debido a la diferencias que existen entre las etiologías, se requiere el abordaje de diferentes modelos experimentales para poder entender esta enfermedad y lograr encontrar blancos terapéuticos que prevengan o frenen la progresión a ERC. Además, es importante contar con moléculas o biomarcadores que puedan evidenciar los mecanismos iniciales de daño para poder establecer el momento adecuado para comenzar el tratamiento.

3. HIPÓTESIS

1. Es posible acelerar la transición de la LRA a ERC con el modelo de uninefrectomia e IR unilateral simultánea.
2. Existen cambios temporales que ocurren en la transición de LRA a ERC.
3. Existen mecanismos clave iniciales involucrados en la ERC inducida por obesidad.
4. Existen biomarcadores que identifiquen oportunamente la LRA y el desarrollo de ERC.
5. La Sirt7 tiene un papel tanto en la LRA como, en la transición de la LRA a ERC.

4. OBJETIVO

Conocer los mecanismos temporales y epigenéticos involucrados en el desarrollo de daño renal inducido por diversos etiologías, como LRA, transición de LRA a ERC y obesidad; así como la búsqueda de métodos de diagnóstico oportuno de la ERC.

4.1 OBJETIVOS PARTICULARES

1. Caracterizar el efecto de la unifrectomia + IR unilateral a largo plazo en la rata.
2. Evaluar el curso temporal de las alteraciones: funcionales, histopatológicas, inflamación renal, respuesta de estrés oxidante y metilación del DNA en la transición de la LRA a ERC en la rata.
3. Evaluar los mecanismos clave iniciales involucrados en la ERC inducida por obesidad.
4. En base a un análisis proteómico, buscaremos nuevos biomarcadores tempranos de LRA y transición de LRA a ERC en este modelo.
5. Determinar si la ausencia de la desacetilasa de histonas Sirt7 modifica el daño renal por IR y la transición a ERC.

5. METODOLOGÍA

5.1 Modelo de transición de LRA a ERC.

Se incluyeron tres grupos de ratas Wistar macho de entre 300-350 g. Los animales se dividieron en tres grupos, el grupo de cirugía falsa (sham n=16), el grupo de nefrectomía derecha (UNx n=16) y el grupo con nefrectomía derecha e isquemia renal izquierda de 45 min (IR+UNx n=20). El protocolo experimental se muestra en la Figura 6. Los animales se anestesiaron con pentobarbital sódico (30 mg/kg) y se mantuvieron en una cama termoregulada para realizar la cirugía a 37°C. Bajo anestesia se realizó una incisión abdominal para exponer los dos riñones; primero se realizó la nefrectomía del riñón derecho, disecando la grasa peri-renal, así como, separando la glándula suprarrenal del riñón con sutileza para evitar dañarla. Para el grupo con IR+UNx, además de la nefrectomía se colocó un clip en el riñón izquierdo durante 45 min, con la finalidad de provocar el proceso isquémico y la reperfusión se logró al retirar el clip, usando la coloración del riñón, como indicador. Los animales se mantuvieron en ciclos de luz-oscuridad ciclos12-12 h y acceso libre a comida y agua. Los animales se sacrificaron y estudiaron a las 24 h, 1, 2, 3 o 4 meses dependiendo del periodo experimental.

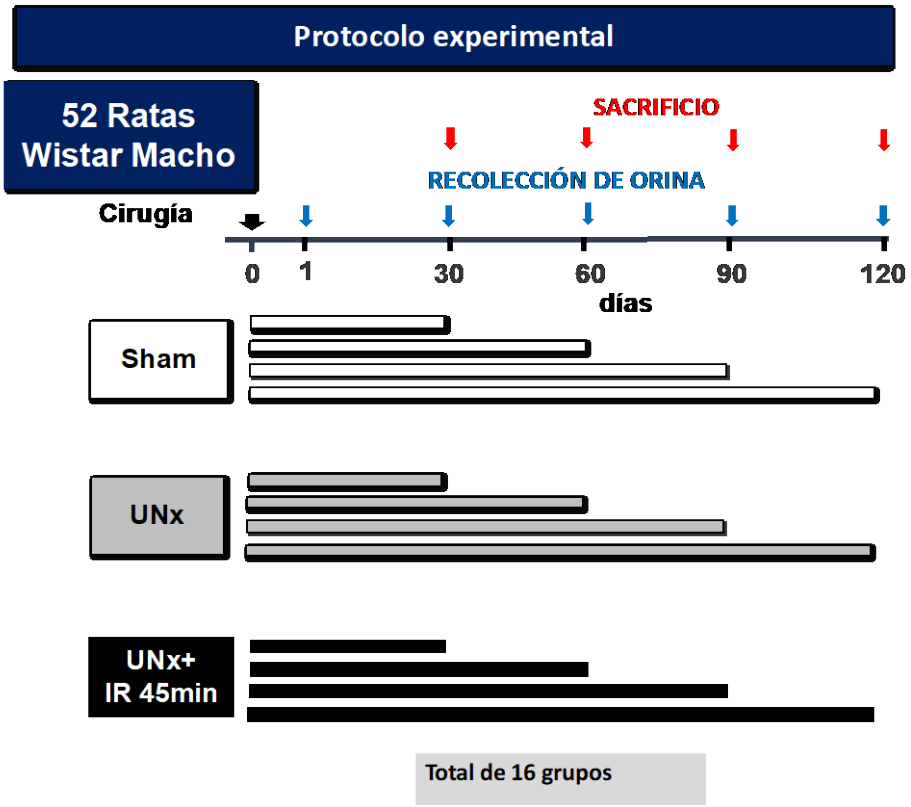

Figura 7. Modelo experimental. Las flechas azueles indican los tiempos en donde se realizaron las recolecciones, y las flechas rojas indican los tiempos en que se realizo la eutanasia. Sham y UNx n=4 por grupo, UNx+ IR n=5 por grupo

-Medición de parámetros fisiológicos

Los animales se colocaron en jaulas metabólicas cada mes, para recolectar la orina de 24 h para determinar el volumen urinario, la excreción urinaria de proteínas y la depuración de creatinina, para la cual también se recolectó una muestra de sangre de forma mensual. Para la determinación de creatinina sérica y urinaria se utilizó el método colorimétrico de ácido pícrico (Creatinine Assay Kit). Para calcular la depuración de creatinina se utilizó la fórmula de C= (U*V)/S, en donde U es la creatinina urinaria multiplicada por el volumen urinario, y S corresponde a la creatinina sérica. La excreción urinaria de proteínas se determinó

por el método turbidimétrico de ácido tricloroacético (TCA), la curva estándar y las muestras se leyeron a 420 nm en un espectrofotómetro.

Para los estudios fisiológicos, los animales fueron anestesiados con pentobarbital sódico (30 mg/kg), se colocaron en una cama de termo regulación, la tráquea se entubó con un tubo de polietileno PE-240 y se cateterizaron las arterias femorales con un tubo de polietileno PE-90. La medición de la presión arterial media se registró por uno de los catéteres colocado en la arteria femoral, usando un transductor de presión. Posteriormente se realizó una incisión abdominal para exponer el riñón izquierdo en donde se separó la arteria renal, después se colocó una sonda de ultrasonido para determinar el flujo sanguíneo renal.

-Histopatología y Análisis Morfométrico

Después de las mediciones hemodinámicas, el riñón derecho se ligó con una sutura y se retiró para separar la médula y la corteza renal y enseguida se congelaron a -70°C, ambas secciones para el análisis molecular: En el caso de los animales controles y en el caso de los animales uninefrectomizados, se escindió el polo superior y el inferior. Después, el riñón izquierdo se perfundió a través del catéter de la arteria femoral con 20 ml de solución salina, y después se fijó con 20 ml de formaldehído al 4%, siempre manteniendo la presión que tenía previamente la rata. El riñón se incluyó en parafina con el fin de realizar cortes de 4 µm de grosor. Los cortes se colocaron en laminillas y se tiñeron con ácido periódico de Schiff (PAS) o rojo de sirio.

Se realizó el análisis ciego de las lamillas teñidas con PAS, tomando 10 microfotografías (Magnificación 100x) de diferentes campos de la corteza renal de cada riñón, usando una cámara Nixon incorporada al microscopio y se cuantificó el

diámetro glomerular en al menos 40 glomérulos por animal. También se usaron estas microfotografías para determinar la dilatación tubular. En las laminillas teñidas con rojo de sirio se capturaron cinco campos subcorticales del riñón para cuantificar la fibrosis tubulointersticial usando un software Eclipse Net de morfometría, se consideraron las áreas de fibrosis, las zonas con deposición de colágena que se tiñen de rojo.

-Determinación de parámetros bioquímicos

-Peróxidos de Hidrógeno

La orina recolectada durante el seguimiento se guardó a -70°C. Se realizó la determinación de peróxidos de hidrogeno de orina como marcador de estrés oxidante¸ mediante el kit comercial Amplex Red Hydrogen Peroxide/ Peroxidase Assay y siguiendo las instrucciones del fabricante. La determinación se basa en la presencia de peroxidasa que, al reaccionar con el peróxido de hidrógeno, produce un compuesto rojo-fluorescente. Se utilizaron 50 µL de cada muestra que se incubaron en el buffer que proporciona el kit durante 30 min a temperatura ambiente. Las muestras y la curva estándar fueron leídas a 560 nm.

-Extracción de RNA y PCR Tiempo Real

Para la extracción de RNA se utilizó el tejido previamente almacenado a -70°C y usando TRIZoL y siguiendo las instrucciones de la compañía. Con el fin de conocer la calidad y la concentración de RNA se realizó una medición por espectrofotometría de UV (280/260 nm) y se analizó su integridad mediante electroforesis en gel de agarosa al 1%.

Para realizar la transcripción reversa (TR) se utilizó 1µg de RNA total de tejido. Se calentó el RNA a 65°C durante 10 min, se utilizó 200 U de transcriptasa reversa (MMLV), 100 pmol de hexámeros al azar, 0.5 mM de cada Dntp, y buffer 1X de TR (75Mm KCl: 50 Mm Tris-HCl; 3mM MgCl2; 10mM DTT, pH: 8.3), se incubó durante una hora a 37°C, en un volumen final de 20 µL. Al final se calentaron las muestras durante 5 min a 95°C para inactivar a la enzima.

Para la PCR en tiempo real se utilizaron sondas TaqMan, para la amplificación de DNA complementario. Se utilizaron sondas específicas para TGF-β, HIF-1α, factor de crecimiento vascular y endotelial (VEGF), IL-6, interleucina 10 (IL-10), TNF-α (FAM) y 18S RNAr (VIC) como control de amplificación. FAM y VIC son colorantes fluorescentes para detectar la amplificación de producto. La cantidad liberada por la sonda TaqMan depende de la actividad exonucleasa de la reacción de PCR. La amplificación se detectó en un termociclador en tiempo real ABI 7300 Prism o QuantStuido5. Se utilizó el método relativo al gen control mediante la fórmula comparativa de Ct.

-Niveles de biomarcadores urinarios

Se utilizó 1 µl de orina de cada animal y se sometieron a electroforesis en un gel de acrilamida al 8.5% desnaturalizante con Sodium dodecyl sulfate (SDS). Las muestras se prepararon con buffer de carga en relación 1:1 con un volumen final de 20 µL. Después se transfirieron a una membrana de difloruro de polivinilo (PVDF) previamente equilibrada con buffer de transferencia 1x (190 mM glicina, 2 mM Tris base, SDS 0.1%) en un transblot durante 60 min a 9 volts. Posteriormente se bloqueó 90 min con el buffer TBS con 5% de agente bloqueante y al terminar el bloqueó, la membrana se incubó con el anticuerpo primario HSP72 (1:5000) durante

toda la noche a 4°C. Al terminar la incubación se realizaron tres lavados de 10 min con TBS-1x Tween, para después incubar con el anticuerpo secundario acoplado a HRP, anti-mouse IgG (1:5000).

-Extracción de DNA y evaluación de la metilación global de DNA.

Para la extracción del DNA, se utilizaron 50 mg de tejido y se homogenizaron con 200 µL de PBS 1X (10 mM PO_4, 137 mM NaCl, y 2.7 mM KCl), se agregó 60 µL de buffer de digestión, para después agregar 26 µL de proteínasa K (10 mg/mL) y se mantuvo en hielo por 5 min. Posteriormente, la mezcla se dejó toda la noche a 56°C, después, las muestras se trataron con 3 µL de RNAasa A (10 mg/mL) y se incubaron durante 3 h a 37°C. Al final se agregaron 250 µL de fenol-cloroformo-isoamil alcohol, se centrifugaron a 14,000 rpm por 20 min a 4°C. Se tomó solo la fase superior, se agregaron 83 µL de acetato de amonio (7.5 M) y 250 µL de etanol absoluto. Las muestras se incubaron a -20°C durante toda la noche, se centrifugaron y se desechó el sobrenadante. Se hicieron dos lavados con 250 µL de etanol al 70%. El pellet se re-suspendió en 200 µL de agua libre de DNAsas. Finalmente, se hizo una medición por espectrofotometría de UV (280/260nm) para determinar la pureza y la concentración del DNA y se analizó su integridad mediante electroforesis en gel de agarosa al 1%.

Para analizar la metilación global de DNA se utilizó el kit de metilación de DNA 5-mC. Se usaron 100 ng de DNA de cada muestra y se llevó a un volumen de 100 µl con 5-mC de Coating Buffer, se incubó a 98°C por 5 min y después se dejó en hielo durante 10 min. Se agregaron a la placa y se incubó a 37°C por una hora. Posteriormente se desechó el excedente y se lavó con 200µl de 5-mC Elisa Buffer. Se añadieron 200 µl de 5-mC Elisa Buffer a cada pozo y se incubó a 37°C por 30

minutos. Se agregó una mezcla de anticuerpo primario anti-5-metil citosina (dilución 1:2,000) y anticuerpo secundario anti rabitt acoplado a HRP (diución 1:1,1000). Para finalizar se agregaron 100 µl de HRP Developer a cada pozo, se incubó 1 h y se midió en espectrómetro a 405-450nm. Los resultados se extrapolaron con una curva estándar y se hizo la corrección por el porcentaje de islas de citocinas y guaninas (CpGs), que se han reportado previamente presentes en el genoma de la rata.

-Análisis de secuencia y diseño de oligos para bisulfito

Se han identificado previamente tres secuencias de unión de Hif1α en el gen promotor Vegfa en la rata y se denominaron región 1 (-976 a -857), región 2 (-724 a -645) y región 3 (-470 a -369), respectivamente (93). La base de datos de las islas CpG y la herramienta analítica (DBCAT) (http://dbcat.cgm.ntu.edu.tw) nos ayudaron a identificar las islas CpG en el promotor y la primera parte de las regiones codificantes del gen Vegfa. Este análisis mostró que solo las regiones 2 y 3 estaban enriquecidas con islas CpG, lo que sugiere que, estas regiones son susceptibles a la metilación. En consecuencia, se diseñaron cebadores óptimos en el software Methyl Primer Express para la secuenciación de bisulfito de los promotores de genes Hif-1α y Vegfa. Para Hif-1α, los cebadores fueron: 5´-GTAGAGAGTAGAGATTGAGTT-3´ (hacia delante) y 5´-CAAAACCTAACCAAACACTAC-3´ (hacia atrás) que amplificaron la región de -1390 a -688 (702 pb). Hay tres secuencias de unión de HIF1α en el promotor de Vegfa, pero solo dos son susceptibles de metilación: la región 2, de -724 a -645 y la región 3, de -470 a -369, amplificamos junto con los siguientes cebadores : 5´-

GGTTTTGTTAGAT (hacia adelante) y 5´- CCATAACCTAAAAATTATCTATC-3´ (hacia atrás) dando un producto de 763 pb.

-Conversión de bisulfito de sodio y secuenciación de DNA

El DNA genómico (3 µg) se procesó con bisulfito de sodio (94), los fragmentos de DNA de interés se amplificaron por PCR. Los fragmentos de DNA amplificados se clonaron en el sistema pGEM-T Easy y se secuenció por el método de Sanger usando su cebador inverso respectivo. Se evaluaron al menos 8 clonas para cada región.

5.2 Modelo de ERC inducido por obesidad

Se utilizaron ratones macho C57BL / 6 (Charles River Laboratories International, Inc.) de 5 a 6 semanas y con un peso de 17 a 22 g, que se mantuvieron en condiciones controladas de temperatura y humedad con un ciclo día / noche de 12:12 h, con libre acceso a agua y comida. No usamos un método para generar la secuencia de aleatorización, los ratones solo se asignaron al azar en dos grupos de al menos 10 ratones por grupo, de la siguiente manera: 1) ratones de control alimentados con una dieta control (C) y 2) ratones obesos (OB) alimentados con una dieta moderadamente alta en grasas (MHFD). El protocolo experimental se muestra en la Figura 8. El tamaño de la muestra se calculó según el porcentaje de acierto y error de la prueba (95). El estudio no fue cegado porque no se realizó ninguna intervención farmacológica. Todos los ratones completaron nuestros criterios de inclusión y ninguno fue excluido. Ambos grupos fueron seguidos durante

14 semanas. Las dietas experimentales fueron realizadas por nuestros laboratorios, como fue previamente reportado por Castro-Rodríguez, et al 2020 (95). La dieta de control estuvo compuesta por: 22.0% de proteína, 5.0% de grasa vegetal (aceite de maíz), 31.0% de polisacárido, 31.0% de azúcares simples, 4.0% de fibra, 6.0% de minerales y 1.0% de vitaminas (p/p), y energía 4.0 kcal g^{-1}, en el que la grasa representa el 11.3% del aporte calórico. Mientras que, la MHFD contenía 23.5% de proteína, 20.0% de manteca de cerdo, 5.0% de grasa vegetal (aceite de maíz), 20.2% de polisacárido, 20.2% de azúcares simples, 5.0% de fibra, 5.0% de minerales, 1.0% de vitaminas (p/p) y energía 4.9 kcal. g^{-1}, donde la grasa representa el 45% del aporte calórico total (95). El peso corporal se registró semanalmente y se registró el consumo diario de alimento.

Al final del período experimental, se recolectó una muestra de orina durante un período de 24 h en jaulas metabólicas. Luego, los ratones fueron anestesiados con pentobarbital sódico (30 mg/kg) para obtener muestras de sangre mediante punción cardíaca. Uno de los riñónes fue fijado en paraformaldehído al 4% para análisis histopatológico. Se pesaron ambos riñones y uno de ellos se conservó en nitrógeno líquido (-80ºC) hasta su análisis.

La concentración de creatinina en orina se midió con el kit de ensayo de creatinina.

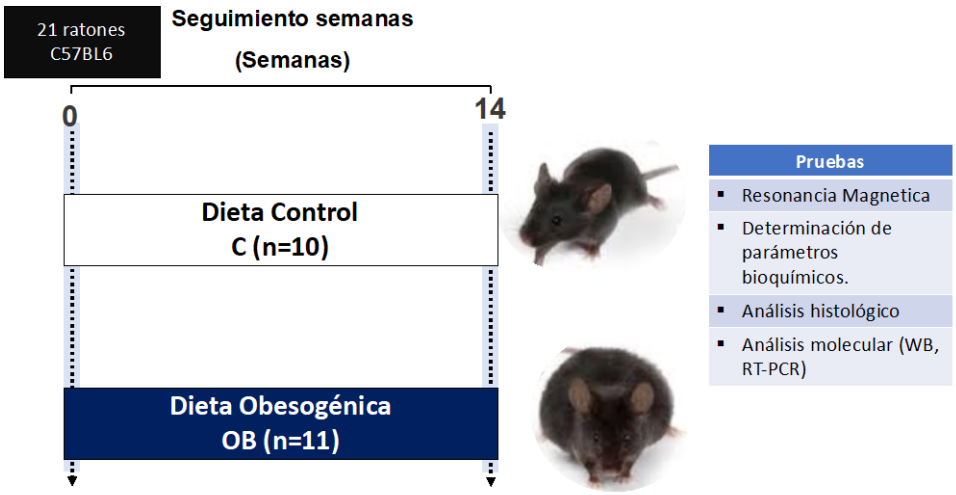

Figura 8. Modelo experimental ratones obesos. La dieta se dio vía sonda gástrica durante 14 días, todos los días.

-Parámetros metabólicos y composición corporal.

El análisis de la composición corporal se realizó en 6 animales por grupo utilizando una resonancia magnética de animales pequeños 4 en 1. El análisis sérico de glucosa, triglicéridos y colesterol se determinó enzimáticamente con un analizador automático SynchronCX.

5.3 Modelo de Lesión Renal Aguda

Se utilizaron dos grupos de ratas. El primer grupo incluyó 20 ratas macho (320-350 g de peso corporal) distribuidas en cinco niveles diferentes de severidad de LRA de la siguiente manera: 0, 15, 30, 45 o 60 min de isquemia y 24 h de reperfusión (n = 4 por período de isquemia). Una hora después de la cirugía, las ratas se colocaron en jaulas metabólicas y se recolectaron muestras de orina de 24 h y se almacenaron a -70 ° C para su posterior análisis. El segundo grupo incluyó 44 ratas macho que se sometieron a 45 minutos de isquemia bilateral. Estas ratas se realizó eutanasia

y estudiaron en diferentes períodos de reperfusión (3, 6, 9, 12, 18, 24, 48, 72, 96 y 120 h) y se compararon con los grupos control correspondientes (n = 4 por período).

-Recolección de muestras de pacientes diagnosticados con LRA

Se recolectaron muestras de orina de pacientes diagnosticados con LRA. El diagnóstico se realizó por la elevación significativa de la creatinina sérica y/o la reducción del flujo urinario y la severidad de la LRA se hizo de acuerdo con la clasificación KDIGO (9).

-Inmunohistoquímica de serpinA3K

Se usó tejido de rata embebida en parafina para obtener rebanadas de 4 µm colocados en portaobjetos cargados, que luego se desparafinaron. La recuperación de anticuerpos se realizó con buffer de citrato (BSB 0022, Bio SB) durante 12 min a alta presión. Los portaobjetos se bloquearon con el bloqueador de fondo inmunoDNA durante 20 min y se incubaron con el anticuerpo primario serpinA3K (1:500, SC-162175) durante 2 h a 23 °C, y luego se incubaron con un anticuerpo secundario de cabra en roedor-HRP, y revelado con sustrato de peroxidasa DAB.

-Cuantificación de la serpinA3 por ELISA

Se utilizó el kit ELISA para determinar la concentración de serpinA3 de acuerdo con las instrucciones y recomendaciones del fabricante. La orina de pacientes y voluntarios sanos se diluyeron a 1:500 y el volumen final fue de 100 µl para cada muestra.

5.4 Clonación de la Serpina3k

Se amplificó serpina3k de rata a partir de DNAc de hígado y se clonó en el vector pcDNA3.1 (-) junto con una secuencia que codifica para una etiqueta FLAG en el extremo C-terminal de la proteína. Esto fue realizado por la tecnología de FastCloning Li, et al. 2011 (102). FastCloning: a highly simplified, purification-free, sequence- and ligation-independent PCR cloning method). Este método independiente de ligación consiste en la amplificación por PCR de la secuencia que será clonada (en este caso el ORF de serpin3k), así como, la amplificación por PCR del vector de clonación. Ambos amplicones se producen con colas que se sobrelapan y la mezcla de los dos amplicones de PCR se transforman directamente en *E. coli* para obtener la clona deseada. La reacción de PCR se realizó con la DNA polimerasa de alta fidelidad Phusion. Los oligonucleótidos utilizados para amplificar el inserto fueron: 5'-CGCCTGGCCCTTCCCATGGCCTTCATTGCAGCTTTGG-3' (forward) y 5'-ATGGTGATGATGATGGTGCATGGGGTTAGTGACTTTGCCCATA-3' (reverse), mientras que el vector se amplificó con 5'-CATGGGAAGGGCCAGGCG-3' (forward) y 5'-GACTACAAAGACGATGACGACAAGTAAGGTACCAAGCTTAAGTTTAAACCGCTGATC-3' (reverse). Varias de las clonas se analizaron por digestión con enzimas de restricción del plásmido. Las que mostraron las bandas del peso correcto, se confirmaron después por secuenciación de Sanger y una clona fue elegida para los experimentos de transfección.

-Transfección de rSerpin3k en células HEK293

Las células HEK293 (ATCC CRL-1573) se usaron para la transfección transitoria de serpin3A-FLAG o vector vacío, (0.25, 0.5, 1, 2 o 3 μg de DNA). Las células se cultivaron hasta un 70-80% de confluencia y se transfectaron con el plásmido usando Lipofectamine 2000. Después de 24, 48 o 72 h de transfección, el medio fue recuperado y guardado con un coctel que contiene inhibidores de proteasas (Complete) para analizar las proteínas secretadas, mientras que las células se lavaron con PBS y se lisaron con un buffer que contenía 50mM HEPES pH 7.4, 250mM NaCl, 5mM EDTA, 0.1% NP-40 and y el coctel con Complete. Posteriormente se cuantificó la concentración de proteínas.

-Respuesta de la rSerpin3k transfectada frente al estrés celular

Después de 24 h de la transfección con rserpin3k, indujimos estrés celular mediante la depleción de nutrientes, es decir, al eliminar la albúmina de suero bovino del medio (BSA) o mediante la adición de dosis crecientes de peróxido de hidrógeno (0, 25, 50, 100 μM) durante 3 h. El sobrenadante y las células se almacenaron como previamente se describió.

-Tratamiento con PNGasa

Los lisados y los sobrenadantes de células transfectadas con rSerpin3k-FLAG, así como lisados de hígado y riñón, plasma y orinas de rata con LRA, fueron desnaturalizados e incubados con o sin PNGAasa F siguiendo las instrucciones del fabricante, para analizar los cambios en la movilidad por electroforesis de SerpinA3 después de remover los N-oligosacáridos.

-Análisis estadístico

Las variables se presentan como media ± SEM. Los grupos se compararon con ANOVA y posterior Bonferroni para comparaciones múltiples. La significancia estadística se definió como un valor $p < 0.05$.

5.4 Modelo de LRA en los ratones silvestres y deficientes para SIRT7

Se incluyeron 60 ratones con fondo genético C57Bl/6 de dos meses de edad: 20 ratones silvestres (WT), 20 ratones deficientes para SIRT7 (KO-Sirt7) y 20 ratones heterocigotos (HT), que se dividieron en seis grupos: 1) WT con cirugía falsa, 2) WT sometidos a isquemia/reperfusión bilateral por 22.5 min (IRB), 3) KO-Sirt7 con cirugía falsa, 4) KO-Sirt7 con IRB, 5) HT con cirugía falsa y 6) HT+IRB. Se realizó la recolección de orina de 24-h, se tomo una muestra de sangre y se estudiaron al término de la recolección. Los riñones se separaron en médula y corteza, la mitad se almacenó a -70ºC para las pruebas moleculares y la otra mitad se fijó para su análisis histológico. El protocolo experimental se muestra en la Figura 9.

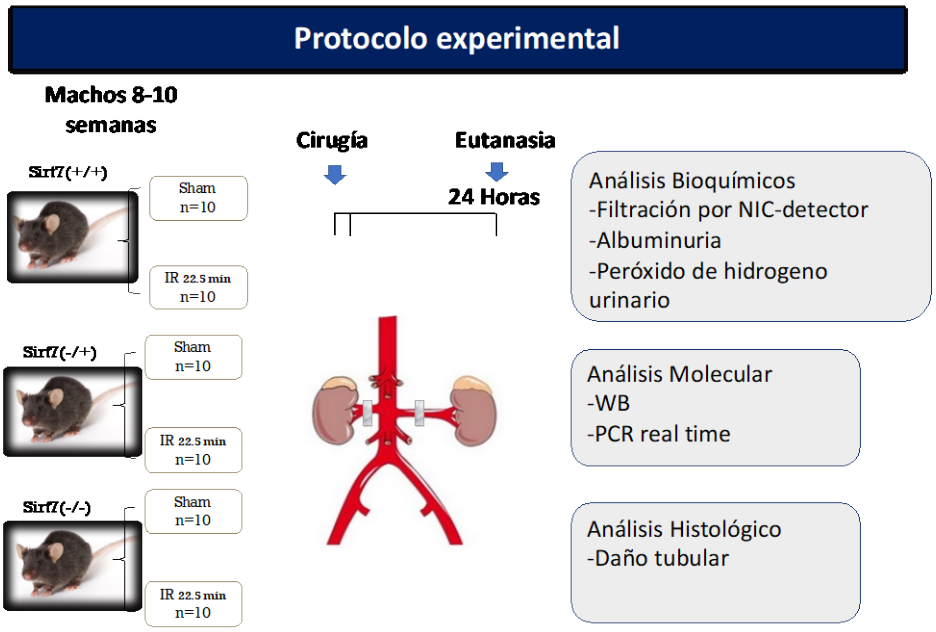

Figura 9. Modelo experimental ratones sirt7. Las flechas azueles indican los tiempos en donde se realizaron las intervenciones.

-Evaluación de función renal

Se determinó la tasa de filtrado glomerular por el método de fluoresceína-5-isotiocianato (FITC)-sinistrina, con un monitor de fluorescencia. Los animales fueron parcialmente sedados con pentobarbital sódico (15 mg/kg), posteriormente se colocó sobre la piel depilada el equipo de filtración, que fue fijado para que no se moviera. Se realizó una lectura basal de un minuto, posteriormente se inyectaron 7 mg/kg de peso de FITC-sinistrina y se determinó la tasa de decaimiento durante 1 h, con el fin de calcular la tasa de filtrado glomerular. Al mismo tiempo, se determinó la concentración de creatina sérica, como marcador subrogado de la función renal.

-Detección de biomarcadores urinarios de daño renal

Se determinó la albuminuria con el kit de ELISA y se siguieron las instrucciones del fabricante, usando 10 ul de orina.

Al mismo tiempo, se determinaron en la orina los biomarcadores, HSP72, KIM-1 y serpinA3 mediante un análisis de Western Blot. En un gel de acrilamida se cargó 0.1 μl de cada orina, diluida en 9.9 μl de solución salina 0.9%. El gel se transfirió en membrana de PVDF, las membranas fueron bloqueadas con agente bloqueante al 5%, posteriormente se incubaron toda la noche a 4ºC con anti-HSP72 (hibridoma, 1: 10,000), anti-KIM-1 (1: 5000), o con anti-serpinA3K (1 : 5000). Más tarde, se incubaron con los anticuerpos secundarios, anti-ratón (1: 10,000) para HSP72 o anti-conejo (1: 5,000) para KIM-1 y serpinA3K. Las proteínas se detectaron usando un kit de quimioluminiscencia comercial y se normalizaron mediante creatinina urinaria (CrU).

-Evaluación de niveles de RNAm

Se extrajo RNA con el método de trizol y se realizó la retro trascripción para generar el cDNA. Las sondas que se usaron son la siguientes: Sirt7 (Mm01248607_m1), Sirt1 (Mm01168521_m1), Il10 (Mm01288386_m1), Il6 (Mm00446190_m1), Mcp1 (Rn00580555_m1), Tnfalpha (Mm0443258_m1), Tgfb1 (Mm03024053_m1), Nfe2l2 (Rn00582415_m1), Hif1a, (Mm00468869_m1), Vegfa (Rn01511602_m1) y Cat (Mm00437992_m1). Como control endógeno, se utilizó rRNA 18S eucariota. La cuantificación relativa de cada expresión génica se realizó con el método del ciclo umbral comparativo (Ct).

-Análisis de Western Blot y anticuerpos utilizados

Las proteínas de la corteza renal se homogeneizaron con un buffer de lisis que contenía: HEPES 50 mM pH 7,4, NaCl 250 mM, EDTA 5 mM, NP-40 al 0,1% e

Complete. La concentración de proteínas se evaluó mediante el ensayo de proteínas de Lowry. Se sometieron a electroforesis individualmente 20 µg de proteínas en un gel desnaturalizante de acrilamida al 8.5% con SDS. Las membranas se incubaron con el anticuerpo primario Sirt7 (1: 1000), Sirt3 (1: 1000), IL-6 (1: 1000) y el anticuerpo β-actina/HRP [AC-15] (1: 1,000,000) durante la noche a 4ºC. Se realizaron tres lavados de 10 min con TBS-Tween 1x y luego se incubaron con el anticuerpo secundario acoplado a HRP, IgG anti-conejo o anti-ratón (respectivamente, 1: 5000). Las proteínas tisulares evaluadas por Western blot se normalizaron mediante detección de beta -actina.

La evaluación de los niveles de TNF-α en plasma se analizó mediante un ensayo de ELISA, siguiendo las instrucciones del fabricante.

6. RESULTADOS PUBLICADOS

6.1 ARTICULO 1 https://pubmed.ncbi.nlm.nih.gov/33888767/

Resumen de los resultados de la evaluación del curso temporal de la transición de LRA a ERC que fueron publicados en la revista Scientific Reports, 11(1):8769, 2021, como parte del objetivo 1 y 2.

La hipoxia crónica es un factor importante que contribuye a la ERC después de una LRA. Sin embargo, la relación temporal entre la lesión aguda y la respuesta renal inadecuada a la hipoxia sigue sin conocerse con exactitud. En este estudio, analizamos la evolución temporal de la hemodinámica renal, el estrés oxidativo, la inflamación y la fibrosis, así como las modificaciones epigenéticas, con especial atención a la señalización de HIF1α / VEGF, en la transición de LRA a ERC. Se incluyeron tres grupos de ratas: operación simulada, nefrectomía derecha (UNx) y UNx más isquemia renal (IR + UNx) y se estudiaron a los 1, 2, 3 o 4 meses. Como hemos reportado previamente, el grupo IR+UNx desarrolló ERC caracterizada por proteinuria progresiva, disfunción renal, proliferación tubular y fibrosis. En el primer mes posterior a la isquemia, hubo un aumento significativo dos veces mayor en el estrés oxidativo y una reducción en la metilación global del ADN que se mantuvo durante todo el estudio. La expresión de Hif1α y Vegfa se deprimió en el primer y segundo mes después de la isquemia y luego se recuperó la expresión de Hif1α, pero no de Vegfa. Interesantemente, encontramos hipermetilación del promotor del gen de Vegfa, particularmente la región 2, en el sitio de unión de HIF1α, desde la primera etapa de la progresión de la ERC. Nuestros hallazgos sugieren que la hipoperfusión renal, la respuesta hipóxica ineficiente, el aumento del estrés oxidativo, la hipometilación del DNA y la hipermetilación del gen promotor de Vegfa

en el sitio de unión de HIF1α, son determinantes tempranos de la transición de AKI a ERC.

scientific reports

Check for updates

OPEN

Vegfa promoter gene hypermethylation at HIF1α binding site is an early contributor to CKD progression after renal ischemia

Andrea Sánchez-Navarro[1,2], Rosalba Pérez-Villalva[1,2], Adrián Rafael Murillo-de-Ozores[1,2], Miguel Ángel Martínez-Rojas[1,2], Jesús Rafael Rodríguez-Aguilera[3], Norma González[2], María Castañeda-Bueno[2], Gerardo Gamba[1,2], Félix Recillas-Targa[3] & Norma A. Bobadilla[1,2]✉

Chronic hypoxia is a major contributor to Chronic Kidney Disease (CKD) after Acute Kidney Injury (AKI). However, the temporal relation between the acute insult and maladaptive renal response to hypoxia remains unclear. In this study, we analyzed the time-course of renal hemodynamics, oxidative stress, inflammation, and fibrosis, as well as epigenetic modifications, with focus on HIF1α/VEGF signaling, in the AKI to CKD transition. Sham-operated, right nephrectomy (UNx), and UNx plus renal ischemia (IR + UNx) groups of rats were included and studied at 1, 2, 3, or 4 months. The IR + UNx group developed CKD characterized by progressive proteinuria, renal dysfunction, tubular proliferation, and fibrosis. At first month post-ischemia, there was a twofold significant increase in oxidative stress and reduction in global DNA methylation that was maintained throughout the study. *Hif1α* and *Vegfa* expression were depressed in the first and second-months post-ischemia, and then *Hif1α* but not *Vegfa* expression was recovered. Interestingly, hypermethylation of the *Vegfa* promoter gene at the HIF1α binding site was found, since early stages of the CKD progression. Our findings suggest that renal hypoperfusion, inefficient hypoxic response, increased oxidative stress, DNA hypomethylation, and, *Vegfa* promoter gene hypermethylation at HIF1α binding site, are early determinants of AKI-to-CKD transition.

Clinical, epidemiological, and experimental studies have shown that AKI is an independent risk factor for the development of CKD and end-stage renal disease (ESRD)[1,2]. In this transition, the initial insult severity and duration is proportional to the risk of CKD, besides, age is another preponderant factor[3–6].

AKI is characterized by an abrupt reduction in renal blood flow with consequent hypoxia, endothelial and proximal epithelial injury, and renal dysfunction. After an AKI episode, a cascade of events occurs, such as brush border loss, cell polarity alterations, increased oxidative stress, and mitochondrial dysfunction of proximal tubular epithelial cells[7,8], as a result, some of these cells undergo necrosis or apoptosis[9]. These processes are also accompanied by macrophage infiltration and inflammation[7,10,11]. Although the tubular epithelium has the capacity for regeneration[12], the injured epithelium is no longer the same. A subpopulation of dedifferentiated and proliferating tubular cells that recover from the acute renal insult suffer cell cycle arrest and cannot be re-differentiated, leading to tubular atrophy; all these events contribute greatly to the tubulointerstitial fibrosis that is observed in the long term[12,13].

Consequently, a maladaptive repair occurs[11,14,15], where there is persistent macrophage infiltration[16–18], dissociation of pericytes from the tubular capillaries[19], and arrest of some tubular cells in the G2/M phase[20], leading to a progressive fibrotic kidney[20–22]. Some mechanisms involved have been elucidated, such as trans-differentiation of pericytes into myofibroblasts[19,23], uncontrolled proliferation of epithelial cells[22], the emergence of an abnormal proximal-tubule phenotype[24], excessive production of TGFβ by both the tubular epithelium[22] and

[1]Molecular Physiology Unit, Instituto de Investigaciones Biomédicas, Universidad Nacional Autónoma de México, Av. Universidad 3000, UNAM, CU, 04510 Coyoacán, Mexico City, Mexico. [2]Department of Nephrology, Instituto Nacional de Ciencias Médicas y Nutrición Salvador Zubirán, Vasco de Quiroga No. 15, Tlalpan 14080, Mexico City, Mexico. [3]Department of Molecular Genetics, Instituto de Fisiología Celular, Universidad Nacional Autónoma de México, Mexico City, Mexico. ✉email: nab@iibiomedicas.unam.mx

local myofibroblasts[25,26], accumulation of extracellular matrix proteins[27,28], vascular rarefaction[29–31], chronic hypoxia[30,32], and chronic stress of the endoplasmic reticulum[33].

In addition, it has been recently shown that epigenetic modifications may be involved in several renal pathologies. However, the specific molecular mechanisms by which epigenetic modifications alter renal physiology are little known. The most studied epigenetic regulations in AKI are the chromatin compaction, DNA methylation and histone acetylation/deacetylation. In AKI, obstructive renal injury, and diabetic nephropathy, epigenetic modifications induced an increase in proinflammatory and profibrotic cytokines such as monocyte chemoattractant protein-1 (MCP-1), complement protein 3 (C3), transforming growth factor β (TGF-β), which in turn perpetuate inflammation and promote epithelial-to-mesenchymal transition (EMT) that contributes to renal fibrosis[34–38]. Although some mechanisms have been elucidated, many others remain unknown, and less is known about temporal changes during CKD progression, such as renal hemodynamics, structural injury, HIF signaling, and epigenetic modifications.

We have previously shown that an AKI episode induced by moderate or severe bilateral renal ischemia/reperfusion (IR) in male rats is sufficient to induce CKD progression after nine months[22,27]. Interestingly, this transition was not observed in female rats, despite a similar magnitude of AKI in both male and female rats. The unique difference in the early phase post-ischemia was that females did not exhibit oxidative stress, suggesting a pivotal role of reactive oxygen species generation in this transition[21].

Thus, it is relevant to establish a temporal understanding of the pathophysiological mechanisms throughout the AKI-to-CKD transition. In this study, we used the model of unilateral renal IR plus contralateral nephrectomy, which allowed us to induce CKD after four months. We found abnormal renal hemodynamics, reduced HIF-1α signaling, increased oxidative stress, and global DNA hypomethylation in the early phase of the AKI to CKD transition. We also showed that the *HIF-1α/Vegfa* signaling reduction was associated with the DNA hypermethylation of the *Vegfa* gene promoter, beginning at an early stage post-ischemia and suggesting that reduced VEGF expression is an early contributor that triggers renal hypoxia and the consequent fibrosis.

Results

Renal injury induced by unilateral ischemia after 24 h of reperfusion. First, we corroborated that the initial insult induced by IR in the uninephrectomized rats was similar among the groups studied at 1, 2, 3, or 4 months postischemia. All IR + UNx rats were randomly assigned to the different periods of follow-up. After 24 h of inducing renal ischemia, all the IR + UNx rats exhibited significant proteinuria that was of the same magnitude among the groups assigned to 1, 2, 3 and, 4 months of follow-up (Fig. 1A), together with a similar reduction in renal function (Fig. 1B); these alterations were not observed in the S (n = 16) or UNx (n = 16) groups after 24 h of the surgery as is shown by the individual data presented in Fig. 1A, B. Consequently, the S or UNx rats were also randomly assigned to the different periods of follow-up. The urinary hydrogen peroxide levels were also evaluated and reflected significant oxidative stress in all IR + UNx groups (Fig. 1C). The urinary HSP72 levels, known to be a sensitive AKI biomarker, were also analyzed[39–42]. As expected, all rats that underwent IR + UNx exhibited a significant and similar increase in urinary HSP72 levels corrected by urinary creatinine (UHSP72/UCreat), (Fig. 1D). These findings show that all the IR + UNx rats exhibited a similar AKI degree. This was important to ensure that the changes observed in the long term were due to the initial insult itself rather than differences in the severity of the ischemic injury.

Temporal progression of renal dysfunction and structural injury after an AKI episode. To evaluate the precise moment at which the functional, structural, and molecular alterations occur along with AKI to CKD transition, the groups were euthanized at 1, 2, 3, or 4 months after the initial ischemic insult. No differences in body weight were found among the studied groups (Fig. 2A). As expected, the UNx and IR + UNx groups showed a significant increase in kidney weight/body weight (KW/BW) starting in the first-month compared to that of the S group (Fig. 2B). All experimental groups remained normotensive at the time of evaluation (Fig. 2C). The IR + UNx group exhibited a progressive increase in proteinuria starting in the second month of follow-up that was not evident in the S and UNx groups (Fig. 2D). Due to the renal mass reduction, the UNx group exhibited renal hyperperfusion, but when it was correct to the kidney weight, renal blood flow (RBF) was similar to the S group (Fig. 2E). This finding, in the UNx group, was related to the maintenance of normal renal function (Fig. 2F). Interestingly, this compensatory response was not seen in the IR + UNx group. RBF/KW was significantly lower than that of the S and UNx groups, starting in the first-month, and renal hypoperfusion was maintaining along the study course (Fig. 2E). At the end of the study, the IR + UNx group had significant renal dysfunction (Fig. 2F). The renal urinary biomarker HSP72 and KIM1 normalized by urinary creatinine, were significantly elevated starting in the first-month and third-month respectively, and increased even more by the end of the study (Fig. 2G, H). In Table 1 appears urinary flow, fractional excretion of sodium (FENa) and osmolarity. No differences were found among the groups along the study, except that the osmolarity was lower in the IR + UNx group at fourth-month compared to S group.

The long-term consequences of an AKI episode were also evidenced by the presence of tubulointerstitial fibrosis starting in the second-month post-ischemia, which progressively increased, whereas this injury was not detected in the UNx group (Fig. 3A). Although increased *Tgfb1* mRNA levels were not observed in the early stages of the AKI to CKD transition, a significant upregulation in *Tgfb1* mRNA and protein levels was evident in the fourth-month post-ischemia compared to that of the S and UNx groups (Fig. 3B, C). Accordingly with this, *Col1a1* (collagen 1*)* mRNA levels were significantly increased in the fourth-month (Fig. 3D). We only measured TGFβ protein levels at the fourth-month, because the *Tgfb1* mRNA levels and its target gene *Col1a1* were only significantly increased in this point of the follow-up. Besides, the IR + UNx group exhibited higher levels of Ki67 positive tubular cells (Fig. 3E, F), similar to our previous findings[22].

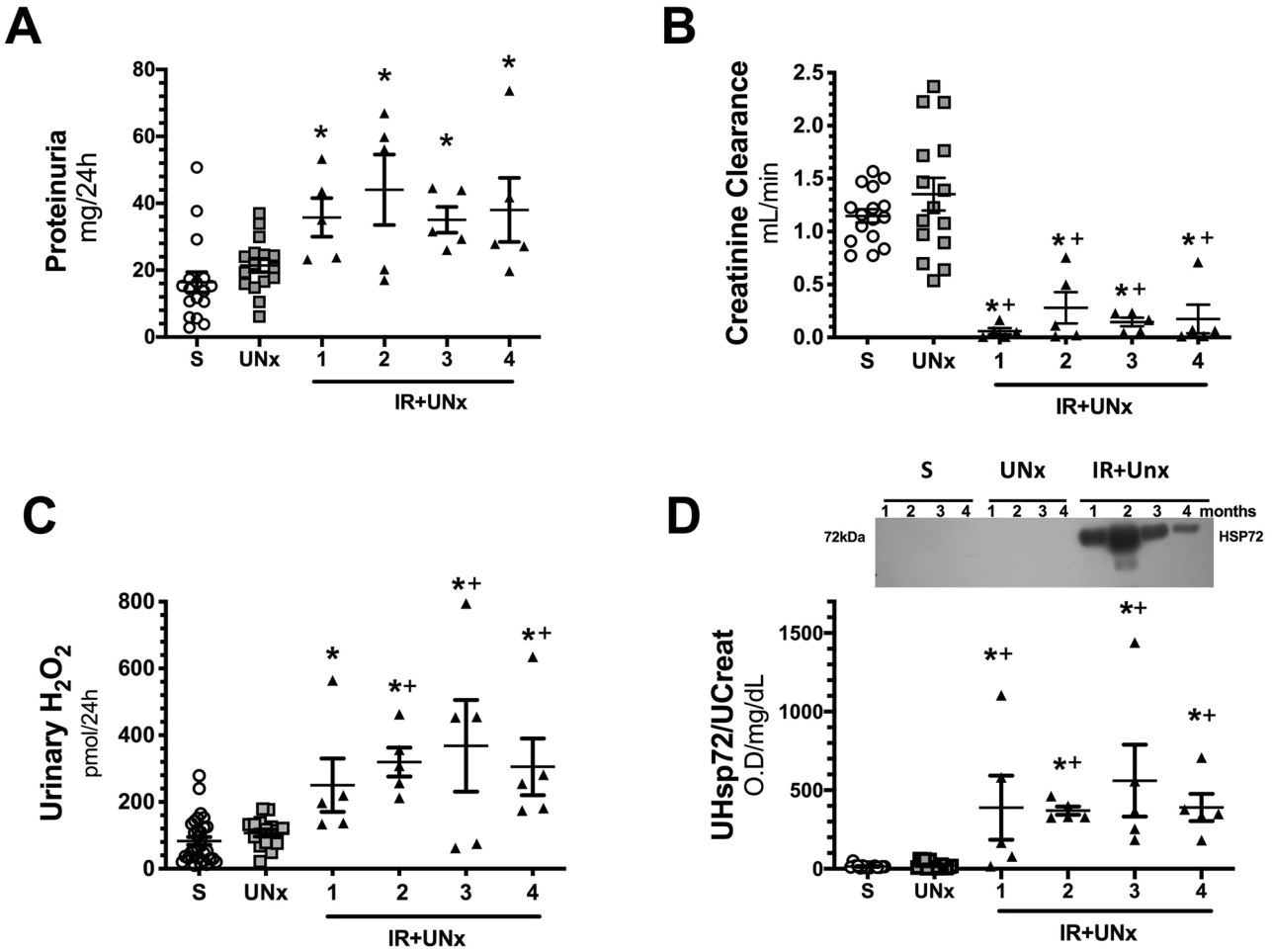

Figure 1. Renal injury induced by unilateral ischemia after 24 h of reperfusion. (**A**) Proteinuria, (**B**) Creatinine clearance, (**C**) Urinary hydrogen peroxide, and (**D**) Urinary HSP72 corrected by urinary creatinine, including a representative cropped blot image. Data are represented as the mean ± SE (for S, n = 16, for UNx, n = 16 and n = 20 for IR + UNx groups). White bars represent the S, gray bars represent UNx, and black bars represent IR + UNx groups. The one-way analysis of variance (ANOVA) was used to determine statistical differences, using the Bonferroni correction for multiple comparisons. *$p < 0.05$ versus S group and +$p < 0.05$ versus UNx group. Full-length blots are presented in Supplementary Fig. 3.

These results show that an AKI episode induced functional and structural alterations that mostly appear beginning at an early stage, highlighting the fact that there was no compensatory renal hyperperfusion expected by the renal mass lost in the IR + UNx group.

Temporal course of oxidative stress and vasoactive factors in the CKD progression induced by an AKI episode. Oxidative stress and renal inflammation have a pivotal role in CKD progression; thus, the temporality of these two pathways was also analyzed. An increase in oxidative stress (Fig. 4A) and a reduction in mRNA levels of the transcription factor *Nfe2l2*, which stimulates the antioxidant response, was observed beginning in the initial stage of the AKI to CKD transition (Fig. 4B), even though *Nox4* mRNA levels were reduced in the late stage of the disease (Fig. 4C). An imbalance in vasoactive factors was also observed at the end of the study. *NOS3* mRNA levels were significantly decreased (Fig. 4D), whereas the endothelin vasoconstrictor effect was increased (Fig. 4E, F).

Inflammatory pathways in the time course of CKD induced by AKI. The mRNA levels of interleukin 6 (*Il6*), monocyte chemoattract protein (*Mcp1*), and interleukin 10 (*Il10*) were measured throughout the study. *Il6* was upregulated in the IR + UNx group in the fourth-month after renal ischemia, as demonstrated by the significant elevation in interleukin 6 mRNA and protein levels (Fig. 5A, B). Because, we only observed a significant increase in *Il6* mRNA levels in the IR + UNx group at fourth-month post-ischemia, the IL6 protein levels were only evaluated in the Sham and IR + UNx groups in this specific time of the study. *Mcp1* mRNA levels increased in the first-month, and this elevation was observed again in the fourth month (Fig. 5C). The mRNA levels of the anti-inflammatory cytokine *Il10* showed a reduction starting in the first-month that became

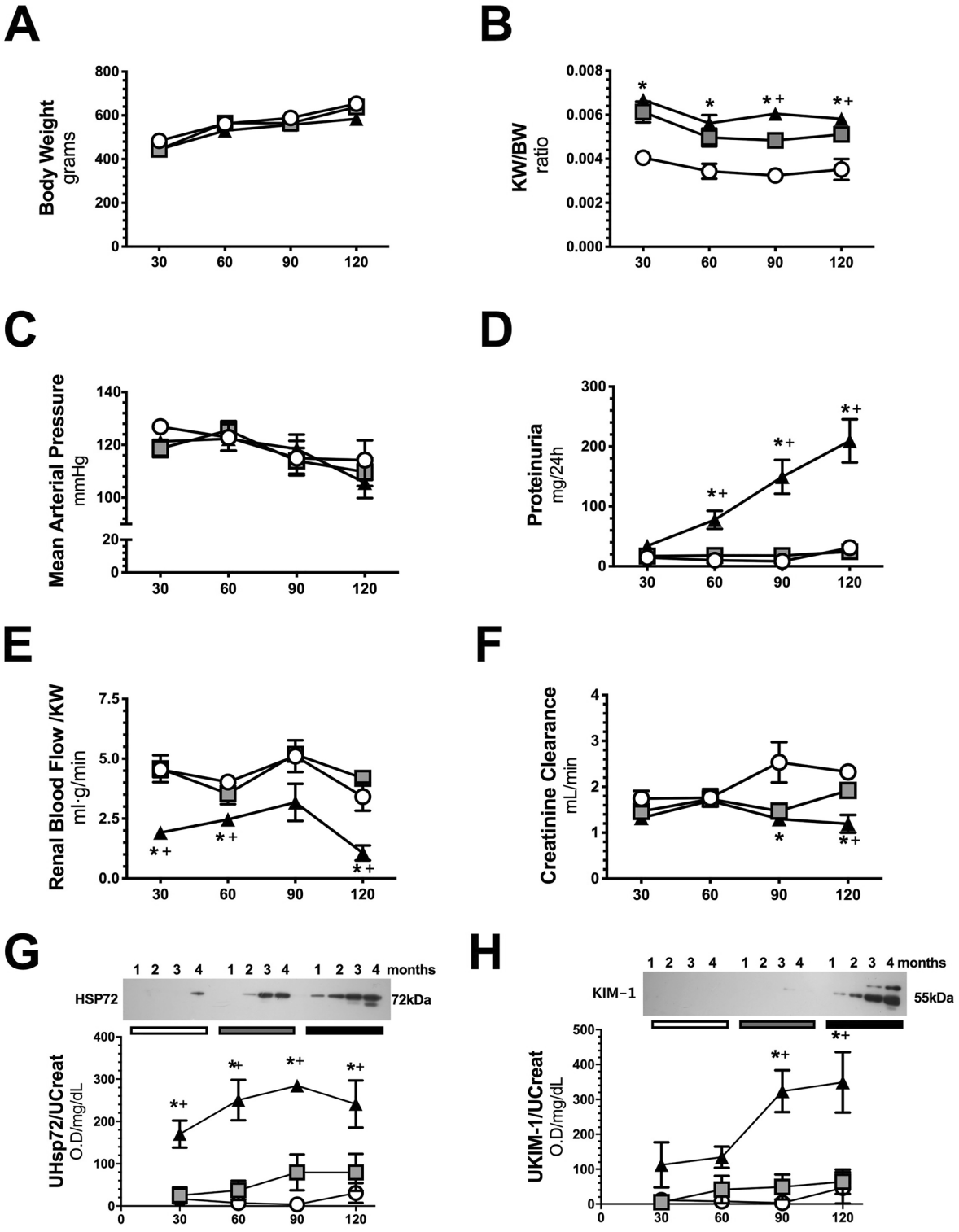

Figure 2. Follow-up of renal function in the AKI to CKD transition. (**A**) Body weight, (**B**) Ratio kidney weight/body weight, (**C**) Mean arterial Pressure, (**D**) Proteinuria, (**E**) Renal blood flow / kidney weight, (**F**) Creatinine clearance, (**G**) Urinary HSP72 corrected by urinary creatinine, and (**H**) Urinary KIM-1 corrected by urinary creatinine, including representative cropped blots, along the follow-up. Data are represented as the mean ± SE. n = 4, 4, and 5 for the S, UNx, and IR + UNx groups in each studied period: 30, 60, 90, and 120 days post-ischemia. White circles represent the S, gray squares represent UNx and black triangles represent IR + UNx groups. The one-way analysis of variance (ANOVA) was used to determine statistical differences, using the Bonferroni correction for multiple comparisons. *$p < 0.05$ versus S group and + $p < 0.05$ versus UNx group in their respective period. Full-length blots are presented in Supplementary Figs. 4 and 5.

	Urinary flow (mL/min)	FENa (%)	Osmolarity (mOsm/L)
Sham			
30 days	0.031 ± 0.004	0.17 ± 0.03	350 ± 77
60 days	0.026 ± 0.007	0.10 ± 0.00	481 ± 107
90 days	0.023 ± 0.003	0.11 ± 0.02	729 ± 123
120 days	0.014 ± 0.003	0.08 ± 0.03	1226 ± 178
UNx			
30 days	0.029 ± 0.005	0.19 ± 0.04	494 ± 172
60 days	0.025 ± 0.005	0.15 ± 0.05	703 ± 119
90 days	0.014 ± 0.007	0.16 ± 0.04	936 ± 72
120 days	0.024 ± 0.004	0.09 ± 0.02	746 ± 129
IR + UNx			
30 days	0.026 ± 0.005	0.21 ± 0.07	448 ± 59
60 days	0.037 ± 0.003	0.26 ± 0.14	440 ± 39
90 days	0.030 ± 0.002	0.24 ± 0.07	501 ± 30
120 days	0.024 ± 0.004	0.20 ± 0.08	678 ± 145*

Table 1. Urine Chemistries along the study for all the included groups. *$p < 0.05$ versus respective Sham.

significant in the second month and returned to normal levels by the third month compared to that of the S and UNx groups (Fig. 5D).

These findings suggest that oxidative stress, rather than renal inflammation, is an initial trigger of the subsequent damage.

Hypoxic response in the timing of CKD progression. As we showed, the UNx group exhibited renal hyperperfusion starting in the first-month post ischemia (Fig. 2E). In contrast, because renal compensatory hyperperfusion was absent in the IR + UNx group, the HIF1α signaling pathway was studied. The gene expression *Hif1a* and one of its target genes, *Vegfa*, were assessed during AKI to CKD transition. In the UNx group, *Hif1a* mRNA levels were significantly reduced in the first and second-month post-ischemia, whereas HIF1α protein levels remained unaltered during follow-up. This response was explained and expected in part by the compensatory renal hyperperfusion seen in these rats. In contrast, there was an inefficient response to hypoxia in the IR + UNx group that exhibited renal hypoperfusion because there was a significant decrease in *Hif1a* mRNA levels in the first and second-month after ischemia (Fig. 6A). In support of this inefficient response, *Vegfa* mRNA and protein levels were significantly reduced starting in the first-month and remained so on during follow-up (Fig. 6B–D), despite *Hif1a* mRNA and protein levels being reestablished by the third-month, suggesting that an independent mechanism maintains *Vegfa* gene expression downregulation and could be related with the vascular rarefaction characteristic of the AKI to CKD transition[29–31].

Time course global DNA methylation during CKD progression induced by AKI. Numerous studies have demonstrated that renal injury is associated with epigenetic changes, including histone modifications, DNA methylation, and the expression of various non-coding RNAs[43]. We found that rats experiencing the AKI to CKD transition exhibited mainly hypomethylation of global DNA, which started in the first-month post-ischemia and was maintained throughout follow-up (Fig. 7A). These changes were only seen in the renal cortex, whereas no differences were observed in the renal medulla (Fig. 7B). In general, the renal medulla exhibited lower levels of DNA methylation compared to that of the renal cortex.

Based on the changes observed in the global methylation of DNA and the possible independent mechanisms regulating the decreased expression of VEGF in the AKI to CKD transition, we decided to evaluate the specific methylation of the *Vegfa* gene promoter.

Vegfa gene promoter DNA methylation during AKI to CKD transition. With the interest to know if DNA methylation was associated with the modulation of *Vegfa* and *Hif1a* expression in AKI to CKD transition, we assessed the methylation state on 5′-upstream promoter region by bisulfite sequencing. According to the decreased *Vegfa* gene expression, we localized a DNA hypermethylated region in the noncoding upstream region of this gene, since the first-month post-ischemia (Fig. 8A), which was maintained until the fourth-month of follow-up (Fig. 8B). Therefore, we discovered that in the binding site for HIF1α, located at the region 2 of the *Vegfa* gene promoter, contains a specific CpG that was highly methylated in the IR + UNx group since the first-month and (75%) compared to that of the S (12%) and UNx groups (30%) (Fig. 8A). Moreover, the hypermethylated region was maintained at the end of the study in the IR + UNx group (91%) compared to that of the S (18%) and UNx (40%) groups (Fig. 8B).

Consistent with our transcriptional findings, we did not found any methylation in the noncoding upstream promoter region of *Hif1a* among the groups (Suppl. Fig. 2).

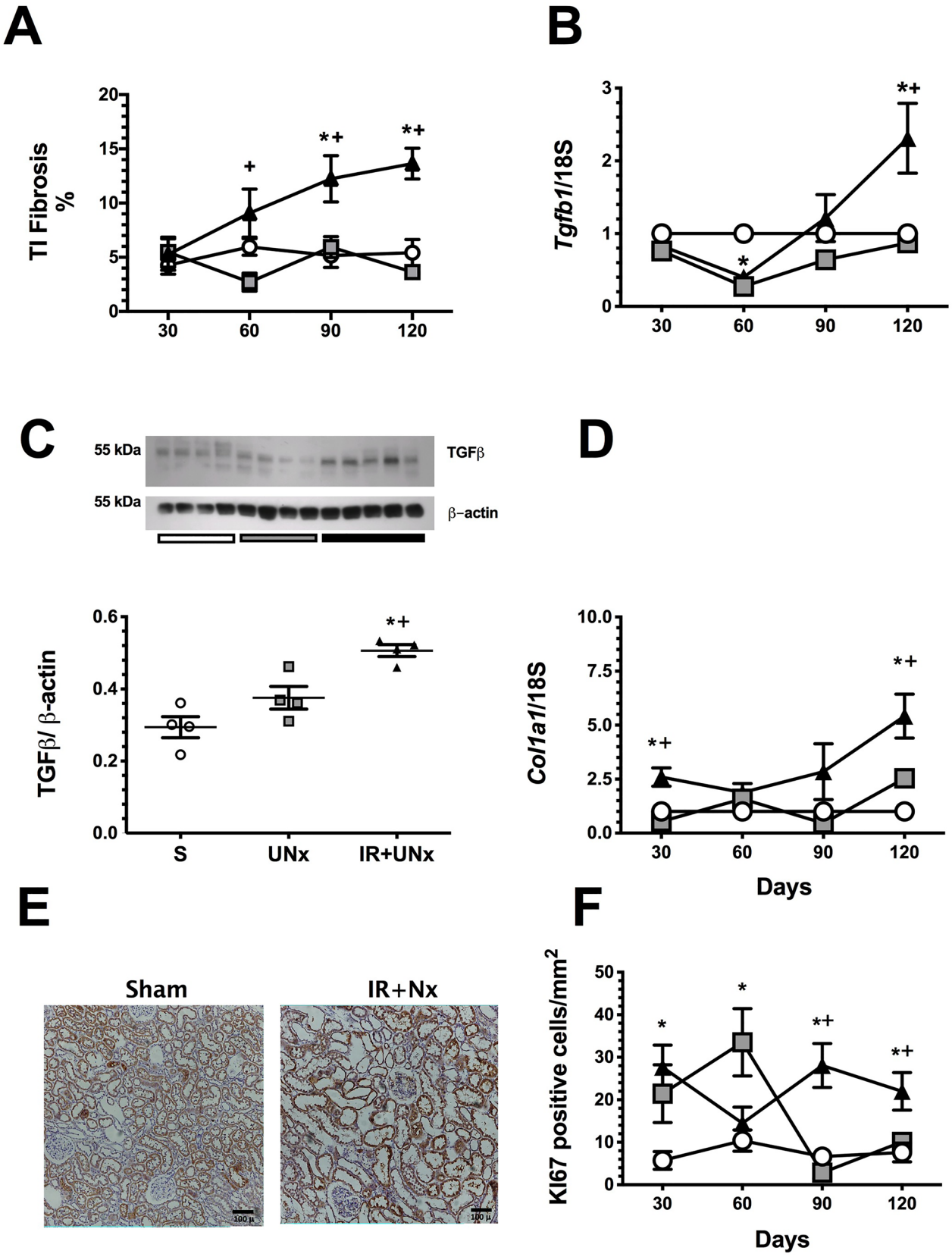
A
TI Fibrosis %
20
15
10
5
0
30
60
90
120
+
*+
*+
B
Tgfb1/18S
3
2
1
0
*
*+
C
55 kDa
TGFβ
55 kDa
β-actin
TGFβ/ β-actin
0.6
0.4
0.2
0.0
S
UNx
IR+UNx
D
Col1a1/18S
10.0
7.5
5.0
2.5
0.0
Days
E
Sham
IR+Nx
F
KI67 positive cells/mm2
50
40
30
20
10
0
Days

◂**Figure 3.** Temporally induction of tubulointersticial fibrosis by TGFβ activation. (**A**) Tubulointersticial fibrosis, (**B**) mRNA levels of *Tgfb1*, (**C**) Protein levels of TGFβ, at fourth-month post-ischemia, including a representative cropped blots. (**D**) mRNA levels of *Collagen1a1*, (**E**) Representative microphotographs of Ki67 immunostaining for the S and IR + UNx groups. (**F**) Quantification of Ki67 positive epithelial cells (cells/mm^2). Data are represented as the mean ± SE. n = 4, 4, and 5 for S, UNx, and IR + UNx groups, in each studied period: 30, 60, 90, and 120 days post-ischemia. White circles/bar represent the S, gray squares/bar represent the UNx and black triangles/bar represent the IR + UNx groups. The one-way analysis of variance (ANOVA) was used to determine statistical differences, using the Bonferroni correction for multiple comparisons. *$p < 0.05$ versus S group and +$p < 0.05$ versus UNx group in their respective period. Full-length blots are presented in Supplementary Fig. 6.

Discussion

Acute kidney injury is a public health problem and despite the advances in modern medicine, its incidence has not diminished in recent decades[44]. Also, the alarming increase in patients with CKD worldwide[45], coupled with the recent recognition that AKI is an independent risk factor for CKD development[1,2] requires joint work between biomedical and clinical researchers to avoid this complication. Therefore, it is imperative to study the temporality of the mechanisms that affect and lead to the AKI to CKD transition, which will allow for the identification of the key points and mediators in the development of this disease and propose specific therapeutic targets according to the stages of CKD. Many efforts have been made, and some pathways, such as trans-differentiation of pericytes into myofibroblasts[19,23], uncontrolled proliferation of epithelial cells[22], excessive production of TGFβ by both tubular epithelium[22] and local myofibroblasts[25,26], accumulation of extracellular matrix proteins[27,28], chronic hypoxia[30,32], vascular rarefaction[29,31,46], and chronic stress of the endoplasmic reticulum[33], have been identified, but many others remain to be elucidated.

In this study, we evaluated ischemic renal damage after 24 h of reperfusion plus right nephrectomy compared to that of the S and UNx groups. AKI induced by IR was characterized by elevated proteinuria, renal dysfunction, and oxidative stress. All IR + UNx rats exhibited the same magnitude of AKI. In the long term, the nephrectomy plus I/R model was able to accelerate the development of CKD. After four months, the IR + UNx group presented a progressive increase in proteinuria and a significant decrease in renal function. Among the alterations that occurred in the early phase of the transition, we found a significant increase in oxidative stress that was maintained throughout the study follow-up and a significant decrease in global DNA methylation, suggesting that both are early key players in the AKI to CKD transition.

As expected, the UNx group exhibited renal hyperperfusion and hyperfiltration to compensate the renal mass reduction for maintaining renal function within standard values, as the S group had. Interestingly, the IR + UNx group displayed sustained hypoperfusion that was observed beginning at an early phase and impacted the expected renal function compensation. Our results suggest that this poor renal hemodynamic response after an AKI episode could be one of the responsible mechanisms involved in the AKI to CKD transition, contributing to chronic renal hypoxia.

Previous studies have demonstrated that chronic hypoxia is a trigger mechanism in the AKI to CKD transition that coordinates the interaction between inflammation, oxidative stress, and progressive fibrosis[13,16–18,20–22,47]. Hif1α serves as a master regulator of adaptive responses against hypoxia, although, the levels of HIF1α can also be regulated by oxygen independent pathways[48]. This transcription factor induces an angiogenic pathway throughout the induction of *Vegfa* gene expression[49,50]. In this regard, we found an inefficient response against renal hypoxia in the IR + UNx group. *Hif1α* mRNA levels were decreased in the first and second-month post-ischemia, similar to those observed in the UNx group. Although, this response could be explained in the UNx group due to the compensatory elevation in RBF, which when normalized by kidney weight was similar to the S group. Since, HIF1α is regulated by proteasomal degradation pathways in response to oxygen levels[51], it is very likely that in the UNx group, there is a greater metabolic work to maintain renal function and therefore, the state of renal oxygenation could not have changed. But this HIF1α response was unexpected in the IR + UNx group that exhibited renal hypoperfusion, a condition in which proteasomal degradation is not expected to occur. This inefficient response of HIF1α was also demonstrated by the reduction in its target gene *Vegfa*. Thus, *Vegfa* mRNA levels were reduced starting in the first-month, and interestingly, they remained reduced throughout the study, despite the restoration of HIF1α levels. The decreased *Vegfa* expression was also corroborated at the protein level throughout the study. Recent studies have reported that the late response of HIF1α could be related to the activation of inflammatory processes and the generation of renal fibrosis[52]. It is well known that the reduction in *Vegfa* gene expression is partly responsible for vascular rarefaction[46,53–55] that accompanies the AKI to CKD transition, which also perpetuates chronic hypoxia. Although *Hif1a* mRNA levels were restored at the end of the study and protein levels remained unaltered, *Vegfa* levels continued diminishing; this opened the possibility of an alternative regulation of *Vegfa* gene expression through the involvement of epigenetic mechanisms.

It has been shown that the hypoxia response element (HRE) in the *Vegfa* promoter gene contains several cytosines in a CpG context that are potentially methylated. This methylation could reduce the HIF1α interaction with the *Vegfa* gene promoter[56,57]. In vitro studies have demonstrated that DNA hypermethylation in the *Vegfa* promoter region induces silencing of this gene[58]. To understand the reduction in *Vegfa* expression despite sustained renal hypoperfusion and recovery of *Hif1a* mRNA levels, we analyzed the methylation of the noncoding upstream region of *Vegfa* during the AKI to CKD transition. Interestingly, we found DNA hypermethylation in the promoter region of *Vegfa*. More importantly, we demonstrated that the HRE, as well as the core region for HIF1α interaction was hypermethylated since the first-month post-ischemia and it was maintained at the fourth-month of the follow-up. This site matches with the region 2, previously described to be important in *Vegf*

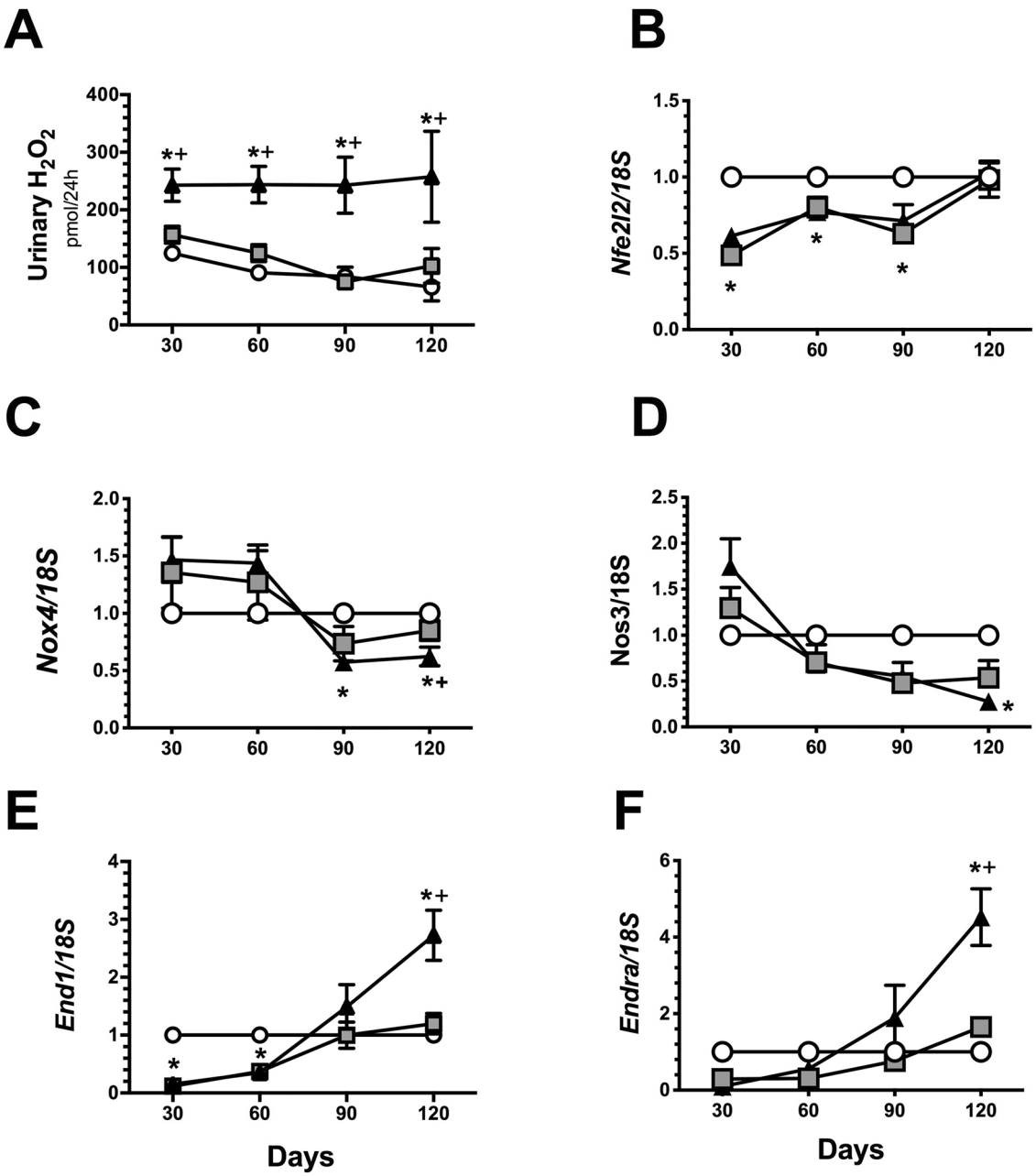

Figure 4. Oxidative stress and vasoactive mediators over the course of AKI to CKD transition. (**A**) Urinary hydrogen peroxide, (**B**) mRNA levels of *Nfe2l2* (**C**) mRNA levels of *Nos3,* (**D**) mRNA levels of NOX4, (**E**) mRNA levels of *Edn1* and (**F**) mRNA levels of endothelin receptor A (*Endra*). Data are represented as the mean ± SE. n = 4, n = 4, and n = 5 for the S, UNx, and IR + UNx groups, in each studied period: 30, 60, 90, and 120 days post-ischemia. The one-way analysis of variance (ANOVA) was used to determine statistical differences, using the Bonferroni correction for multiple comparisons. *$p < 0.05$ versus S group and + $p < 0.05$ versus UNx group in their respective period.

gene transcription regulation[59]. Using the transcription factor binding site predictor tool PROMO (version 8.3 of TRANSFAC, http://alggen.lsi.upc.es), TFsitescan (http://www.ifti.org/cgi-bin/ifti/Tfsitescan.pl) and JASPAR database (http://dbcat.cgm.ntu.edu.tw), we found that this hypermethylated region contains a putative binding sequence responsible for the interaction of Hif1α, C/EBPα and the p300. This complex is essential for *Vegfa* transcription regulation and contributes to the pro-angiogenic pathway[60,61]. Our findings suggest that the reduction in *Vegfa* gene expression in the IR + UNx group resulted from epigenetic regulation, which could be partially responsible for inducing vascular rarefaction and chronic renal hypoxia, which are mechanisms implicated in the AKI to CKD transition[19,29–31,46]. In agreement with our results, it has been demonstrated that treatment with VEGF-121 was effective in suppressing the AKI to CKD transition induced by IR in rats. Although VEGF-121 did not affect AKI, the loss of peritubular capillaries in the cortex and outer stripe of the outer medulla was

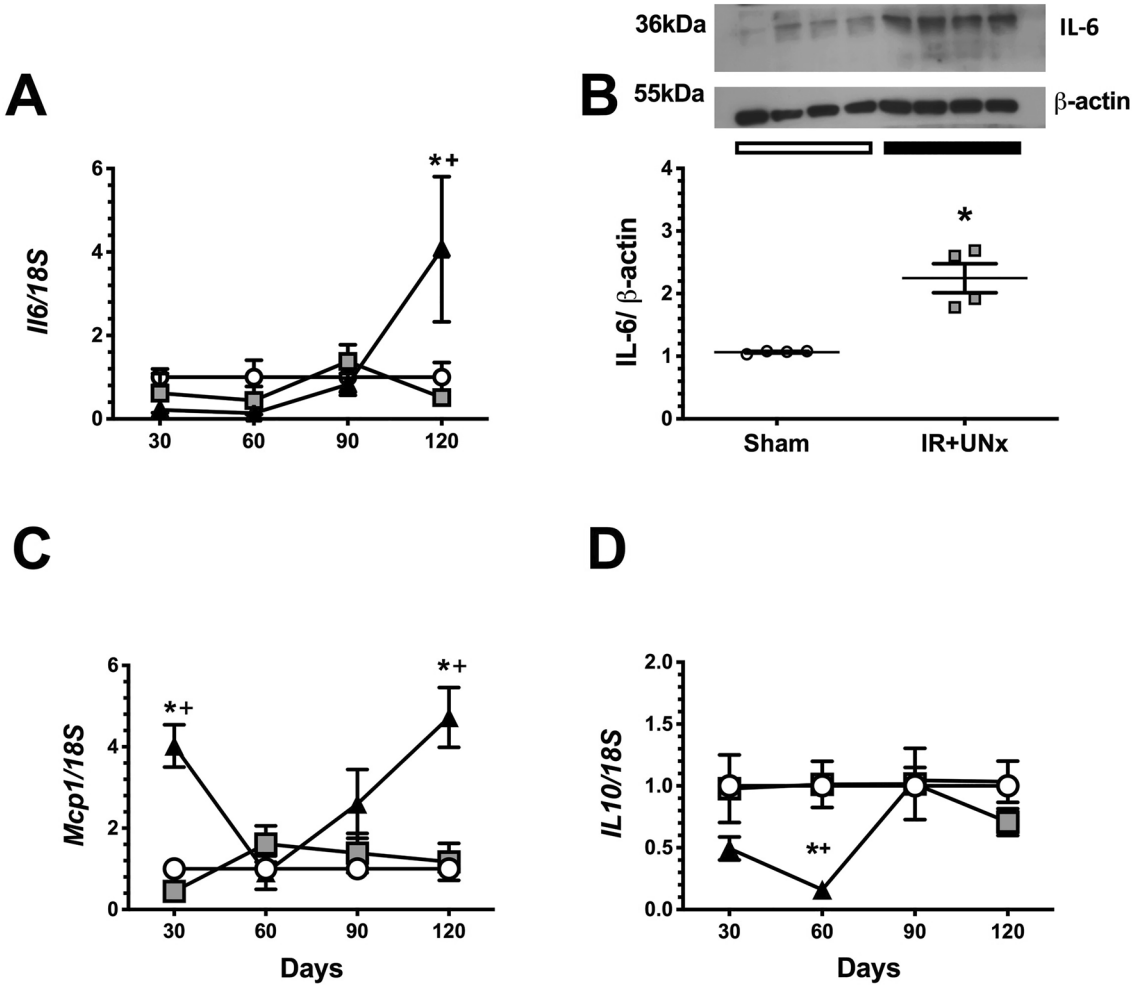

Figure 5. Inflammatory mediators participation during AKI to CKD transition. (**A**) mRNA levels of *Il6*, (**B**) Protein levels of IL-6 at fourth-month post-ischemia, including a representative cropped blots, (**C**) mRNA levels of *Mcp1* and (**D**) mRNA levels of *Il10*. Data are represented as the mean ± SE. n = 4, 4, and 5 for the S, UNx, and IR + UNx groups in each studied period: 30, 60, 90, and 120 days post-ischemia. White circles/bar represent the S, gray squares represent the UNx and black triangles/bar represent the IR + UNx groups. The one-way analysis of variance (ANOVA) was used to determine statistical differences, using the Bonferroni correction for multiple comparisons. *$p < 0.05$ versus S group and + $p < 0.05$ versus UNx group in their respective period. Full-length blots are presented in Supplementary Fig. 7.

significantly attenuated[55]. Further experimental and clinical studies are required to evaluate VEGF therapeutic power in preventing the AKI to CKD transition. In this hypermethylated region, we also found a putative binding site for Nrf2, which is a master regulator of the antioxidant response[62]. Because hypermethylation of the *Vegfa* promoter region occurred from the first-month post-ischemia, it suggests that this epigenetic mechanism plays an important role in the onset of the disease, promoting chronic hypoxia and concomitant development of renal fibrosis. In a recent study, it was observed that indeed, epigenetic modifications occur early after folic acid-induced kidney damage. In particular, it was observed that de novo methylation of histone H3K4 is necessary for the differentiated cells to re-enter mitosis and regenerate the proximal tubular epithelium[63]. These findings together, highlighted the crucial role of the early epigenetic modifications in the long consequences after an ischemic insult. Furthermore, our results open an exciting research field to explore the mechanisms by which hypermethylation of the *Vegfa* promoter gene is occurring, in which cell subpopulations occur, as well as the molecular mediators of this phenomenon, such as histone modifications and the enzymes involved in this pathophysiological condition. In this context, previous reports have demonstrated that the up-regulation of DNA methyltransferase 1 (Dnmt1), DNA methylation, and transcriptional silencing are linked to fibroblast activation and kidney fibrosis[37].

In addition to the mentioned changes, the IR + UNx group exhibited activation of renal inflammation. Pro-inflammatory molecules, as indicated by *Mcp1* and *Il6* mRNA levels, increased, while the anti-inflammatory molecule, *Il10*, decreased beginning at the early phase of the transition of this disease. These changes could result from the global DNA hypomethylation observed in the IR + UNx, as previous studies have shown in AKI, diabetic nephropathy, and CKD models[34,37,38].

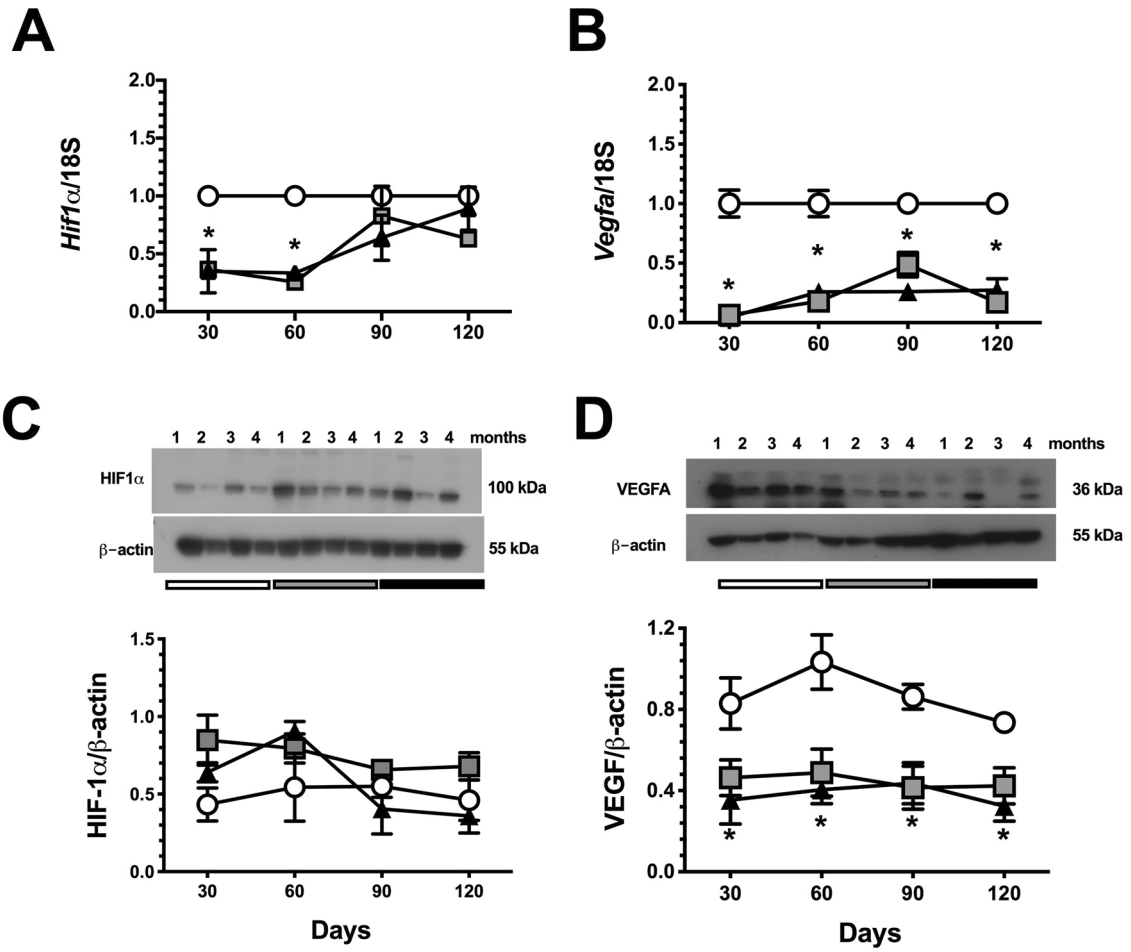

Figure 6. Temporal course of HIF-1α signaling during AKI to CKD transition. (**A**) mRNA levels of *Hif1a*, (**B**) mRNA levels of *Vegfa*, (**C**) Protein levels of HIF-1α, including a representative cropped blot, and (**D**) Protein levels of VEGF, including a representative cropped blot. Data are represented as the mean ± SE. n = 4, for S, UNx, and IR + UNx groups, in each studied period: 30, 60, 90, and 120 days post-ischemia. White circles represent the S, gray squares represent the UNx and black triangles represent the IR + UNx groups. The one-way analysis of variance (ANOVA) was used to determine statistical differences, using the Bonferroni correction for multiple comparisons. *$p < 0.05$ versus S group and + $p < 0.05$ versus UNx group in their respective period. Full-length blots are presented in Supplementary Figs. 8 and 9.

In summary, our study shows that early renal hypoperfusion, inefficient hypoxia response, increased oxidative stress, and increased inflammation play an important role in the AKI to CKD transition. Specifically, the inefficient hypoxia response results from the inadequate hypermethylation of the *Vegfa* promoter gene at the site of HIF1α binding that occurs in the early stage post-ischemia.

Methods

All the experimental procedures in the animals were conducted following the Guide for the Care and Use of Laboratory Animals and were approved by the animal research ethics committee of the *Instituto Nacional de Ciencias Médicas y Nutrición Salvador Zubirán* with the approval number NMM-1852. The study was carried out in compliance with the ARRIVE guidelines.

Experimental model: right nephrectomy and contralateral ischemia. Fifty-nine male Wistar rats weighing between 300 and 320 g were included. Seven rats did not meet our inclusion and exclusion criteria, two were excluded due to bleeding during the nephrectomy surgical procedure and five due to postoperative death in the first 72 h as a consequence of renal ischemia–reperfusion injury. Therefore, a total of 52 rats were included and randomly divided into three groups: the sham surgery group (S, n = 16), the right nephrectomy group (UNx, n = 16), and the group with right nephrectomy and simultaneous left renal ischemia of 45 min in the left kidney (IR + UNx, n = 20). Based on our previous experience with the IR experimental model, we calculated the sample size for comparison of two means, using the creatinine elevation after 24 h post-ischemia. Although, we did not use a method to generate the randomization sequence, each block of 3 rats was randomly assigned to each of the studied groups: S, UNx or IR + UNx and so on. The study was not blinded because no pharmacological intervention was carried out.

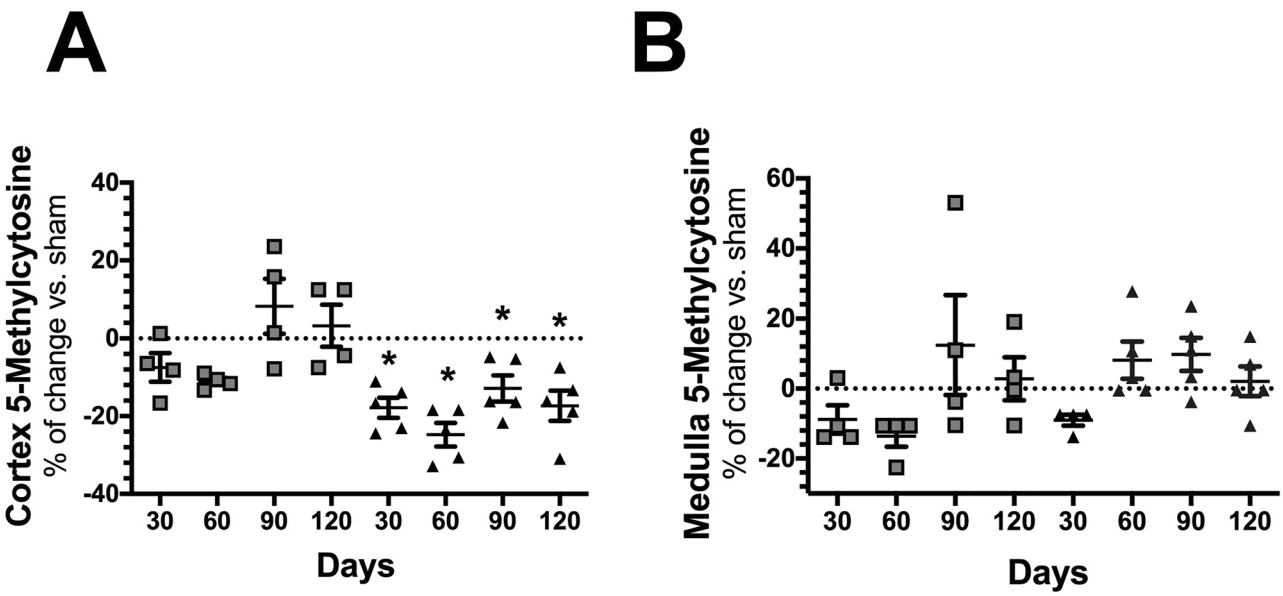

Figure 7. Global DNA methylation over the course of AKI to CKD transition. (**A**) Percentage change of global DNA methylation in renal cortex from the UNx (gray squares) and IR + UNx (black triangles) groups. (**B**) Percentage change of global DNA methylation in renal medulla from the UNx (gray squares) and IR + UNx (black triangles) groups, for each studied period: 30, 60, 90, and 120 days The one-way analysis of variance (ANOVA) was used to determine statistical differences, using the Bonferroni correction for multiple comparisons. *$p < 0.05$ versus S group.

The animals were anesthetized with sodium pentobarbital (30 mg/kg) and kept in a thermoregulated bed to perform the surgery at 37 °C. Under anesthesia, an abdominal incision was made to expose the two kidneys, first, the nephrectomy of the right kidney was performed, dissecting the peri-renal fat, as well as, separating the adrenal gland from the kidney with delicacy to avoid damaging it. For the IR + UNx group, in addition to the nephrectomy, a clip was placed in the left kidney for 45 min, to induce the ischemic process and the reperfusion was achieved when the clip was removed, using the recovery of the coloration of the kidney, as an indicator. The animals were bred and kept in our animal facility; on a 12/12 h light/dark cycles and permitted ad libitum access to food and water. Each studied group was followed for 1, 2, 3, and 4 months, respectively. At the end of each experimental period, the following parameters were assessed: mean arterial pressure (MAP), renal blood flow (RBF), creatinine clearance, glomerular diameter, tubule-interstitial fibrosis, Ki67 positive cells, urinary H_2O_2 excretion urinary biomarkers of renal injury, RNA and protein levels of antioxidant enzymes and anti-inflammatory cytokines, DNA methylation and promoter VEGF methylation.

Renal functional studies. The animals were placed in metabolic cages every month, to collect urine for at least 18 h to determine urinary protein excretion and creatinine clearance. A blood sample from the retro-orbital plexus was also collected monthly. Urine collections were carried out at the same schedule in all animals, starting between 4 and 6 pm and ended 18 h later, to avoid diurnal variations. For the determination of serum and urine creatinine, the colorimetric method of picric acid was used and quantified at 510 nm in a spectrophotometer. To calculate the creatinine clearance, the formula of C = (U*V)/S was used, where U is the urinary creatinine multiplied by the urinary volume (V), and S corresponds to the serum creatinine. Urinary protein excretion was determined by the turbidimetric method of trichloroacetic acid (TCA) and quantified at 420 nm in a spectrophotometer.

By the end of each experimental period, the animals were anesthetized with sodium pentobarbital (30 mg/kg) and were placed in a thermoregulated pad. The trachea was cannulated with a PE-240 polyethylene tube and the femoral arteries were catheterized with a polyethylene tube PE-90. The mean arterial pressure was recorded by one of the catheters placed in the femoral artery, using a pressure transducer (Model p23 db, Gould, Puerto Rico). Subsequently, an abdominal incision was made to expose the left kidney, the renal artery was dissected and an ultrasound probe was placed to register the renal blood flow (1RB, Transonic, Ithaca, NY).

The right kidney from the S group was ligated and removed and the left kidney upper and lower pole for the UNx and the IR + UNx groups were excised to separate renal medulla and cortex, both sections were immediately frozen at − 70 °C for further molecular analysis. The left kidney was then perfused through the femoral artery catheter with 20 mL of saline and then fixed with 20 mL of 4% formaldehyde, and removed immediately after. The animals were euthanized with an intraperitoneal delivery of an overdose of pentobarbital (100 mg/kg) after 1, 2, 3, and 4 months of renal reperfusion.

Light microscopy and immunohistochemistry analysis. After tissue fixation, the kidneys were dehydrated and embedded in paraffin. Renal slices of 4 μm were obtained and stained with Periodic Acid Schiff

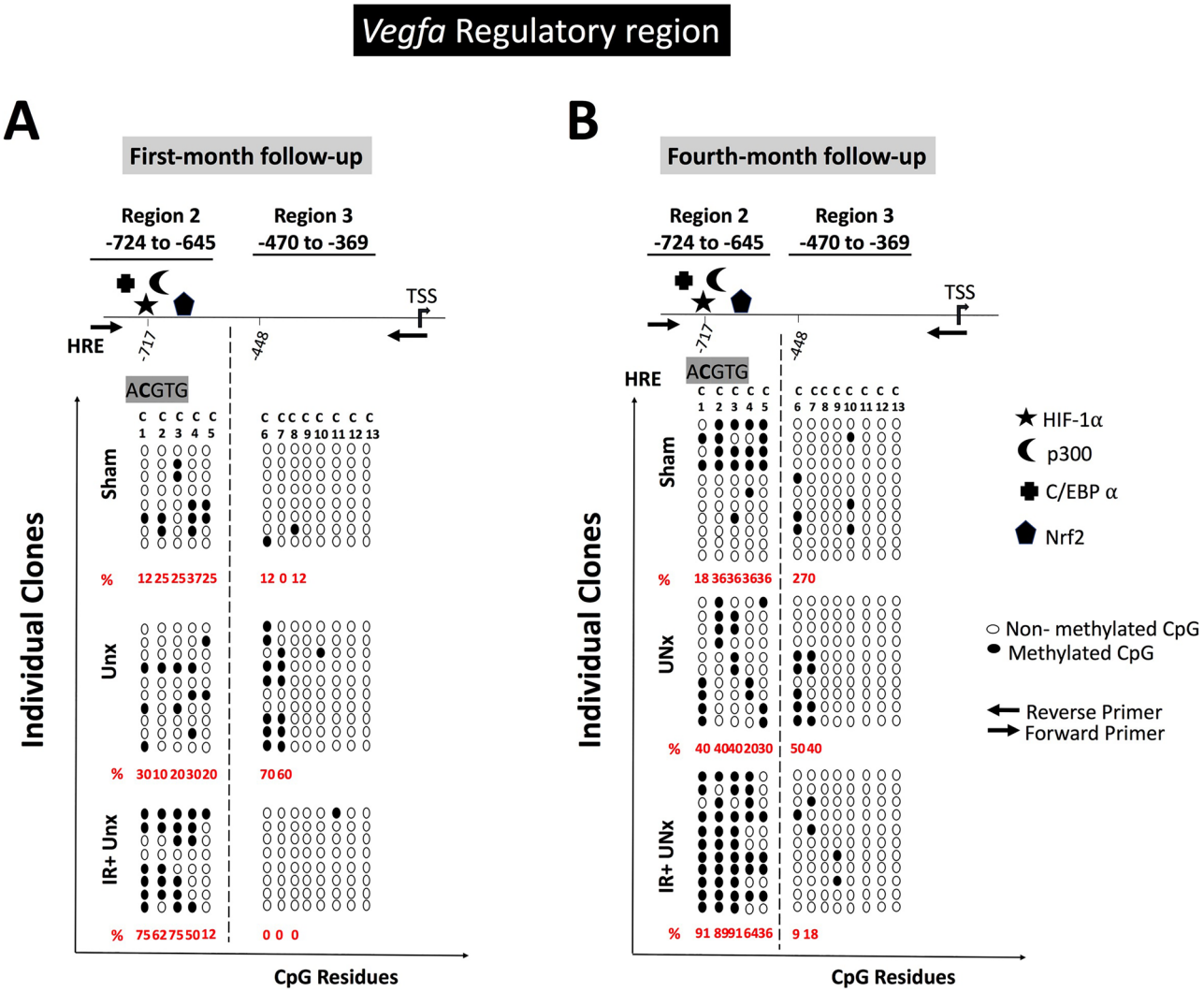

Figure 8. Bisulfite sequencing of two non-codifying upstream regions of *Vegfa* promoter for (**A**) the first-month and (**B**) the fourth month of follow-up for the Sham, UNx and IR + UNx groups, respectively. Arrows represented the forward and reverse primers for each amplicon. HIF-1α, p300, C/EBPα, and Nrf2 binding sites as is stated. White circles represented non-methylated CpG, and black circles represented methylated CpG, each circle represented an individual clone. Each C represented a cytosine in CpG context. TSS-Transcription star site; HRE-Hypoxia response element (ACGTG).

(PAS) or Sirius red. In the slices stained with PAS, ten microphotographs (Magnification 400x) were obtained from different renal cortex fields of each kidney and glomerular diameter was quantified in at least 40 glomeruli per rat using a Nixon camera incorporated to the microscope. In the slices stained with Sirius red, five to eight subcortical periglomerular fields per section were randomly selected in kidneys from the groups studied (Magnification 100x). Tubulo-interstitial fibrosis consisted of extracellular matrix expansion with collagen deposition together with distortion and collapse of the tubules; fibrosis was evidenced by red coloration in Sirus red-stained slides. The affected area was delimited and the percentage of tubulointerstitial fibrosis was calculated by dividing the fibrotic by the total area, excluding the glomerular area. Researchers were blind to the experimental group.

To evaluate tubular cell proliferation, conventional immunoperoxidase assays for Ki67 (anti-Ki67 antibody, Abcam Cat. No. ab66155) were performed. For signal detection, HRP/DAB Detection System (Bio SB, Santa Barbara CA, USA Cat. No. BSB 0001) was used, slides were counterstain with hematoxylin. The number of Ki-67-positive epithelial cells on each slide was counted in at least 10-subcortical fields (100 × magnification).

Hydrogen peroxide urinary excretion. In the urine collected during the follow-up time, the determination of urine hydrogen peroxides as an oxidative stress marker was carried out, using a commercial kit (Amplex Red Hydrogen Peroxide/Peroxidase Assay, Roche, Cat. No. A22188) following the manufacturer's instructions. The determination is based on the presence of peroxidase which, when reacted with hydrogen peroxide, produces a red-fluorescent compound, which was quantified in a spectrophotometer at 560 nm and extrapolated with a standard curve.

RNA extraction and quantitative PCR. The total RNA was isolated from the kidneys using the TRIzol method (Invitrogen, Carlsbad, CA, Cat. No. 15596026) and checked for integrity using 1% agarose gel electrophoresis. To avoid DNA contamination, total RNA samples were treated with DNase (DNase I; Invitrogen, Carlsbad, CA, Cat. No. 18068015). Reverse transcription (RT) was carried out with 1 µg of total RNA and 200 U of Moloney murine leukemia virus reverse transcriptase (Invitrogen). The mRNA levels of *Hif1a*, *Vegfa*, pre-pro-endothelin (*Edn1*), endothelin receptor A (*Ednra*), endothelial NOS 3 (*NOS3),* transforming growth factor *(Tgfb1)*, monocyte chemoattractant protein *1 (Mcp1),* nuclear factor erythroid 2 like 2 *(Nfe2l2),* NADPH oxidase *4 (Nox4),* collagen-1 *(Col1a1)* interleukin 6 *(Il6), and* interleukin 10 *(Il10)* were quantified by real-time PCR on an ABI Prism 7300 Sequence Detection System (TaqMan, ABI, Foster City, CA, Cat. No. 4331182). Primers and probes were ordered as a kit as follows: *Hif1a*, (Rn0057756_m1), *Vegfa* (Rn01511602_m1), *Edn1* (Rn00561129_m1), *Ednra* (Rn00561137_m1), *NOS3* (Rn004352204_m1), *Tgfb1* (Rn00572010_m1), *Mcp1* (Rn00580555_m1), *Nfe2l2* (Rn00582415_m1), *Nox4* (Rn00585380_m1), *Col1a1* (Rn1463848_m1), *Il6* (Rn01410330_m1), and *Il10* (Rn99999012_m1). As an endogenous control, eukaryotic 18S rRNA (predesigned assay reagent Applied by ABI, external run, Rn03928990_g1, Cat. No. 4319413E was used. The relative quantification of each gene expression was performed with the comparative threshold cycle (Ct) method.

Western blot and antibodies. The renal cortex proteins were homogenized with a lysis buffer containing: 50 mM HEPES pH 7.4, 250 mM NaCl, 5 mM EDTA, 0.1% NP-40 and complete protease inhibitor (Roche, Cat. No.. 11,697,498,001). The proteins concentration was assessed by Lowry protein assay (Bio-Rad, Cat. No. 5000113 and 5,000,114). Renal cortex protein levels were detected by Western blot, tissue proteins (20–40 µg) were electrophoresed in a denaturing 8.5% acrylamide gel with SDS. The samples were prepared with loading buffer in a 1:1 ratio with a final volume of 20 µL. The membranes were incubated with the primary antibody TGFβ (Thermo Fisher, Cat. No. MA5-15,065, 1:1000), HIF-1alpha (Abcam, Cat. No.. ab2185, 1:5000) VEGFA (Invitrogen, MA1-16,629, 1:5000), IL-6 (Abcam, Cat. No. ab9324, 1:1000), and HRP β-Actin antibody [AC-15] (Abcam, Cat. No. ab49900, 1:1,000,000) overnight at 4 °C. Three 10-min washes were performed with TBS-1 × Tween and then incubated with the secondary antibody coupled to HRP, anti-rabbit or anti-mouse IgG (Santa Cruz, Cat. No. sc-2031 or sc-2004, respectively 1: 5000). Tissue proteins assessed by Western blot were normalized by β-Actin detection.

Detection of urinary biomarkers by western blot. Urinary HSP72 levels were detected by Western blot, each urine was diluted 1:10 in 0.9% saline solution, and 10 µL of each dilution was loaded and resolved by 8.5% SDS-PAGE, as previously described[39–42,64]. The membranes were incubated with mouse anti-HSP72 antibody (ENZO Life Sciences, Cat. No. ADI-SPA-819F, 1:5000 dilution) or KIM-1 (Boster, Cat. No. PA1632, 1:5000) overnight at 4 °C. Thereafter; membranes were incubated with a secondary antibody, HRP-conjugated goat anti-mouse IgG, or anti-rabbit IgG, respectively (1:5000, Cat. No. sc-2031 or sc-2004, respectively, Santa Cruz). The proteins were detected using a commercial chemiluminescence kit (Millipore, Cat. No. WBKLS0500) and were normalized by urinary creatinine (UCreat).

Genomic DNA extraction and quantification of global DNA methylation. For genomic DNA extraction, 50 mg of tissue was homogenized in 200 µL of 1X PBS (10 mM PO4, 137 mM NaCl, and 2.7 mM KCl), 60 µL of digestion buffer (Tris–HCl 1 M, EDTA 0.5 M, SDS 10%, NaCl 5 M, pH = 8), then 26 µL of Proteinase K (Sigma, Cat. No. P2308-100 mg, 10 mg/mL) was added and kept on ice for 5 min. Subsequently, the mixture was left overnight at 56 °C, then the samples were treated with 3 µL of RNase A (Qiagen, Cat. No. 19101, 10 mg/mL) and incubated for 3 h at 37 °C. By the end, 250 µL of phenol–chloroform-isoamyl alcohol (Sigma, Cat. No. 77617-100ML) was added, centrifuged for 20 min, 16.1 g at 4 °C. Only the upper phase was taken and 83 µL of ammonium acetate (7.5 M) and 250 µL of absolute ethanol were added. The samples were incubated at − 20 °C overnight, centrifuged and the supernatant was discarded. Two washes were made with 250 µL of 70% ethanol. The pellet was re-suspended in 200 µL of DNase/RNase-Free Distilled Water. To analyze the global DNA methylation, the commercial methylation kit of 5mC DNA (Zymo Research Cat. No. D5326) was used, 100 ng of DNA from each sample was used and it was taken to a volume of 100 µL with 5mC of coating buffer. The mix was incubated at 98 °C for 5 min and then left on ice for 10 min. Then it was added to the plate and incubated at 37 °C for 1 h and the excess was discarded and washed with 200 µL of 5mC Elisa Buffer. Thereafter, 200 µL of 5mC Elisa buffer was added to each well and incubated at 37 °C for 30 min. A mixture of 5-methyl cytosine primary antibody (1:2,000) and HRP-coupled secondary anti-rabbit antibody (1:1000) was added. Finally, 100 µL of HRP developer was added to each well, incubated 1 h, and measured in a spectrometer at 405–450 nm. The results were extrapolated with a standard curve and the correction was made for the percentage of cytosines and guanine dinucleotides (CpGs), which have been previously reported for the rat genome[65].

Sequence analysis and bisulfite primer design. Three binding Hif1α sequences in the promoter *Vegf* gene in the rat have been previously identified and were named as region 1 (− 976 to − 857), region 2 (− 724 to − 645), and region 3 (− 470 to − 369), respectively (Suppl. Fig. 1)[59]. DataBase of CpG islands and Analytical Tool (DBCAT) (http://dbcat.cgm.ntu.edu.tw) software-assisted us to identify the CpG islands in the promoter and the first part of the coding regions of *Vegf* gene. This analysis showed that only regions 2 and 3 were enriched of CpG islands, suggesting that these regions are susceptible to methylation. Consequently, optimal primers were designed in the Methyl Primer Express software for bisulfite sequencing of *Hif-1α* and *Vegf* gene promoters. For *Hif-1α* the primers were: 5′-GTAGAGAGTAGAGATTGAGTT-3′ (forward) and 5′-CAAAACCTAACC AAACACTAC-3′ (reverse) that amplified the region from − 1390 to − 688 (702 bp): As was commented before there are three HIF1α binding sequences in the promoter of *Vegfa*, but only two are susceptible to methylation:

the region 2, from − 724 to − 645, and the region 3. from − 470 to − 369, we amplified together with the following primers: 5′-GGTTTTGTTAGATTTTATAGTG-3′ (forward) and 5′-CCATAACCTAAAAATTATCTATC-3′ (reverse) yielding a product of 763 bp.

Sodium bisulfite DNA conversion and sequencing. Genomic DNA (3 µg) was processed with sodium bisulfite[66], DNA fragments of interest were PCR-amplified. The amplified DNA fragments were cloned into the pGEM-T Easy system (Promega, Cat. No. A1360), and Sanger sequenced using its respective reverse primer. At least 8 clones were evaluated for each region.

Statistical analysis. The results are presented as the mean ± SE. The significance of the differences between groups was assessed by 1-way ANOVA using the Bonferroni correction for multiple comparisons. All comparisons passed the normality test. Statistical significance was defined when the p-value was < 0.05. All the graphs and statistical analyses were performed using the statistical GraphPad Prisma 8 software for Mac (GraphPad Software, San Diego, CA, USA).

Received: 5 November 2020; Accepted: 6 April 2021
Published online: 22 April 2021

References

1. Chawla, L. S., Eggers, P. W., Star, R. A. & Kimmel, P. L. Acute kidney injury and chronic kidney disease as interconnected syndromes. *N. Engl. J. Med.* **371**, 58–66 (2014).
2. Hsu, C. Y. *et al.* Impact of AKI on urinary protein excretion: analysis of two prospective cohorts. *J. Am. Soc. Nephrol.* **30**, 1271–1281. https://doi.org/10.1681/ASN.2018101036 (2019).
3. Bucaloiu, I. D., Kirchner, H. L., Norfolk, E. R., Hartle, J. E. & Perkins, R. M. Increased risk of death and de novo chronic kidney disease following reversible acute kidney injury. *Kidney Int.* **81**, 477–485 (2012).
4. Chawla, L. S., Amdur, R. L., Amodeo, S., Kimmel, P. L. & Palant, C. E. The severity of acute kidney injury predicts progression to chronic kidney disease. *Kidney Int.* **79**, 1361–1369 (2011).
5. Hatakeyama, Y. *et al.* Transition from acute kidney injury to chronic kidney disease: a single-centre cohort study. *Clin. Exp. Nephrol.* **22**, 1281–1293. https://doi.org/10.1007/s10157-018-1571-5 (2018).
6. Ishani, A. *et al.* Acute kidney injury increases risk of ESRD among elderly. *J. Am. Soc. Nephrol.* **20**, 223–228 (2009).
7. Funk, J. A. & Schnellmann, R. G. Persistent disruption of mitochondrial homeostasis after acute kidney injury. *Am. J. Physiol. Ren. Physiol.* **302**, F853–F864. https://doi.org/10.1152/ajprenal.00035.2011 (2012).
8. Zuk, A. & Bonventre, J. V. Acute kidney injury. *Annu. Rev. Med.* **67**, 293–307. https://doi.org/10.1146/annurev-med-050214-013407 (2016).
9. Linkermann, A. *et al.* Two independent pathways of regulated necrosis mediate ischemia-reperfusion injury. *Proc. Natl. Acad. Sci. U. S. A.* **110**, 12024–12029. https://doi.org/10.1073/pnas.1305538110 (2013).
10. Dong, Y. *et al.* Ischemic duration and frequency determines AKI-to-CKD progression monitored by dynamic changes of tubular biomarkers in IRI mice. *Front Physiol.* **10**, 153. https://doi.org/10.3389/fphys.2019.00153 (2019).
11. Fiorentino, M., Grandaliano, G., Gesualdo, L. & Castellano, G. Acute kidney injury to chronic kidney disease transition. *Contrib. Nephrol.* **193**, 45–54. https://doi.org/10.1159/000484962 (2018).
12. Bonventre, J. V. Dedifferentiation and proliferation of surviving epithelial cells in acute renal failure. *J. Am. Soc. Nephrol.* **14**(Suppl 1), S55-61. https://doi.org/10.1097/01.asn.0000067652.51441.21 (2003).
13. Bonventre, J. V. & Yang, L. Cellular pathophysiology of ischemic acute kidney injury. *J. Clin. Invest.* **121**, 4210–4221 (2011).
14. Bonventre, J. V. Maladaptive proximal tubule repair: cell cycle arrest. *Nephron Clin. Pract.* **127**, 61–64. https://doi.org/10.1159/000363673 (2014).
15. Okamura, D. M. & Pennathur, S. The balance of powers: redox regulation of fibrogenic pathways in kidney injury. *Redox Biol.* **6**, 495–504. https://doi.org/10.1016/j.redox.2015.09.039 (2015).
16. Lech, M. *et al.* Macrophage phenotype controls long-term AKI outcomes–kidney regeneration versus atrophy. *J. Am. Soc. Nephrol.* **25**, 292–304 (2014).
17. Lee, S. *et al.* Distinct macrophage phenotypes contribute to kidney injury and repair. *J. Am. Soc. Nephrol.* **22**, 317–326 (2011).
18. Zhang, M. Z. *et al.* CSF-1 signaling mediates recovery from acute kidney injury. *J. Clin. Invest.* **122**, 4519–4532 (2012).
19. Kramann, R., Wongboonsin, J., Chang-Panesso, M., Machado, F. G. & Humphreys, B. D. Gli1(+) pericyte loss induces capillary rarefaction and proximal tubular injury. *J. Am. Soc. Nephrol.* **28**, 776–784. https://doi.org/10.1681/ASN.2016030297 (2017).
20. Yang, L., Besschetnova, T. Y., Brooks, C. R., Shah, J. V. & Bonventre, J. V. Epithelial cell cycle arrest in G2/M mediates kidney fibrosis after injury. *Nat. Med.* **16**, 535–543, 531p (2010).
21. Lima-Posada, I. *et al.* Gender differences in the acute kidney injury to chronic kidney disease transition. *Sci. Rep.* **7**, 12270. https://doi.org/10.1038/s41598-017-09630-2 (2017).
22. Rodriguez-Romo, R. *et al.* AT1 receptor antagonism before ischemia prevents the transition of acute kidney injury to chronic kidney disease. *Kidney Int.* **89**, 363–373. https://doi.org/10.1038/ki.2015.320 (2016).
23. Humphreys, B. D. *et al.* Fate tracing reveals the pericyte and not epithelial origin of myofibroblasts in kidney fibrosis. *Am. J. Pathol.* **176**, 85–97. https://doi.org/10.2353/ajpath.2010.090517 (2010).
24. Kirita, Y., Wu, H., Uchimura, K., Wilson, P. C. & Humphreys, B. D. Cell profiling of mouse acute kidney injury reveals conserved cellular responses to injury. *Proc. Natl. Acad. Sci. U. S. A.* **117**, 15874–15883. https://doi.org/10.1073/pnas.2005477117 (2020).
25. Iwano, M. *et al.* Evidence that fibroblasts derive from epithelium during tissue fibrosis. *J. Clin. Invest.* **110**, 341–350. https://doi.org/10.1172/JCI15518 (2002).
26. Moll, S. *et al.* Epithelial cells as active player in fibrosis: findings from an in vitro model. *PLoS ONE* **8**, e56575 (2013).
27. Barrera-Chimal, J. *et al.* Spironolactone prevents chronic kidney disease caused by ischemic acute kidney injury. *Kidney Int.* **83**, 93–103 (2013).
28. Horbelt, M. *et al.* Acute and chronic microvascular alterations in a mouse model of ischemic acute kidney injury. *Am. J. Physiol. Ren. Physiol.* **293**, F688–F695 (2007).
29. Basile, D. P., Donohoe, D., Roethe, K. & Osborn, J. L. Renal ischemic injury results in permanent damage to peritubular capillaries and influences long-term function. *Am. J. Physiol. Ren. Physiol.* **281**, F887–F899 (2001).
30. Basile, D. P., Donohoe, D. L., Roethe, K. & Mattson, D. L. Chronic renal hypoxia after acute ischemic injury: effects of L-arginine on hypoxia and secondary damage. *Am. J. Physiol. Ren. Physiol.* **284**, F338–F348 (2003).

31. Kramann, R., Tanaka, M. & Humphreys, B. D. Fluorescence microangiography for quantitative assessment of peritubular capillary changes after AKI in mice. *J. Am. Soc.* **25**, 1924–1931 (2014).
32. Li, L. *et al.* FoxO3 activation in hypoxic tubules prevents chronic kidney disease. *J. Clin. Invest.* **130**, 2374–2389. https://doi.org/10.1172/JCI122256 (2019).
33. Shu, S. *et al.* Endoplasmic reticulum stress is activated in post-ischemic kidneys to promote chronic kidney disease. *EBioMedicine* **37**, 269–280. https://doi.org/10.1016/j.ebiom.2018.10.006 (2018).
34. Huang, N., Tan, L., Xue, Z., Cang, J. & Wang, H. Reduction of DNA hydroxymethylation in the mouse kidney insulted by ischemia reperfusion. *Biochem. Biophys. Res. Commun.* **422**, 697–702 (2012).
35. Pang, M. *et al.* Inhibition of histone deacetylase activity attenuates renal fibroblast activation and interstitial fibrosis in obstructive nephropathy. *Am. J. Physiol. Ren. Physiol.* **297**, F996–F1005 (2009).
36. Naito, M., Zager, R. A. & Bomsztyk, K. BRG1 increases transcription of proinflammatory genes in renal ischemia. *J. Am. Soc. Nephrol.* **20**, 1787–1796 (2009).
37. Bechtel, W. *et al.* Methylation determines fibroblast activation and fibrogenesis in the kidney. *Nat. Med.* **16**, 544–550 (2010).
38. Rodriguez-Romo, R., Berman, N., Gomez, A. & Bobadilla, N. A. Epigenetic regulation in the acute kidney injury (AKI) to chronic kidney disease transition (CKD). *Nephrol. (Carlton)* **20**, 736–743 (2015).
39. Barrera-Chimal, J. *et al.* Hsp72 is an early and sensitive biomarker to detect acute kidney injury. *EMBO Mol. Med.* **3**, 5–20 (2011).
40. Morales-Buenrostro, L. E. *et al.* Hsp72 is a novel biomarker to predict acute kidney injury in critically ill patients. *PLoS ONE* **9**, e109407 (2014).
41. Ortega-Trejo, J. A. *et al.* Heat shock protein 72 (Hsp72) specific induction and temporal stability in urine samples as a reliable biomarker of acute kidney injury (AKI). *Biomarkers* **20**, 453–459. https://doi.org/10.3109/1354750X.2015.1096305 (2015).
42. Perez-Villalva, R. *et al.* HSP72 is an early biomarker to detect cisplatin and acetaminophen nephrotoxicity. *Biomarkers* **22**, 548–556. https://doi.org/10.1080/1354750X.2017.1315616 (2017).
43. Reddy, M. A. & Natarajan, R. Recent developments in epigenetics of acute and chronic kidney diseases. *Kidney Int.* **88**, 250–261. https://doi.org/10.1038/ki.2015.148 (2015).
44. Ronco, C., Bellomo, R. & Kellum, J. A. Acute kidney injury. *Lancet* **394**, 1949–1964. https://doi.org/10.1016/S0140-6736(19)32563-2 (2019).
45. Mehta, R. L. *et al.* International society of nephrology's 0by25 initiative for acute kidney injury (zero preventable deaths by 2025): a human rights case for nephrology. *Lancet* **385**, 2616–2643. https://doi.org/10.1016/S0140-6736(15)60126-X (2015).
46. Basile, D. P. Rarefaction of peritubular capillaries following ischemic acute renal failure: a potential factor predisposing to progressive nephropathy. *Curr. Opin. Nephrol. Hypertens.* **13**, 1–7 (2004).
47. Rius, J. *et al.* NF-kappaB links innate immunity to the hypoxic response through transcriptional regulation of HIF-1alpha. *Nature* **453**, 807–811. https://doi.org/10.1038/nature06905 (2008).
48. Iommarini, L., Porcelli, A. M., Gasparre, G. & Kurelac, I. Non-canonical mechanisms regulating hypoxia-inducible factor 1 alpha in cancer. *Front Oncol.* **7**, 286. https://doi.org/10.3389/fonc.2017.00286 (2017).
49. Liu, Y., Cox, S. R., Morita, T. & Kourembanas, S. Hypoxia regulates vascular endothelial growth factor gene expression in endothelial cells. Identification of a 5' enhancer. *Circ. Res.* **77**, 638–643. https://doi.org/10.1161/01.res.77.3.638 (1995).
50. Pugh, C. W. & Ratcliffe, P. J. Regulation of angiogenesis by hypoxia: role of the HIF system. *Nat. Med.* **9**, 677–684. https://doi.org/10.1038/nm0603-677 (2003).
51. Semenza, G. L. Hydroxylation of HIF-1: oxygen sensing at the molecular level. *Physiol. Bethesda* **19**, 176–182. https://doi.org/10.1152/physiol.00001.2004 (2004).
52. Yu, X. *et al.* The balance of beneficial and deleterious effects of hypoxia-inducible factor activation by prolyl hydroxylase inhibitor in rat remnant kidney depends on the timing of administration. *Nephrol. Dial. Trans.* **27**, 3110–3119 (2012).
53. Basile, D. P. *et al.* Impaired endothelial proliferation and mesenchymal transition contribute to vascular rarefaction following acute kidney injury. *Am. J. Physiol. Ren. Physiol.* **300**, F721–F733 (2011).
54. Basile, D. P., Fredrich, K., Chelladurai, B., Leonard, E. C. & Parrish, A. R. Renal ischemia reperfusion inhibits VEGF expression and induces ADAMTS-1, a novel VEGF inhibitor. *Am. J. Physiol. Ren. Physiol.* **294**, F928–F936 (2008).
55. Leonard, E. C., Friedrich, J. L. & Basile, D. P. VEGF-121 preserves renal microvessel structure and ameliorates secondary renal disease following acute kidney injury. *Am. J. Physiol. Ren. Physiol.* **295**, F1648–F1657 (2008).
56. Pisani, F. *et al.* Potential role of the methylation of VEGF gene promoter in response to hypoxia in oxygen-induced retinopathy: beneficial effect of the absence of AQP4. *J. Cell Mol. Med.* **22**, 613–627. https://doi.org/10.1111/jcmm.13348 (2018).
57. Sundrani, D. P. *et al.* Differential placental methylation and expression of VEGF, FLT-1 and KDR genes in human term and preterm preeclampsia. *Clin. Epigenet.* **5**, 6. https://doi.org/10.1186/1868-7083-5-6 (2013).
58. Siddique, A. N. *et al.* Targeted methylation and gene silencing of VEGF-A in human cells by using a designed Dnmt3a-Dnmt3L single-chain fusion protein with increased DNA methylation activity. *J. Mol. Biol.* **425**, 479–491. https://doi.org/10.1016/j.jmb.2012.11.038 (2013).
59. Shinagawa, M. *et al.* C/EBPbeta regulates Vegf gene expression in granulosa cells undergoing luteinization during ovulation in female rats. *Sci. Rep.* **9**, 714. https://doi.org/10.1038/s41598-018-36566-y (2019).
60. Lando, D., Peet, D. J., Whelan, D. A., Gorman, J. J. & Whitelaw, M. L. Asparagine hydroxylation of the HIF transactivation domain a hypoxic switch. *Science* **295**, 858–861. https://doi.org/10.1126/science.1068592 (2002).
61. Mahon, P. C., Hirota, K. & Semenza, G. L. FIH-1: a novel protein that interacts with HIF-1alpha and VHL to mediate repression of HIF-1 transcriptional activity. *Genes Dev.* **15**, 2675–2686. https://doi.org/10.1101/gad.924501 (2001).
62. Schmidlin, C. J., Dodson, M. B., Madhavan, L. & Zhang, D. D. Redox regulation by NRF2 in aging and disease. *Free Radic. Biol. Med.* **134**, 702–707. https://doi.org/10.1016/j.freeradbiomed.2019.01.016 (2019).
63. Soofi, A., Kutschat, A. P., Azam, M., Laszczyk, A. M. & Dressler, G. R. Regeneration after acute kidney injury requires PTIP-mediated epigenetic modifications. *JCI Insight* https://doi.org/10.1172/jci.insight.130204 (2020).
64. Institute of Laboratory Animal Resources (U.S.). Committee on care and use of laboratory animals. In *NIH Publication Volumes* (U.S. Dept. of Health and Human Services, Public Health Service, Bethesda, Md.).
65. Han, L., Su, B., Li, W. H. & Zhao, Z. CpG island density and its correlations with genomic features in mammalian genomes. *Genome Biol.* **9**, R79. https://doi.org/10.1186/gb-2008-9-5-r79 (2008).
66. Valdes-Quezada, C., Arriaga-Canon, C., Fonseca-Guzman, Y., Guerrero, G. & Recillas-Targa, F. CTCF demarcates chicken embryonic alpha-globin gene autonomous silencing and contributes to adult stage-specific gene expression. *Epigenetics* **8**, 827–838. https://doi.org/10.4161/epi.25472 (2013).

Acknowledgements

We are grateful to Mariela Contreras´s staff for their aid with animal care. The results presented in this paper have not been published previously in whole or in part, except as an abstract presented at the American Society of Nephrology Kidney Week Meeting 2016 (Chicago. IL), and World Congress of Nephrology ISN 2017 (Mexico City, Mexico).

Author contributions

Conception and design A.S.N. and N.A.B. Performed the experiments and analytical techniques A.S.N., R.P.V., A.R.M.O., M.A.M.R., J.R.R.A., N.G. and M.C.B. Acquisition of data: A.S.N., and N.A.B. Analysis and interpretation of data; N.A.B., A.S.N. and F.R.T. Drafting the article and revising it critically for important intellectual content; N.A.B., A.S.N., F.R.T. and G.G.

Funding

This study was supported by Grants from the Mexican Council of Science and Technology (CONACyT) (A1-S-8715, 300151, 235855, and 235964 to NAB) and from the Universidad Nacional Autónoma de México (IN201619 to NAB). This study was performed in partial fulfillment of the requirements for the PhD degree, Andrea Sánchez-Navarro is a doctoral student from Programa de Doctorado en Ciencias Biomédicas, Universidad Nacional Autónoma de México (UNAM) and received a fellowship from CONACYT (607517).

Competing interests

The authors declare no competing interests.

Additional information

Supplementary Information The online version contains supplementary material available at https://doi.org/10.1038/s41598-021-88000-5.

Correspondence and requests for materials should be addressed to N.A.B.

Reprints and permissions information is available at www.nature.com/reprints.

Publisher's note Springer Nature remains neutral with regard to jurisdictional claims in published maps and institutional affiliations.

6.2 ARTÍCULO 2 https://pubmed.ncbi.nlm.nih.gov/34291592/

Resumen de los resultados de los mecanismos clave iniciales involucrados en la ERC inducida por obesidad, publicados en la revista Physiological Reports, Jul;9(14): e14937, 2021, correspondientes al objetivo 3.

La mayoría de los modelos murinos de obesidad en los que se induce daño renal utilizan alimentos ricos en calorías, donde la grasa representa el 60% del aporte calórico total, sin embargo, esta estrategia duplica la proporción estándar de ingestión de grasas en pacientes obesos. Por lo tanto, es crucial estudiar el impacto de una ingesta alta en grasas en la fisiología renal que se asemeja a la obesidad común en humanos para comprender los mecanismos desencadenantes de las consecuencias renales a largo plazo del sobrepeso y la obesidad.

En este estudio, analizamos si la alimentación crónica con una dieta moderadamente alta en grasas (MHFD) que representa el 45% de las calorías totales, puede inducir daño funcional y estructural del riñón en comparación con los ratones C57BL/ 6 alimentados con una dieta de control. Después de 14 semanas, MHFD indujo obesidad significativa en ratones. A nivel funcional, los ratones obesos mostraron signos de lesión renal caracterizados por un aumento del cociente albuminuria/creatinina y una mayor excreción de biomarcadores urinarios de daño renal. Mientras que, a nivel estructural, se observó hipertrofia glomerular. Aunque no detectamos fibrosis renal, los ratones obesos exhibieron una elevación significativa de los niveles de RNAm de *Tgfb1*. El daño renal causado por la exposición a MHFD se asoció con un mayor estrés oxidante, inflamación renal, mayor estrés en el retículo endoplásmico (RE) y alteración de la dinámica mitocondrial.

En resumen, nuestros datos demuestran que la obesidad inducida por una dieta de menor contenido en grasa es suficiente para establecer daño renal, donde el estrés oxidativo, la inflamación, el estrés ER y el daño mitocondrial cobran relevancia, señalando la importancia de llevar a cabo intervenciones oportunas para evitar las consecuencias de la obesidad y el síndrome metabólico a largo plazo.

Received: 27 April 2021 | Accepted: 4 May 2021

DOI: 10.14814/phy2.14937

ORIGINAL ARTICLE

Physiological Reports

Early triggers of moderately high-fat diet-induced kidney damage

Andrea Sánchez-Navarro[1,2] | **Miguel Ángel Martínez-Rojas**[1,2] | **Rebecca I. Caldiño-Bohn**[1,2] | **Rosalba Pérez-Villalva**[1,2] | **Elena Zambrano**[3] | **Diana C. Castro-Rodríguez**[3,4] | **Norma A. Bobadilla**[1,2]

[1]Molecular Physiology Unit, Instituto de Investigaciones Biomédicas, Universidad Nacional Autónoma de México, Mexico City, Mexico

[2]Department of Nephrology, Instituto Nacional de Ciencias Médicas y Nutrición, Salvador Zubirán, Mexico City, Mexico

[3]Department of Biology of Reproduction, Instituto Nacional de Ciencias Médicas y Nutrición, Salvador Zubirán, Mexico City, Mexico

[4]CONACyT-Cátedras, Mexico City, Mexico

Correspondence
Norma A. Bobadilla, Unidad de Fisiología Molecular, Vasco de Quiroga No. 15, Tlalpan, 14080, Mexico City, Mexico.
Emails: nab@biomedicas.unam.mx; norma.bobadillas@incmnsz.mx

Funding information
This project was supported by grants from the Mexican Council of Science and Technology (CONACyT) (235855, 000000000300151, and A1-S-8715 to NAB), from the Universidad Nacional Autónoma de México (IN223915 and IN201619 to NAB) and from Consejo Nacional de Ciencia y Tecnología-Secretaría de Educación Pública (CONACyT-SEP) (287912 to EZ). This study was performed in partial fulfillment of the requirements for the PhD degree, Andrea Sánchez-Navarro is a doctoral student from Programa de Doctorado en Ciencias Biomédicas, Universidad Nacional Autónoma de México (UNAM) and received a fellowship 607517 from CONACYT.

Abstract

Most of the obesity murine models inducing renal injury use calorie-enriched foods, where fat represents 60% of the total caloric supply, however, this strategy doubles the standard proportion of fat ingestion in obese patients. Therefore, it is crucial to study the impact of a high-fat intake on kidney physiology that resembles common obesity in humans to understand the trigger mechanisms of the long-term consequences of overweight and obesity. In this study, we analyzed whether chronic feeding with a moderately high fat diet (MHFD) representing 45% of total calories, may induce kidney function and structural injury compared to C57BL/6 mice fed a control diet. After 14 weeks, MHFD induced significant mice obesity. At the functional level, obese mice showed signs of kidney injury characterized by increased albuminuria/creatinine ratio and higher excretion of urinary biomarkers of kidney damage. While, at the structural level, glomerular hypertrophy was observed. Although, we did not detect renal fibrosis, the obese mice exhibited a significant elevation of *Tgfb1* mRNA levels. Kidney damage caused by the exposure to MHFD was associated with greater oxidative stress, renal inflammation, higher endoplasmic reticulum (ER)-stress, and disruption of mitochondrial dynamics. In summary, our data demonstrate that obesity induced by a milder fat content diet is enough to establish renal injury, where oxidative stress, inflammation, ER-stress, and mitochondrial damage take relevance, pointing out the importance of opportune interventions to avoid the long-term consequences associated with obesity and metabolic syndrome.

KEYWORDS

ER-stress, glomerular hypertrophy, mitochondrial dynamics disruption, renal inflammation

1 | INTRODUCTION

The global overweight/obesity epidemic has worsened in the last decades, it has nearly tripled since 1975, affecting more than 1.9 billion adults and 350 million children in 2016, which has resulted in an increase in obesity-related health complications with a significant impact on the economic burden of disease and mortality, accounting for 4 million deaths globally, most of them related to cardiovascular disease (Collaborators et al., 2017; Ogden et al., 2014; Tsuboi et al., 2017; Wang et al., 2008).

The higher cost of a balanced diet may explain why many families around the world face food insecurity and have a higher risk of developing overweight or obesity (Popkin et al., 2012). People choose less expensive foods that often have a high caloric density and low nutrient content, this has not only been reported in low- and middle-income countries, but also in high-income countries (FAO I, UNICEF, WFP, & WHO, 2020). It is well known that obesity predisposes to many cardiometabolic diseases, including type 2 diabetes mellitus (T2D), hypertension (HTN), chronic kidney disease (CKD), fatty liver disease, and several types of cancer, among others (Bluher, 2019; Eknoyan, 2011; Kovesdy et al., 2017; Tsuboi et al., 2017). In numerous large population-based studies, having a higher body mass index (BMI) was associated with the reduction of estimated glomerular filtration rate (eGFR) (Chang et al., 2018; Foster et al., 2008; Pinto-Sietsma et al., 2003; Tsuboi et al., 2017). In fact, when considering that the main causes of CKD are all related to high-BMI states, we can highlight the impact of overweight and obesity in kidney health (Camara et al., 2017). The relationship between obesity and kidney damage is multifactorial and bidirectional, involving insulin resistance, hyperlipidemia, increased renin-angiotensin-aldosterone system activity, oxidative stress, chronic inflammation and mitochondrial dysfunction (Kovesdy et al., 2017; Takagi et al., 2018).

In most models of murine obesity in which kidney abnormalities have been reported, animals have free access to high-calorie foods, where fat represents 60% of the total caloric intake, which is known as a high-fat diet (HFD) and the follow-up fluctuates between 12 and 34 weeks (Borgeson et al., 2017; Cheng et al., 2019; Kim et al., 2019; Luo et al., 2019; Pereira et al., 2020; Saito et al., 2019; Szeto et al., 2016; Xu et al., 2019; Yamamoto et al., 2017). Although this strategy leads effectively to the establishment of obesity in rodents and is capable of reproducing many of the multi-organ alterations known in humans, it doubles the typical proportion of fat ingestion in obese patients (Botchlett & Wu, 2018). More realistic diets that resemble different degrees of obesity in humans are crucial to understand the trigger mechanisms of the long-term consequences of overweight and obesity. Unfortunately, very little is known about calorie-enriched foods containing a lesser content of fat on renal function in mice.

There is evidence that C57BL/6 mice fed with a diet containing 60% of fat for at least 12 weeks develop renal functional alterations like glomerular hyperfiltration and increased urinary excretion of albumin, as well as structural injury such as: glomerulopathy, podocytopathy and vacuolization of the tubular epithelium (Borgeson et al., 2017; Cheng et al., 2019; Kim et al., 2019; Luo et al., 2019; Pereira et al., 2020; Saito et al., 2019; Szeto et al., 2016; Xu et al., 2019; Yamamoto et al., 2017). These functional and structural abnormalities have been associated with increased reactive oxygen species (ROS) (Borgeson et al., 2017), endoplasmic reticulum stress (Li et al., 2019a), and more recently with disruption of mitochondrial homeostasis (Sun et al., 2020; Yamamoto et al., 2017). Since most of these studies have used the typical HFD, we decided to study the impact of chronic feeding of male C57BL/6 mice with a moderately high fat diet (MHFD) on kidney function and structure. We consider that this model resembles more accurately what happens to people with overweight, which is relevant in order to identify early pathophysiological events and find possible targets to prevent CKD development. We found that renal inflammation, oxidative stress, altered balance of mitochondrial fission/fusion, and endoplasmic reticulum stress (ER-stress) are induced by feeding a MHFD in the mice for a relatively short period, showing deleterious outcomes of a moderate fat consumption in promoting renal injury.

2 | METHODS

All experiments involving animals were conducted in accordance with the NIH Guide for the Care and Use of Laboratory Animals (https://grants.nih.gov/grants/olaw/guide-for-the-care-and-use-of-laboratory-animals.pdf) and with the Mexican Federal Regulation for animal reproduction, care, and experimentation (NOM-062-ZOO-2001). The Animal Care Committee at Instituto Nacional de Ciencias Médicas y Nutrición Salvador Zubirán approved our experimental study.

2.1 | Experimental protocol

Male C57BL/6 mice (Charles River Laboratories International, Inc.) aged 5–6 weeks and weighing 17–22 g were maintained in controlled conditions of temperature and humidity in our animal housing facility with 12:12 h day/night cycle, with free access to water and food. We did not use a method to generate the randomization sequence, the mice were only randomly assigned into two groups of at least 10 mice per group, as follows: (1) control mice fed with a control diet (C) and (2) obese mice (OB) fed with a moderately high fat diet (MHFD). The sample size

was calculated according to the percentage of success and error test (Dell et al., 2002). The study was not blinded because no pharmacological intervention was carried out. All mice fill out our inclusion criteria and none was excluded. Both groups were follow-up for 14 weeks. The experimental diets were homemade, as was previously reported by Castro-Rodríguez et al. control diet contained 22.0% protein, 5.0% vegetable fat (corn oil), 31.0% polysaccharide, 31.0% simple sugars, 4.0% fiber, 6.0% minerals and 1.0% vitamins (w/w), and energy 4.0 kcal/g, in which fat represents 11.3% of caloric supply (Zeigler Rodent RQ 22–5). The MHFD contained 23.5% protein, 20.0% lard, 5.0% vegetable fat (corn oil), 20.2% polysaccharide, 20.2% simple sugars, 5.0% fiber, 5.0% minerals, 1.0% vitamins (w/w), and energy 4.9 kcal/g, where fat represents 45% of total caloric supply (Castro-Rodriguez et al., 2020). Body weight was measured weekly and daily food consumption was recorded.

At the end of the experimental period, urine samples were collected over a 24-h period in metabolic cages. Then, mice were anesthetized with sodium pentobarbital (30 mg/kg) to obtain blood samples by cardiac puncture. A slide of the kidney was fixed in paraformaldehyde 4% for histopathological analysis and both kidneys were weighed and preserved in liquid nitrogen (−80ºC) until analysis.

Urinary creatinine concentration was measured with the Quantichrom creatinine assay kit (DICT-500).

2.2 | Metabolic parameters and body composition

Analysis of body composition was performed in 6 animals per group using a 4- in-1 small animal MRI (Echo Medical Systems). Serum analysis of glucose, triglycerides, and cholesterol were determined enzymatically with a SynchronCX auto analyzer (Beckman Coulter).

2.3 | Hydrogen peroxide urinary excretion

The determination of urinary hydrogen peroxide as an oxidative stress marker was carried out, using a commercial kit (Amplex Red Hydrogen Peroxide/Peroxidase Assay, Roche, cat. no. A22188) following the manufacturer's instructions.

2.4 | Albuminuria excretion

As a marker of kidney damage, urinary albumin concentration was analyzed by using a commercial kit Albuwell M (Exocell Inc., cat. no. 1011) following the manufacturer's instructions. This assay is a competitive ELISA completed in a direct mode, consisting of mouse-specific albumin recognition by the provided horseradish peroxidase-conjugated antibody, absorbance spectrophotometry, and concentration estimation using linear regression of a standard curve, and were normalized by urinary creatinine (UCr).

2.5 | Detection of urinary biomarkers by Western Blot

Using Western blot technique, urinary HSP72 (Barrera-Chimal et al., 2011; Morales-Buenrostro et al., 2014; Ortega-Trejo et al., 2015; Perez-Villalva et al., 2017), KIM-1 (Perez-Rojas et al., 2007; Vaidya et al., 2005, 2006), and SerpinA3K (Sanchez-Navarro et al., 2019) levels were detected in the diluted urine (1:10 in 0.9% saline solution) as follows: 10 µl of each dilution was loaded and resolved in 8.5% SDS-PAGE. A mouse anti-HSP72 (ENZO Life Sciences, cat. no. ADI-SPA-819F 1:5000 dilution), anti-KIM-1 (Boster, cat. no. PA1632, 1:5000) or anti-SerpinA3K antibody (Proteintech, cat. no. 55480-1-AP, 1:1000) was incubated overnight at 4℃. Thereafter, membranes were incubated with a secondary antibody, HRP-conjugated goat anti-mouse IgG or anti-rabbit IgG, respectively (Santa Cruz, cat. no. sc-2031 and sc-2004, respectively 1:5000). The proteins were detected using a commercial chemiluminescence kit (Millipore, Cat. No. WBKLS0500) and were normalized by urinary creatinine (UCr).

2.6 | Western Blot and antibodies

The renal proteins were homogenized with a lysis buffer containing: 50 mM HEPES pH 7.4, 250 mM NaCl, 5 mM EDTA, 0.1% NP-40 and complete protease inhibitor (Roche, cat. no. 11697498001). The proteins concentration was assessed by Lowry protein assay (Bio-Rad, Cat. No. 5000113 and 5000114). Renal protein levels were detected by Western blot, tissue proteins (20 µg) were electrophoresed in a denaturing 8.5% acrylamide gel with SDS. The membranes were incubated with the primary antibody IL-6 (Santa Cruz, cat. no. sc57315, 1:1000), BiP-1 (Cell Signaling, cat. no. 3177, 1:1000), CHOP (Cell Signaling, cat. no. 2895, 1:5000), FOXO3 (Santa Cruz, cat. no. sc11351, 1:5000), Mitofusin-1+Mitofusin-2 (Abcam, cat. no. ab57602, 1:1000), Drp1 (Santa Cruz, cat. no. sc-271583, 1:1000) and HRP β-Actin antibody [AC-15] (Abcam, cat. no. ab49900, 1:1,000,000) overnight at 4℃. Three of 10-min washes were performed with TBS-1x Tween, and then incubated with a secondary antibody coupled to HRP, anti-rabbit or anti-mouse IgG (Santa Cruz, cat. no. sc-2031 or sc-2004, respectively 1:5000). Tissue proteins assessed by Western blot were normalized by β-actin detection.

2.6.1 | RNA extraction and quantitative PCR

Total RNA was isolated from whole kidneys using the TRIzol method (Invitrogen, cat. no. 15596026) and RNA integrity was evaluated using 1% agarose gel electrophoresis, to analyze rRNA. To avoid DNA contamination, total RNA samples were treated with DNase (DNase I; Invitrogen, cat. no. 18068015). Reverse transcription (RT) was carried out with 1 μg of total RNA and 200 U of Moloney murine leukemia virus reverse transcriptase (Invitrogen, cat. no. 18064022). The mRNA levels of Interleukin 6 (*Il-6*), tumor necrosis factor alpha (*Tnfa*), interleukin 10 (*Il10*), transforming growth factor (*Tgfb1*) vascular endothelial growth factor (*Vegfa*), catalase (*Cat*), superoxide dismutase (*Sod2*) and glutathione peroxidase 1 (*Gpx1*) were quantified by real-time PCR on an ABI Prism 7300 Sequence Detection System (TaqMan, ABI, Foster City, CA, cat. no. 4331182). Probes were ordered as follows: *Il*6 (Mm00446190_m1), *Tnfa* (Mm0443258_m1), *Il10* (Mm01288386_m1), *Tgfb1* (Mm03024053_m1), *Vegfa* (Rn01511602_m1), *Cat* (Mm00437992_m1), *Sod2* (Mm01313000_m1) and *Gpx1* (Mm00656767_g1). As an endogenous control, eukaryotic *18S* rRNA (predesigned assay reagent Applied by ABI, external run, Rn03928990_g1, Cat. No. 4319413E) was used. The relative quantification of each gene expression was performed using the comparative threshold cycle (Ct) method.

2.6.2 | Histopathological analysis

After tissue fixation, the kidneys were dehydrated and embedded in paraffin. Renal slices of 4 μm were obtained and stained with Periodic Acid Schiff (PAS). Twelve high-power fields (Magnification 200×) were captured from the renal cortex of each kidney to ensure the presence of at least 12 glomeruli per kidney using a camera incorporated onto the microscope. The glomerulus size was evaluated by measuring glomerular area in each captured glomerulus per mouse using the NIS-Elements software (Nikon Instruments Inc.). Because glomeruli are spheroidal in shape and in each section of the kidney, each glomerulus can be cut at the lower, upper, or middle pole, the glomerular area was organized by ranks and then the differences between the C and MHDF groups were determined by a contingency analysis, as we have previously reported (Barrera-Chimal et al., 2013, 2018; Garcia-Ortuno et al., 2019; Perez-Rojas et al., 2007). Researchers were blind to the experimental group.

2.6.3 | Statistical analysis

The results are presented as the mean ± SE. The significance of the differences between groups was assessed by unpaired *t*-test. All comparisons passed the normality test. The differences in the ranks of glomerular area among the groups were evaluated by contingency analysis, and the differences were assessed using the chi-squared test with Yates correction. Statistical significance was defined when the p value was <0.05. All the graphs and statistical analyses were performed using the statistical GraphPad Prism 8 software for Mac (GraphPad Software).

3 | RESULTS

3.1 | Overweight and renal damage induced by a MHFD

The experimental group was fed with a MHFD for fourteen weeks. We observed that the MHFD group exhibited an increase in body weight (BW) by 48% compared to the control group (Figure 1a), without changes in the kidney weight (KW) (Figure 1b). In addition, no statistical difference was observed in the ratio kidney weight g/lean % (0.0034 ± 0.0002 vs. 0.0026 ± 0.0003, respectively, p = NS). However, the ratio kidney/body weight (KW/BW) was reduced (Figure 1c). We also observed that the MHFD group had decreased urine output (Figure 1d).

In Table S1 (https://figshare.com/s/753eb0b268daba362bf6) (https://doi.org/10.6084/m9.figshare.14224199) appears the corporal composition and metabolic parameters for the studied groups. Serum glucose and cholesterol levels were significantly increased by 35.6% and 45.1%, respectively in the MHDF group. In the MHFD group there was an increase in fat tissue percentage compared to the control group (33.6% vs. 8.4%, respectively). Similarly, the visceral adipose tissue was greater in the MHFD than in the C group (2.9 vs. 0.4 g, respectively). These alterations resulted in a reduction in lean tissue percentage in the MHDF compared to the control group (66.2% vs. 91.2%, respectively). At the end of the study, the MHFD group exhibited mild metabolic dysfunction characterized by a significant increase in serum glucose and in cholesterol, without changes in triglycerides levels.

Renal dysfunction induced by MHFD was evaluated by albuminuria/UCr (Figure 2a) and urinary biomarkers of kidney injury: HSP72 (Figure 2b), KIM-1 (Figure 2c), and serpinA3K (Figure 2d). The HFD group exhibited a significant increase in albuminuria/UCr compared to the C group (0.048 vs. 0.004, respectively). In accordance with these results a significant increase in UHSP72, UKIM-1 and UserpinA3K was observed in the MHFD group by 2.1, 3.7 and 1.9-fold, respectively, compared to the control group.

Because hyperfiltration and glomerular injury are associated with albuminuria in obese subjects (D'Agati et al., 2016), we quantified glomerular area in at least 12

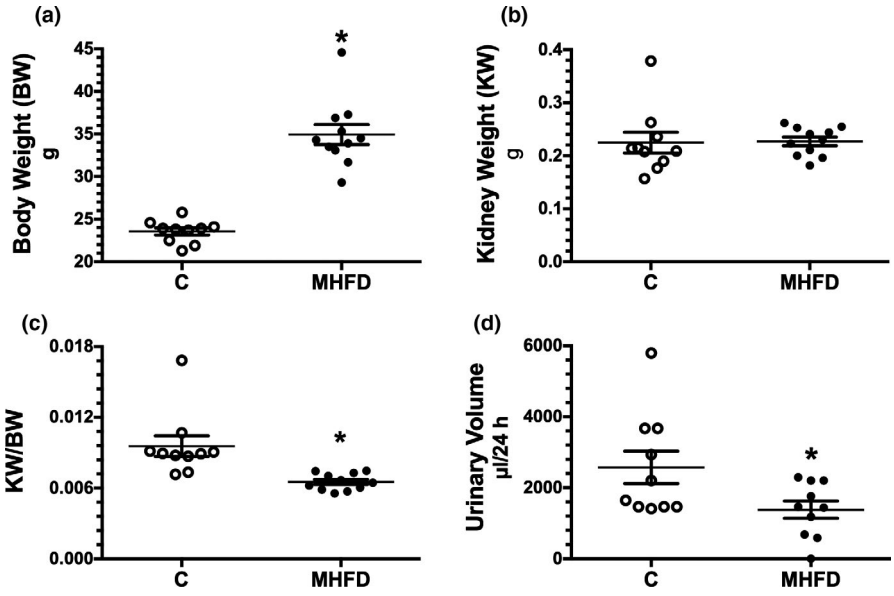

FIGURE 1 Physiological parameters induced by a MHFD at the end of the study. (a) Body weight (BW) and (b) kidney weight (KW) (g), respectively. (c) Kidney weight/body weight ratio (KW/BW). (d) urinary volume (µl/24 h). The group fed with a control diet (c) is represented in white circles, while the MHFD group in black circles, $n = 10/11$ per group, respectively for (a), (b), (c) and $n = 10$ per group for (d). Lines stated in each group represent the mean ± SE. *$p < 0.05$ versus the C group assessed by unpaired *t*-test

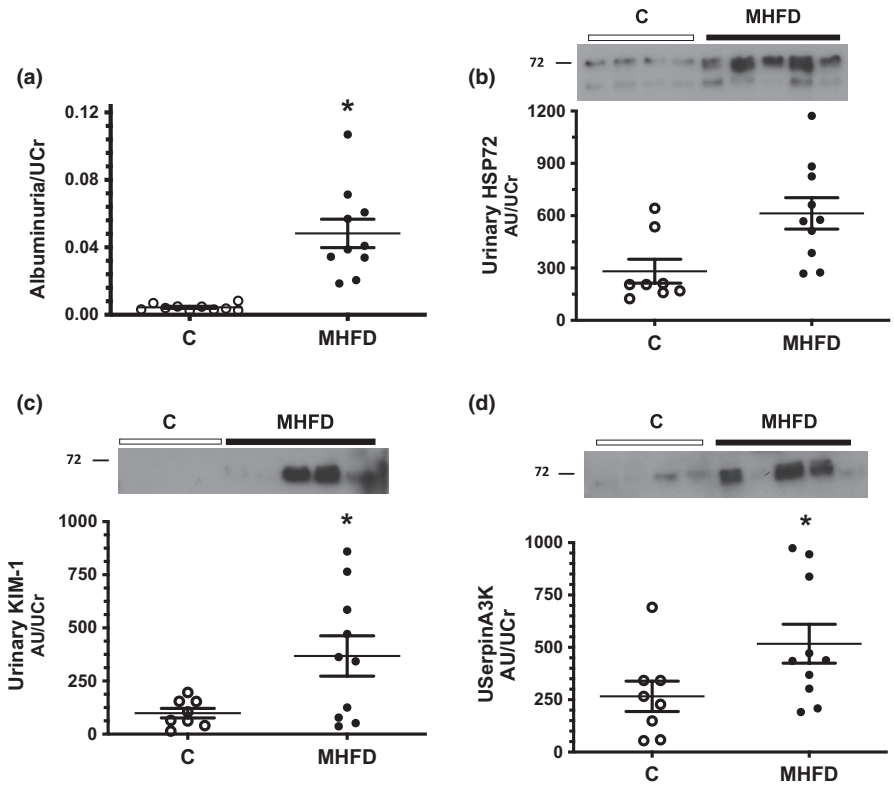

FIGURE 2 Kidney biomarkers of renal injury. (a) Albuminuria/UCr evaluated by ELISA (µg/ml). (b, c, and d) Urinary HSP72, urinary KIM-1, and urinary SerpinA3K respectively, detected by WB analysis and corrected by urinary creatinine (AU/UCr), in these graphs insets of representative blots are included. The group fed a control diet (C) is represented in white circles, while the MHFD group in black circles, $n = 8/10$ per group, respectively for (b), (c), (d) and $n = 10$ per group for (a). Lines reflect mean ± SE. *$p < 0.05$ versus the C group assessed by unpaired *t*-test

glomeruli of each mouse. In seven ranges, the glomerular areas were distributed, the percentage in each range was calculated and the statistical differences between the C and MHDF groups were analyzed by contingency analysis (Figure 3). Interestingly we found a higher proportion of large glomeruli (>3200 µm^2) in the kidney microphotographs from obese mice, whereas the C group exhibited a normal distribution in the glomerular areas, where most of the glomeruli were between 2001 and 2400 µm^2 (Figure 3b), indicating that glomerular hypertrophy is part of the renal structural abnormalities in our model. To address the establishment of chronic kidney disease, we also evaluated fibrotic area using Sirius Red stain, as a final common pathway of chronic kidney injury; however, we did not find extracellular matrix (ECM) expansion in any of the obese mice compared to the C group (Figure 3e,f). These results indicated that mice fed with a MHFD exhibited clear signs of early renal injury.

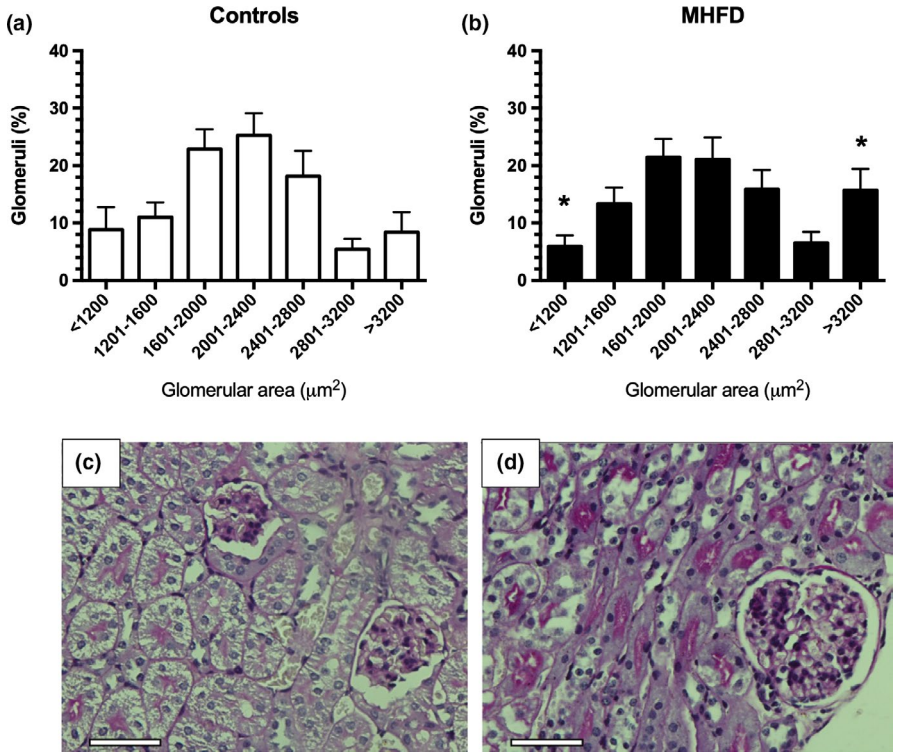

FIGURE 3 Glomerular hypertrophy induced by MHFD. (a,b) Glomerular area distribution along seven ranks are represented in white bars for the control diet group (a), and in black for MHFD group (b). (c,d) Representative micrographs staining with PAS showing glomerular hypertrophy induced by MHFD. Scale bar 50 μm (Original magnification 200×). *$p < 0.01$ versus the C group assessed by a contingency analysis

3.2 | Mice fed a MHFD exhibited renal inflammation, oxidative stress and ER-stress

Obese mice fed a MHFD exhibited inflammation as is shown by the increase in interleukin-6 (*Il6*) mRNA (Figure 4a) and protein levels (Figure 4b), as well as by the increase in *Tnfa* mRNA levels (Figure 4c), and a significant reduction were observed in the anti-inflammatory cytokine: interleukin-10 (*Il10*) (Figure 4d). Interestingly, transforming growth factor β (*Tgfb1*) mRNA levels were significantly increased in the kidney of obese mice (Figure 4e). In addition, significant increase of vascular endothelial growth factor (*Vegf*) mRNA levels was observed in the HFD group compared to the C group (Figure 4f).

Oxidative stress was indirectly evaluated by urinary hydrogen peroxide levels (Urinary H_2O_2) and by antioxidant enzymes mRNA levels. Urinary H_2O_2 was clearly enhanced in the MHFD group compared to the C group (10.5 ± 2.3 vs. 4.2 ± 0.5 pMol/24 h) (Figure 5a). Although, we did not observe changes in nuclear factor erythroid 2 Like 2 (*Nfe2l2*) mRNA levels between the studied groups (Figure 5b), catalase (*Cat*) mRNA levels were significantly reduced in the MHFD group compared to the C group (Figure 5c), whereas no changes in superoxide dismutase 2 (*Sod2*) or glutathione peroxidase (*Gpx*) mRNA levels were found (Figure 5d,e). We also evaluated the protein levels of FOXO3, because of its critical role in the regulation of metabolism, oxidative stress and hypoxic response, as well as, its role in the cell-cycle (Senf et al., 2011). We found a significant reduction in FOXO3 protein levels in the obese animals, consistent with the oxidative stress found in the MHFD group (Figure 5f).

Additionally, we studied the protein levels of BiP-1 and CHOP involved in ER-stress in response to energetic or cellular stress. A significant increase by almost 2-fold in BiP-1 was observed in the MHFD group compared to the C group (Figure 6a). Similarly, a higher increase by 2.5-fold was found in CHOP expression in the MHFD group compared to the C group (Figure 6b).

3.3 | Obese mice exhibited disruption of mitochondrial dynamics

Finally, we evaluated the mitochondrial dynamics by analyzing the protein levels of Mitofusin-1+Mitofusin-2 (Mfn1/2) and Dynamin-related Protein-1 (Drp1) by western blot, as subrogates of mitochondrial damage. We found a significant increase in Drp1 protein levels (Figure 7a), whereas Mfn1/2, a basic component of the mitochondrial outer membrane fusion machinery, did not change (Figure 7b). Nevertheless, we found an increased Drp1-to-Mfn1/2 expression ratio in the animals fed a MHFD (Figure 7c). These results reflect the increased mitochondrial fragmentation and damage, that could be related to the oxidative and ER-stress.

4 | DISCUSSION

In this study, we demonstrated that feeding male mice with a lesser content of fat (45%) for a relatively short period induced relevant renal alterations characterized by a

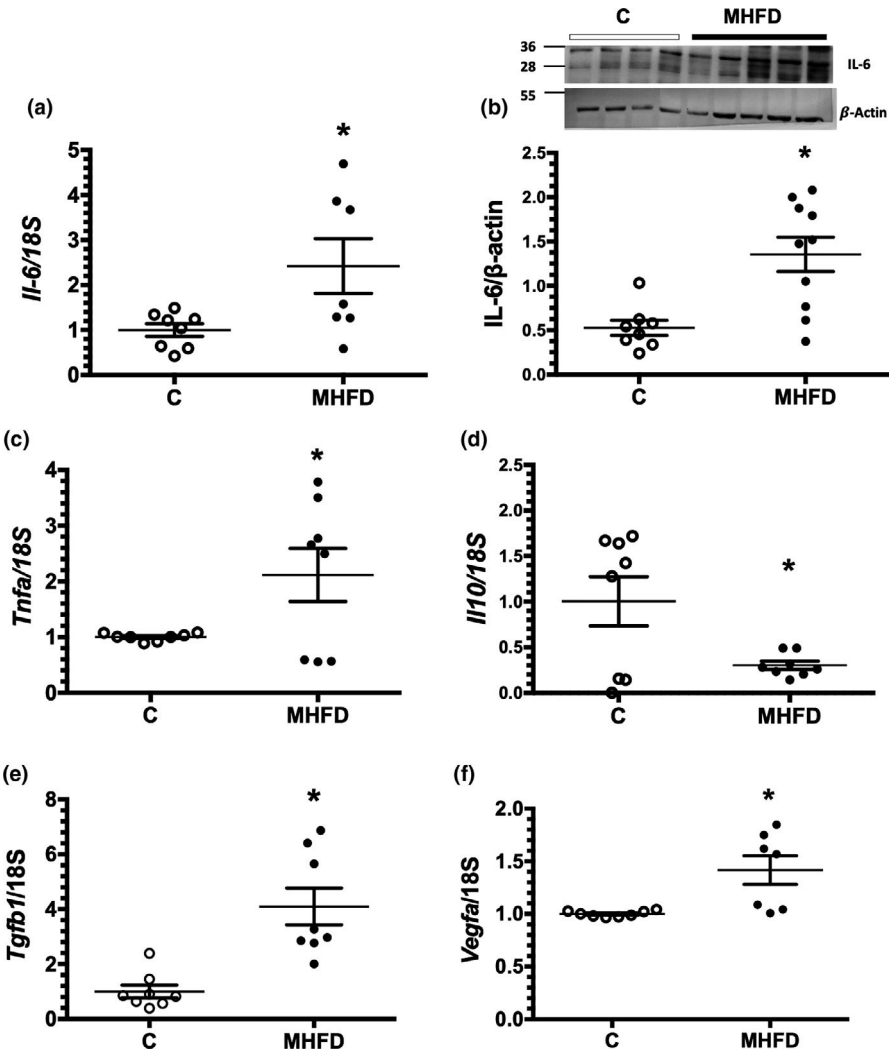

FIGURE 4 Kidney inflammation induced by MHFD. (a) Relative expression of *Il-6* mRNA and (b) Protein levels of IL-6, including a representative blot. (c) Relative expression of *Tnfa* mRNA levels. (d) Relative expression of *Il-10* mRNA levels. (e) Relative expression of *Tgfb1* mRNA levels and (f) Relative expression of *Vegfa* mRNA levels. In the IL-6 detection by WB: the first four samples corresponded to the control group (C) and the remaining five samples are from the MHFD mice and corrected by β-actin. The group fed a control diet (C) is represented in white circles, while the MHFD group in black circles, $n = 8/10$ per group, respectively for (b) and $n = 8$ per group for (a), (c), (d), (e), (f). Lines reflect mean ± SE. $^*p < 0.05$ versus the C group assessed by unpaired *t*-test

significant increase in albuminuria, glomerular hypertrophy, and increased excretion of urinary kidney injury biomarkers (Hsp72, Kim1, and serpinA3), in spite of a discretional metabolic impairment. All these abnormalities were associated with altered balance of mitochondrial fission/fusion, renal inflammation, and increased oxidative and ER-stress.

Despite the efforts that have been made to study the mechanisms involved in the relationship between obesity and renal damage, there is an inadequate understanding of the crucial events that lead to long-term alterations in the kidney. A high-fat diet induces an initial adaptation of mitochondrial bioenergetics to balance the energy supply and demand, in order to optimize nutrient overload and consumption. However, this adaptation is accompanied by a reduced respiratory efficiency, increased proton leakage, ROS generation and increased mito-autophagy (Garrison et al., 2017; Ruggiero et al., 2011). Accordingly, we found that mice fed a MHFD exhibit greater oxidative stress that was evidenced by a significant increase in urinary H_2O_2 excretion and a significant reduction in catalase mRNA levels. In addition, FOXO3 protein levels were reduced in the kidney from the MHFD group, which could contribute to more ROS generation. In this regard, it has been shown that the conditional deletion of FOXO3 exacerbates acute kidney injury (AKI) to CKD transition by reducing epithelial autophagy and lowering SOD2 expression. On the contrary, FOXO3 activation in hypoxic tubules prevents CKD (Li et al., 2019b).

Although we did not measure GFR, the presence of glomerular hypertrophy suggests an increase in intraglomerular pressure (D'Agati et al., 2016), which leads to enhanced solute and fluid delivery along the nephrons, therefore increasing metabolic demand, and possibly contributing to oxidative stress perpetuation. The presence of albuminuria and the increased excretion of tubular injury biomarkers in the MHDF group suggest a deterioration of both, glomerular filtration barrier and tubular epithelium.

Factors associated with obesity, like elevated circulating levels of free fatty acids (FFA) can lead to ER-stress in several tissues. ER is essential for the biosynthesis of proteins, lipid metabolism and regulation of calcium metabolism (Martin-Jimenez et al., 2017). However, the precise mechanisms that lead to ER-stress induced by obesity, is still unknown. Recent evidence suggests that ER-stress is dependent on dysregulation of calcium homeostasis, increased ROS,

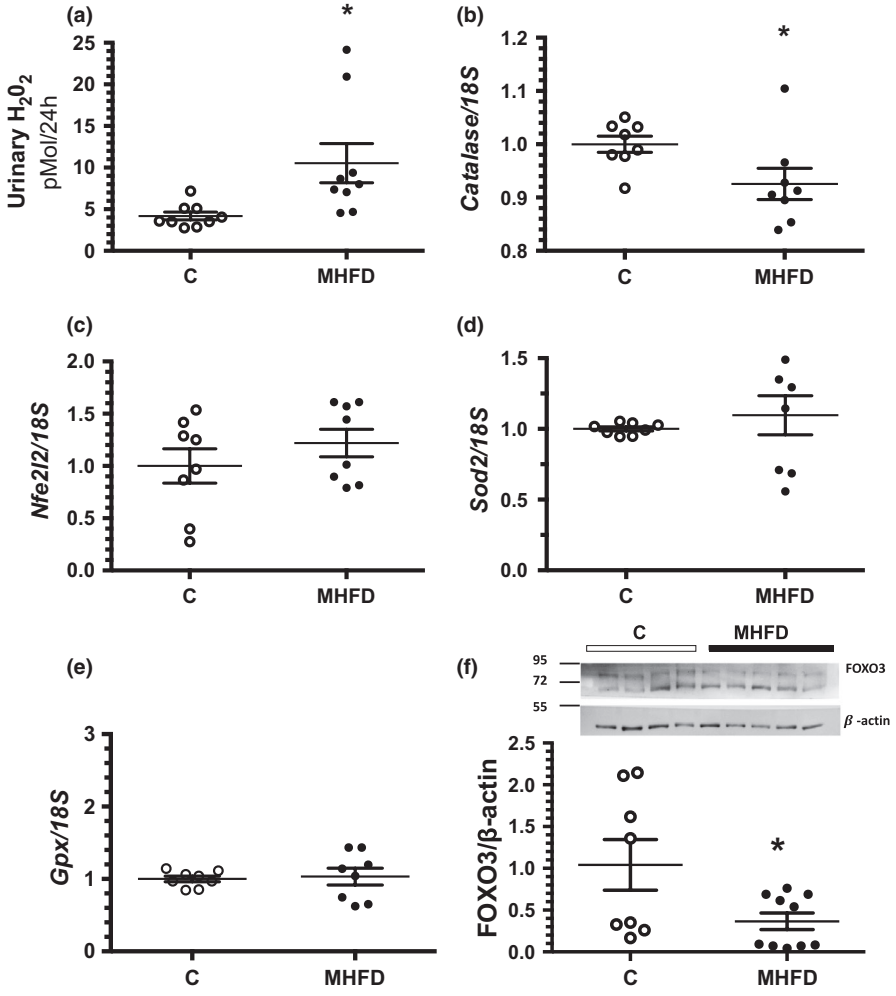

FIGURE 5 Oxidative stress after 14 weeks of MHFD. (a) Urinary Hydrogen Peroxide (Urinary H_2O_2) (b–e) Relative expression of *Catalase*, *Nrfe2l2*, *Sod2*, and *Gpx*, respectively (f) Protein levels of FOXO3 and β-actin detected by WB including the insets of a representative blot. The first four samples correspond to the control group (C) and the remaining five to the MHFD group, the graph represents FOXO3 corrected by β-actin. The group fed a control diet (C) is represented in white circles, while the MHFD group in black circles, $n = 9$ per group for (a); $n = 8$ per group for (b), (c), (d), (e) and $n = 8/10$ per group, respectively for (f). Lines reflect mean ± SE. $^*p < 0.05$ versus the C group assessed by unpaired *t*-test

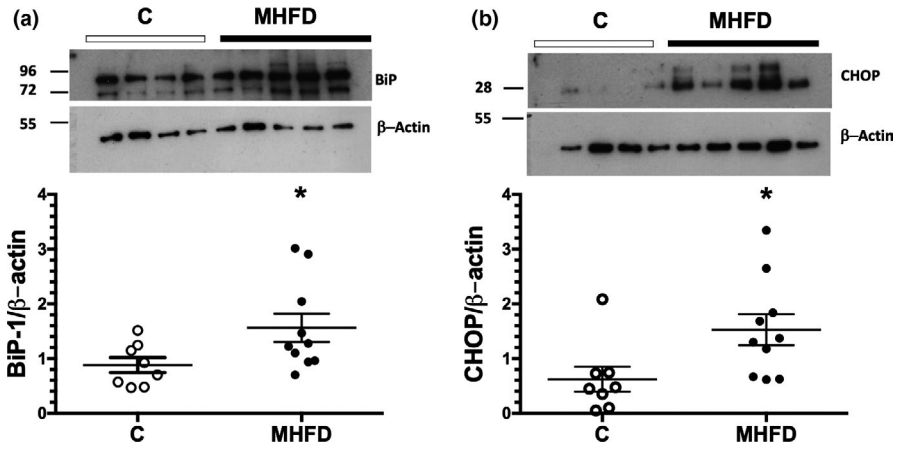

FIGURE 6 Renal endoplasmic reticulum stress induced by a MHFD in the mice. (a) Protein levels of BIP-1 and (b) Protein levels of CHOP, including representative blots. In the WB image inset: the first four samples correspond to the controls (C) and the remaining five to the MHFD mice group and corrected by β-actin. The bars reflect mean ± SE. $^*p < 0.05$ versus control group. The group fed a control diet (C) is represented in white circles, while the MHFD group in black circles, $n = 8/10$ per group, respectively. Lines reflect mean ± SE. $^*p < 0.05$ versus the C group assessed by unpaired *t*-test

and FFA accumulation (Cnop et al., 2012; Martin-Jimenez et al., 2017). In HFD-fed mice, excessive ectopic accumulation of FFA has been demonstrated in several tissues, leading to cellular lipotoxicity, remarkable ER-stress, and an activated unfolded protein response (UPR) (Li et al., 2019a; Tanaka et al., 2012). Indeed, UPR becomes activated with

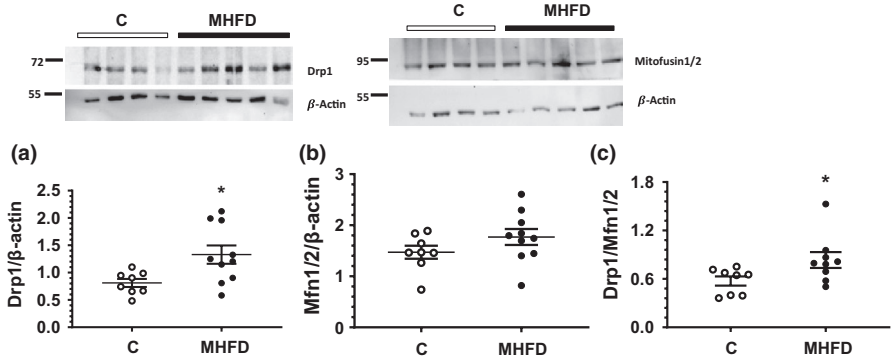

FIGURE 7 Altered balance of mitochondrial fission/fusion in the kidney of MHFD mice. (a) Protein levels of Drp1 and (b) Protein levels of Mitofusin1, including a representative blot. (c) Ratio Drp1/Mitofusin1. In the WB image insets: the first four samples correspond to the controls (C) and the remaining five are from the MHFD mice group and corrected by β-actin. The bars reflect mean ± SE. *$p < 0.05$ versus control group. The group fed a control diet (C) is represented in white circles, while the MHFD group in black circles, $n = 8/10$ per group, respectively. Lines reflect mean ± SE. *$p < 0.05$ versus the C group assessed by unpaired *t*-test

the accumulation of misfolded proteins in the ER lumen (Martin-Jimenez et al., 2017) that intends to balance the ER functional capacity. Additionally, oxidative and ER-stress are closely interrelated phenomena because oxidative stress can disturb the ER redox balance leading to the disruption of disulfide bonds, the misfolding of proteins and the generation of ROS (Cao & Kaufman, 2014; Victor et al., 2021).

Moreover, it has been shown that ER-stress contributes to the development of insulin resistance and inflammation. In fact, ER-stress preceded inflammation in the liver mediated by lipotoxicity (Martin-Jimenez et al., 2017; Ozcan et al., 2004; Townsend et al., 2019). During ER-stress, protein kinase RNA-like ER kinase (PERK), inositol-requiring protein 1α (IRE1α) and activating transcription factor 6 (ATF6) dissociate from the ER chaperone immunoglobulin heavy chain-binding protein (BiP), which then increases its binding to misfolded proteins found in the lumen (Cnop et al., 2012; Martin-Jimenez et al., 2017). Consistent with this, we found a significant increase in BiP expression, suggesting that feeding the mice a MHFD for 14 weeks is enough to induce renal ER-stress. The BiP up-regulation is associated with the prevention of protein translation, and inefficient removal of misfolded proteins, which favors apoptosis of damaged cells, as an adaptive mechanism (Dandekar et al., 2015; Kim et al., 2018a). Furthermore, in chronic ER-stress, signaling switches from pro-survival to pro-apoptosis by upregulating the C/EBP homologous protein (CHOP) driven by ATF4 associated to the PERK/eIF2-α pathway to trigger apoptosis (Groenendyk et al., 2010; Li et al., 2019a). Chronic ER-stress also leads to oxidative stress and inflammation (Kim et al., 2018b). In fact, in human obesity and models of genetic or dietary obesity, ER-stress leads to the activation of UPR and the expression of CHOP. The upregulation of CHOP has been related with the induction of inflammation, leading to lower number of macrophages-M2 and lymphocytes Th2, well known to establish and anti-inflammatory response (Suzuki et al., 2017). In human obesity, UPR pathways' activation, evaluated by CHOP and BiP upregulation, happens together with oxidative stress and inflammation (Banuls et al., 2017; Komura et al., 2010; Sage et al., 2012) this data supports the existence of cross-linked mechanisms that occur in the kidneys as a result of obesity.

There is also evidence that ER-stress also leads to inflammation through the liberation of Ca^{2+} and ROS from the ER that trigger the Toll-like receptor (TLR) pathways, including nuclear factor κB (NF-κB), mitogen-activated protein kinase (MAPK), and glycogen synthase kinase-3β (GSK-3β) (Victor et al., 2021). Accordingly, we found that the MHFD group exhibited an increase in interleukin-6 mRNA and protein levels, as well as an increase in *Tnfa* mRNA levels. Additionally, *Tgfb1* mRNA levels were significantly increased too. This cytokine is well known to be associated with renal fibrosis by promoting the proliferation and the activation of interstitial fibroblasts and the epithelial-mesenchymal transition (Iwano et al., 2002; Lovisa et al., 2015). Although, we did not find ECM expansion, the elevation of *Tgfb1* could represent the initiation of a pro-fibrotic state into the kidney, which could be histologically evidenced in future studies with a longer follow-up.

In this study, we also found a significant increase in *Vegf* mRNA levels in the MHFD group. VEGF-A is a protein that can be secreted by podocytes and its function is critical for podocytes, mesangial and endothelial cells survival. VEGF-A regulates slit-diaphragm signaling and podocyte shape through VEGF receptor 2-nephrin-actin interactions. Previous studies have demonstrated that chronic hyperglycemia induced an excess of podocyte VEGF-A expression and low endothelial nitric oxide (NO) generation. The abnormal crosstalk between VEGF-A and NO pathways results in an increased oxidative stress (Tufro & Veron, 2012). Moreover, elevation of VEGF alone reproduces some aspects of glomerulopathy, and its antagonism attenuates diabetic albuminuria and other associated features of the podocytopathy (Cooper et al., 1999; Sung et al., 2006).

Emerging evidence suggest that dysfunctional mitochondria have a primary role in the development of CKD. There are some hallmark features of mitochondrial dysfunction, such as, changes in morphology, remodeling, and decrease in both mitochondrial biogenesis and ATP production (Galvan et al., 2017). Considering that we found an interesting bioenergetic dysregulation, reflected by the oxidative and ER-stress, we decided to analyze the mitochondrial dynamics as subrogate of mitochondrial dysfunction. Under normal conditions, both mitochondrial fission and fusion occur continuously and are precisely controlled by associated modulators (Chan, 2012). We found that Drp1 protein levels, that is a member of the GTPase family, and controls the final step in mitochondrial fission (Correa-Rotter & Gamba, 1997), was significantly elevated in the MHFD group, while Mfn1/2, a basic component of the mitochondrial fusion machinery did not change (Chan, 2012). Therefore, our results suggest that increased mitochondrial fragmentation is another implicated mechanism in renal injury induced by a MHFD (Jeong et al., 2018). In this regard, increased numbers of fragmented mitochondria have been observed in renal diseases, such as diabetic nephropathy (Brooks et al., 2009; Lee et al., 2017).

In summary, this model of MHFD-induced kidney damage has given us a great opportunity to detect key initiators, suggesting relevant interactions that can lead to the development of CKD. At the same time, it has taught us the possible kidney disorders that can occur in obese patients. We also believe that this model could be a useful tool to study the role of antioxidant molecules and drugs to protect ER and mitochondrial dynamics as new therapeutic targets for obesity-induced kidney damage.

CONFLICT OF INTEREST

The authors declare no conflict of interest.

AUTHOR CONTRIBUTIONS

Conception and design: EZ and NAB. Inclusion and following of experimental mice, and metabolic analysis: DCCR and EZ. Performed renal functional and structural analysis, as well as biochemical and molecular assessment: ASN, MAMR, RICB, and RPV. Acquisition of data: ASN, and MAMR. Analysis and interpretation of data: ASN, MAMR, and NAB. Drafting the article and revising it critically for important intellectual content: N.A.B, A.S.N. and MAMR.

ORCID

Norma A. Bobadilla https://orcid.org/0000-0002-3153-9151

REFERENCES

Banuls, C., Rovira-Llopis, S., Martinez de Maranon, A., Veses, S., Jover, A., Gomez, M., Rocha, M., Hernandez-Mijares, A., & Victor, V. M. (2017). Metabolic syndrome enhances endoplasmic reticulum, oxidative stress and leukocyte-endothelium interactions in PCOS. *Metabolism*, *71*, 153–162. https://doi.org/10.1016/j.metabol.2017.02.012

Barrera-Chimal, J., Perez-Villalva, R., Cortes-Gonzalez, C., Ojeda-Cervantes, M., Gamba, G., Morales-Buenrostro, L. E., & Bobadilla, N. A. (2011). Hsp72 is an early and sensitive biomarker to detect acute kidney injury. *EMBO Molecular Medicine*, *3*, 5–20. https://doi.org/10.1002/emmm.201000105

Barrera-Chimal, J., Perez-Villalva, R., Rodriguez-Romo, R., Reyna, J., Uribe, N., Gamba, G., & Bobadilla, N. A. (2013). Spironolactone prevents chronic kidney disease caused by ischemic acute kidney injury. *Kidney International*, *83*, 93–103. https://doi.org/10.1038/ki.2012.352

Barrera-Chimal, J., Rocha, L., Amador-Martinez, I., Perez-Villalva, R., Gonzalez, R., Cortes-Gonzalez, C., Uribe, N., Ramirez, V., Berman, N., Gamba, G., & Bobadilla, N. A. (2018). Delayed spironolactone administration prevents the transition from acute kidney injury to chronic kidney disease through improving renal inflammation. *Nephrology Dialysis Transplantation*, *34*(5), 794–801. https://doi.org/10.1093/ndt/gfy246

Bluher, M. (2019). Obesity: Global epidemiology and pathogenesis. *Nature Reviews Endocrinology*, *15*, 288–298.

Borgeson, E., Wallenius, V., Syed, G. H., Darshi, M., Lantero Rodriguez, J., Biorserud, C., Ragnmark Ek, M., Bjorklund, P., Quiding-Jarbrink, M., Fandriks, L., Godson, C., & Sharma, K. (2017). AICAR ameliorates high-fat diet-associated pathophysiology in mouse and ex vivo models, independent of adiponectin. *Diabetologia*, *60*, 729–739. https://doi.org/10.1007/s00125-017-4211-9

Botchlett, R., & Wu, C. (2018). Diet composition for the management of obesity and obesity-related disorders. *Journal of Diabetes Mellitus and Metabolic Syndrome*, *3*, 10–25. https://doi.org/10.28967/jdmms.2018.01.18002

Brooks, C., Wei, Q., Cho, S. G., & Dong, Z. (2009). Regulation of mitochondrial dynamics in acute kidney injury in cell culture and rodent models. *Journal of Clinical Investigation*, *119*, 1275–1285. https://doi.org/10.1172/JCI37829

Camara, N. O., Iseki, K., Kramer, H., Liu, Z. H., & Sharma, K. (2017). Kidney disease and obesity: Epidemiology, mechanisms and treatment. *Nature Reviews Nephrology*, *13*, 181–190

Cao, S. S., & Kaufman, R. J. (2014). Endoplasmic reticulum stress and oxidative stress in cell fate decision and human disease. *Antioxidants & Redox Signaling*, *21*, 396–413. https://doi.org/10.1089/ars.2014.5851

Castro-Rodriguez, D. C., Reyes-Castro, L. A., Vega, C. C., Rodriguez-Gonzalez, G. L., Yanez-Fernandez, J., & Zambrano, E. (2020). *Leuconostoc mesenteroides* subsp. mesenteroides SD23 prevents metabolic dysfunction associated with high-fat diet-induced obesity in male mice. *Probiotics and Antimicrobial Proteins*, *12*, 505–516. https://doi.org/10.1007/s12602-019-09556-3

Chan, D. C. (2012). Fusion and fission: Interlinked processes critical for mitochondrial health. *Annual Review of Genetics*, *46*, 265–287.

Chang, T. J., Zheng, C. M., Wu, M. Y., Chen, T. T., Wu, Y. C., Wu, Y. L., Lin, H. T., Zheng, J. Q., Chu, N. F., Lin, Y. M., Su, S. L., Lu, K. C., Chen, J. S., Sung, F. C., Lee, C. T., Yang, Y., Hwang, S. J., Wang, M. C., Hsu, Y. H., … Lin, Y. F. (2018). Relationship between body mass index and renal function deterioration among the Taiwanese chronic kidney disease population. *Scientific Reports*, *8*, 6908. https://doi.org/10.1038/s41598-018-24757-6

Cheng, K., Song, Z., Chen, Y., Li, S., Zhang, Y., Zhang, H., Zhang, L., Wang, C., & Wang, T. (2019). Resveratrol protects against renal damage via attenuation of inflammation and oxidative stress in high-fat-diet-induced obese mice. *Inflammation*, *42*, 937–945. https://doi.org/10.1007/s10753-018-0948-7

Cnop, M., Foufelle, F., & Velloso, L. A. (2012). Endoplasmic reticulum stress, obesity and diabetes. *Trends in Molecular Medicine*, *18*, 59–68. https://doi.org/10.1016/j.molmed.2011.07.010

Collaborators, G. B. D. O., Afshin, A., Forouzanfar, M. H., Reitsma, M. B., Sur, P., Estep, K., Lee, A., Marczak, L., Mokdad, A. H., Moradi-Lakeh, M., Naghavi, M., Salama, J. S., Vos, T., Abate, K. H., Abbafati, C., Ahmed, M. B., Al-Aly, Z., Alkerwi, A., Al-Raddadi, R., … Murray, C. J. L. (2017). Health effects of overweight and obesity in 195 countries over 25 years. *The New England Journal of Medicine*, *377*, 13–27.

Cooper, M. E., Vranes, D., Youssef, S., Stacker, S. A., Cox, A. J., Rizkalla, B., Casley, D. J., Bach, L. A., Kelly, D. J., & Gilbert, R. E. (1999). Increased renal expression of vascular endothelial growth factor (VEGF) and its receptor VEGFR-2 in experimental diabetes. *Diabetes*, *48*, 2229–2239. https://doi.org/10.2337/diabetes.48.11.2229

Correa-Rotter, R., & Gamba, G. (1997). Molecular biology in medicine. VIII. Analysis of gene expression. *Revista de Investigación Clínica*, *49*, 163–166.

D'Agati, V. D., Chagnac, A., de Vries, A. P., Levi, M., Porrini, E., Herman-Edelstein, M., & Praga, M. (2016). Obesity-related glomerulopathy: Clinical and pathologic characteristics and pathogenesis. *Nature Reviews Nephrology*, *12*, 453–471.

Dandekar, A., Mendez, R., & Zhang, K. (2015). Cross talk between ER stress, oxidative stress, and inflammation in health and disease. *Methods in Molecular Biology*, *1292*, 205–214.

Dell, R. B., Holleran, S., & Ramakrishnan, R. (2002). Sample size determination. *ILAR Journal*, *43*, 207–213. https://doi.org/10.1093/ilar.43.4.207

Eknoyan, G. (2011). Obesity and chronic kidney disease. *Nefrologia*, *31*, 397–403.

FAO I, UNICEF, WFP and WHO. (2020). *The state of food security and nutritition in the world 2020. Transforming food systems for affordable healthy diets*. FAO.

Foster, M. C., Hwang, S. J., Larson, M. G., Lichtman, J. H., Parikh, N. I., Vasan, R. S., Levy, D., & Fox, C. S. (2008). Overweight, obesity, and the development of stage 3 CKD: The Framingham Heart Study. *American Journal of Kidney Diseases*, *52*, 39–48.

Galvan, D. L., Green, N. H., & Danesh, F. R. (2017). The hallmarks of mitochondrial dysfunction in chronic kidney disease. *Kidney International*, *92*, 1051–1057. https://doi.org/10.1016/j.kint.2017.05.034

Garcia-Ortuno, L. E., Barrera-Chimal, J., Perez-Villalva, R., Ortega-Trejo, J. A., Luna-Bolanos, E., Lima-Posada, I., Sanchez-Navarro, A., Reyes-Castro, L., Gamba, G., Zambrano, E., & Bobadilla, N. A. (2019). Resilience to acute kidney injury in offspring of maternal protein restriction. *American Journal of Physiology. Renal Physiology*, *317*, F1637–F1648. https://doi.org/10.1152/ajprenal.00356.2019

Garrison, C. B., Lastwika, K. J., Zhang, Y., Li, C. I., & Lampe, P. D. (2017). Proteomic analysis, immune dysregulation, and pathway interconnections with obesity. *Journal of Proteome Research*, *16*, 274–287. https://doi.org/10.1021/acs.jproteome.6b00611

Groenendyk, J., Sreenivasaiah, P. K., Kim, D. H., Agellon, L. B., & Michalak, M. (2010). Biology of endoplasmic reticulum stress in the heart. *Circulation Research*, *107*, 1185–1197. https://doi.org/10.1161/CIRCRESAHA.110.227033

Iwano, M., Plieth, D., Danoff, T. M., Xue, C., Okada, H., & Neilson, E. G. (2002). Evidence that fibroblasts derive from epithelium during tissue fibrosis. *Journal of Clinical Investigation*, *110*, 341–350. https://doi.org/10.1172/JCI0215518

Jeong, H. Y., Kang, J. M., Jun, H. H., Kim, D. J., Park, S. H., Sung, M. J., Heo, J. H., Yang, D. H., Lee, S. H., & Lee, S. Y. (2018). Chloroquine and amodiaquine enhance AMPK phosphorylation and improve mitochondrial fragmentation in diabetic tubulopathy. *Scientific Reports*, *8*, 8774. https://doi.org/10.1038/s41598-018-26858-8.

Kim, K., Ahn, N., & Jung, S. (2018). Comparison of endoplasmic reticulum stress and mitochondrial biogenesis responses after 12 weeks of treadmill running and ladder climbing exercises in the cardiac muscle of middle-aged obese rats. *Brazilian Journal of Medical and Biological Research*, *51*, e7508. https://doi.org/10.1590/1414-431x20187508

Kim, K., Ahn, N., Jung, S., Ju, Y., Lee, G., Kim, M., & Jeong, Y. (2018). Effects of resistance exercise and fermented soybean consumption on glucose tolerance and expressions of immune senescence-related myokines in middle-aged obese rats. *Journal of Obesity & Metabolic Syndrome*, *27*, 186–194. https://doi.org/10.7570/jomes.2018.27.3.186.

Kim, S. R., Jiang, K., Ogrodnik, M., Chen, X., Zhu, X. Y., Lohmeier, H., Ahmed, L., Tang, H., Tchkonia, T., Hickson, L. J., Kirkland, J. L., & Lerman, L. O. (2019). Increased renal cellular senescence in murine high-fat diet: Effect of the senolytic drug quercetin. *Translational Research*, *213*, 112–123.

Komura, T., Sakai, Y., Honda, M., Takamura, T., Matsushima, K., & Kaneko, S. (2010). CD14+ monocytes are vulnerable and functionally impaired under endoplasmic reticulum stress in patients with type 2 diabetes. *Diabetes*, *59*, 634–643. https://doi.org/10.2337/db09-0659.

Kovesdy, C. P., Furth, S. L., Zoccali, C., & World Kidney Day Steering C. (2017). Obesity and kidney disease: Hidden consequences of the epidemic. *Future Science OA*, *3*, FSO159.

Lee, S. Y., Kang, J. M., Kim, D. J., Park, S. H., Jeong, H. Y., Lee, Y. H., Kim, Y. G., Yang, D. H., & Lee, S. H. (2017). PGC1alpha activators mitigate diabetic tubulopathy by improving mitochondrial dynamics and quality control. *Journal of Diabetes Research*, *2017*, 6483572.

Li, B., Leung, J. C. K., Chan, L. Y. Y., Yiu, W. H., Li, Y., Lok, S. W. Y., Liu, W. H., Chan, K. W., Tse, H. F., Lai, K. N., & Tang, S. C. W. (2019). Amelioration of endoplasmic reticulum stress by mesenchymal stem cells via hepatocyte growth factor/c-Met signaling in obesity-associated kidney injury. *Stem Cells Translational Medicine*, *8*, 898–910. https://doi.org/10.1002/sctm.18-0265.

Li, L., Kang, H., Zhang, Q., D'Agati, V. D., Al-Awqati, Q., & Lin, F. (2019). FoxO3 activation in hypoxic tubules prevents chronic kidney disease. *Journal of Clinical Investigation*, *130*, 2374–2389. https://doi.org/10.1172/JCI122256

Lovisa, S., LeBleu, V. S., Tampe, B., Sugimoto, H., Vadnagara, K., Carstens, J. L., Wu, C. C., Hagos, Y., Burckhardt, B. C., Pentcheva-Hoang, T., Nischal, H., Allison, J. P., Zeisberg, M., & Kalluri, R. (2015). Epithelial-to-mesenchymal transition induces cell cycle arrest and parenchymal damage in renal fibrosis. *Nature Medicine*, *21*, 998–1009. https://doi.org/10.1038/nm.3902.

Luo, Y., Wu, M. Y., Deng, B. Q., Huang, J., Hwang, S. H., Li, M. Y., Zhou, C. Y., Zhang, Q. Y., Yu, H. B., Zhao, D. K., Zhang, G.,

Qin, L., Peng, A., Hammock, B. D., & Liu, J. Y. (2019). Inhibition of soluble epoxide hydrolase attenuates a high-fat diet-mediated renal injury by activating PAX2 and AMPK. *Proceedings of the National Academy of Sciences of the United States of America*, *116*, 5154–5159. https://doi.org/10.1073/pnas.1815746116

Martin-Jimenez, C. A., Garcia-Vega, A., Cabezas, R., Aliev, G., Echeverria, V., Gonzalez, J., & Barreto, G. E. (2017). Astrocytes and endoplasmic reticulum stress: A bridge between obesity and neurodegenerative diseases. *Progress in Neurobiology*, *158*, 45–68.

Morales-Buenrostro, L. E., Salas-Nolasco, O. I., Barrera-Chimal, J., Casas-Aparicio, G., Irizar-Santana, S., Perez-Villalva, R., & Bobadilla, N. A. (2014). Hsp72 is a novel biomarker to predict acute kidney injury in critically ill patients. *PLoS ONE*, *9*, e109407. https://doi.org/10.1371/journal.pone.0109407

Ogden, C. L., Carroll, M. D., & Flegal, K. M. (2014). Prevalence of obesity in the United States. *JAMA*, *312*, 189–190. https://doi.org/10.1001/jama.2014.6228

Ortega-Trejo, J. A., Perez-Villalva, R., Barrera-Chimal, J., Carrillo-Perez, D. L., Morales-Buenrostro, L. E., Gamba, G., Flores, M. E., & Bobadilla, N. A. (2015). Heat shock protein 72 (Hsp72) specific induction and temporal stability in urine samples as a reliable biomarker of acute kidney injury (AKI). *Biomarkers*, *20*, 453–459. https://doi.org/10.3109/1354750X.2015.1096305

Ozcan, U., Cao, Q., Yilmaz, E., Lee, A. H., Iwakoshi, N. N., Ozdelen, E., Tuncman, G., Gorgun, C., Glimcher, L. H., & Hotamisligil, G. S. (2004). Endoplasmic reticulum stress links obesity, insulin action, and type 2 diabetes. *Science*, *306*, 457–461. https://doi.org/10.1126/science.1103160

Pereira, B. M. V., Thieme, K., de Araujo, L., & Rodrigues, A. C. (2020). Lack of adiponectin in mice accelerates high-fat diet-induced progression of chronic kidney disease. *Life Sciences*, *257*, 118061. https://doi.org/10.1016/j.lfs.2020.118061

Perez-Rojas, J., Blanco, J. A., Cruz, C., Trujillo, J., Vaidya, V. S., Uribe, N., Bonventre, J. V., Gamba, G., & Bobadilla, N. A. (2007). Mineralocorticoid receptor blockade confers renoprotection in preexisting chronic cyclosporine nephrotoxicity. *American Journal of Physiology-Renal Physiology*, *292*, F131–F139. https://doi.org/10.1152/ajprenal.00147.2006

Perez-Villalva, R., Barrera-Chimal, J., Aguilar-Carrasco, J. C., Lima-Posada, I., Cruz, C., Ramirez, V., Gonzalez-Bobadilla, Y., Uribe, N., Trumper, L., & Bobadilla, N. A. (2017). HSP72 is an early biomarker to detect cisplatin and acetaminophen nephrotoxicity. *Biomarkers*, *22*, 548–556. https://doi.org/10.1080/1354750X.2017.1315616

Pinto-Sietsma, S.-J., Navis, G., Janssen, W. M. T., de Zeeuw, D., Gans, R. O. B., de Jong, P. E., & Group PS. (2003). A central body fat distribution is related to renal function impairment, even in lean subjects. *American Journal of Kidney Diseases*, *41*, 733–741. https://doi.org/10.1016/S0272-6386(03)00020-9.

Popkin, B. M., Adair, L. S., & Ng, S. W. (2012). Global nutrition transition and the pandemic of obesity in developing countries. *Nutrition Reviews*, *70*, 3–21. https://doi.org/10.1111/j.1753-4887.2011.00456.x

Ruggiero, C., Ehrenshaft, M., Cleland, E., & Stadler, K. (2011). High-fat diet induces an initial adaptation of mitochondrial bioenergetics in the kidney despite evident oxidative stress and mitochondrial ROS production. *American Journal of Physiology-Endocrinology and Metabolism*, *300*, E1047–1058. https://doi.org/10.1152/ajpendo.00666.2010.

Sage, A. T., Holtby-Ottenhof, S., Shi, Y., Damjanovic, S., Sharma, A. M., & Werstuck, G. H. (2012). Metabolic syndrome and acute hyperglycemia are associated with endoplasmic reticulum stress in human mononuclear cells. *Obesity (Silver Spring)*, *20*, 748–755. https://doi.org/10.1038/oby.2011.144

Saito, H., Tanaka, T., Sugahara, M., Tanaka, S., Fukui, K., Wakashima, T., & Nangaku, M. (2019). Inhibition of prolyl hydroxylase domain (PHD) by JTZ-951 reduces obesity-related diseases in the liver, white adipose tissue, and kidney in mice with a high-fat diet. *Laboratory Investigation*, *99*, 1217–1232. https://doi.org/10.1038/s41374-019-0239-4

Sanchez-Navarro, A., Mejia-Vilet, J. M., Perez-Villalva, R., Carrillo-Perez, D. L., Marquina-Castillo, B., Gamba, G., & Bobadilla, N. A. (2019). SerpinA3 in the early recognition of acute kidney injury to chronic kidney disease (CKD) transition in the rat and its potentiality in the recognition of patients with CKD. *Scientific Reports*, *9*, 10350. https://doi.org/10.1038/s41598-019-46601-1

Senf, S. M., Sandesara, P. B., Reed, S. A., & Judge, A. R. (2011). p300 Acetyltransferase activity differentially regulates the localization and activity of the FOXO homologues in skeletal muscle. *American Journal of Physiology: Cell Physiology*, *300*, C1490–1501. https://doi.org/10.1152/ajpcell.00255.2010.

Sun, Y., Ge, X., Li, X., He, J., Wei, X., Du, J., Sun, J., Li, X., Xun, Z., Liu, W., Zhang, H., Wang, Z. Y., & Li, Y. C. (2020). High-fat diet promotes renal injury by inducing oxidative stress and mitochondrial dysfunction. *Cell Death & Disease*, *11*, 914. https://doi.org/10.1038/s41419-020-03122-4

Sung, S. H., Ziyadeh, F. N., Wang, A., Pyagay, P. E., Kanwar, Y. S., & Chen, S. (2006). Blockade of vascular endothelial growth factor signaling ameliorates diabetic albuminuria in mice. *Journal of the American Society of Nephrology*, *17*, 3093–3104. https://doi.org/10.1681/ASN.2006010064

Suzuki, T., Gao, J., Ishigaki, Y., Kondo, K., Sawada, S., Izumi, T., Uno, K., Kaneko, K., Tsukita, S., Takahashi, K., Asao, A., Ishii, N., Imai, J., Yamada, T., Oyadomari, S., & Katagiri, H. (2017). ER Stress protein CHOP mediates insulin resistance by modulating adipose tissue macrophage polarity. *Cell Reports*, *18*, 2045–2057. https://doi.org/10.1016/j.celrep.2017.01.076

Szeto, H. H., Liu, S., Soong, Y., Alam, N., Prusky, G. T., & Seshan, S. V. (2016). Protection of mitochondria prevents high-fat diet-induced glomerulopathy and proximal tubular injury. *Kidney International*, *90*, 997–1011.

Takagi, S., Li, J., Takagaki, Y., Kitada, M., Nitta, K., Takasu, T., Kanasaki, K., & Koya, D. (2018). Ipragliflozin improves mitochondrial abnormalities in renal tubules induced by a high-fat diet. *Journal of Diabetes Investigation*, *9*, 1025–1032. https://doi.org/10.1111/jdi.12802.

Tanaka, Y., Kume, S., Kitada, M., Kanasaki, K., Uzu, T., Maegawa, H., & Koya, D. (2012). Autophagy as a therapeutic target in diabetic nephropathy. *Experimental Diabetes Research*, *2012*, 628978. https://doi.org/10.1155/2012/628978

Townsend, L. K., Medak, K. D., Peppler, W. T., Meers, G. M., Rector, R. S., LeBlanc, P. J., & Wright, D. C. (2019). High-saturated-fat diet-induced obesity causes hepatic interleukin-6 resistance via endoplasmic reticulum stress. *Journal of Lipid Research*, *60*, 1236–1249. https://doi.org/10.1194/jlr.M092510

Tsuboi, N., Okabayashi, Y., Shimizu, A., & Yokoo, T. (2017). The renal pathology of obesity. *Kidney International Reports*, *2*, 251–260. https://doi.org/10.1016/j.ekir.2017.01.007

Tufro, A., & Veron, D. (2012). VEGF and podocytes in diabetic nephropathy. *Seminars in Nephrology*, *32*, 385–393. https://doi.org/10.1016/j.semnephrol.2012.06.010

Vaidya, V. S., Ramrez, V., Bobadilla, N. A., & Bonventre, J. V. (2005). A microfluidics based assay to measure Kidney Injury Molecule-1 (Kim-1) in the urine as a biomarker for early diagnosis of acute kidney injury. *Journal of the American Society of Nephrology*, *16*, 192A.

Vaidya, V. S., Ramirez, V., Ichimura, T., Bobadilla, N. A., & Bonventre, J. V. (2006). Urinary kidney injury molecule-1: A sensitive quantitative biomarker for early detection of kidney tubular injury. *American Journal of Physiology-Renal Physiology*, *290*, F517–F529.

Victor, P., Umapathy, D., George, L., Juttada, U., Ganesh, G. V., Amin, K. N., Viswanathan, V., & Ramkumar, K. M. (2021). Crosstalk between endoplasmic reticulum stress and oxidative stress in the progression of diabetic nephropathy. *Cell Stress and Chaperones*, *26*, 311–321. https://doi.org/10.1007/s12192-020-01176-z

Wang, Y., Chen, X., Song, Y., Caballero, B., & Cheskin, L. J. (2008). Association between obesity and kidney disease: A systematic review and meta-analysis. *Kidney International*, *73*, 19–33.

Xu, S., Luo, W., Xu, X., Qian, Y., Xu, Z., Yu, W., Shan, X., Guan, X., Lum, H., Zhou, H., & Wang, Y. (2019). MD2 blockade prevents oxLDL-induced renal epithelial cell injury and protects against high-fat-diet-induced kidney dysfunction. *Journal of Nutritional Biochemistry*, *70*, 47–55. https://doi.org/10.1016/j.jnutbio.2019.04.003

Yamamoto, T., Takabatake, Y., Takahashi, A., Kimura, T., Namba, T., Matsuda, J., Minami, S., Kaimori, J. Y., Matsui, I., Matsusaka, T., Niimura, F., Yanagita, M., & Isaka, Y. (2017). High-fat diet-induced lysosomal dysfunction and impaired autophagic flux contribute to lipotoxicity in the kidney. *Journal of the American Society of Nephrology*, *28*, 1534–1551. https://doi.org/10.1681/ASN.2016070731

SUPPORTING INFORMATION

Additional supporting information may be found online in the Supporting Information section.

How to cite this article: Sánchez-Navarro, A., Martínez-Rojas M. Á., Caldiño-Bohn R. I., Pérez-Villalva R., Zambrano E., Castro-Rodríguez D. C., & Bobadilla N. A. (2021). Early triggers of moderately high-fat diet-induced kidney damage. *Physiological Reports*, 9, e14937. https://doi.org/10.14814/phy2.14937

6.3 ARTÍCULO 3 https://pubmed.ncbi.nlm.nih.gov/31316093/

Resumen de los resultados de un nuevo biomarcador para el diagnóstico de LRA y de la transición de LRA a ERC, publicados en la revista en Scientific Reports, 9(1), 1–11, 2019, correspondientes al objetivo 4.

Identificar a los pacientes en las primeras fases de la enfermedad renal crónica (ERC) es difícil y resulta aún más complicado predecir la lesión renal aguda (LRA) y su transición a la ERC. El estándar de oro para identificar oportunamente la fibrosis renal es la biopsia renal, un procedimiento invasivo que no suele realizarse con este fin en la práctica clínica. Identificamos mediante espectrometría de masas de alta resolución la presencia anormal de SerpinA3 en la orina de animales con ERC. Se observó una elevación temprana y progresiva de SerpinA3 urinario (uSerpinA3) durante la transición de LRA a ERC, junto con la reubicación de SerpinA3 desde el citoplasma a la membrana tubular apical en el riñón de rata. uSerpinA3 aumentó significativamente en pacientes con ERC secundaria a GSFS, vasculitis asociada a ANCA (VAA) y nefritis lúpica proliferativa de clases III y IV (NL). Los niveles de uSerpinA3 se asociaron de forma independiente y positiva con la fibrosis renal. En pacientes con NL de clase V, los niveles de uSerpinA3 no fueron diferentes de los de voluntarios sanos. La uSerpinA3 no se encontró en pacientes con enfermedades inflamatorias sistémicas sin disfunción renal. Nuestras observaciones sugieren que la uSerpinA3 puede detectar la fibrosis y la inflamación renal, con un potencial particular de su detección no invasiva y de manera oportuna.

SCIENTIFIC REPORTS

OPEN

SerpinA3 in the Early Recognition of Acute Kidney Injury to Chronic Kidney Disease (CKD) transition in the rat and its Potentiality in the Recognition of Patients with CKD

Received: 24 October 2018
Accepted: 29 June 2019
Published online: 17 July 2019

Andrea Sánchez-Navarro[1,2], Juan M. Mejía-Vilet[2], Rosalba Pérez-Villalva[1,2], Diego L. Carrillo-Pérez[4,5], Brenda Marquina-Castillo[3], Gerardo Gamba[1,2,5] & Norma A. Bobadilla[1,2]

Recognizing patients at early phases of chronic kidney disease (CKD) is difficult, and it is even more challenging to predict acute kidney injury (AKI) and its transition to CKD. The gold standard to timely identify renal fibrosis is the kidney biopsy, an invasive procedure not usually performed for this purpose in clinical practice. SerpinA3 was identified by high-resolution-mass-spectrometry in urines from animals with CKD. An early and progressive elevation of urinary SerpinA3 (uSerpinA3) was observed during the AKI to CKD transition together with SerpinA3 relocation from the cytoplasm to the apical tubular membrane in the rat kidney. uSerpinA3/alpha-1-antichymotrypsin was significantly increased in patients with CKD secondary to focal and segmental glomerulosclerosis (FSGS), ANCA associated vasculitis (AAV) and proliferative class III and IV lupus nephritis (LN). uSerpinA3 levels were independently and positively associated with renal fibrosis. In patients with class V LN, uSerpinA3 levels were not different from healthy volunteers. uSerpinA3 was not found in patients with systemic inflammatory diseases without renal dysfunction. Our observations suggest that uSerpinA3 can detect renal fibrosis and inflammation, with a particular potential for the early detection of AKI to CKD transition and for the differentiation among lupus nephritis classes III/IV and V.

Chronic kidney disease (CKD) is a silent disease that is often not recognized in clinical practice until the global renal function is impaired or proteinuria is detected in urine assays. Over the past two decades, the incidence of CKD has increased more than threefold, and according to the World Health Organization, it will be one of the three main causes of death and disability in the world by 2020[1]. To assess renal function, international organizations such as the National Kidney Foundation in the Kidney Disease Outcomes Quality Initiative (NKF-KDOQI) or the Kidney Disease Improving Global Outcomes (KDIGO) have proposed a series of guidelines for CKD detection that recommend CKD screening with serum creatinine, urea nitrogen and the abnormal presence of proteins in the urine[2,3]. Unfortunately, these classical kidney injury markers are only detectable when the disease is already advanced, and pharmacological treatments are possibly less effective. Moreover, tubulointerstitial fibrosis has been shown to occur earlier than renal dysfunction, and when proteinuria appears, the disease has been already established[4,5]. The presence of renal fibrosis, before glomerular filtration rate (GFR) reduction, can only be documented by kidney biopsy. Additionally, for most glomerular diseases, as is the case for lupus nephritis

[1]Molecular Physiology Unit, Instituto de Investigaciones Biomédicas, Universidad Nacional Autónoma de México, Mexico City, Mexico. [2]Department of Nephrology and Mineral Metabolism, Instituto Nacional de Ciencias Médicas y Nutrición Salvador Zubirán, Mexico City, Mexico. [3]Department of Experimental Pathology, Instituto Nacional de Ciencias Médicas y Nutrición Salvador Zubirán, Mexico City, Mexico. [4]Deparment of Internal Medicine, Instituto Nacional de Ciencias Médicas y Nutrición Salvador Zubirán, Mexico City, Mexico. [5]Tecnológico de Monterrey, Escuela de Medicina y Ciencias de la Salud, Monterrey, Nuevo León, Mexico. Correspondence and requests for materials should be addressed to N.A.B. (email: nab@biomedicas.unam.mx)

(LN), kidney biopsy represents the gold standard for diagnosis and the only way to classify histological damage for diagnostic and prognostic purposes[5].

Acute kidney injury (AKI) represents another important renal disease around the globe. It affects 21% of hospitalized patients in general wards and up to 60% of patients in critical care units[6,7]. It was previously speculated that patients who completely recovered from an AKI episode had no further repercussions on kidney function and structure; however, recent evidence based on epidemiological and experimental observations has demonstrated that in many cases, AKI leads to CKD[8–13]. Therefore, AKI is now acknowledged as a risk factor for the development of CKD and an accelerating factor for the transition from CKD to end-stage renal disease (ESRD)[13–15].

Currently, CKD diagnosis is made through urine proteinuria or albuminuria, serum creatinine elevation, urine sediment abnormalities, imaging studies or histopathology. The disadvantage to these approaches is the late detection of renal disease and, for the case of histopathological studies, the invasiveness and impracticability. Therefore, current efforts are under way to identify a timely non-invasive biomarker for CKD and the AKI to CKD transition.

We identified the abnormal presence of serpinA3 in urine samples from animals with CKD by high-resolution mass spectrometry, and here, we present evidence that uSerpinA3 is a potentially useful diagnostic marker to detect the AKI to CKD transition and CKD from different etiologies.

Methods

All experiments involving animals were conducted in accordance with the NIH Guide for the Care and Use of Laboratory Animals (https://grants.nih.gov/grants/olaw/guide-for-the-care-and-use-of-laboratory-animals.pdf) and with the Mexican Federal Regulation for animal reproduction, care, and experimentation (NOM-062-ZOO-2001). All methods involving humans were performed in accordance with the relevant guidelines and regulations. The study was approved by both the Animal Care and Use Committee and the Ethical Committee for human research at Instituto Nacional de Ciencias Médicas y Nutrición Salvador Zubirán. Informed consent was obtained from all the patients included in this study.

All the animals used in this study were maintained in controlled conditions of temperature and humidity in our animal housing facility with 12:12 h day/night cycle, with free access to water and food.

AKI to CKD transition model. 36 male Wistar rats (320–350 g) were included and randomly distributed into two groups as follows: control animals who underwent sham surgery and were studied and sacrificed at 1, 2, 3, or 4-months (n = 4 per period), and rats who underwent right nephrectomy and unilateral 45-min left renal ischemia who were studied and sacrificed at 1, 2, 3, or 4-months (n = 5 per period). In our experience, 30–40% of the animals died after 24 h of ischemic injury, but none was lost during the follow-up (4 months). The animals were maintained in controlled conditions in our animal facility. All the samples of the included animals were evaluated and included in the analyses.

Ischemia/reperfusion model. After an intra-peritoneal injection of sodium pentobarbital (30 mg/kg), the rats were placed on a heating pad to maintain core body temperature at 37 °C. Unilateral renal ischemia was induced using a non-traumatic clamp on left renal artery for 45 min. Then, the clip was released to allow the return of oxygenated blood to the kidney and right nephrectomy was performed. 3–0 vicryl and silk sutures were used to close the muscle and the skin, respectively. For sham surgery, laparotomy and renal pedicle dissection, without clamping, was performed.

Functional studies. At the end of the experimental period, rats were anesthetized with sodium pentobarbital (30 mg/kg) and placed on a homoeothermic table. The femoral arteries were catheterized with polyethylene tubing (PE-50). The mean arterial pressure (MAP) was monitored with a pressure transducer (model p23 db, Gould) and recorded on a polygraph (Grass Instruments, Quincy, MA). An ultrasound transit-time flow probe (transonic flow probe, New York, NY) was placed around the left artery and filled with ultrasonic coupling gel (HR Lubricating Jelly, Carter-Wallace, New York, NY) to record the renal blood flow (Transonic flowmeter, New York, NY). Blood samples were taken at the end of the study as we previously reported[16,17].

Biochemical studies. Turbidimetric method with trichloroacetic acid (TCA) was employed to measure urinary protein excretion monthly in 24-h urine collections throughout the follow-up in all studied groups. Quantichrom creatinine assay kit (DICT-500) was used to determine urine and serum creatinine concentrations and renal creatinine clearance was obtained using the standard formula.

Percentage of tubulo-interstitial fibrosis. Paraffin embedded renal tissue was deparaffinized and 3 µm sections were stained with Sirius red. Eight to ten subcortical fields (magnification x400) were recorded from each kidney slide using a digital camera incorporated in a Nikon Light microscope to measure the degree of tubulo-interstitial fibrosis by morphometry. The affected area of tubulo-interstitial fibrosis was automatically quantified by an eclipse net software. All the analyses were performed by an observer blind to the experiments as we previously reported[16,17].

High-resolution urine mass spectrometry. Bands of 55 and 70 kDa were cut from an 8.5% acrylamide gel stained with Coomassie R-250 blue to perform a tryptic protein digestion in gel, following the protocol of the Laboratory of Proteomics from our University. The collected peptides were desalted with Zip Tip C18 millipore tips (LUP protocol) and dried in a speedvac. Samples were kept at −80 °C until analysis. The sample ionization and subsequent analysis was performed by high-resolution mass spectrometry (LTQ Orbitrap, Thermo Fisher Scientific).

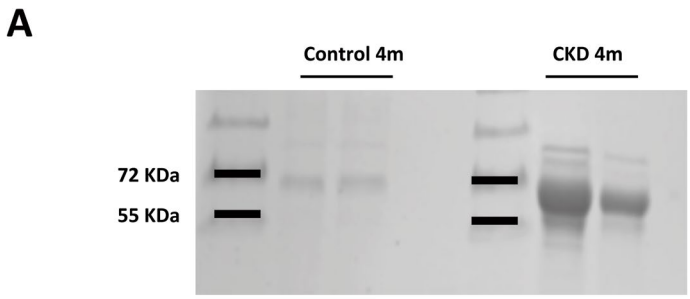

B **High Resolution Mass Spectometry**

MAFIAALGLL MAGICPAVLC DGILGRDTLP HEDQGKGRQL HSLTLASINT DFTLSLYKKL ALRNPDKNVV FSPLSISAAL AILSLGAKDS TMEEILEVLK FNLTEITEEE

IHQGFGHLLQ RLSQPEDQAE INTGSALFID KEQPILSEFQ EKTRALYQAE AFVADFKQCN EAKKFINDYV SNQTQGKIAE LFSELDERTS MVLVNYLLFK GKWKVPFNPN

D

DTFEEEFYLD EKRSVKVPMM KIKDLTTPYI RDEELSCSVL ELKYTGNASA LFILPDQGKM QQVESSLQPE TLKKWKDSLR PRIISELRMP KFSISTDYNL EEVLPELGIR

KIFSQQADLS RITGTKNLHV SQVVHKAVLD VDETGTEGAA ATAVTAALKS LPQTIPLLNF NRPFMLVITD NNGQSVFFMG KVTNPM

Accession	Description	Score	Coverage	# Peptides	MW [kDa]
P05545	Serine protease inhibitor A3K OS=Rattus norvegicus GN=Serpina3k PE=1 SV=3 - [SPA3K_RAT]	256.18	44.7	6	46.5

Figure 1. Urine high-resolution mass spectrometry in CKD rats. (**A**) Representative acrylamide gel under denaturing conditions and subsequent staining with Coomassie blue of urines from rats with CKD compared to control rats (sham). The identified proteins were mainly between 55 and 72 KDa. (**B**) SerpinA3 was identified with high-resolution mass spectrometry with a high coverage (44.7%) in urine samples from CKD rats.

Renal SerpinA3 mRNA levels. At every predefined period, animals were sacrificed and half of the left kidney was quickly removed and frozen for molecular studies. Total RNA was isolated from the kidney using the TRIzol method (Invitrogen, Carlsbad, CA) and its integrity checked integrity using 1% agarose gel electrophoresis. To avoid DNA contamination, total RNA samples were treated with DNAase (DNAase I; Invitrogen). Reverse transcription (RT) was carried out with 1 μg of total RNA and 200 U of Moloney's murine leukemia virus reverse transcriptase (Invitrogen) as we previously reported[16,17]. SerpinA3 mRNA levels (Rn04280570_m1) were quantified by real-time PCR on an ABI Prism 7300 Sequence Detection System (TaqMan, ABI, Foster City, CA). Eukaryotic 18S rRNA (predesigned assay reagent Applied by ABI, external run, Rn03928990_g1) was used as endogenous control. The relative quantification of each gene expression was performed with the comparative threshold cycle (Ct) method.

SerpinA3 protein levels in tissue, urine and plasma. Electrophoresis on an 8.5% denaturing acrylamide gel was performed with 40 μg of renal tissue proteins, 1 μl of rat urine, 15 μl of human urine or 30 nl of human plasma as appropriate. Proteins were then transferred to pre-equilibrated polyvinyl difluoride (PVDF, Millipore) membranes with 1x transfer buffer (190 mM glycine, 2 mM Tris base, 0.1% SDS) in a transblot (SD cell, BioRad) for 60 min at 9 volts. Subsequently, membranes were blocked for 90 min with TBS buffer 5% blocking agent (BioRad). After blockade, membranes were incubated with the primary antibody serpinA3K (1:2000, Santa Cruz, SC-162175 for rat samples) and antibody serpinA3/alpha-1-antichymotrypsin (Proteintech, 55480-1-AP for human samples) overnight at 4 °C. The membranes were then incubated with the HRP-coupled anti-goat secondary antibody or HRP-coupled anti-rabbit secondary antibody, respectively (1:10000, Millipore or Thermo Scientific Pierce, respectively).

Urine Hsp72 levels. Urine Hsp72 levels were detected by Western blot. Each urine sample was diluted 1:10 in 0.9% saline solution, and 10 μL were loaded and resolved by 8.5% SDS-PAGE electrophoresis and then electroblotted. The membranes were incubated with mouse anti-Hsp72 antibody (ENZO Life Sciences, 1:5000 dilution) for 2-h. Thereafter; membranes were incubated with a secondary antibody, HRP-conjugated goat anti-mouse IgG (1:5000, Santa Cruz Biotechnology). The proteins were detected using a commercial chemiluminiscence kit (Millipore), as we previously described[18].

CKD patient sample collection. Plasma and urine samples were collected pre-biopsy from male and female patients diagnosed with focal and segmental glomerulosclerosis (FSGS, n = 14), lupus nephritis (LN, n = 47), and ANCA associated vasculitis (AAV, n = 19). Lupus nephritis biopsies were classified according to the ISN/RPS classification[19] into class III (n = 18), class IV (n = 18) and class V (n = 11). The sample size was based on the availability of biological samples and not statistically determined. The percentage of tubulointerstitial fibrosis was evaluated in renal biopsies by an expert nephropathologist. Patients with inflammatory diseases but without renal dysfunction were also included: liver cirrhosis (LC, n = 6), acute pancreatitis (AP, n = 6) and active rheumatoid arthritis (RA, n = 6). All the groups were compared to healthy volunteers (n = 20).

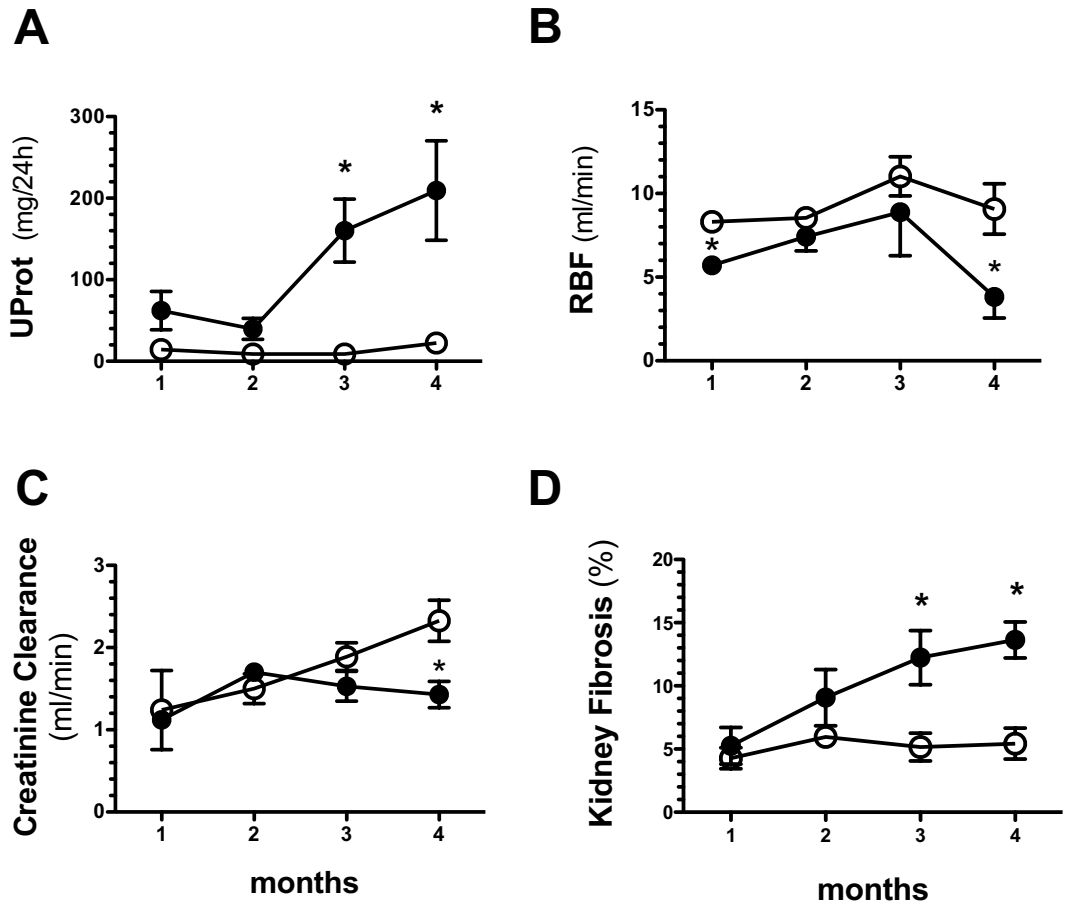

Figure 2. Temporal course of renal dysfunction and fibrosis in AKI to CKD transition in the rat. (**A**) Proteinuria, (**B**) Renal blood flow (RBF), (**C**) Creatinine clearance, and (**D**) Tubulo-interstitial fibrosis since the 1st until the 4th month post-ischemia. Data are represented as the mean ± SE (for sham, n = 4, and for the AKI to CKD transition groups, n = 5 per period). White circles represent sham and black circles represent AKI to CKD transition groups. *$p < 0.05$ vs. sham group in their respective period.

*Acute pancreatitis w*as defined by the presence of two of the following: acute onset of persistent, severe, epigastric pain often radiating to the back, elevation in serum lipase or amylase to three times or greater than the upper limit of normal, or characteristic findings in the image studies[20]. RA was diagnosed by the 2010 ACR/EULAR classification criteria. Active RA was defined as Disease Activity Score-28 joints (DAS28)-erythrocyte sedimentation rate (ESR) ≥ 3.2[21]. LC was diagnosed by liver biopsy and/or clinical, biochemical, ultrasound, and/or endoscopic findings, and classified according to the patient's Child-Pugh score[22].

SerpinA3 Immunohistochemistry. Tissues from rat or human biopsies embedded in paraffin and cut into 4 μm sections in charged slides. Once deparaffinized, the antibody recovery was performed with citrate buffer (Bio SB) for 12 min in high pressure. The slides were then blocked with a inmunoDNA background blocker (Bio SB) for 20 min and incubated with the primary serpinA3 antibody (1:500, Santa Cruz, SC-162175) for 2 h at 23 °C. Then the slides were incubated with a goat-on-rodent-HRP-polymer-secondary antibody (Biocare medical), and revealed with DAB peroxidase Substrate (Bio SB).

uSerpinA3 levels by ELISA. Human serpinA3/Alpha-1-antichymotrypsin concentration in the urine samples was analyzed by ELISA kit (Catalog No. ELH-serpinA3, Raybiotech Inc.) The procedure was performed following the instructions of the manufacturer. Urine samples from healthy volunteers and patients were diluted at 1:100 or 1:200–500, respectively.

Statistical analysis. Data distribution was evaluated by the Shapiro-Wilk test. The variables with normal distributions are presented as mean ± SD, while variables with non-normal distributions are presented as median and interquartile range. The groups were compared with ANOVA or the Kruskal Wallis test as appropriate, with Bonferroni's and Dunn's tests for multiple comparisons. Correlations were evaluated by Spearman's test. The factors independently associated with interstitial fibrosis in LN patients were determined by a linear regression model. Variables were log-transformed and collinearity assessed by the variation inflation factor (VIF). Statistical significance was defined as a p-value < 0.05.

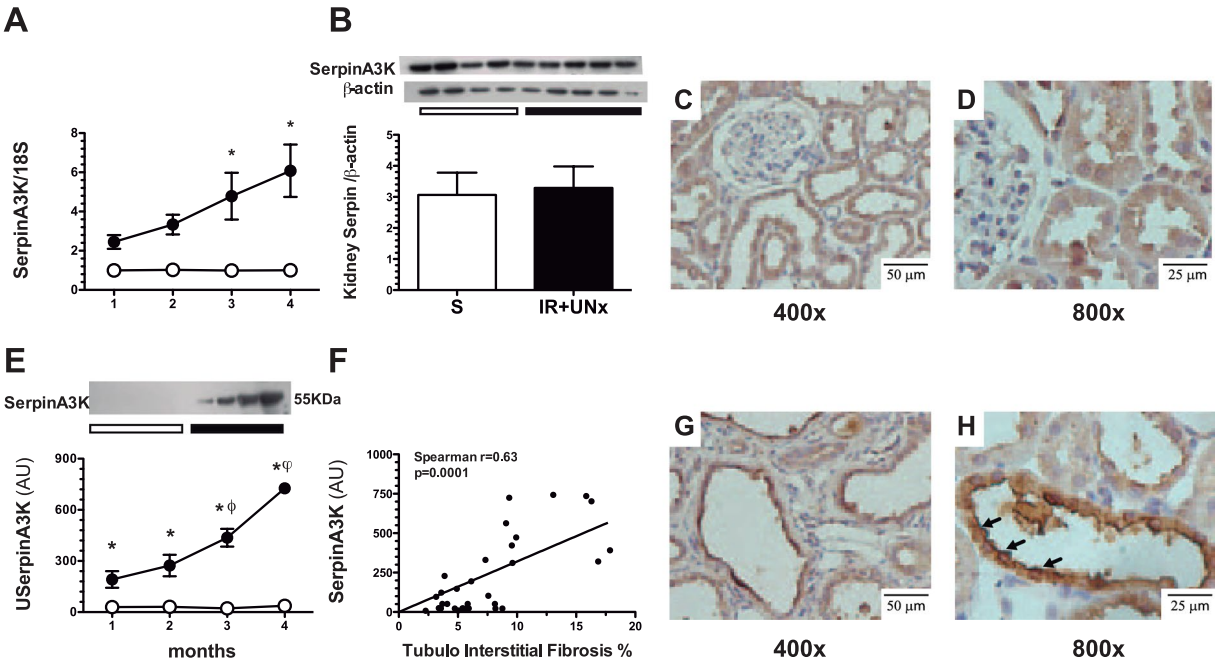

Figure 3. Timely AKI to CKD transition detection by serpinA3. (**A**) SerpinA3 mRNA levels in renal cortex during the follow-up of the animals, (**B**) SerpinA3 protein levels in the renal cortex evaluated by Western Blot 4 months post-ischemia, (**C**,**D**) representative microphotographs of serpinA3 immunostaining in renal cortex from the control group, magnification 400 and 800x respectively, (**E**) Urinary serpinA3 levels during AKI to CKD transition and compared with the control group, (**F**) Spearman correlation between urine serpinA3 and tubulo-interstitial fibrosis, and (**G**,**H**) representative microphotographs of serpinA3 immunostaining in renal cortex from the AKI to CKD transition group, magnification 400 and 800x respectively. Data are represented as mean ± SE. (for sham, n = 4, and for the AKI to CKD transition groups, n = 5 per period). White circles or bar represent sham and black circles or bar represent AKI to CKD transition groups and. *$p < 0.05$ vs. the sham group in their respective period, $^{\phi}p < 0.05$ vs. IR + UNx 2nd month and $\omega p < 0.05$ vs. IR + UNx 3rd month.

Results

Identification of SerpinA3 in the urine from rats with CKD. CKD was induced in male rats using the model of right nephrectomy plus contralateral renal ischemia for 45-min then followed for four months. By the end of the study, all animals developed CKD and exhibited higher amounts of urine proteins between 55 and 72 kDa compared to the control group (Fig. 1A). The bands were isolated, and the proteins were extracted from the gel to be analyzed by high-resolution mass spectrometry. As expected, albuminuria was present in the urine. In addition, serpinA3 was identified in these samples with a coverage of 44.7%. Other identified proteins were serotransferrin, alpha-1-antiproteinase, serine A3M protease inhibitor, LOC299282 protein, serpinC1, kininogen T, B-fetuin, and type I keratin. However, albumin and serpinA3 constituted the most abundant proteins (Fig. 1B).

uSerpinA3 levels in the AKI to CKD transition. We analyzed the time course of the AKI to CKD transition by studying and euthanizing groups of animals on a monthly basis, starting in the 1st month and continuing up to the 4th month post-ischemia. The AKI to CKD transition was characterized by a progressive elevation of proteinuria that was statistically significant starting at the 3rd month (Fig. 2A), together with a significant reduction of renal blood flow (Fig. 2B) and renal dysfunction at the 4th month (Fig. 2C). The development of tubulointerstitial fibrosis was also observed starting at the 3rd month post-ischemia (Fig. 2D). These results show that uninephrectomized rats exposed to an AKI episode developed progressive CKD that was detected between three- and four-months post-AKI by the classic renal injury biomarkers.

Renal tissue serpinA3 mRNA and protein levels, as well as uSerpinA3 were analyzed during the time course of the AKI to CKD transition, as shown in Fig. 3. We observed a significant increase in serpinA3 mRNA levels starting at the 3rd month post-ischemia compared to the control group (Fig. 3A); however, this difference was not reflected at the protein level, as is shown by the Western blot analysis, in which no differences between groups were observed (Fig. 3B). Immunohistochemical analysis revealed that in the control group, serpinA3 is expressed mostly in the cytoplasm of tubular epithelium (Fig. 3C,D). Interestingly, in the AKI to CKD transition group serpinA3 is relocated to the apical membrane (Fig. 3G,H). The Supp. Fig. 1 shows the serpinA3 relocation along the AKI to CKD transition, that was slightly observed since the 1st month and the relocation was even more evident throughout the CKD progression. Moreover, we found that the AKI to CKD transition was timely revealed by a progressive increase in uSerpinA3 levels, which were significantly elevated starting at the 1st month, even before the proteinuria appearance (Fig. 2A). In contrast, this protein was not detected in the urine from the control group (Fig. 3E). It is noteworthy that 15 days after the AKI episode was resolved, serpinA3 was not found in the

	Volunteers n = 20	Class III LN n = 18	Class IV LN n = 18	Class V LN n = 11	AAV n = 19	FSGS n = 14
Age, years	31 ± 10	31 ± 10	30 ± 11	33 ± 14	54 ± 15	36 ± 10
Female, n (%)	6 (30)	14 (75)	16 (89)	9 (82)	14 (74)	4 (29)
Months from SLE diagnosis, median (IQR)	—	23 (0–62)	36 (4–83)	27 (8–116)	—	—
Months from renal symptoms start, median (IQR)	—	2 (1–5)	2 (1–4)	3 (1–5)	1 (0–2)	6 (2–11)
Creatinine, mg/dl, median (IQR)	0.8 (0.7–0.9)	0.8 (0.7–1.3)	1.2 (0.7–2.1)$^{\Phi}$	0.7 (0.5–0.9)	2.6 (1.2–3.6)*	0.9 (0.8–1.4)
eGFR, ml/min/1.73 m^2, median (IQR)	118 (105–129)	99 (50–119)	64 (31–119)*	111 (103–132)	24 (14–90)*	85 (61–107)
Proteinuria, g/g, median (IQR)	0.1 (0.0–0.1)	2.7 (1.9–4.0)*	5.7 (3.4–8.4)*	2.9 (1.9–4.3)*	2.2 (0.7–3.1)*	3.3 (1.6–6.2)*
Hematuria, n (%)	0 (0)	12 (67)	17 (94)	7 (64)	18 (95)	11 (79)
+ve dsDNA antibodies, n (%)	ND	15 (83)	16 (89)	7 (64)	0 (0)	0 (0)
Complement C3, mg/dl	ND	73 (60–90)	53 (41–72)	111 (71–131)	119 (103–132)	148 (126–189)
Complement C4, mg/dl	ND	9 (8–14)	8 (8–14)	14 (11–18)	32 (20–42)	32 (30–46)
Interstitial fibrosis, %, median (IQR)	ND	15 (10–20)	20 (12.5–40)$^{\Phi}$	10 (0–15)	30 (25–50)$^{+}$	17.5 (10–40)
Tubular atrophy, %, median (IQR)	ND	15 (10–20)	20 (12.5–30)$^{\Phi}$	10 (0–15)	30 (30–60)$^{+}$	15 (15–40)

Table 1. Clinical characteristics of the studied patients. Abbreviations. LN, lupus nephritis; AAV, ANCA-associated vasculitis; FSGS, focal and segmental glomerulosclerosis; SLE, systemic lupus erythematosus; eGFR, estimated glomerular filtration rate calculated by the CKD-EPI formula; +ve dsDNA antibodies, positive antibodies directed to double-strand DNA; ND, not determined. Mean ± S.D. $^{*}p < 0.05$ vs. volunteers, $^{\Phi}p < 0.05$ vs. class V LN, and $^{+}p < 0.05$ vs. FSGS.

urine (Supp. Fig. 2). Thus, the abnormal uSerpinA3 levels and the gradual increment along the time course reflect the AKI to CKD transition. Accordingly to these findings, there was a significant correlation between renal fibrosis and uSerpinA3 levels, as is shown in Fig. 3F ($r = 0.63$, $p < 0.001$).

uSerpinA3 in CKD secondary to lupus nephritis. To translate these findings to the clinical setting, we evaluated whether serpinA3 could be used as a biomarker in CKD patients. For this purpose, we analyzed serpinA3/Alpha-1-antichymotrypsin levels in patients diagnosed with class III, IV and V lupus nephritis, focal and segmental glomerulosclerosis (FSGS), ANCA associated vasculitis (AAV), and compared them with healthy volunteers. As these patients were diagnosed by kidney biopsy, CKD diagnosis was based on the histopathological analysis, severe proteinuria, and/or renal dysfunction. The patients with LN were classified using the ISN/RPS classification by a qualified nephropathologist. A representative microphotograph of hematoxylin/eosin staining and immunofluorescence that allowed the LN classification are shown in the Supp. Fig. 3. In this study, we included 47 LN patients of different classes and compared them with 20 healthy volunteers. The demographical characteristics of these patients are shown in Table 1. As expected in LN, the proportion of women was greater in all the groups and most were young patients. The time of evolution from systemic lupus erythematosus diagnosis and the time elapsed between the first renal symptom and the biopsy appears also in Table 1. In accordance with previous studies, the worst renal fibrosis and tubular atrophy was seen in class III and IV LN patients (proliferative LN)[5]. As shown in Fig. 4A, the serum creatinine levels were higher in class IV LN compared to class V patients (membranous LN). All LN patients exhibited severe proteinuria and variable renal fibrosis degrees (Fig. 4B,C). uSerpinA3 was not detected in the urine from healthy volunteers, but it was significantly elevated in classes III/IV LN patients, whereas class V LN group exhibited lower uSerpinA3 levels as is shown by the Western blot analysis in Fig. 4D. The absolute uSerpinA3 values are presented in Fig. 4E and the uSerpinA3 corrected by urinary creatinine in Fig. 4F. The results obtained by ELISA were similar to those by Western blot analysis (Fig. 4G). There were no differences in plasma serpinA3/Alpha-1-antichymotrypsin levels among LN groups and between LN and healthy volunteers (Supp. Fig. 4A) and there was no correlation between plasma and uSerpinA3 levels (Supp. Fig. 4B). As found in the rat model, we observed a significant correlation between the uSerpinA3 levels (ELISA) and interstitial fibrosis % ($r = 0.34$, $p = 0.02$, Fig. 4H). Moreover, uSerpinA3 levels discriminated between class III/ IV LN patients from class V LN, with a c-statistic of 0.85 (Supp. Fig. 5). We constructed a linear regression model to determine factors associated to renal interstitial fibrosis (dependent variable). The model included age, serum creatinine, proteinuria, histological activity score, plasma and urinary SerpinA3 (Suppl. Table 2). Urinary SerpinA3, serum creatinine and proteinuria were independently associated to the degree of interstitial fibrosis. There was no collinearity among the included variables (VIF < 1.4 for all variables).

In accordance to our experimental findings, serpinA3 was found in the cytosol of tubular epithelial cells from kidney donor's biopsies (Fig. 5A–C). By contrast, in class III/IV LN patients, serpinA3 was relocated to the apical tubular membrane (Fig. 5D–I). Interestingly, class V LN patients, whom exhibited lower uSerpinA3 levels, the relocation was minimal (Fig. 5J–L).

uSerpinA3 levels in CKD secondary to FSGS and AAV. To explore other etiologies of renal injury, we included patients diagnosed with FSGS and AAV. The Table 1 shows also the demographical characteristics of these two groups compared with the volunteers group. The AAV patients were older than the other groups and the percentage of women was higher in all the groups. The worst renal structural injury was seen in the AAV group.

The AAV group exhibited severe renal injury characterized by a significant elevation of serum creatinine, proteinuria, renal fibrosis and tubular atrophy (Fig. 6A–C, Table 1). In the FSGS group, serum creatinine was

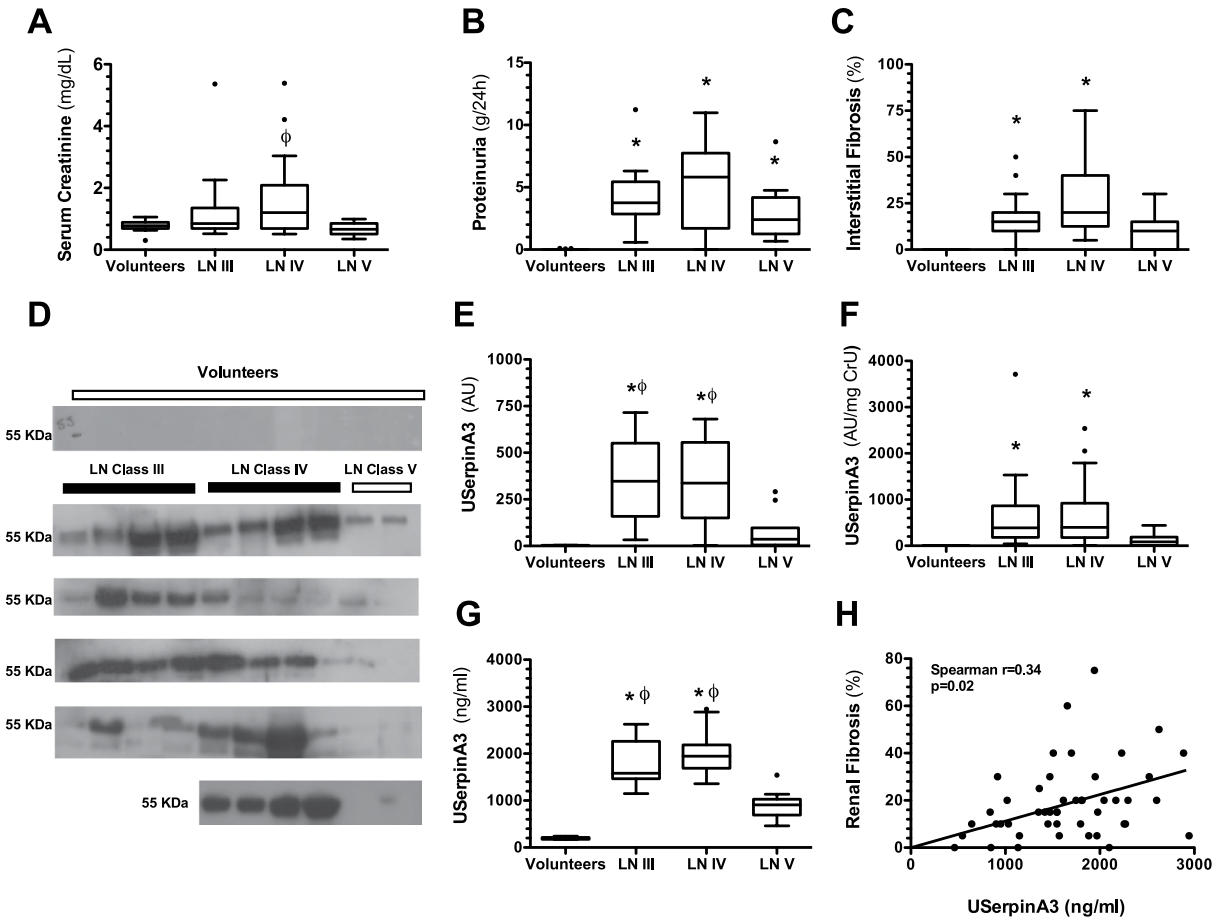

Figure 4. Renal clinical characteristics and urinary serpinA3 in patients diagnosed with LN. (**A**) Serum creatinine, (**B**) Proteinuria, (**C**) Percentage of renal fibrosis, and (**D**) WB autoradiography for urinary serpinA3 levels showing all the patients included. (**E**) Densitometric analysis for WB. (**F**) Urinary serpinA3 corrected by urinary creatinine. (**G**) Urinary serpinA3 levels determined by ELISA. (**H**) Spearman's correlation of urinary serpinA3 and tubule-interstitial fibrosis. LN III = class III lupus nephritis (n = 18); LN IV = class IV lupus nephritis (n = 18); LN V = class V lupus nephritis (n = 11). Data are presented as Tukey's box and whiskers plots. Healthy volunteers (n = 20), *$p < 0.001$ vs. Healthy volunteers, $^{\phi}p < 0.001$ vs. class V LN.

not different from the volunteers group (Fig. 6A), but the proteinuria was more severe than in the AAV group (Fig. 6B), despite similar tubular interstitial fibrosis (Fig. 6C). As shown in Fig. 6D, uSerpinA3 was significantly higher in patients with FSGS and AAV compared to the volunteer's group as is shown by the Western blot, the densitometric analysis (Fig. 6E) and the uSerpinA3 corrected by urine creatinine (Fig. 6F). All results obtained by Western blot were later confirmed by a commercial serpinA3/alpha-1-antichymotrypsin ELISA (Fig. 6G). As we could not determine renal fibrosis in healthy volunteers group, no significant correlation between uSerpinA3 levels and renal fibrosis % was found, but it can be appreciated that to greater fibrosis, uSerpinA3 levels were higher (Fig. 6H).

uSerpinA3 levels in patients with inflammatory diseases without renal dysfunction. To determine the specificity of uSerpinA3 for detecting kidney injury, we evaluated uSerpinA3/alpha-1-antichemotrypsin in patients with inflammatory diseases, but without renal dysfunction. For this purpose, patients with liver cirrhosis (LC), acute pancreatitis (AP) and active rheumatoid arthritis (RA) were included. The clinical characteristics of these patients are shown in the Suppl. Table 1. As shown in the Suppl. Fig. 6A,B, uSerpinA3 was not detected in LC, AP, and RA groups by either Western blot or ELISA.

Discusion

Using high-resolution mass spectrometry, we isolated urine proteins from animals with CKD. Among the identified proteins were: albumin, serpinA3, serotransferrin, alpha-1-antiproteinase, serine A3M protease inhibitor, LOC299282 protein, serpinC1, kininogen T, B-fetuin, and type I keratin. Albumin and serpinA3 constituted the most abundant proteins.

Serpins are a family of serine protease inhibitors. Thirty-four serpins from nine classes have been identified and characterized in humans to date; within these proteins is the serpinA3/Alpha-1-Antichymotrypsin

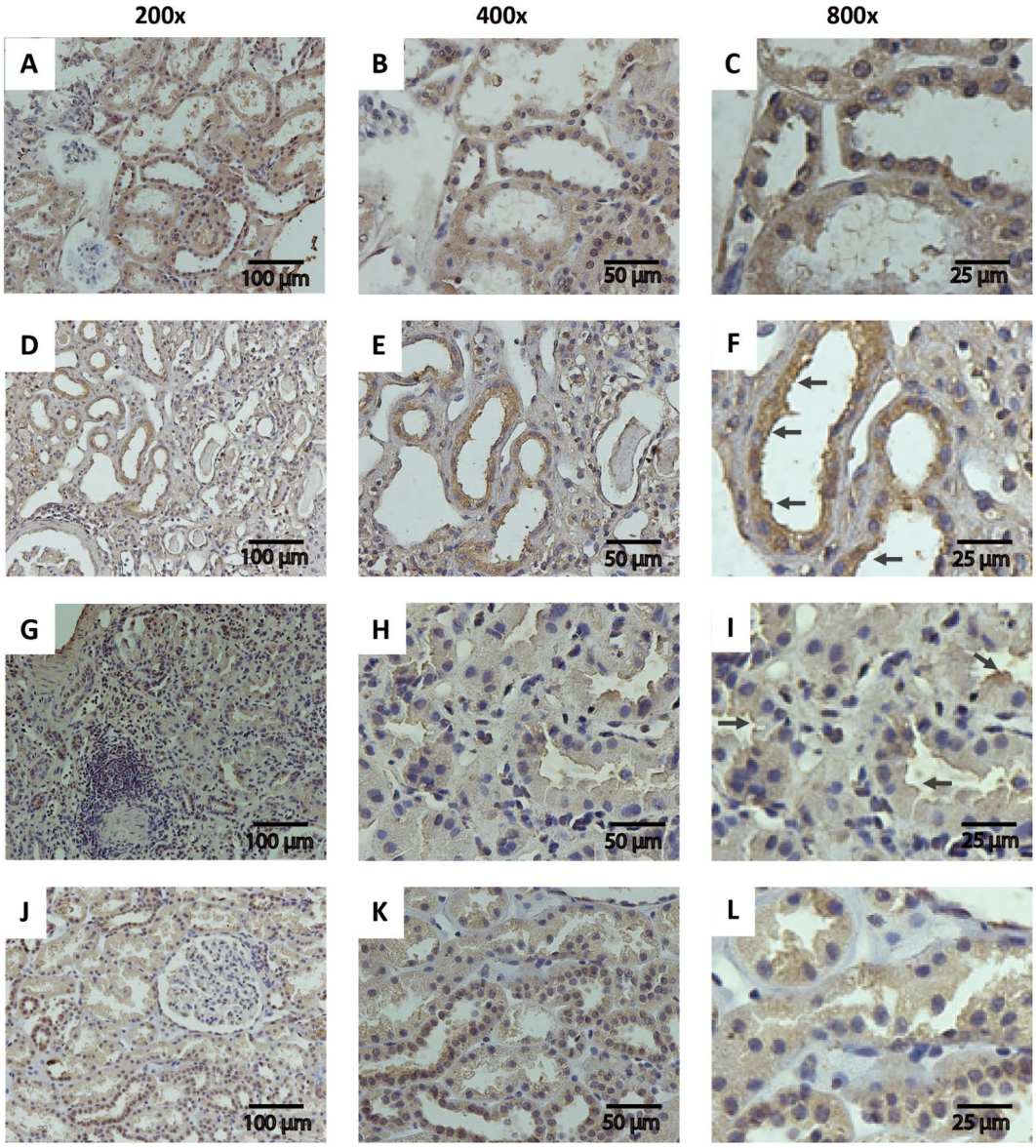

Figure 5. Serpin A3K immunohistochemistry in renal biopsies. (**A**–**C**) Representative micrographs of serpinA3 in a biopsy from healthy donor (Magnification 200x, 400x and 800x, respectively); (**D**–**F**) Representative micrographs of serpinA3 from a patient diagnosed with LN class III (Magnification 200x, 400x and 800x, respectively); (**G**–**I**) Representative micrographs of serpinA3 from a patient with LN class IV (Magnification 200x, 400x and 800x, respectively); (**J**–**L**) Representative micrographs of serpinA3 from patient with LN class V (Magnification 200x, 400x and 800x, respectively). Black arrows point the relocation to apical membrane in CKD patients.

(serine-proteinase inhibitor, class A, member 3), whereas the homologous for rodents is serpinA3K[23]. The genecards website, a database of human genes (http://www.genecards.org/cgi-bin/carddisp.pl?gene=SERPINA3&keywords=serpinA3), has reported serpinA3 expression in different tissues, evaluated by three different approaches: RNAseq, microarrays and a serial analysis of gene expression (SAGE), with the largest expression in retina, kidney, liver, and pancreas (Suppl. Fig. 7). In the kidney, Fleming S. *et.al.*[24] identified serpinA3 in the tubular proximal epithelium, the mesenchyme of nephroblastomas and the adult renal cell carcinoma. Similarly, Khan T.N. *et al.*[25] found serpinA3 immunostaining in proximal tubules from control biopsies. We confirmed these findings in this work showing that in the kidney from control rats and in kidney from donor biopsies, serpinA3 is mainly located in the cytoplasm of tubular epithelial cells (Figs 3C,D and 5A–C).

SerpinA3 has been involved in different pathologies such as hypertension, inflammation, and angiogenesis[26]. Specifically, in cornea and retina, serpinA3 promotes anti-inflammatory, anti-angiogenic, anti-oxidant and anti-fibrotic actions[26–30]. However, little is known about the specific role of serpinA3 in the renal pathophysiology. One study showed increased serpinA3 staining in the proximal renal tubules in biopsies from a variety of primary and secondary glomerulonephritis, such as minimal-change disease (MCD), FSGS, diffuse mesangial

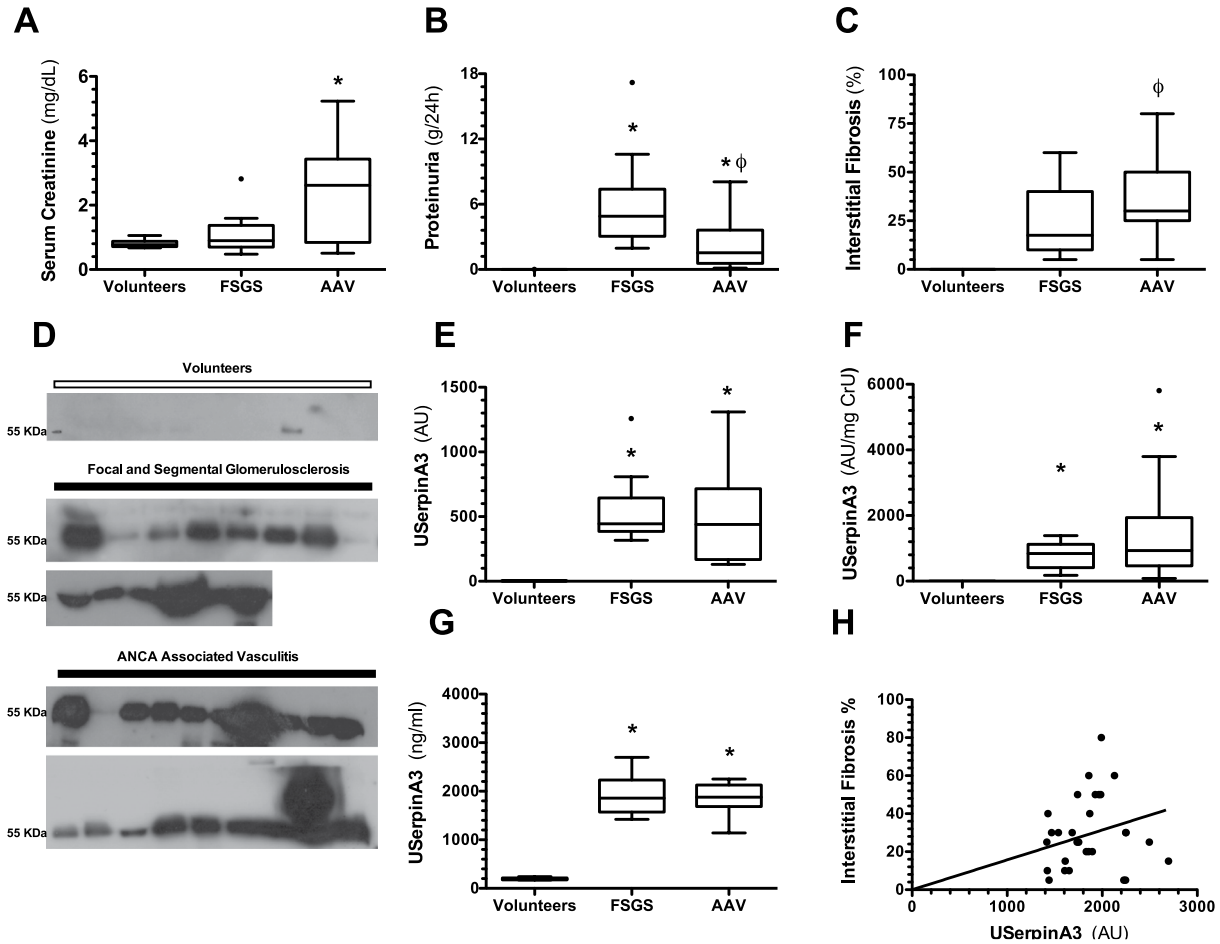

Figure 6. Renal clinical characteristics and urinary serpinA3 in patients diagnosed with FSGS and AAV. (**A**) Serum creatinine, (**B**) Proteinuria, (**C**) Percentage of renal fibrosis, and (**D**) WB autoradiography for urinary serpinA3 levels showing all the patients included. (**E**) Densitometric analysis for WB. (**F**) Urinary serpinA3 corrected by urinary creatinine. (**G**) Urinary serpinA3 levels determined by ELISA. (**H**) Spearman's correlation of urinary serpinA3 and tubule-interstitial fibrosis. Focal Segmental Glomerulosclerosis = FSGS (n = 14); ANCA-associated vasculitis = AAV (n = 19). Data are presented as Tukey's box and whiskers plots. *$p < 0.001$ vs. Healthy volunteers, $^{\phi}p < 0.001$ vs. FSGS.

proliferative glomerulonephritis (MeGN), membranous glomerulonephritis (MGN), diabetic nephropathy, IgA nephritis and LN compared to normal renal tissues[31].

In the present study, using a model of AKI to CKD transition in rats, we found that serpinA3 appears in the urine since the first month post-ischemia, when the rats do not even exhibit proteinuria or any sign of glomerular damage. Moreover, uSerpinA3 levels positively correlated with renal fibrosis, hence higher uSerpinA3 levels associate with higher renal tissue fibrosis.

To address if urinary serpinA3 was being filtrated, we measured plasma serpinA3 and found no correlation between plasma serpinA3 with urinary serpinA3 levels. Furthermore, plasma serpinA3 levels were similar in healthy volunteers and among the different lupus nephritis classes (Suppl. Fig. 5) and uSerpinA3 levels were independently associated with interstitial fibrosis. We cannot fully exclude that some fraction of serpinA3 may be filtered in pathophysiological conditions, however, in our rat model, we showed that serpinA3 appears in the urine since the first month post renal ischemia, much earlier than proteinuria. Furthermore, the subgroup of class V LN patients with higher degrees of proteinuria (>3 g per day) still exhibited minimal serpinA3 urine excretion. As serpinA3 is mainly expressed in organs such as liver or pancreas, we also included patients with acute inflammation (pancreatitis) or chronic damage (cirrhosis). Urinary serpinA3 levels were not modified in these conditions. These evidences together strongly suggest that most of the serpinA3 found in the urine has renal origin.

In pathologic conditions, serpinA3 was relocated from the cytoplasm to the apical epithelial membrane (Fig. 3). This suggests: 1) that uSerpinA3 reflects intra-renal injury, 2) that during renal injury, serpinA3 is probably secreted into the luminal space explaining its emergence in the urine, and 3) that uSerpinA3 is an early and timely marker of AKI to CKD transition.

We then analyzed the expression of uSerpinA3 in human renal diseases. We showed that uSerpinA3 is not detectable in healthy volunteers but it increases in kidney diseases from different etiologies: LN, FSGS and AAV.

In LN patients, uSerpinA3 levels were found elevated in severe classes III/IV LN that are usually associated with greater kidney fibrosis, and less elevated, in the less inflammatory class V LN that usually carries better prognosis[32]. It has also been reported increased uSerpinA3 levels in active LN patients but not in systemically active lupus without renal involvement[33]. These suggests that uSerpinA3 derives from kidney and its elevation is probably associated with higher inflammation and fibrosis. However, the potential use of uSerpinA3 as a biomarker needs further evaluation in larger studies.

SerpinA3 has been described to have anti-inflammatory properties[8–12,26,28], therefore, we decided to evaluate uSerpinA3 in AAV, a severe renal inflammatory disease, and compared it to FSGS patients, a proteinuric but less inflammatory disease. Urinary SerpinA3 levels were equally elevated in both groups despite different degrees of proteinuria and positively correlated with the percentage of renal fibrosis in the biopsy. Furthermore, we studied patients with extrarenal inflammatory diseases (rheumatoid arthritis, pancreatitis, liver cirrhosis) with preserved renal function. Urinary SerpinA3 levels were similar in these patients compared to those observed in healthy volunteers. This also supports that uSerpinA3 is kidney-derived and probably more related to fibrosis than to sytemuc inflammation.

The specific role of serpins in the renal physiology or pathophysiology has not been studied. Zhang B. *et al.*[27,29,30], Liu X. *et al.*[26] and Hu, J. *et al.*[28] have demonstrated that serpinA3 blocks reactive oxygen species (ROS) generation, inflammation and pro-fibrotic pathways in the cornea and retina. Thus, our results suggest that serpinA3's role in the kidney could be to counterbalance the inflammation, oxidative stress and renal fibrosis that follows renal damage. This hypothesis will require further study. As it is possible that serpinA3 may have a different role depending on the pathophysiological scenery, we need to wait for serpinA3's transgenic mice that will be soon available to more profoundly evaluate its role in AKI and CKD.

The limitations of the present study are: 1) uSerpinA3 levels were measured in biological samples at a single time point, and further work has to be undertaken to evaluate the course of this protein longitudinally, and 2) although there was a good correlation with kidney fibrosis, it cannot be ignored that uSerpinA3 levels could be increased secondary to other ongoing inflammatory processes in the kidney.

This study supports that uSerpinA3 is an early and effective biomarker for the detection of renal injury, with a great potential to be used in the diagnosis of the AKI to CKD transition and CKD from different etiologies. Our observations in humans suggest that uSerpinA3 can be a useful marker for renal fibrosis and inflammation, with a potential role to differentiate between class III/IV and class V lupus nephritis.

References

1. Lozano, R. *et al.* Global and regional mortality from 235 causes of death for 20 age groups in 1990 and 2010: a systematic analysis for the Global Burden of Disease Study 2010. *Lancet.* **380**, 2095–2128 (2012).
2. Levin, A. & Stevens, P. E. Summary of KDIGO 2012 CKD Guideline: behind the scenes, need for guidance, and a framework for moving forward. *Kidney Int* **85**, 49–61, https://doi.org/10.1038/ki.2013.444 (2014).
3. Kidney Disease: Improving Global Outcomes, C. K. D. M. B. D. U. W. G. KDIGO 2017 Clinical Practice Guideline Update for the Diagnosis, Evaluation, Prevention, and Treatment of Chronic Kidney Disease-Mineral and Bone Disorder (CKD-MBD). *Kidney Int Suppl* 7, 1–59, https://doi.org/10.1016/j.kisu.2017.04.001 (2017).
4. Lima-Posada, I. *et al.* Gender Differences in the Acute Kidney Injury to Chronic Kidney Disease Transition. *Sci Rep* **7**, 12270, https://doi.org/10.1038/s41598-017-09630-2 (2017).
5. Parikh, S. V., Alvarado, A., Malvar, A. & Rovin, B. H. The Kidney Biopsy in Lupus Nephritis: Past, Present, and Future. *Semin Nephrol* **35**, 465–477, https://doi.org/10.1016/j.semnephrol.2015.08.008 (2015).
6. Mehta, R. L. *et al.* International Society of Nephrology's 0by25 initiative for acute kidney injury (zero preventable deaths by 2025): a human rights case for nephrology. *Lancet* **385**, 2616–2643, https://doi.org/10.1016/S0140-6736(15)60126-X (2015).
7. Susantitaphong, P. *et al.* World incidence of AKI: a meta-analysis. *Clin J Am Soc Nephrol* **8**, 1482–1493, https://doi.org/10.2215/CJN.00710113 (2013).
8. Venkatachalam, M. A. *et al.* Acute kidney injury: a springboard for progression in chronic kidney disease. *Am. J. Physiol Renal Physiol* (2010).
9. Chawla, L. S., Eggers, P. W., Star, R. A. & Kimmel, P. L. Acute kidney injury and chronic kidney disease as interconnected syndromes. *N.Engl.J.Med.* **371**, 58–66 (2014).
10. Block, C. A. & Schoolwerth, A. C. Acute renal failure: outcomes and risk of chronic kidney disease. *Minerva Urol Nefrol* **59**, 327–335 (2007).
11. Ponte, B., Felipe, C., Muriel, A., Tenorio, M. T. & Liano, F. Long-term functional evolution after an acute kidney injury: a 10-year study. *Nephrol Dial Transplant* **23**, 3859–3866, https://doi.org/10.1093/ndt/gfn398 (2008).
12. Iwashima, F. *et al.* Aldosterone induces superoxide generation via Rac1 activation in endothelial cells. *Endocrinology* **149**, 1009–1014 (2008).
13. Lewington, A. J., Cerda, J. & Mehta, R. L. Raising awareness of acute kidney injury: a global perspective of a silent killer. *Kidney Int.* **84**, 457–467 (2013).
14. Coca, S. G., Singanamala, S. & Parikh, C. R. Chronic kidney disease after acute kidney injury: a systematic review and meta-analysis. *Kidney Int* (2011).
15. Bucaloiu, I. D., Kirchner, H. L., Norfolk, E. R., Hartle, J. E. & Perkins, R. M. Increased risk of death and de novo chronic kidney disease following reversible acute kidney injury. *Kidney Int.* **81**, 477–485 (2012).
16. Barrera-Chimal, J. *et al.* Spironolactone prevents chronic kidney disease caused by ischemic acute kidney injury. *Kidney Int*. **83**, 93–103 (2013).
17. Rodriguez-Romo, R. *et al.* AT1 receptor antagonism before ischemia prevents the transition of acute kidney injury to chronic kidney disease. *Kidney Int* **89**, 363–373, https://doi.org/10.1038/ki.2015.320 (2016).
18. Barrera-Chimal, J. *et al.* Hsp72 is an early and sensitive biomarker to detect acute kidney injury. *EMBO Mol.Med.* **3**, 5–20 (2011).
19. Weening, J. J. *et al.* The classification of glomerulonephritis in systemic lupus erythematosus revisited. *Kidney Int* **65**, 521–530, https://doi.org/10.1111/j.1523-1755.2004.00443.x (2004).
20. Banks, P. A. *et al.* Classification of acute pancreatitis–2012: revision of the Atlanta classification and definitions by international consensus. *Gut* **62**, 102–111, https://doi.org/10.1136/gutjnl-2012-302779 (2013).
21. van Riel, P. L. & Renskers, L. The Disease Activity Score (DAS) and the Disease Activity Score using 28 joint counts (DAS28) in the management of rheumatoid arthritis. *Clin Exp Rheumatol* **34**, S40–S44 (2016).
22. Child, C. G. & Turcotte, J. G. Surgery and portal hypertension. *Major Probl Clin Surg* **1**, 1–85 (1964).

23. van Gent, D., Sharp, P., Morgan, K. & Kalsheker, N. Serpins: structure, function and molecular evolution. *Int J Biochem Cell Biol* **35**, 1536–1547 (2003).
24. Fleming, S. & Gibson, A. A. Proteinase inhibitors in the kidney and its tumours. *Histopathology* **10**, 1303–1313 (1986).
25. Khan, T. N. & Sinniah, R. Renal tubular antiproteinase (alpha-1-antitrypsin and alpha-1-antichymotrypsin) response in tubulo-interstitial damage. *Nephron* **65**, 232–239 (1993).
26. Liu, X. *et al*. Anti-angiogenic and anti-inflammatory effects of SERPINA3K on corneal injury. *PLoS One* **6**, e16712, https://doi.org/10.1371/journal.pone.0016712 (2011).
27. Zhang, B., Hu, Y. & Ma, J. X. Anti-inflammatory and antioxidant effects of SERPINA3K in the retina. *Invest Ophthalmol Vis Sci* **50**, 3943–3952, https://doi.org/10.1167/iovs.08-2954 (2009).
28. Hu, J. *et al*. Serine protease inhibitor A3K protects rabbit corneal endothelium from barrier function disruption induced by TNF-alpha. *Invest Ophthalmol Vis Sci* **54**, 5400–5407, https://doi.org/10.1167/iovs.12-10145 (2013).
29. Zhang, B. & Ma, J. X. SERPINA3K prevents oxidative stress induced necrotic cell death by inhibiting calcium overload. *PLoS One* **3**, e4077, https://doi.org/10.1371/journal.pone.0004077 (2008).
30. Zhang, B., Zhou, K. K. & Ma, J. X. Inhibition of connective tissue growth factor overexpression in diabetic retinopathy by SERPINA3K via blocking the WNT/beta-catenin pathway. *Diabetes* **59**, 1809–1816, https://doi.org/10.2337/db09-1056 (2010).
31. Conz, P. *et al*. Alpha-1-antichymotrypsin in renal biopsies. *Nephron* **56**, 387–390 (1990).
32. Sun, H. O. *et al*. Long-term outcome of Chinese patients with membranous lupus nephropathy. *Lupus* **17**, 56–61, https://doi.org/10.1177/0961203307083443 (2008).
33. Chatterjee, P. K. *et al*. GW274150, a potent and highly selective inhibitor of iNOS, reduces experimental renal ischemia/reperfusion injury. *Kidney Int.* **63**, 853–865 (2003).

Acknowledgements

We are grateful to Martha Carrasco and Silvia Ivonne Mora for their technical assistance, to Dr. Mariela Contreras and Erika Miguel-Cruz for their aid with the animal care, and to Dr. Norma Uribe who facilitated us the kidney biopsy paraffin blocks. The results presented in this paper have not been published previously in whole or in part, except as an abstract presented at the American Society of Nephrology Kidney Week Meeting 2017 and 2018 (New Orleans, LO, and San Diego, CA. respectively). Dr. Norma A. Bobadilla and BS Andrea Sánchez-Navarro have presented a Mexican patent application. The studies from our laboratory cited in the review were supported by grants from the Mexican Council of Science and Technology (CONACyT) (235855, 235964, 272390, and A1-S-8715 to NAB) and from the National University of Mexico (IN223915 and IN201619 to NAB). This study was performed in partial fulfillment of the requirements for the PhD degree, Andrea Sánchez-Navarro is a doctoral student from Programa de Doctorado en Ciencias Biomédicas, Universidad Nacional Autónoma de México (UNAM) and received a fellowship from CONACYT (607517).

Author Contributions

Conception and design N.A.B. and A.S.N. Performed the experiments and analytical techniques A.S.N., R.P.V. and B.M.C. Acquisition of data: A.S.N., J.M.M.V. and N.A.B. Inclusion of patients: D.L.C.P. and J.M.M.V. Analysis and interpretation of data; N.A.B., A.S.N., J.M.M.V. and G.G. Drafting the article and revising it critically for important intellectual content; N.A.B., A.S.N., J.M.M.V. and G.G.

Additional Information

Supplementary information accompanies this paper at https://doi.org/10.1038/s41598-019-46601-1.

Competing Interests: The authors declare no competing interests.

Publisher's note: Springer Nature remains neutral with regard to jurisdictional claims in published maps and institutional affiliations.

6.4 SOLICITUD DE PATENTE SERPINA3K

Derivado de la descripción de la proteína SerpinA3 como un biomarcador temprano y oportuno para la detección de la ERC y la LRA, sometimos la solicitud de patente en 2017.

Instituto Mexicano de la Propiedad Industrial

[X] Solicitud de Patente
[ ] Solicitud de Registro de Modelo de Utilidad

[ ] Solicitud de Registro de Diseño Industrial, especifique cuál:
[ ] Modelo Industrial [ ] Dibujo Industrial

Antes de llenar la forma lea las consideraciones generales al reverso

Uso exclusivo Delegaciones Subdelegaciones de la Secretar Economía y Oficinas Regionales IMPI.

Sello

Folio de entrada

Fecha y hora de recepción

INSTITUTO MEXICANO DE LA PROPIEDAD INDUSTRIAL
Dirección Divisional de Patentes

Solicitud Expediente: MX/a/2017/010805
Fecha: 23/AGO/2017 Hora: 11:29:22
Folio: MX/E/2017/061900 869699

MX/E/2017/061900

I DATOS DEL (DE LOS) SOLICITANTE(S)

El solicitante es el inventor [ ] El solicitante es el causahabiente [X]

1) Nombre (s): **UNIVERSIDAD NACIONAL AUTÓNOMA DE MÉXICO**

2) Nacionalidad (es): MEXICANA

3) Domicilio; calle, número, colonia y código postal: 9° PISO DE LA TORRE DE RECTORÍA S/N, CIUDAD UNIVERSITARIA, C.P. 04510

Población, Estado y País: COYOACÁN, CIUDAD DE MÉXICO, MÉXICO.

4) Teléfono (clave): (55) 56 22 63 29 AL 31 5) Fax (clave): (55) 56 65 46 44

II DATOS DEL (DE LOS) INVENTOR(ES)

6) Nombre (s):NORMA ARACELI BOBADILLA SANDOVAL Y ANDREA SÁNCHEZ NAVARRO.

7) Nacionalidad (es): MEXICANAS.

8) Domicilio; calle, número, colonia y código postal: ÁGUILA TRIANA N°55, COL. FUEGO NUEVO, IZTAPALAPA, C.P. 09800.

Población, Estado y País: CIUDAD DE MÉXICO, MÉXICO.

9) Teléfono (clave): 10) Fax (clave):

III DATOS DEL (DE LOS) APODERADO (S)

11) Nombre (s): MARTHA FIGUEROA PÉREZ 12) RGP-DDAJ-14782

13) Domicilio; calle, número, colonia y código postal: 3er PISO DEL EDIFICIO "B" DE LAS OFICINAS ADMINISTRATIVAS EXTERIORES DE LA ZONA CULTURAL DE CIUDAD UNIVERSITARIA, C.P. 04510.

Población, Estado y País: COYOACÁN, CIUDAD DE MÉXICO, MÉXICO. 14) Teléfono (clave): (55) 56 22 63 29 AL 31 15) Fax (clave): (55) 56 65 46 44

16) Personas Autorizadas para oír y recibir notificaciones:

DANIEL OJESTO MARTÍNEZ PORCAYO, ROCIO JUÁREZ VÁZQUEZ Y ANACLARA ALVARADO DE LA CUESTA.

17) **Denominación o Título de la Invención:**

"MÉTODO DE DIAGNOSTICO PARA DETECTAR LA ENFERMEDAD RENAL CRÓNICA Y LA LESIÓN RENAL AGUDO MEDIANTE EL USO DE LA SERPINA A3K"

18) **Fecha de divulgación previa** Día Mes Año

19) **Clasificación Internacional** **uso exclusivo del IMPI**

20) **Divisional de la solicitud** Número Figura jurídica

21) **Fecha de presentación** Día Mes Año

22) **Prioridad Reclamada:**

País	Fecha de presentación Día Mes Año	No. de serie

Lista de verificación (uso interno)

No. Hojas			No. Hojas	
X	1	Comprobante de pago de la tarifa	X	2 Documento de cesión de derechos
X	21	Descripción y reivindicación (es) de la invención		Constancia de depósito de material biológico
X	11	Dibujo (s) en su caso		Documento (s) comprobatorio(s) de divulgación previa
X	1	Resumen de la descripción de la invención		Documento (s) de prioridad
X	1	Documento que acredita la personalidad del apoderado		Traducción
			37	TOTAL DE HOJAS

Observaciones:
Se anexa hoja de descuento.

Bajo protesta de decir verdad, manifiesto que los datos asentados en esta solicitud son ciertos.

LIC. MARTHA FIGUEROA PÉREZ
Nombre y firma del solicitante o su apoderado

CIUDAD UNIVERSITARIA, CD. MX., A 22 DE AGOSTO DE 2017
Lugar y fecha

IMPI-00-009

6.5 ARTÍCULO 4 **https://pubmed.ncbi.nlm.nih.gov/33112643/**

La identificación de la serpinA3 en la orina de animales y pacientes con ERC, así como, el poco conocimiento que existe en este contexto, decidimos realizar una revisión sobre esta proteína que fue publicada en American journal of physiology. Cell physiology, 320(1), C106–C118.

Am J Physiol Cell Physiol 320: C106–C118, 2021.
First published October 28, 2020; doi:10.1152/ajpcell.00366.2020

american physiological society

AMERICAN JOURNAL OF PHYSIOLOGY
CELL PHYSIOLOGY

REVIEW

An integrative view of serpins in health and disease: the contribution of SerpinA3

Andrea Sánchez-Navarro,[1,2] Isaac González-Soria,[1,2,3] Rebecca Caldiño-Bohn,[1,2] and Norma A. Bobadilla[1,2]

[1]*Molecular Physiology Unit, Instituto de Investigaciones Biomédicas, Universidad Nacional Autónoma de México, Mexico City, Mexico;* [2]*Department of Nephrology, Instituto Nacional de Ciencias Médicas y Nutrición Salvador Zubirán, Mexico City, Mexico; and* [3]*MD/PhD (PECEM) Program, Facultad de Medicina, Universidad Nacional Autónoma de México, Mexico City, Mexico*

Abstract

Serpins are a superfamily of proteins characterized by their common function as serine protease inhibitors. So far, 36 serpins from nine clades have been identified. These proteins are expressed in all the organs and are involved in multiple important functions such as the regulation of blood pressure, hormone transport, insulin sensitivity, and the inflammatory response. Diseases such as obesity, diabetes, cardiovascular diseases, and kidney disorders are intensively studied to find effective therapeutic targets. Given the serpins' outstanding functionality, the deficiency or overexpression of certain types of serpin has been associated with diverse pathophysiological events. In particular, we focus here on reviewing the studies evaluating the participation of serpins, and particularly SerpinA3, in diverse diseases that occur in relevant organs such as the brain, retinas, corneas, lungs, cardiac vasculature, and kidneys. In this review, we summarize the role of serpins in physiological and pathophysiological processes as well as recent evidence on the crucial role of SerpinA3 in several pathologies. Finally, we emphasize the importance of SerpinA3 in regulating cellular processes such as angiogenesis, apoptosis, fibrosis, oxidative stress, and the inflammatory response.

angiogenesis; inflammation; physiopathology; serine protease inhibitors; suicide substrate inhibition

THE SERPIN SUPERFAMILY

The serpin superfamily is composed of ~1,500 serpin sequences that have been identified in the genomes of five kingdoms. The name coined for serpins originated from their main function: they are described as serine proteinase inhibitors. Serpin protein structure is characterized by a core domain with three β-sheets and eight or nine α-helices. This domain is responsible for the structural and functional properties that determine the most notable function of the entire serpin superfamily, their activity as serine protease inhibitors (1). The molecular mass of serpins is ~46–55 kDa (2), and they are typically 330–500 amino acids in length (3). The nomenclature for each serpin member consists of two parts: clades with alphabetic and numerical designations. However, this nomenclature does not refer to their evolutionary proximity to each other but rather to their order of discovery. Phylogenetic study of the serpin superfamily divided the eukaryotic serpins into 16 clades, designated from A to P, although many serpins have alternative names that were given before this classification was proposed. In humans, serpins are a superfamily of 36 protein-coding genes from nine clades: A, B, C, D, E, F, G, H, and I (Table 1) (3,4).

The main structural similarity in the serpin superfamily corresponds to 350 residues with a conserved conformation. Variation occurs either at the NH_2- or COOH-terminal tail, which can lead to polypeptide extension, glycosylation, or other posttranscriptional modifications (5). Several conformational structures have been found in serpin crystal structures: native, cleaved, latent, and δ-conformation. All these conformational structures depend on the reactive center loop (RCL) that interacts with specific substrates. The native serpin form is a metastable conformation that is converted to a more stable state during protease inhibition (4). The native form spontaneously shifts to the latent form; however, this confirmation requires a lot of energy, and therefore most of the serpins are not found in this state. Notably, the effectiveness of protease inhibition is primarily modulated by RCL and protein flexibility. Indeed, it has been demonstrated that mutations in the RCL increase the serpins' stability but significantly reduce their function as serine protease inhibitors (6). One example of this is a δ-conformation that is induced by the partial insertion of four residues of the RCL into the top of β-sheet A. This conformation is inactive because this partial insertion in the RCL prevents the interaction with their respective proteases and is a natural variant (p.Leu55Pro) of SerpinA3 (Fig. 1*E*) (7). Another

Correspondence: N. A. Bobadilla (nab@biomedicas.unam.mx or norma.bobadillas@incmnsz.mx).
Submitted 21 July 2020 / Revised 1 October 2020 / Accepted 20 October 2020

Table 1. *Human serpins: function and associated diseases*

Serpin	Other Names	Target	Associated Pathologies
SerpinA1	Antitrypsin	Neutrophil elastase	Liver and lung diseases
SerpinA2	Antitrypsin-related protein	Not characterized	
SerpinA3	Antichymotrypsin	Cathepsin G	Alzheimer´s disease, emphysema, eye and renal damage
SerpinA4	Kallistatin (PI4)	Kallikrein	
SerpinA5	Protein C inhibitor (PAI-3)	Active protein C	Edema
SerpinA6	Corticosteroid-binding globulin	Cortisol binding	Chronic fatigue
SerpinA7	Thyroxine-binding globulin	Thyroxine binding	Hypothyroidism
SerpinA8	Angiotensinogen	Release of angiotensin I by renin	Hypertension
SerpinA9	Centerin	Maintenance of naive B cells	B-cell lymphomas
SerpinA10	Protein Z-dependent proteinase inhibitor	Inhibition of activated factor Z and XI	Venous thromboembolic disease
SerpinA11	XP_170754.3	Not characterized	
SerpinA12	Vaspin	Kallikrein 7	anti-insulin resistance and obesity
SerpinA13	XM_370772	Not characterized	
SerpinB1	Monocyte neutrophil elastase inhibitor	Neutrophil elastase	Pulmonary emphysema and impetigo herpetiformis
SerpinB2	Plasminogen activator inhibitor 2 (PAI-2)	Inhibition of uPA	Gingivitis and preeclampsia
SerpinB3	Squamous cell carcinoma antigen I	Cathepsins L and V	Tumor metastasis and autoimmunity
SerpinB4	Squamous cell carcinoma antigen 2	Cathepsin G and chymase	Squamous cell carcinoma
SerpinB5	Maspin		Tumor growth
SerpinB6	Proteinase inhibitor-6 (PI6)	Cathepsin G	
SerpinB7	Megsin	Megakaryocyte maturation	IgA nephropathy
SerpinB8	Cytoplasmic antiproteinase 8 (PI8)	Furin	Peeling skin syndrome 5 and exfoliative ichthyosis
SerpinB9	Cytoplasmic antiproteinase 9 (PI9)	Granzyme B	Autoinflammatory disease
SerpinB10	Bomapin (PI10)	Thrombin and trypsin	Chronic myelomonocytic leukemia and cardiomyopathy
SerpinB11	Epipin		Ovarian endometrial cancer and endometrioid ovary carcinoma
SerpinB12	Yukopin	Trypsin	
SerpinB13	Headpin (PI13)	Cathepsins L and K	
SerpinC1	Antithrombin	Thrombin and factor Xa inhibitor	Thrombosis
SerpinD1	Heparin cofactor II	Thrombin inhibitor	Thrombotic risk
SerpinE1	Plasminogen activator inhibitor 1 (PAI1)	Inhibitor of thrombin, uPA, tPA, and plasmin	Abnormal bleeding
SerpinE2	Protease nexin I (PI7)	Inhibition of uPA and tPA	Cardiac fibrosis
SerpinE3	Hs.512272	Not characterized	
SerpinF1	Pigment epithelium-derived factor	Potent antiangiogenic molecule	
SerpinF2	Alpha-2-antiplasmin	Plasmin inhibitor	Fibrinolytic activity, bleeding
SerpinG1	C1 inhibitor	C1 esterase inhibitor	Angioedema
SerpinH1	47-kDa heat-shock protein	Chaperone for collagens	
SerpinI1	Neuroserpin (PI12)	Inhibitor of tPA, uPA, and plasmin	
SerpinI2	Myoepithelium-derived serine proteinase inhibitor (PI14)	Inhibition of cancer metastasis	Polymerization results in dementia

tPA, tissue plasminogen activator; uPA, urokinase plasminogen activator.

conformation that has been crystallized is the cleaved serpin (Fig. 1*D*). Some serpin mutations, especially nonconservative substitutions within the RCL, result in this conformation, which is also inactive (3, 8).

Contrary to what happens with most enzymes and non-serpin serine protease inhibitors, serpins establish a covalent ester bond with their target protease, thus inhibiting the activity of the protease by distorting their target protein. This mechanism has been named "suicide substrate inhibition" (Fig. 1*C*), where the reactive loop center (RLC), a conserved sequence of the serpin, acts as bait to attract the protease, and the subsequent interactions are the same as those occurring during usual protease catalysis. Serine proteases form a noncovalent complex with their usual substrates, which activates them to attack some of the typical peptide bonds, and therefore they form a covalent enzyme-peptide acyl ester intermediate (Fig. 1*B*). This action releases the free amino side of the substrate so that water breaks the bond between the protease and the remaining product (3, 8).

Serpin Clades in Humans

Serpins are widely distributed among eukaryotes and located intracellularly, extracellularly, or both (3). In humans, there are two large clades of 36 serpins that have been

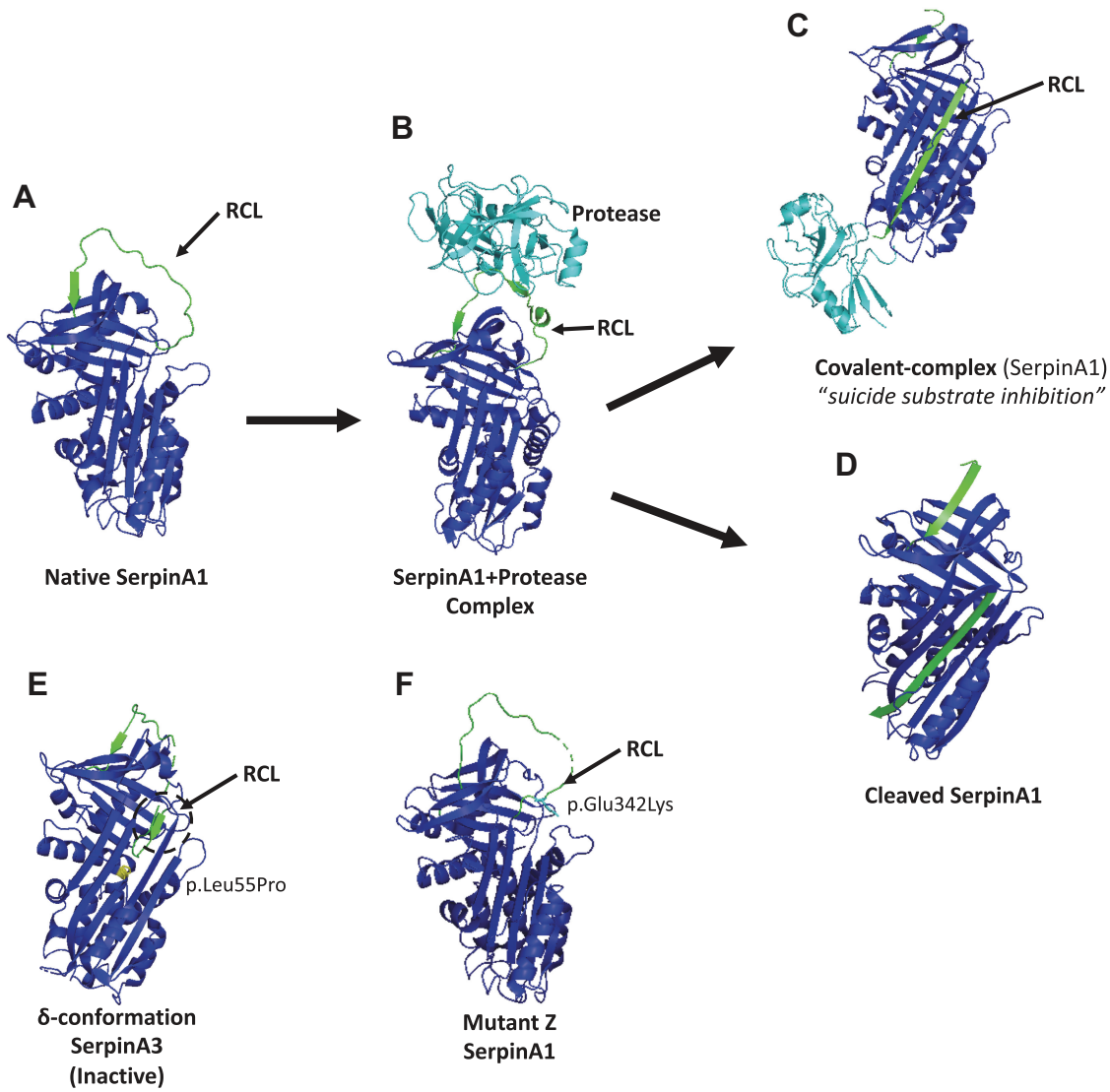

Fig. 1. Serpin structure and the mechanism by which serine proteases are inhibited. *A*: the structure of native SerpinA1 (blue) [Protein Data Bank (PDB): 1QLP]. *B*: the Michaelis complex between SerpinA1 and trypsin (PDB: 1OPH). RCL, reactive center loop. *C*: the final serpin enzyme complex or "suicide substrate inhibition" (PDB: 1EZX). The RCL changes the conformation of the protein to form the fourth strand of β-sheet A, and the inactive protease hangs distorted at the base of the molecule. *D*: cleaved SerpinA1 (PDB: 7API) is inactive. *E*: δ-conformation of SerpinA3 (PDB: 1QMN); the partial insertion of 4 residues of the RCL into the top of β-sheet A is in the circle shown in yellow, caused by a natural variant (p.Leu55Pro). This conformation is constitutively inactive and related to chronic obstructive pulmonary disease (COPD). *F*: mutant Z of SerpinA1 (PDB: 5IO1) (p.Glu342Lys) shown in cyan is related to liver and lung disease. The RCL is shown in green and the protease in cyan. The modeling was performed with PyMOL version 1.20.

identified within clade A, with 13 members clustered on chromosomes 1, 14, and X. The clade B/ovalbumin-related serpins (ov-serpins) have 13 members on chromosomes 18 and 6. There are also one of each for clades C, D, G, and H, three of clade E, and two of each for clades F and I. Inside these clades, there are six noninhibitory human serpins: corticosteroid-binding protein (CBG), T4-binding globulin (TBG), angiotensinogen, mammary serine protease inhibitor (maspin), pigment epithelium-derived factor (PEDF), and heat shock protein 47 (HSP47), which perform diverse physiological functions (3, 9) (Table 1).

The principal function of serpins is to inhibit functional proteases that are implicated in the coagulation process, such as factor Xa, factor XIa, plasmin, tissue plasminogen activator (tPA), and urokinase plasminogen activator (uPA). Several of these serpins can also be bound to heparin and other glycosaminoglycans, regulating their functions (10). Serpins are also involved in the regulation of blood pressure, hormone transport, and insulin sensitivity as well as in inflammatory processes, such as acute phase cellular response and complement system activation (11, 12).

Several functions have been demonstrated for serpins; however, more studies are needed to determine all the roles each member of the serpin superfamily may play in physiological and pathophysiological conditions. Fortunately, the similarity of the serpins in humans and mice allows us to exploit experimental models to understand the role that serpins may play in diverse human diseases (12) (Table 1).

GENERALITIES ABOUT SERPINS IN CHRONIC DISEASES

The varied functions that serpins exert throughout the body have been of interest to different research groups around the world. Despite its participation in a series of cellular events, it is crucial to study the functionality of each serpin from different perspectives, which include its structural conformation and/or its location (intracellular, extracellular, or both).

Here we present a description of some of the molecular mechanisms exerted by serpins that have been related to chronic diseases. We focus on SerpinA3, which can be of interest as a target in clinical settings.

Serpins in Brain Diseases

The participation of serpins in brain physiology has attracted the attention of neuroscientists. One of the most important serpins expressed in the brain is SerpinI1 (neuroserpin), which is associated with effects on emotional behavior, synaptic plasticity, and neuroprotection (13, 14). SerpinI1 is expressed in neural, endocrine, and immune cells and inhibits both the plasminogen activator and plasmin (3, 15), but its main target is tPA. In the brain, tPA might be deleterious, but SerpinI1 efficiently regulates the neurotoxic effects of tPA (16). It has been shown that a mutation in the SerpinI1 gene produces the serpinopathy known as familial encephalopathy with neuroserpin inclusion bodies (FENIB). It is characterized by SerpinI1 inclusion bodies, which in turn, lead to neurodegeneration, epilepsy, and dementia. Moreover, the accumulation of SerpinI1 polymers in the brain causes endoplasmic reticulum (ER) stress and inflammation (13, 17). SerpinI1 overexpression has also been associated with the accumulation of amyloid-β protein in patients with Alzheimer's disease (AD), which seems to result from a reduction in the degradation of amyloid-β by plasmin (18). These results suggest that the inhibition of tPA by SerpinI1 is a possible mechanism involved in AD. This is supported by the decreased activity of tPA, which converts plasminogen into plasmin in AD brains (19). However, further studies are required to achieve better therapeutic options that attenuate the progression of this disease.

Serpins in Obesity and Diabetes

Another relevant area in which serpin contribution has been explored is the endocrine system, particularly in diabetes and obesity states. Several studies have found a potential role of SerpinA12, also known as visceral adipose tissue-derived serpin (Vaspin), in countering deleterious effects of obesity by inducing insulin resistance and anti-inflammatory effects (20, 21). Classically, SerpinA12 inhibits kallikrein 7, which is involved in the cleavage and degradation of the A and B chains of insulin, suggesting that the SerpinA12 antidiabetic effect is due to the reduction of insulin degradation (11, 22). Another possible target of SerpinA12 is the phosphatidylinositol 3-kinase (PI3-kinase)/AKT pathway, which seems to ameliorate atherosclerosis (22,23). There is also evidence that intraperitoneal administration of SerpinA12 reduces food intake, improves glucose metabolism, and regulates candidate genes for insulin resistance in obese mice (24). These data suggest that SerpinA12 could be a pivotal regulator of weight gain and metabolic function, suggesting SerpinA12 as an attractive candidate for drug development.

Serpins in Liver Disease

Liver tissue is the main producer of SerpinA1, also known as alpha-1-antitrypsin (ATT). During its synthesis, SerpinA1 is transcribed and translated, with the resulting nascent peptide being translocated to the endoplasmic reticulum (ER) for its proper protein folding (25,26). There is a homozygous genetic disease caused by a mutant Z allele of the SerpinA1 gene, in which a punctual mutation occurs, provoking a change of glutamic acid for lysine at position 342 (p.Glu342Lys) (Fig. 1*F*). This mutant protein is unable to fold, so it is accumulated in the ER, forming polymers, and this, in turn, leads to liver damage. Teckman et al. (26) have demonstrated that autophagy is an important pathway of intracellular degradation for the mutant Z protein. Intriguingly, not all patients with this mutation develop liver disease. This discrepancy has been explained by the activation of a variety of proteolytic processes, such as ubiquitin-dependent and ubiquitin-independent pathways, as well as ER-associated degradation (27).

Heterozygous individuals for mutant Z represent 2% of the White population and are generally asymptomatic. However, retrospective studies reported a three- to fivefold overrepresentation of heterozygous patients who developed liver and lung diseases (28,29).

To treat genetic diseases, promising new technologies have been developed, such as stimulation of proteolysis via autophagy (30), small-molecule chaperones (31), gene therapy, siRNAs (32), or gene repair by clustered regularly interspersed short palindromic repeats (CRISPR) (33,34). However, none of these has yet been approved for human use. A challenge for future research will be to study these new clinical approaches and to design effective clinical trials.

Serpins in Lung Diseases

SerpinA1 is the major source of protection against proteolytic damage in the lungs. This protein is a potent inhibitor of neutrophil elastase, cathepsin G, and proteinase-3. During inflammation, neutrophils express cathepsin G on their surfaces and release neutrophil elastase into the lungs, which induces severe damage by degrading elastin and collagen. Patients with SerpinA1 mutant Z develop emphysema through an excess of elastase activity (Fig. 1*F*) (35). Additionally, patients with this mutation who smoke present a rapid onset of emphysema and die by the age of 50 yr.

Another associated disease is cystic fibrosis; in this pathology, patients express normal amounts of SerpinA1, but their elevated elastase levels overcome the neutralizing activity of this serpin.

SerpinC1, also known as antithrombin III, regulates coagulation processes by inhibiting thrombin, factors IXa, Xa, XIa, and XIIa, and kallikrein (36). Defects in SerpinC1 result in thrombosis; however, in animal models of sepsis and ischemia, SerpinC1 reduced sepsis-related lung dysfunction by improving fibrin deposition and lung function (37).

SerpinA5/peptidase C inhibitor has been associated with protection from pulmonary hypertension. Transgenic mice overexpressing SerpinA5 in the lungs and displaying

pulmonary hypertension exhibited a significant reduction in proinflammatory cytokines, such as tumor necrosis factor-alpha (TNF-α) and monocyte chemoattractant protein 1 (MCP1). Because SerpinA5 inhibits proteases associated with blood coagulation, the authors suggest that these transgenic mice had lower levels of complex SerpinA5-thrombin, and thus minor activation of the coagulation system, although SerpinA5's protection against pulmonary hypertension was, in part, mediated by both anti-inflammatory and anticoagulant activities in the lung (38). Furthermore, new evidence indicates that SerpinA5 exerts antimicrobial activity against bacterial pathogens by interacting with lipid membranes, leading to bacterial permeabilization and death (38). This additional antibacterial effect provides a novel perspective to study the effect of serpins beyond their protease activity.

Serpins in Cancer

Several studies have implicated the serpin superfamily in the development of different types of cancer. Here we present some specific studies relevant to this topic. According to Valiente et al. (39), SerpinI1 and SerpinB2 selectively inhibit tPA. Plasmin acts as a defense against metastatic invasion; therefore, the inhibition of tPA by these serpins promotes metastasis in brain, lung, and breast cancer.

SerpinB9 is an endogenous inhibitor of granzyme B in humans, which protects against cytotoxic granule leakage (40). Vycital et al. (41) have shown that SerpinB9 expression can be used as a prognostic factor for colorectal cancer because of the association of SerpinB9 with lymph node metastasis.

Although SerpinB5, also known as maspin, has been linked with tumor growth and metastasis, its expression can be upregulated or downregulated depending on the type of cancer cells. These opposite expression levels result from its localization (cytoplasmatic, nuclear, membranal, or secreted), epigenetic regulation, or both (42).

All of these studies suggest that serpins participate in several cancer scenarios; however, it is imperative to study the localization and contribution of the serpin in question in each specific type of cancer to understand its role in pathology and to design possible therapeutic targets.

Serpins in Eye Diseases

Hatcher et al. (43) is a pioneering work that demonstrated the existence of a decrease in SerpinA4 expression (also known as kallistatin) in an animal model of diabetic retinopathy. This finding suggests that the lack of this protein promotes deterioration in the retina; however, the underlying mechanisms were not elucidated. SerpinA4 has been found in the cornea, ciliary body, sclera, choroid, vitreous, and retina, but its expression is reduced in diabetic patients, suggesting the importance of SerpinA4 in the eye physiology and pathophysiology (44). In addition, SerpinA4 seems to be a possible inhibitor of vascular endothelial growth factor (VEGF) (45). Gao et al. (46) have shown that SerpinA4 attenuates retinal angiogenesis in a rat model of oxygen-induced retinopathy. This effect seems to be mediated by the interaction of SerpinA4 with VEGF receptors, promoting the downregulation of VEGF and angiogenesis (46).

The SerpinF1 gene encodes the pigment epithelium-derived factor (PEDF) (47). Although PEDF is not a serine protease inhibitor, it has been associated with neuroprotective and antiangiogenic activity in the retina (48). Supporting this, SerpinF1-knockout mice exhibited a reduced retinal vasculature during the first through the seventh postnatal day, which was associated with increased vessel obliteration in a model of oxygen-induced retinopathy compared with wild-type mice (49). Additionally, the binding of SerpinF1 to its receptors promotes antiapoptotic activity in the retina (50).

These studies suggest that the serpin family could have an important role in ocular diseases that are affected by angiogenesis; therefore, it is crucial to know whether the balance among the involved serpins is sufficient to regulate adequate neovascularization.

Serpins in Cardiovascular Diseases

Evidence from in vivo and in vitro studies has shown that serpins are related to cardiovascular pathologies. In experimental cardiovascular injury, SerpinE1, also known as tPA inhibitor type 1 (PAI-1), has been demonstrated to be a regulator of cardiac fibrosis by stimulating transforming growth factor-β (TGF-β) production in cardiomyocytes (51). Moreover, cultured cardiomyocytes treated with proinflammatory mediators, such as interleukin-1α and TNF-α, showed upregulation of SerpinE1 expression. These data indicate that PAI-1 acts as a mediator between proinflammatory and fibrotic responses (52).

SerpinA4 seems to inhibit oxidative stress and inflammation after experimental cardiac injury. In patients with coronary artery disease SerpinA4 is significantly reduced, which is associated with worse outcomes in these patients. In support of this, the depletion of SerpinA4 aggravates aortic injury by inducing senescence, oxidative stress, and inflammation in streptozotocin-induced diabetic mice (53). The role of serpins in cardiovascular physiology is obvious because of their participation in coagulation, but little is known about the specific role of each expressed serpin in cardiovascular diseases. Recent evidence suggests that serpins could exert activities independent of their canonical pathways as protease inhibitors, for example, the participation of SerpinA4 in the regulation of the VEGF pathway in the retina by antagonizing the VEGF receptor (46). These data suggest that this effect could occur in cardiovascular diseases as well. However, this hypothesis needs to be verified.

Serpins in Renal Pathologies

Deficiency in SerpinB2, also known as plasminogen activator inhibitor-2 (PAI-2), has been associated with delayed development of diabetic nephropathy and chronic kidney disease (54). The main function of this serpin has been related to the immunological Th1 response (55), which is upregulated in activated macrophages (56). Recently, Sen et al. (57) pointed out that SerpinB2 has an immune regulatory function through enhancing phagocytosis and attenuating persistent migration of proinflammatory type M1 macrophages; these are implicated in chronic inflammation leading to fibrosis and a maladaptive response. This phenomenon was mediated by the induction of monocyte chemoattractant protein 1 (MCP1 or CCL2) by tubular epithelium expression

that allows appropriate transient inflammatory infiltration of reparative type M2 macrophages in the kidney, stimulating a reparative response (57).

The intraperitoneal administration of SerpinA1 in mice that underwent bilateral renal ischemia-reperfusion improved renal function and reduced tubular necrosis and macrophage infiltration, but the renoprotective mechanisms were not elucidated (58).

Finally, in *db/db* obese mice, gene transfer of SerpinA4 into the kidneys induced a reduction of inflammation, oxidative stress, and angiogenesis as well as the attenuation of tubular damage and fibrosis (59).

As mentioned above, even though there is evidence that several members of the serpin superfamily have been implicated in the physiology and pathophysiology of different organs (Fig. 2), very little has been known about other members of this superfamily until now. This review also focuses on collecting the most relevant information about SerpinA3, which has been of interest to us since we previously demonstrated its potential as a biomarker of damage in several kidney diseases (60).

GENERALITIES ABOUT SERPINA3

SerpinA3, also known as antichymotrypsin, is codified in chromosome 14q32.1 with a length of 11.66 kb. It is one of the 13 group A serpins and has 423 amino acids, with a molecular mass of ~55–66 kDa. SerpinA3 is subjected to multiple glycosylations; this posttranscriptional modification is characteristic of plasma serpins. Glycosylation modifications are responsible for generating a tag that selectively targets the native protein for intracellular processing to ensure the correct folding of SerpinA3 in the endoplasmic reticulum and posterior secretion (61). Nevertheless, the posterior glycosylation processing in the Golgi apparatus is not well understood. The promotor and enhancers possess binding sites for nuclear factor-κB (NF-κB), activator protein 1 (AP-1), nuclear factor-1-X (NF1), and signal transducer and activator of

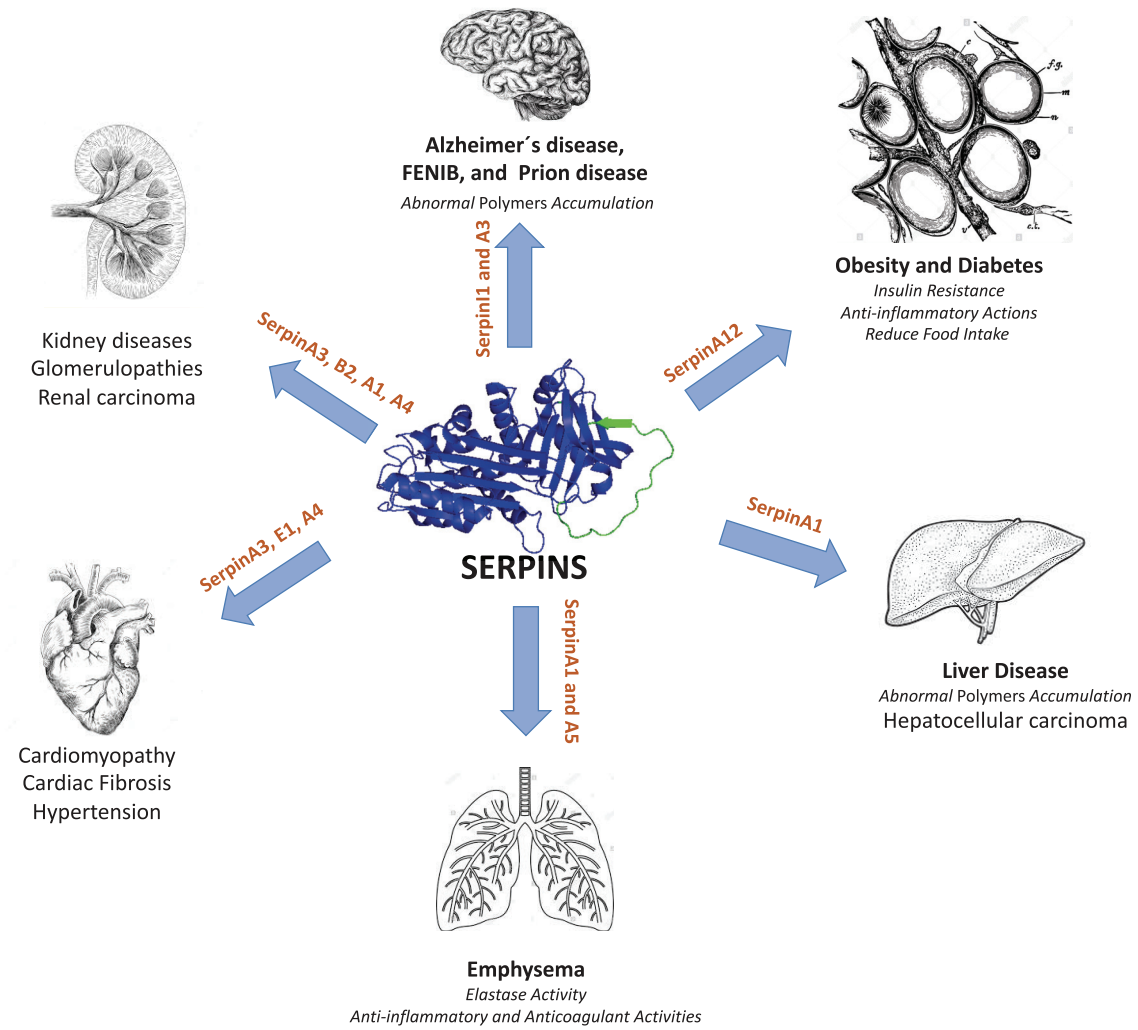

Fig. 2. Serpin involvement in pathophysiological events. Serpins are expressed throughout the body; alteration in their expression or conformational structure may participate in diverse diseases. The structure of native SerpinA1 [Protein Data Bank (PDB): 1QLP], which was the first crystallized structure, is shown. In addition, the involvement of each serpin in the corresponding disease is illustrated. FENIB, familial encephalopathy with neuroserpin inclusion bodies.

transcription (STAT) (62). The SerpinA3 gene is regulated by different cytokines, such as IL-1, IL-6, and oncostatin M, probably through the regulation of the translocation of transcription factors to the nucleus to induce the transcription of these cytokines; however, the specific mechanism is unknown. SerpinA3, like other members of the superfamily, has a RCL of 23 amino acids located near the carboxy end (16). When a protease binds to the RCL of SerpinA3, the latter is inserted into β-sheet A, leading to irreversible inactivation of the protease (Fig. 1*C*). This complex is then metabolized in the liver (63).

The GeneCards website (https://www.genecards.org/cgi-bin/carddisp.pl?gene=SERPINA3&keywords=serpinA3) has reported SerpinA3 expression in different tissues. This was found by using three different tools: RNA-seq, microarrays, and serial analysis of gene expression (SAGE), with the highest expression being in the retinas, kidneys, liver, and pancreas.

SerpinA3 inhibited several serine proteases, such as pancreatic chymotrypsin, leukocyte cathepsin G, mast cell chymases, human glandular kallikrein 2, kallikrein 3 (also known as prostate-specific antigen), pancreatic cationic elastase, and lung serum protease (62, 64). Within these proteases, cathepsin G is the major target for SerpinA3. Cathepsin G is expressed in neutrophil granules and is secreted during inflammation. One special feature of SerpinA3 is its ability to bind to DNA, but the physiological significance of this binding remains unclear (65).

Polymorphisms and mutations can occur, affecting SerpinA3's function, which could predispose the host to diseases. In some cases, this serpin is elevated within the nucleus of malignant cells, particularly in pancreatic, stomach, liver, breast, prostatic, and lymphatic cancers. SerpinA3 appears to bind to DNA polymerase and DNA primase, and this may be a regulatory mechanism to control cell replication (66).

SERPINA3 INVOLVEMENT IN PATHOPHYSIOLOGICAL PROCESSES

An imbalance in the serpin-protease equilibrium may have severe effects, leading to pathophysiological consequences. The negative effect of this imbalance has been evidenced by the study of its mutations, which result in deficiency or complete loss of serpin expression. This leads to an excess in target protease activity and thus a disruption of the downstream pathway. Mutations in key structural regions of SerpinA3, such as the hinge, RCL, or shutter domains, could destabilize the structure and initiate the polymerization and accumulation of this protein (62, 67).

In the context of human diseases, two familial SerpinA3 mutations in p.Leu55Pro and p.Pro229Ala result in a deficiency of SerpinA3 that is related to chronic obstructive pulmonary disease (COPD) (Fig. 1*E*). Also, in cystic fibrosis SerpinA3 deficiency has been associated with milder lung disease. Nevertheless, these mutations are rare, and this association is controversial (68,69).

SerpinA3 in Brain Pathogenesis

In the brain, serpins are synthesized by astrocytes that are involved in neurodegeneration and neuroinflammation. The most-studied brain disease associated with SerpinA3 is Alzheimer's disease. It has been reported that SerpinA3 might bind to β-amyloid proteins, and thus SerpinA3 makes up part of amyloid deposits (70). In vivo studies with transgenic mice suggest that SerpinA3 mediates β-amyloid protein clearance. This finding was supported by the fact that SerpinA3 is highly expressed in regions of the brain associated with Alzheimer's disease, including the hippocampus (71). Moreover, higher SerpinA3 levels have been found in the serum and cerebrospinal fluid of patients with severe Alzheimer's disease (72). Genetic evidence for the role of SerpinA3 in Alzheimer's disease pathogenesis in humans has been difficult to prove, and these results remain inconclusive. However, SerpinA3 signal peptide polymorphism at codon −17 (A > T) has been linked to an earlier age of onset of Alzheimer's disease (73).

Another brain disease linked to SerpinA3 upregulation is prion disease. This is a rare disorder in which misfolded prion proteins accumulate, causing a neural loss in gray matter, vacuolation, and the accumulation of glial fibrillary acidic protein (GFAP). These neuropathological alterations lead to death. Creutzfeldt–Jakob disease (CJD) is the most common form of human prion disease. Vanni et al. (74) found that in all patients with this disease there was a significant elevation of SerpinA3 mRNA and protein levels. They suggest that this upregulation may be a consequence of a cycle in which elevated levels of the misfolded prion protein are also affecting the production of SerpinA3; therefore, this leads to the propagation of prions. They also have reported that SerpinA3 could be able to translocate to the nucleus and regulate chromatin condensation, which in turn downregulates the prion protein gene transcription, a common factor in prion disease. Interestingly, it has been proposed that SerpinA3 expression might be a useful tool for prion disease diagnosis, even in the presymptomatic stage (74). Furthermore, after a traumatic brain injury in mice, SerpinA3 has been identified as a neuroprotective influence resulting from the regulation of the MAPK signal pathway, which promotes antioxidant protection and the reduction of endogenous mitochondrial apoptosis (15).

Together, all these findings suggest that SerpinA3 is involved in the pathogenesis of brain diseases. SerpinA3 could be an important diagnostic tool, not only for early identification of AD and CJD but also for many degenerative brain diseases in which the diagnosis remains unclear. Undoubtedly more studies are needed to understand the mechanisms by which SerpinA3 can exert protective or adverse function in the brain (Fig. 2).

SerpinA3/Antichymotrypsin in Eye Diseases

Disease in eye tissues has been one of the most-studied pathological processes in which SerpinA3 is involved. The administration of recombinant SerpinA3 was able to reduce cornea neovascularization and inflammation in a murine model of corneal alkaline burn. This effect was mediated by the negative regulation of angiogenic and inflammatory factors (21). Moreover, the same research group that reported the previous effect evaluated the SerpinA3-downregulated components associated with the Wnt pathway in suture-induced corneal neovascularization, which has been

associated with the regulation of inflammatory response and angiogenesis (75). Besides this, inhibition of the Wnt pathway with an intravitreal injection of adenovirus expressing SerpinA3 promoted antifibrotic activity in experimental diabetic retinopathy through the reduction of connective tissue growth factor (CTGF) (76).

In vitro studies in retinal neuronal and Müller cells have shown that SerpinA3 exerts protection against reactive oxygen species (ROS). This effect appears to be mediated by the inhibition of phospholipase C activation, which avoids calcium overload and preserves retinal cells (77). Moreover, in cultured human corneal epithelial cells and in rat corneal epithelium in vivo, SerpinA3 has been reported to increase the activity of superoxide dismutase (SOD) and catalase, which cause lower levels of ROS, as well as blocking NOX4, which is an isoform of NADPH oxidase, decreasing ROS production. SerpinA3 could regulate the KEAP1-NRF2 pathway, which mediates the redox system (78).

In eye pathogenesis, SerpinA3 seems to be a protective molecule, having antiangiogenic, anti-inflammatory, antioxidant, and antifibrotic activities (Fig. 3). Therefore, the evaluation of SerpinA3 in tissue-specific transgenic mice will allow us to evaluate the detailed mechanisms implicated in these pathologies.

SerpinA3/Antichymotrypsin in Oncological Processes

The activity of SerpinA3 is diverse, depending on the type of tumor and the region of the body where the tumor is located. In hepatocellular carcinoma, an overregulation of the PI3-kinase/Akt/mechanistic target of rapamycin (mTOR) pathway exists that counteracts apoptosis-related proteins. It has been reported that SerpinA3 acts as a suppressor of this type of carcinoma through the negative regulation of the PI3-kinase/Akt/mTOR pathway, allowing the induction of apoptosis of cancerous cells (79). On the contrary, the overexpression of SerpinA3 was associated with glioblastoma progression, as indicated by larger tumor sizes, a higher World Health Organization (WHO) grade of glioma, and reduction of patient survival (80). Additionally, in vitro experiments have shown that when astroglia and microglia cell lines are cocultured with SerpinA3, remodeling of the extracellular matrix occurs, which promotes higher invasion of the glioma (81).

SerpinA3 has been detected in the nuclei of pancreas, stomach, breast, hepatic, and lymphatic cancers, despite not being present in the nucleus of normal tissues (82). Furthermore, SerpinA3 levels are elevated in the serum of individuals with malignant diseases. Also, increased SerpinA3 expression has been described in endometrial cancer as well as melanoma, and this has been considered to be a prognostic factor related to high mortality (83,84). Also, it has been reported that SerpinA3 could regulate the cell cycle at the G_2/M phase, allowing proliferation and avoiding apoptosis of endometrial cancer cells that appears to be mediated by the AKT and ERK1/2 pathway (80). Finally, in melanoma and colon cancer, SerpinA3 was closely associated with the migration of, and invasion by, malignant cells (83, 85). Most of these studies show that there is an increase in SerpinA3 levels, but we still do not know if this is to help counteract the tumorigenic process or to increase the invasiveness of cancer cells; therefore, it is necessary to fully explore its participation within each tissue type in cancer proliferation processes.

SerpinA3/Antichymotrypsin in Cardiovascular Diseases

A few studies have explored the contribution of SerpinA3 in the cardiovascular system. In a murine model, an intravenous injection of recombinant human SerpinA3 before reperfusion of the myocardium was able to reduce myocardial ischemia-reperfusion damage. This protective effect was mediated by an inhibition of neutrophil accumulation at the site of the injury (86).

In patients diagnosed with cardiac stenosis, SerpinA3 plasma levels are increased, suggesting that this molecule could be useful as a diagnostic tool. Zhao et al. (87) recently proposed that SerpinA3 could predict adverse cardiac events such as cardiovascular death, recurrent myocardial infarction, advanced heart failure, and any revascularization in patients with myocardial infarction. Although its usefulness is still under investigation to determine the prognosis of these diseases, additional clinical studies could help validate its use as an effective diagnostic test.

SerpinA3 in Renal Diseases

Under normal conditions, SerpinA3 is mainly expressed in epithelial cells of the proximal convoluted tubule, but it is absent in glomerular structures and interstitium. A recent massive proteomic study demonstrated that SerpinA3 is primarily expressed in the S2 proximal tubule segment and the descending thin limb of Henle's loop in the kidneys of rats (88). As in other organs, little is known about the specific role of SerpinA3 in renal physiology and pathophysiology. It is known that increased SerpinA3 is found in stainings of the proximal renal tubules of biopsies compared with normal renal tissues from a variety of primary and secondary glomerulonephritis, such as minimal change disease (MCD), focal and segmental glomerulosclerosis (FSGS), diffuse mesangial proliferative glomerulonephritis (MeGN), membranous glomerulonephritis (MGN), diabetic nephropathy, IgA nephritis, and lupus nephritis (LN) (89).

During kidney injury, it has been reported that several proteolytic molecules are filtered, which could be potentially harmful to the tubules (90). Colocalization of lysozymes with either SerpinA1 or SerpinA3 in proximal tubular cells has been reported, especially in patients with immunological kidney diseases (91). Although it is feasible that serpins regulate inflammatory responses in kidney injuries, there is no evidence of serpin interstitial staining, even in the setting of a nephritic process. SerpinA3 has also been found in cells of different renal tumors, such as nephroblastoma, renal carcinoma, and congenital mesoblastic nephroma (89).

Recently, through high-resolution mass spectrometry we identified the abnormal presence of SerpinA3 in the urine of rats with chronic kidney disease (CKD) (60). In this study, we first assessed whether urinary SerpinA3 (uSerpinA3) could detect early CKD in rodents with an experimental model of transition from acute kidney injury (AKI) to CKD. A progressive elevation of proteinuria and renal fibrosis was observed during AKI-to-CKD transition

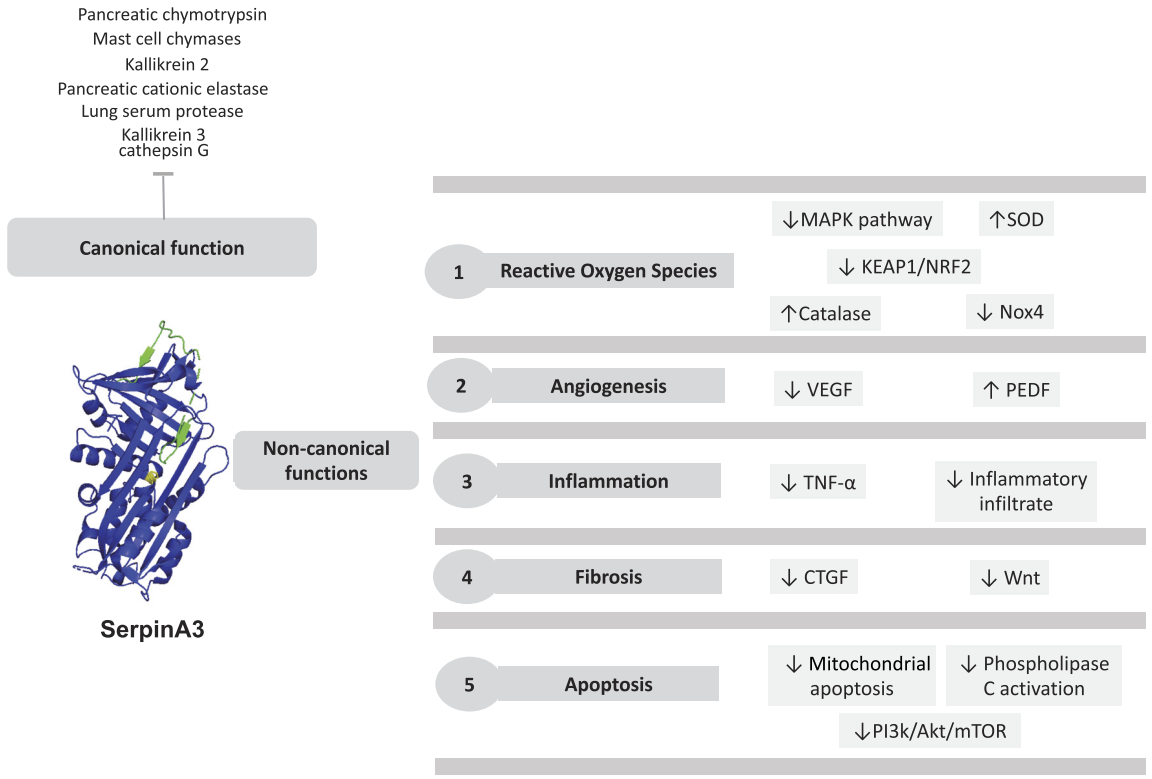

Fig. 3. Noncanonical functions of SerpinA3 during pathophysiological scenarios. SerpinA3 has been identified as a serine protease inhibitor, but additional functions have been identified in pathophysiological situations such as protection against reactive oxygen species, reduction of angiogenesis, inflammation, and fibrosis, as well as decreasing apoptosis. There are several pathways identified in different diseases; however, the mechanisms of regulation of these pathways require more detailed studies. CTGF, connective tissue growth factor; mTOR, mechanistic target of rapamycin; PEDF, pigment epithelium-derived factor; PI3k, phosphatidylinositol 3-kinase; SOD, superoxide dismutase; TNF-α; tumor necrosis factor-α; VEGF, vascular endothelial growth factor.

in the rats. At the same time, we studied the presence of SerpinA3 in the urine of patients with different renal diseases, and we also included patients with inflammatory diseases but without kidney damage. uSerpinA3 had behavior similar to that in rats, but a much earlier elevation was seen, and there was a significant correlation with fibrosis. In the immunohistochemical analysis, SerpinA3 was relocated from the cytoplasm to the tubular apical membrane in CKD. uSerpinA3K levels increased markedly in patients with CKD secondary to focal and segmental glomerulosclerosis (FSGS), ANCA-associated vasculitis (AAV), or proliferative lupus nephritis (LN) class III and IV compared with a group of healthy volunteers. Furthermore, although uSerpinA3 levels were significantly correlated with renal fibrosis in the patient groups, in contrast, in patients with class V LN uSerpinA3 levels were not different from healthy volunteers. Also, uSerpinA3 levels in patients with other inflammatory diseases without renal dysfunction were similar to healthy volunteers. In patients with LN classes III and IV, SerpinA3 was also relocated from the cytoplasm to the apical epithelial membrane, suggesting that during renal injury SerpinA3 is probably secreted into the luminal space, explaining its presence in the urine (60). Urine proteomic studies of patients with acute renal allograft rejection have also pointed out SerpinA3K's possible role as a potential early biomarker (92) for this condition.

These results suggest that SerpinA3 seems to be involved in renal diseases, although it is necessary to evaluate in detail its role in renal inflammation, oxidative stress, cellular proliferation, angiogenesis, and fibrosis.

CONCLUSIONS

In summary, the evolution and conservation of serpins in three different species give us a broad view of their importance in preserving cellular physiology. Advances in knowledge of the functional biochemistry and cell biology of serpins have been reinforced by extensive contributions of structural biology and genomics. These in vitro findings have been supported by the generation and characterization of transgenic mice providing in vivo evidence of the central role of serpins in several chronic diseases.

Despite the earlier belief that the main function of serpins was to act as serine protease inhibitors, many of the effects that serpins exert are related to noncanonical pathways (Fig. 3), such as oxidative stress, cellular proliferation, and apoptosis. In oncological processes, the location of the involved serpin, either intracellular or extracellular, determines whether cancer has a good or bad prognosis. One mechanism for this could be related to the ability to bind to DNA, DNA polymerase, and DNA primase, which have been described for SerpinA3 (65, 66). However, more studies are needed to

determine whether other serpins have the potential to bind to DNA.

Many serpinopathies are related to intracellular accumulation caused by the improper folding of the proteins. Even though the participation of some mutations in serpin misfolding is well described, little is known about the regulation of serpin folding and secretion under conditions of cellular stress. The glycosylation of serpins could play an important role in pathological events, either by increased glycosylation or by its lack, which could modify serpin secretion. This hypothesis could be supported by the fact that the clade B serpins, which are typically intracellular, are not fully glycosylated, but there are examples of secreted and glycosylated clade B serpins, such as SerpinB2 and ovalbumin, although SerpinB5 is predicted to be a cytoplasmic and nonsecreted protein (93). However, in different types of cancer SerpinB5 has been located extracellularly, on the membrane surface, in the cytoplasm, or the nucleus, without any changes in the protein sequence, suggesting that pathological situations could influence posttranscriptional modifications (42). Further investigation is essential to understand whether glycosylation is needed for secretion of serpins as well as whether their glycosylation is implicated in chronic diseases.

Within the serpin superfamily, SerpinA3 has shown a relevant role in the physiology and pathophysiology of the brain, lungs, heart, corneas, retinas, and kidneys. Several studies have demonstrated SerpinA3's involvement in the regulation of angiogenesis, apoptosis, oxidative stress, and inflammatory responses as well as in preserving the balance of pro- and antifibrotic factors. It has been shown that KEAP1-NRF2, SOD2, Wnt, CTGF, phospholipase C, AKT, and ERK1/2 are regulated by SerpinA3 (Fig. 3). Nevertheless, the specific mechanism by which SerpinA3 can regulate these pathways is still unknown. One explanation could be related to the DNA-binding capacity of SerpinA3 (66), which theoretically could allow SerpinA3 to regulate transcription. Another possibility is the ability to interact with some receptors, as is the case for SerpinA4 (46).

Although much remains to be discovered about serpins' functions and the additional roles they may have in various physiological and pathophysiological scenarios, their participation in chronic and degenerative diseases is evident. This opens a niche of opportunity not only to explore signaling pathways that may be activated in different circumstances but also to develop new therapeutic targets, with the possible use of serpins as diagnostic tools for several diseases.

GRANTS

Our laboratory studies cited in this review were supported by grants from the Mexican Council of Science and Technology (CONACyT) (272390, 300151, and A1-S-8715 to N. A. Bobadilla) and Universidad Nacional Autónoma de México (UNAM) (IN223915 and IN201619 to N. A. Bobadilla). This study was performed in partial fulfillment of the requirements for a PhD degree; A. Sánchez-Navarro and I. González-Soria are doctoral students in the Programa de Doctorado en Ciencias Biomédicas and the MD/Ph.D. (PECEM) program of the Facultad de Medicina, UNAM, respectively. Each received fellowships (607517 and 1045949) from CONACyT.

DISCLOSURES

No conflicts of interest, financial or otherwise, are declared by the authors.

AUTHOR CONTRIBUTIONS

A.S.-N., I.G.-S., R.C.-B., and N.A.B. prepared figures; drafted manuscript; edited and revised manuscript; and approved final version of manuscript.

REFERENCES

1. **Loebermann H**, **Tokuoka R**, **Deisenhofer J**, **Huber R.** Human alpha 1-proteinase inhibitor. Crystal structure analysis of two crystal modifications, molecular model and preliminary analysis of the implications for function. *J Mol Biol* 177: 531–557, 1984. doi:10.1016/0022-2836(84)90298-5.
2. **van Gent D**, **Sharp P**, **Morgan K**, **Kalsheker N.** Serpins: structure, function and molecular evolution. *Int J Biochem Cell Biol* 35: 1536–1547, 2003. doi:10.1016/S1357-2725(03)00134-1.
3. **Law RH**, **Zhang Q**, **McGowan S**, **Buckle AM**, **Silverman GA**, **Wong W**, **Rosado CJ**, **Langendorf CG**, **Pike RN**, **Bird PI**, **Whisstock JC.** An overview of the serpin superfamily. *Genome Biol* 7: 216, 2006. doi:10.1186/gb-2006-7-5-216.
4. **Irving JA**, **Pike RN**, **Lesk AM**, **Whisstock JC.** Phylogeny of the serpin superfamily: implications of patterns of amino acid conservation for structure and function. *Genome Res* 10: 1845–1864, 2000. doi:10.1101/gr.GR-1478R.
5. **Gettins PG**, **Olson ST.** Inhibitory serpins. New insights into their folding, polymerization, regulation and clearance. *Biochem J* 473: 2273–2293, 2016. doi:10.1042/BCJ20160014.
6. **Huntington JA**, **Read RJ**, **Carrell RW.** Structure of a serpin-protease complex shows inhibition by deformation. *Nature* 407: 923–926, 2000. doi:10.1038/35038119.
7. **Gooptu B**, **Hazes B**, **Chang WS**, **Dafforn TR**, **Carrell RW**, **Read RJ**, **Lomas DA.** Inactive conformation of the serpin alpha$_1$-antichymotrypsin indicates two-stage insertion of the reactive loop: implications for inhibitory function and conformational disease. *Proc Natl Acad Sci USA* 97: 67–72, 2000. doi:10.1073/pnas.97.1.67.
8. **Tew DJ**, **Bottomley SP.** Intrinsic fluorescence changes and rapid kinetics of proteinase deformation during serpin inhibition. *FEBS Lett* 494: 30–33, 2001. doi:10.1016/S0014-5793(01)02305-5.
9. **Silverman GA**, **Bird PI**, **Carrell RW**, **Church FC**, **Coughlin PB**, **Gettins PG**, **Irving JA**, **Lomas DA**, **Luke CJ**, **Moyer RW**, **Pemberton PA**, **Remold-O'Donnell E**, **Salvesen GS**, **Travis J**, **Whisstock JC.** The serpins are an expanding superfamily of structurally similar but functionally diverse proteins. Evolution, mechanism of inhibition, novel functions, and a revised nomenclature. *J Biol Chem* 276: 33293–33296, 2001. doi:10.1074/jbc.R100016200.
10. **Huntington JA.** Mechanisms of glycosaminoglycan activation of the serpins in hemostasis. *J Thromb Haemost* 1: 1535–1549, 2003. doi:10.1046/j.1538-7836.2003.00305.x.
11. **Heiker JT**, **Klöting N**, **Kovacs P**, **Kuettner EB**, **Sträter N**, **Schultz S**, **Kern M**, **Stumvoll M**, **Blüher M**, **Beck-Sickinger AG.** Vaspin inhibits kallikrein 7 by serpin mechanism. *Cell Mol Life Sci* 70: 2569–2583, 2013. doi:10.1007/s00018-013-1258-8.
12. **Heit C**, **Jackson BC**, **McAndrews M**, **Wright MW**, **Thompson DC**, **Silverman GA**, **Nebert DW**, **Vasiliou V.** Update of the human and mouse SERPIN gene superfamily. *Hum Genomics* 7: 22, 2013. doi:10.1186/1479-7364-7-22.
13. **Lee TW**, **Tsang VW**, **Loef EJ**, **Birch NP.** Physiological and pathological functions of neuroserpin: regulation of cellular responses through multiple mechanisms. *Semin Cell Dev Biol* 62: 152–159, 2017. doi:10.1016/j.semcdb.2016.09.007.
14. **Reumann R**, **Vierk R**, **Zhou L**, **Gries F**, **Kraus V**, **Mienert J**, **Romswinkel E**, **Morellini F**, **Ferrer I**, **Nicolini C**, **Fahnestock M**, **Rune G**, **Glatzel M**, **Galliciotti G.** The serine protease inhibitor neuroserpin is required for normal synaptic plasticity and regulates learning and social behavior. *Learn Mem* 24: 650–659, 2017. doi:10.1101/lm.045864.117.

15. **Jing Y**, **Yang D**, **Fu Y**, **Wang W**, **Yang G**, **Yuan F**, **Chen H**, **Ding J**, **Chen S**, **Tian H.** Neuroprotective effects of Serpina3k in traumatic brain injury. *Front Neurol* 10: 1215, 2019. doi:10.3389/fneur.2019.01215.
16. **Hwang SR**, **Steineckert B**, **Kohn A**, **Palkovits M**, **Hook VY.** Molecular studies define the primary structure of alpha1-antichymotrypsin (ACT) protease inhibitor in Alzheimer's disease brains. Comparison of ACT in hippocampus and liver. *J Biol Chem* 274: 1821–1827, 1999. doi:10.1074/jbc.274.3.1821.
17. **Davies MJ**, **Miranda E**, **Roussel BD**, **Kaufman RJ**, **Marciniak SJ**, **Lomas DA.** Neuroserpin polymers activate NF-kappaB by a calcium signaling pathway that is independent of the unfolded protein response. *J Biol Chem* 284: 18202–18209, 2009. doi:10.1074/jbc.M109.010744.
18. **Tucker HM**, **Kihiko M**, **Caldwell JN**, **Wright S**, **Kawarabayashi T**, **Price D**, **Walker D**, **Scheff S**, **McGillis JP**, **Rydel RE**, **Estus S.** The plasmin system is induced by and degrades amyloid-beta aggregates. *J Neurosci* 20: 3937–3946, 2000. doi:10.1523/JNEUROSCI.20-11-03937.2000.
19. **Fabbro S**, **Seeds NW.** Plasminogen activator activity is inhibited while neuroserpin is up-regulated in the Alzheimer disease brain. *J Neurochem* 109: 303–315, 2009. doi:10.1111/j.1471-4159.2009.05894.x.
20. **Escoté X**, **Gómez-Zorita S**, **López-Yoldi M**, **Milton-Laskibar I**, **Fernández-Quintela A**, **Martínez JA**, **Moreno-Aliaga MJ**, **Portillo MP.** Role of omentin, vaspin, cardiotrophin-1, TWEAK and NOV/CCN3 in obesity and diabetes development. *Int J Mol Sci* 18: 1770, 2017. doi:10.3390/ijms18081770.
21. **Liu X**, **Lin Z**, **Zhou T**, **Zong R**, **He H**, **Liu Z**, **Ma JX**, **Liu Z**, **Zhou Y.** Anti-angiogenic and anti-inflammatory effects of SERPINA3K on corneal injury. *PLoS One* 6: e16712, 2011. doi:10.1371/journal.pone.0016712.
22. **Breitfeld J**, **Wiele N**, **Gutsmann B**, **Stumvoll M**, **Blüher M**, **Scholz M**, **Kovacs P**, **Tönjes A.** Circulating adipokine VASPIN is associated with serum lipid profiles in humans. *Lipids* 54: 203–210, 2019. doi:10.1002/lipd.12139.
23. **Jung CH**, **Lee WJ**, **Hwang JY**, **Seol SM**, **Kim YM**, **Lee YL**, **Park JY.** Vaspin protects vascular endothelial cells against free fatty acid-induced apoptosis through a phosphatidylinositol 3-kinase/Akt pathway. *Biochem Biophys Res Commun* 413: 264–269, 2011. doi:10.1016/j.bbrc.2011.08.083.
24. **Hida K**, **Wada J**, **Eguchi J**, **Zhang H**, **Baba M**, **Seida A**, **Hashimoto I**, **Okada T**, **Yasuhara A**, **Nakatsuka A**, **Shikata K**, **Hourai S**, **Futami J**, **Watanabe E**, **Matsuki Y**, **Hiramatsu R**, **Akagi S**, **Makino H**, **Kanwar YS.** Visceral adipose tissue-derived serine protease inhibitor: a unique insulin-sensitizing adipocytokine in obesity. *Proc Natl Acad Sci USA* 102: 10610–10615, 2005. doi:10.1073/pnas.0504703102.
25. **Patel D**, **Teckman JH.** Alpha-1-antitrypsin deficiency liver disease. *Clin Liver Dis* 22: 643–655, 2018. doi:10.1016/j.cld.2018.06.010.
26. **Teckman JH**, **Burrows J**, **Hidvegi T**, **Schmidt B**, **Hale PD**, **Perlmutter DH.** The proteasome participates in degradation of mutant alpha 1-antitrypsin Z in the endoplasmic reticulum of hepatoma-derived hepatocytes. *J Biol Chem* 276: 44865–44872, 2001. doi:10.1074/jbc.M103703200.
27. **Perlmutter DH.** Alpha-1-antitrypsin deficiency: biochemistry and clinical manifestations. *Ann Med* 28: 385–394, 1996. doi:10.3109/07853899608999097.
28. **American Thoracic Society, European Respiratory Society.** American Thoracic Society/European Respiratory Society statement: standards for the diagnosis and management of individuals with alpha-1 antitrypsin deficiency. *Am J Respir Crit Care Med* 168: 818–900, 2003. doi:10.1164/rccm.168.7.818.
29. **Sveger T.** The natural history of liver disease in alpha 1-antitrypsin deficient children. *Acta Paediatr Scand* 77: 847–851, 1988. doi:10.1111/j.1651-2227.1988.tb10767.x.
30. **Hidvegi T**, **Ewing M**, **Hale P**, **Dippold C**, **Beckett C**, **Kemp C**, **Maurice N**, **Mukherjee A**, **Goldbach C**, **Watkins S**, **Michalopoulos G**, **Perlmutter DH.** An autophagy-enhancing drug promotes degradation of mutant alpha1-antitrypsin Z and reduces hepatic fibrosis. *Science* 329: 229–232, 2010. doi:10.1126/science.1190354.
31. **Kaushal S**, **Annamali M**, **Blomenkamp K**, **Rudnick D**, **Halloran D**, **Brunt EM**, **Teckman JH.** Rapamycin reduces intrahepatic alpha-1-antitrypsin mutant Z protein polymers and liver injury in a mouse model. *Exp Biol Med (Maywood)* 235: 700–709, 2010. doi:10.1258/ebm.2010.009297.
32. **Guo S**, **Booten SL**, **Aghajan M**, **Hung G**, **Zhao C**, **Blomenkamp K**, **Gattis D**, **Watt A**, **Freier SM**, **Teckman JH**, **McCaleb ML**, **Monia BP.** Antisense oligonucleotide treatment ameliorates alpha-1 antitrypsin-related liver disease in mice. *J Clin Invest* 124: 251–261, 2014. doi:10.1172/JCI67968.
33. **Flotte TR**, **Trapnell BC**, **Humphries M**, **Carey B**, **Calcedo R**, **Rouhani F**, **Campbell-Thompson M**, **Yachnis AT**, **Sandhaus RA**, **McElvaney NG**, **Mueller C**, **Messina LM**, **Wilson JM**, **Brantly M**, **Knop DR**, **Ye GJ**, **Chulay JD.** Phase 2 clinical trial of a recombinant adeno-associated viral vector expressing alpha1-antitrypsin: interim results. *Hum Gene Ther* 22: 1239–1247, 2011. doi:10.1089/hum.2011.053.
34. **Loring HS**, **Flotte TR.** Current status of gene therapy for alpha-1 antitrypsin deficiency. *Expert Opin Biol Ther* 15: 329–336, 2015. doi:10.1517/14712598.2015.978854.
35. **Askew DJ**, **Silverman GA.** Intracellular and extracellular serpins modulate lung disease. *J Perinatol* 28: S127–S135, 2008. doi:10.1038/jp.2008.150.
36. **Rau JC**, **Beaulieu LM**, **Huntington JA**, **Church FC.** Serpins in thrombosis, hemostasis and fibrinolysis. *J Thromb Haemost* 5, Suppl 1: 102–115, 2007. doi:10.1111/j.1538-7836.2007.02516.x.
37. **Salvatierra A**, **Guerrero R**, **Rodriguez M**, **Alvarez A**, **Soriano F**, **Lopez-Pedrera R**, **Ramirez R**, **Carracedo J**, **Lopez-Rubio F**, **Lopez-Pujol J**, **Velasco F.** Antithrombin III prevents early pulmonary dysfunction after lung transplantation in the dog. *Circulation* 104: 2975–2980, 2001. doi:10.1161/hc4801.100032.
38. **Nishii Y**, **Gabazza EC**, **Fujimoto H**, **Nakahara H**, **Takagi T**, **Bruno N**, **D'Alessandro-Gabazza CN**, **Maruyama J**, **Maruyama K**, **Hayashi T**, **Adachi Y**, **Suzuki K**, **Taguchi O.** Protective role of protein C inhibitor in monocrotaline-induced pulmonary hypertension. *J Thromb Haemost* 4: 2331–2339, 2006. doi:10.1111/j.1538-7836.2006.02174.x.
39. **Valiente M**, **Obenauf AC**, **Jin X**, **Chen Q**, **Zhang XH**, **Lee DJ**, **Chaft JE**, **Kris MG**, **Huse JT**, **Brogi E**, **Massagué J.** Serpins promote cancer cell survival and vascular co-option in brain metastasis. *Cell* 156: 1002–1016, 2014. doi:10.1016/j.cell.2014.01.040.
40. **Losasso V**, **Schiffer S**, **Barth S**, **Carloni P.** Design of human granzyme B variants resistant to serpin B9. *Proteins* 80: 2514–2522, 2012. doi:10.1002/prot.24133.
41. **Vycital O**, **Pitule P**, **Hosek P**, **Kriz T**, **Treska V**, **Liska V.** Expression of Serpin B9 as a prognostic factor of colorectal cancer. *Anticancer Res* 39: 6063–6066, 2019. doi:10.21873/anticanres.13813.
42. **Lockett J**, **Yin S**, **Li X**, **Meng Y**, **Sheng S.** Tumor suppressive maspin and epithelial homeostasis. *J Cell Biochem* 97: 651–660, 2006. doi:10.1002/jcb.20721.
43. **Hatcher HC**, **Ma JX**, **Chao J**, **Chao L**, **Ottlecz A.** Kallikrein-binding protein levels are reduced in the retinas of streptozotocin-induced diabetic rats. *Invest Ophthalmol Vis Sci* 38: 658–664, 1997.
44. **Ma JX**, **King LP**, **Yang Z**, **Crouch RK**, **Chao L**, **Chao J.** Kallistatin in human ocular tissues: reduced levels in vitreous fluids from patients with diabetic retinopathy. *Curr Eye Res* 15: 1117–1123, 1996. doi:10.3109/02713689608995143.
45. **Miao RQ**, **Agata J**, **Chao L**, **Chao J.** Kallistatin is a new inhibitor of angiogenesis and tumor growth. *Blood* 100: 3245–3252, 2002. doi:10.1182/blood-2002-01-0185.
46. **Gao G**, **Shao C**, **Zhang SX**, **Dudley A**, **Fant J**, **Ma JX.** Kallikrein-binding protein inhibits retinal neovascularization and decreases vascular leakage. *Diabetologia* 46: 689–698, 2003. doi:10.1007/s00125-003-1085-9.
47. **He X**, **Cheng R**, **Benyajati S**, **Ma JX.** PEDF and its roles in physiological and pathological conditions: implication in diabetic and hypoxia-induced angiogenic diseases. *Clin Sci (Lond)* 128: 805–823, 2015. doi:10.1042/CS20130463.
48. **Tombran-Tink J**, **Barnstable CJ.** PEDF: a multifaceted neurotrophic factor. *Nat Rev Neurosci* 4: 628–636, 2003. doi:10.1038/nrn1176.
49. **Huang Q**, **Wang S**, **Sorenson CM**, **Sheibani N.** PEDF-deficient mice exhibit an enhanced rate of retinal vascular expansion and are more sensitive to hyperoxia-mediated vessel obliteration. *Exp Eye Res* 87: 226–241, 2008. doi:10.1016/j.exer.2008.06.003.
50. **Subramanian P**, **Locatelli-Hoops S**, **Kenealey J**, **DesJardin J**, **Notari L**, **Becerra SP.** Pigment epithelium-derived factor (PEDF) prevents retinal cell death via PEDF receptor (PEDF-R): identification of a functional ligand binding site. *J Biol Chem* 288: 23928–23942, 2013. doi:10.1074/jbc.M113.487884.
51. **Flevaris P**, **Khan SS**, **Eren M**, **Schuldt AJ**, **Shah SJ**, **Lee DC**, **Gupta S**, **Shapiro AD**, **Burridge PW**, **Ghosh AK**, **Vaughan DE.** Plasminogen

activator inhibitor type I controls cardiomyocyte transforming growth factor-beta and cardiac fibrosis. *Circulation* 136: 664–679, 2017. doi:10.1161/CIRCULATIONAHA.117.028145.

52. **Macfelda K**, **Weiss TW**, **Kaun C**, **Breuss JM**, **Zorn G**, **Oberndorfer U**, **Voegele-Kadletz M**, **Huber-Beckmann R**, **Ullrich R**, **Binder BR**, **Losert UM**, **Maurer G**, **Pacher R**, **Huber K**, **Wojta J.** Plasminogen activator inhibitor 1 expression is regulated by the inflammatory mediators interleukin-1alpha, tumor necrosis factor-alpha, transforming growth factor-beta and oncostatin M in human cardiac myocytes. *J Mol Cell Cardiol* 34: 1681–1691, 2002. doi:10.1006/jmcc.2002.2117.
53. **Chao J**, **Guo Y**, **Chao L.** Protective role of endogenous kallistatin in vascular injury and senescence by inhibiting oxidative stress and inflammation. *Oxid Med Cell Longev* 2018: 4138560, 2018. doi:10.1155/2018/4138560.
54. **Nicholas SB**, **Aguiniga E**, **Ren Y**, **Kim J**, **Wong J**, **Govindarajan N**, **Noda M**, **Wang W**, **Kawano Y**, **Collins A**, **Hsueh WA.** Plasminogen activator inhibitor-1 deficiency retards diabetic nephropathy. *Kidney Int* 67: 1297–1307, 2005. doi:10.1111/j.1523-1755.2005.00207.x.
55. **Schroder WA**, **Le TT**, **Major L**, **Street S**, **Gardner J**, **Lambley E**, **Markey K**, **MacDonald KP**, **Fish RJ**, **Thomas R**, **Suhrbier A.** A physiological function of inflammation-associated SerpinB2 is regulation of adaptive immunity. *J Immunol* 184: 2663–2670, 2010. doi:10.4049/jimmunol.0902187.
56. **Shea-Donohue T**, **Zhao A**, **Antalis TM.** SerpinB2 mediated regulation of macrophage function during enteric infection. *Gut Microbes* 5: 254–258, 2014. doi:10.4161/gmic.28093.
57. **Sen P**, **Helmke A**, **Liao CM**, **Sörensen-Zender I**, **Rong S**, **Bräsen JH**, **Melk A**, **Haller H**, **von Vietinghoff S**, **Schmitt R.** SerpinB2 regulates immune response in kidney injury and aging. *J Am Soc Nephrol* 31: 983–995, 2020. doi:10.1681/ASN.2019101085.
58. **Maicas N**, **van der Vlag J**, **Bublitz J**, **Florquin S**, **Bakker-van Bebber M**, **Dinarello CA**, **Verweij V**, **Masereeuw R**, **Joosten LA**, **Hilbrands LB.** Human Alpha-1-Antitrypsin (hAAT) therapy reduces renal dysfunction and acute tubular necrosis in a murine model of bilateral kidney ischemia-reperfusion injury. *PLoS One* 12: e0168981, 2017. doi:10.1371/journal.pone.0168981.
59. **Yiu WH**, **Wong DW**, **Wu HJ**, **Li RX**, **Yam I**, **Chan LY**, **Leung JC**, **Lan HY**, **Lai KN**, **Tang SC.** Kallistatin protects against diabetic nephropathy in db/db mice by suppressing AGE-RAGE-induced oxidative stress. *Kidney Int* 89: 386–398, 2016. doi:10.1038/ki.2015.331.
60. **Sánchez-Navarro A**, **Mejía-Vilet JM**, **Pérez-Villalva R**, **Carrillo-Pérez DL**, **Marquina-Castillo B**, **Gamba G**, **Bobadilla NA.** SerpinA3 in the early recognition of acute kidney injury to chronic kidney disease (CKD) transition in the rat and its potentiality in the recognition of patients with CKD. *Sci Rep* 9: 10350, 2019. doi:10.1038/s41598-019-46601-1.
61. **Cabral CM**, **Choudhury P**, **Liu Y**, **Sifers RN.** Processing by endoplasmic reticulum mannosidases partitions a secretion-impaired glycoprotein into distinct disposal pathways. *J Biol Chem* 275: 25015–25022, 2000. doi:10.1074/jbc.M910172199.
62. **Baker C**, **Belbin O**, **Kalsheker N**, **Morgan K.** SERPINA3 (aka alpha-1-antichymotrypsin). *Front Biosci* 12: 2821–2835, 2007. doi:10.2741/2275.
63. **Mast AE**, **Enghild JJ**, **Nagase H**, **Suzuki K**, **Pizzo SV**, **Salvesen G.** Kinetics and physiologic relevance of the inactivation of alpha 1-proteinase inhibitor, alpha 1-antichymotrypsin, and antithrombin III by matrix metalloproteinases-1 (tissue collagenase), -2 (72-kDa gelatinase/type IV collagenase), and -3 (stromelysin). *J Biol Chem* 266: 15810–15816, 1991.
64. **Aslam MS**, **Yuan L.** Serpina3n: potential drug and challenges, mini review. *J Drug Target* 28: 368–378, 2020. doi:10.1080/1061186X.2019.1693576.
65. **Naidoo N**, **Cooperman BS**, **Wang ZM**, **Liu XZ**, **Rubin H.** Identification of lysines within alpha 1-antichymotrypsin important for DNA binding. An unusual combination of DNA-binding elements. *J Biol Chem* 270: 14548–14555, 1995. doi:10.1074/jbc.270.24.14548.
66. **Takada S**, **Tsuda M**, **Yamamura M**, **Katsunuma T.** Effect of alpha-1-antichymotrypsin on activity of DNA primase isolated from human stomach adenocarcinoma cells. *Biochem Int* 16: 949–954, 1988.
67. **Lomas DA**, **Mahadeva R.** Alpha1-antitrypsin polymerization and the serpinopathies: pathobiology and prospects for therapy. *J Clin Invest* 110: 1585–1590, 2002. doi:10.1172/JCI0216782.
68. **Mahadeva R**, **Sharples L**, **Ross-Russell RI**, **Webb AK**, **Bilton D**, **Lomas DA.** Association of alpha$_1$-antichymotrypsin deficiency with milder lung disease in patients with cystic fibrosis. *Thorax* 56: 53–58, 2001. doi:10.1136/thorax.56.1.53.
69. **Sandford AJ**, **Chagani T**, **Weir TD**, **Paré PD.** Alpha 1-antichymotrypsin mutations in patients with chronic obstructive pulmonary disease. *Dis Markers* 13: 257–260, 1998. doi:10.1155/1998/867620.
70. **Meckelein B**, **Marshall DC**, **Conn KJ**, **Pietropaolo M**, **Van Nostrand W**, **Abraham CR.** Identification of a novel serine protease-like molecule in human brain. *Brain Res Mol Brain Res* 55: 181–197, 1998. doi:10.1016/S0169-328X(97)00366-5.
71. **Mucke L**, **Yu GQ**, **McConlogue L**, **Rockenstein EM**, **Abraham CR**, **Masliah E.** Astroglial expression of human alpha$_1$-antichymotrypsin enhances Alzheimer-like pathology in amyloid protein precursor transgenic mice. *Am J Pathol* 157: 2003–2010, 2000. doi:10.1016/S0002-9440(10)64839-0.
72. **DeKosky ST**, **Ikonomovic MD**, **Wang X**, **Farlow M**, **Wisniewski S**, **Lopez OL**, **Becker JT**, **Saxton J**, **Klunk WE**, **Sweet R**, **Kaufer DI**, **Kamboh MI.** Plasma and cerebrospinal fluid alpha1-antichymotrypsin levels in Alzheimer's disease: correlation with cognitive impairment. *Ann Neurol* 53: 81–90, 2003. doi:10.1002/ana.10414.
73. **Kamboh MI**, **Minster RL**, **Kenney M**, **Ozturk A**, **Desai PP**, **Kammerer CM**, **DeKosky ST.** Alpha-1-antichymotrypsin (ACT or SERPINA3) polymorphism may affect age-at-onset and disease duration of Alzheimer's disease. *Neurobiol Aging* 27: 1435–1439, 2006. doi:10.1016/j.neurobiolaging.2005.07.015.
74. **Vanni S**, **Moda F**, **Zattoni M**, **Bistaffa E**, **De Cecco E**, **Rossi M**, **Giaccone G**, **Tagliavini F**, **Haïk S**, **Deslys JP**, **Zanusso G**, **Ironside JW**, **Ferrer I**, **Kovacs GG**, **Legname G.** Differential overexpression of SERPINA3 in human prion diseases. *Sci Rep* 7: 15637, 2017. doi:10.1038/s41598-017-15778-8.
75. **Zhou T**, **Chen L**, **Huang CH**, **Lin Z**, **Zong R**, **Zhu C**, **Pan F**, **Ma JX**, **Liu ZG**, **Zhou Y.** Serine proteinase inhibitor SERPINA3K suppresses corneal neovascularization via inhibiting Wnt signaling and VEGF. *Invest Ophthalmol Vis Sci* 55: 4863–4872, 2014. doi:10.1167/iovs.14-14023.
76. **Zhang B**, **Zhou KK**, **Ma JX.** Inhibition of connective tissue growth factor overexpression in diabetic retinopathy by SERPINA3K via blocking the WNT/beta-catenin pathway. *Diabetes* 59: 1809–1816, 2010. doi:10.2337/db09-1056.
77. **Zhang B**, **Ma JX.** SERPINA3K prevents oxidative stress induced necrotic cell death by inhibiting calcium overload. *PLoS One* 3: e4077, 2008. doi:10.1371/journal.pone.0004077.
78. **Zhou T**, **Zong R**, **Zhang Z**, **Zhu C**, **Pan F**, **Xiao X**, **Liu Z**, **He H**, **Ma JX**, **Liu Z**, **Zhou Y.** SERPINA3K protects against oxidative stress via modulating ROS generation/degradation and KEAP1-NRF2 pathway in the corneal epithelium. *Invest Ophthalmol Vis Sci* 53: 5033–5043, 2012. doi:10.1167/iovs.12-9729.
79. **Zhu H**, **Liu Q**, **Tang J**, **Xie Y**, **Xu X**, **Huang R**, **Zhang Y**, **Jin K**, **Sun B.** Alpha1-ACT functions as a tumour suppressor in hepatocellular carcinoma by Inhibiting the PI3K/AKT/mTOR signalling pathway via activation of PTEN. *Cell Physiol Biochem* 41: 2289–2306, 2017. doi:10.1159/000475648.
80. **Luo D**, **Chen W**, **Tian Y**, **Li J**, **Xu X**, **Chen C**, **Li F.** Serpin peptidase inhibitor, clade A member 3 (SERPINA3), is overexpressed in glioma and associated with poor prognosis in glioma patients. *Onco Targets Ther* 10: 2173–2181, 2017. doi:10.2147/OTT.S133022.
81. **Li Y**, **Dong X**, **Cai J**, **Yin S**, **Sun Y**, **Yang D**, **Jiang C.** SERPINA3 induced by astroglia/microglia co-culture facilitates glioblastoma stem-like cell invasion. *Oncol Lett* 15: 285–291, 2018. doi:10.3892/ol.2017.7275.
82. **Takada S**, **Tsuda M**, **Fujinami S**, **Yamamura M**, **Mitomi T**, **Katsunuma T.** Incorporation of alpha-1-antichymotrypsin into carcinoma cell nuclei of human stomach adenocarcinoma transplanted into nude mice. *Cancer Res* 46: 3688–3691, 1986.
83. **Zhou J**, **Cheng Y**, **Tang L**, **Martinka M**, **Kalia S.** Up-regulation of SERPINA3 correlates with high mortality of melanoma patients and increased migration and invasion of cancer cells. *Oncotarget* 8: 18712–18725, 2017. doi:10.18632/oncotarget.9409.
84. **Zhou ML**, **Chen FS**, **Mao H.** Clinical significance and role of up-regulation of SERPINA3 expression in endometrial cancer. *World J Clin Cases* 7: 1996–2002, 2019. doi:10.12998/wjcc.v7.i15.1996.
85. **Cao LL**, **Pei XF**, **Qiao X**, **Yu J**, **Ye H**, **Xi CL**, **Wang PY**, **Gong ZL.** SERPINA3 silencing inhibits the migration, invasion, and liver metastasis of colon cancer cells. *Dig Dis Sci* 63: 2309–2319, 2018. doi:10.1007/s10620-018-5137-x.

86. **Murohara T**, **Guo JP**, **Lefer AM.** Cardioprotection by a novel recombinant serine protease inhibitor in myocardial ischemia and reperfusion injury. *J Pharmacol Exp Ther* 274: 1246–1253, 1995.
87. **Zhao L**, **Zheng M**, **Guo Z**, **Li K**, **Liu Y**, **Chen M**, **Yang X.** Circulating Serpina3 levels predict the major adverse cardiac events in patients with myocardial infarction. *Int J Cardiol* 300: 34–38, 2020. doi:10.1016/j.ijcard.2019.08.034.
88. **Limbutara K**, **Chou CL**, **Knepper MA.** Quantitative proteomics of all 14 renal tubule segments in rat. *J Am Soc Nephrol* 31: 1255–1266, 2020. doi:10.1681/ASN.2020010071.
89. **Conz P**, **Bevilacqua PA**, **Ronco C**, **Feriani M**, **Brendolan A**, **Dell'Aquila R**, **Pietribiasi G**, **Meli S**, **La Greca G.** Alpha-1-antichymotrypsin in renal biopsies. *Nephron* 56: 387–390, 1990. doi:10.1159/000186180.
90. **Hörl WH**, **Stepinski J**, **Schäfer RM**, **Wanner C**, **Heidland A.** Role of proteases in hypercatabolic patients with renal failure. *Kidney Int Suppl* 16: S37–S42, 1983.
91. **Khan TN**, **Sinniah R.** Renal tubular antiproteinase (alpha-1-antitrypsin and alpha-1-antichymotrypsin) response in tubulo-interstitial damage. *Nephron* 65: 232–239, 1993. doi:10.1159/000187480.
92. **Ziegler ME**, **Chen T**, **LeBlanc JF**, **Wei X**, **Gjertson DW**, **Li KC**, **Khalighi MA**, **Lassman CR**, **Veale JL**, **Gritsch HA**, **Reed EF.** Apolipoprotein A1 and C-terminal fragment of alpha-1 antichymotrypsin are candidate plasma biomarkers associated with acute renal allograft rejection. *Transplantation* 92: 388–395, 2011. doi:10.1097/TP.0b013e318225db6a.
93. **Teoh SS**, **Whisstock JC**, **Bird PI.** Maspin (SERPINB5) is an obligate intracellular serpin. *J Biol Chem* 285: 10862–10869, 2010. doi:10.1074/jbc.M109.073171.

7. MANUSCRITOS EN PREPARACIÓN

7.1 Manuscrito 1: La serpinA3 en respuesta al estrés celular.

Evaluamos si los niveles de serpinA3K en orina podrían servir como un biomarcador temprano de LRA. Utilizamos un modelo de Lesión por Isquemia/Reperfusión (IR) para inducir LRA. Este modelo se caracteriza por hipoxia, estrés oxidante, inflamación y daño y muerte de células tubulares y endoteliales (87). Se incluyeron 20 animales que se sometieron a diferentes períodos de Isquemia / Reperfusión bilateral renal (15, 30, 45 y 60 min) y los comparamos con un grupo simulado (n = 4 para cada grupo). A las 24 h post-isquemia, se evaluaron los parámetros fisiológicos y bioquímicos. No encontramos cambios en la presión arterial media entre los grupos (datos no mostrados), mientras que los animales que se sometieron a isquemia mostraron alteraciones profundas a nivel renal, como la reducción en el flujo sanguíneo renal (FSR), que fue significativo en los grupos de 45 y 60 minutos de isquemia (Figura 1A), aumentos significativos en la creatinina sérica (Figura 1B) y aumento de proteinuria (Figura 1C) a partir de los 30 minutos posteriores a la isquemia, mientras que la elevación de un marcador de estrés oxidante fue estadísticamente significativo después de 45 minutos de LRA (Figura 1D). También analizamos los niveles de Hsp72 en orina, un biomarcador de LRA sensible que hemos descrito previamente. Los niveles de Hsp72 urinario aumentaron progresivamente en paralelo a la gravedad del daño renal inducido (Figura 1E). De manera similar, los niveles de serpinA3K en orina aumentaron progresivamente de manera proporcional a la severidad del LRA (Figura 1F). El incremento en los niveles de serpinA3K en orina fue evidente a partir de los 15 minutos posteriores a la isquemia, pero alcanzó una diferencia estadística a partir

de los 30 minutos posteriores a la isquemia. Estos datos indican que los niveles urinarios de serpinA3K pudieron estratificar el grado de lesión renal.

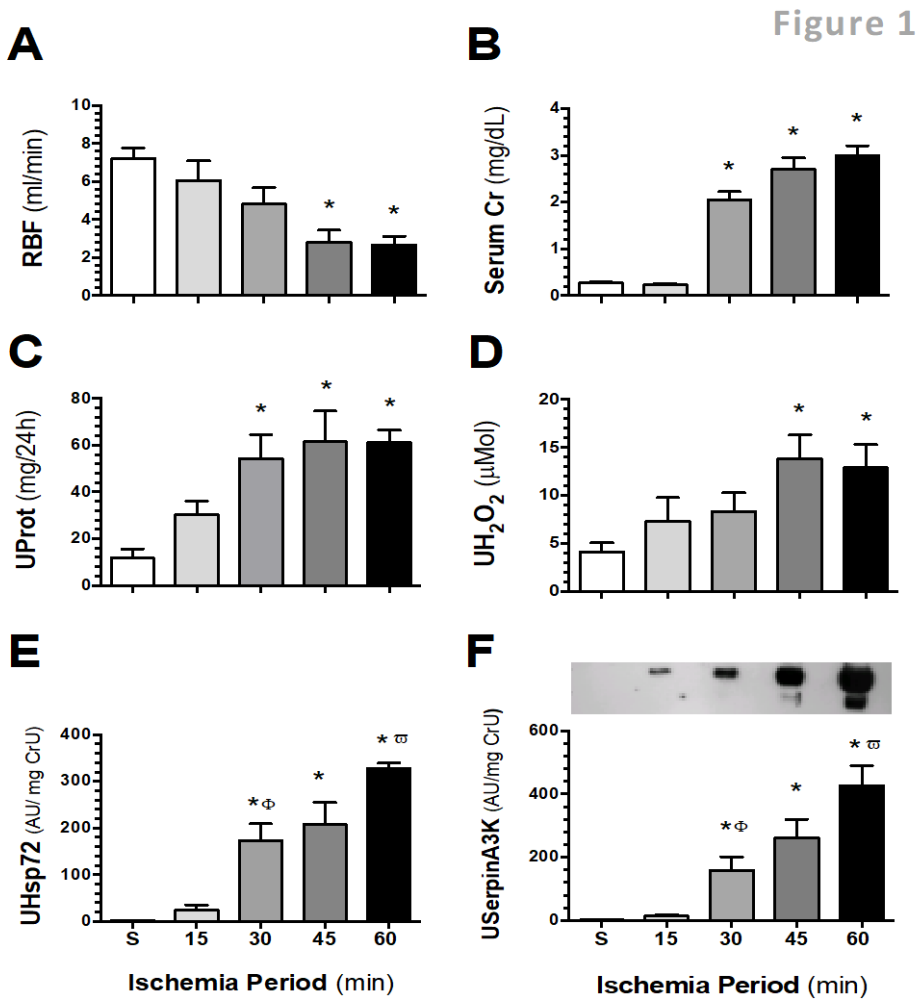

Figura 1. Gravedad de la LRA inducida por diferentes periodos de I/R bilateral en la rata. A) Flujo sanguíneo renal (RBF), B) Creatinina sérica, C) Proteinuria, D) Peróxido de hidrógeno en orina (UH2O2) E) Niveles de proteína HSP72 en orina, y F) Niveles de proteína serpinA3K en orina, una autorradiografía de WB representativa se muestra arriba. Los datos se muestran como media ± SE. (n = 4 por grupo). * p <0,05 frente al grupo simulado, Φ p <0,05 frente al grupo isquémico de 45 min, ϖ p <0,05 frente al grupo isquémico de 60 min.

También evaluamos si serpinA3K podría ser un biomarcador temprano de LRA en ratas. Once grupos fueron incluidos y eutanasiados en diferentes períodos de reperfusión (3, 6, 9, 12, 18, 24, 48, 72, 96 y 120 h). Se encontró una reducción significativa en el FSR (Figura 2A), con una elevación significativa de la creatinina

sérica después de 9 h de isquemia (Figura 2B), mientras que la proteinuria y la excreción urinaria de H_2O_2 no se alteraron hasta las 24 h después de la isquemia (Figura 2C y 2D). Como reportamos anteriormente (61). El aumento de los niveles urinarios de Hsp72 apareció muy temprano, comenzando a las 3 h después de la isquemia (Figura 2E). Del mismo modo, observamos que los niveles de serpinA3K en orina podrían detectar AKI en las primeras etapas, también comenzando a las 3 h post-isquemia (Figura 2F).

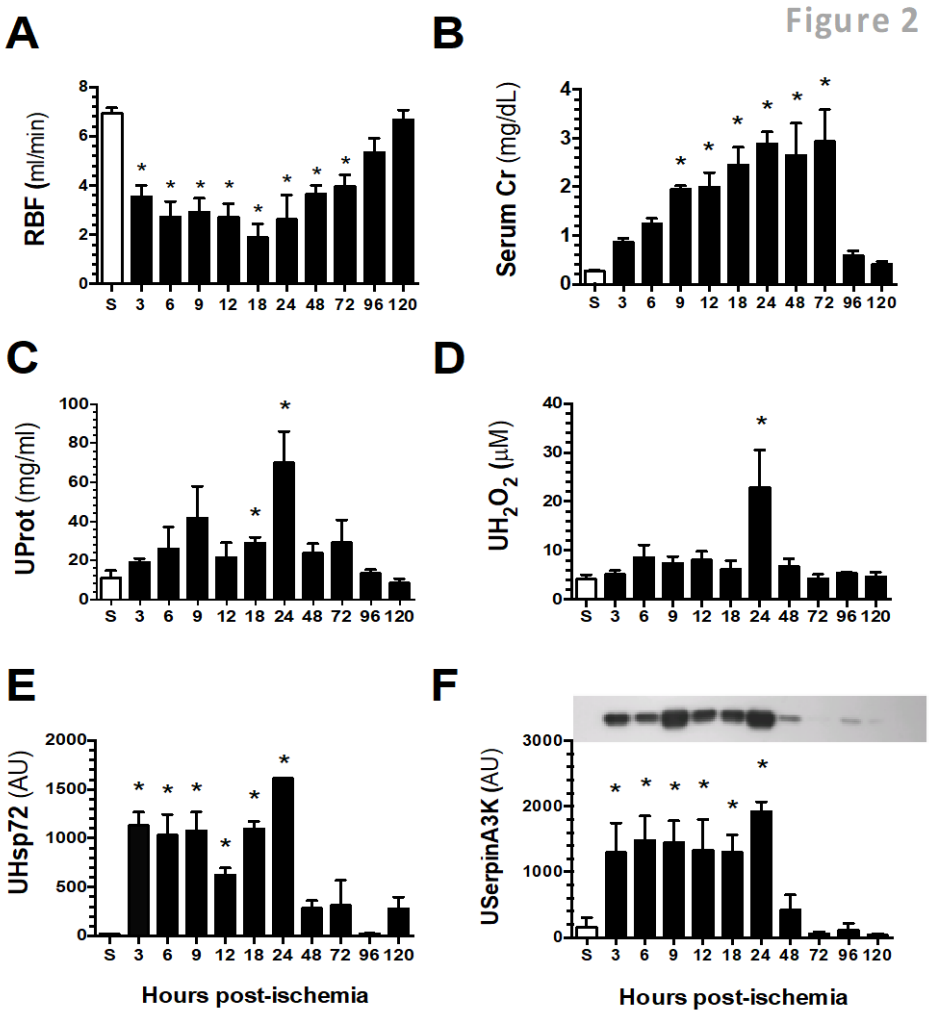

Figura 2. Evolución temporal de los biomarcadores de LRA después de 45 min de isquemia renal bilateral en la rata. A) Flujo sanguíneo renal, B) Creatinina sérica, C) Proteinuria, D) Peróxido de hidrógeno en orina, E) Niveles de proteína HSP72 en orina, y F) Niveles de proteína serpinA3K en orina medidos por Western Blot, incluida una autorradiografía de WB representativa. Los datos se presentan como media ± SE. (n = 4 por grupo). * p <0,05 frente al grupo simulado.

Al analizar la localización de la serpinA3K en el riñón, encontramos que esta se expresaba principalmente en las células tubulares. En el caso del grupo control, la proteína se encontraba distribuida por todo el citoplasma, en comparación con el grupo de LRA encontramos que la serpinA3K, se relocalizó a la membrana apical

(Figura suplem. 1). Este cambio de localización sugiere su posible secreción a la luz tubular y de esa manera su presencia en la orina.

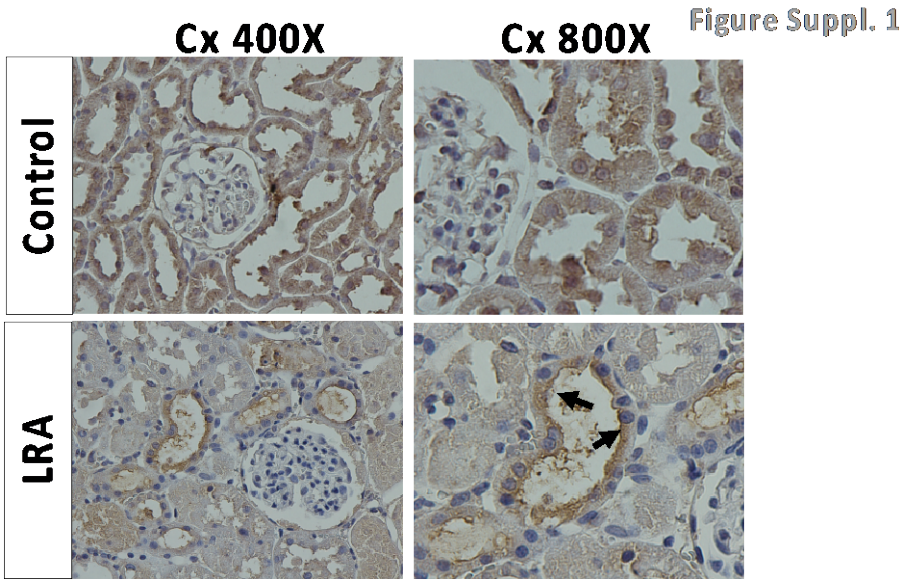

Figura suplementaria 1. Inmunohistoquímica de Serpin A3K en tejido renal. Micrografías representativas de serpinA3 en portaobjetos de riñón de ratas de control o AKI, después de 24 horas. Ampliación 400 xy 800x. Las flechas indican la translocación de serpinA3K a la membrana apical

Con la finalidad de evaluar si la serpina es secretada en condiciones de estrés celular, clonamos a la serpina3k de la rata en un vector de expresión para realizar la transfección transitoria en células HEK293, realizando una curva creciente de plásmido, así como, una curva temporal de la expresión y secreción de serpinA3K. Primero corroboramos que la transfección era eficiente mediante la utilización de un anticuerpo anti-Flag y anti-serpina. Encontramos que el punto máximo de expresión y secreción de la serpinA3K se logró con 1ug de plásmido (Figura 3A). Al evaluar la temporalidad de la expresión y secreción de serpinA3K, encontramos que cambiando el medio cada 24 h, el período entre 24 y 48 h fue donde encontramos mayor secreción, (Figura 3C); es importante mencionar que la transfección continúo siendo eficiente hasta las 72 h, ya que, al hacer un ensayo en

donde no se realizó cambio de medio, podemos ver la acumulación creciente de la serpinA3K en el medio (Figura 3D).

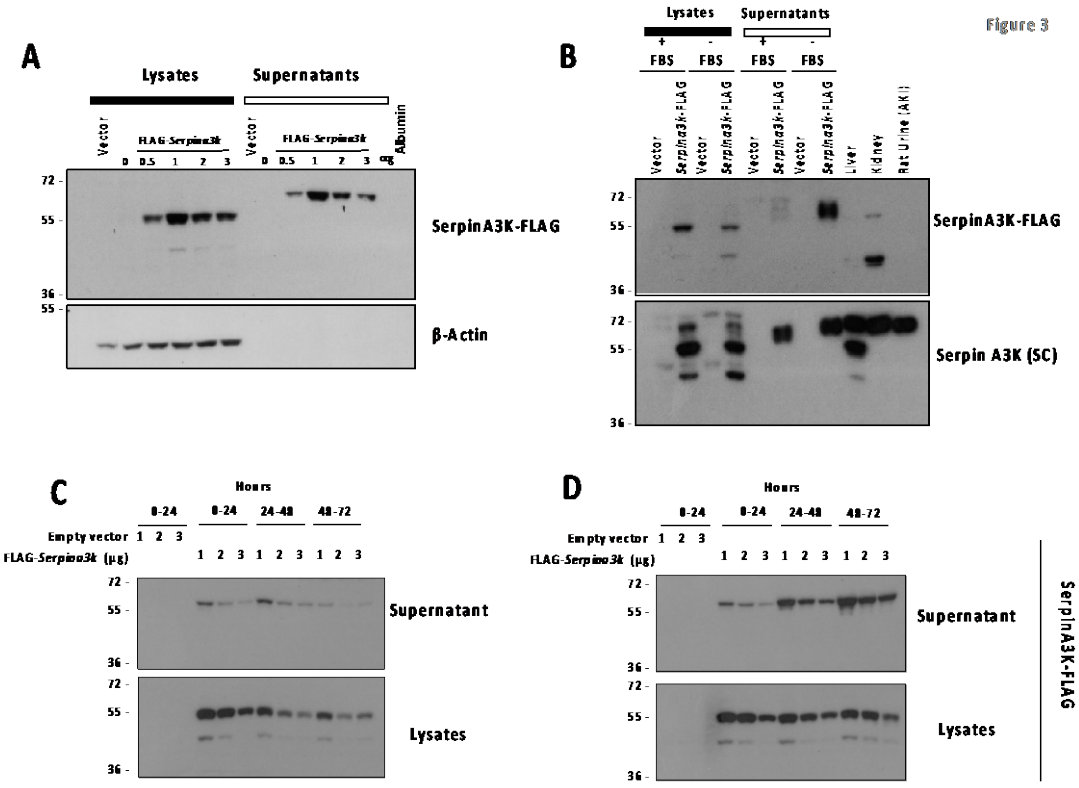

Figura 3. Secreción in vitro de serpinA3 tras estrés celular. A) WB de curva de diferente concentración de DNA para sobreexpresión de serpinA3K. B) WB con estímulos celulares con o sin Albúmina de Suero Bovino (BSA). C) Curva temporal de secreción de serpinA3K cambiando el medio cada 24hr. D) Curva temporal de secreción de serpinA3K sin cambiar el medio.

Para evaluar si el estrés celular era capaz de inducir mayor secreción de serpinA3K, eliminamos el suero fetal bovino del medio durante 24h. Encontramos que el estrés celular indujo una mayor secreción serpinA3K (Figura 3B).

Observamos también que el peso molecular de la proteína secretada era mayor que la intracelular. Esto nos sugirió que, la serpinA3K para ser secretada, requiere una modificación postraduccional. La N-glicosilación es una modificación previamente identificada en esta proteína (88, 89). Por esta razón, analizamos si

esta modificación se estaba produciendo y si era encontrada en la serpinA3K secretada. Realizamos un ensayo de PNG-glicanasa, enzima encargada de remover las N-glicosilaciones. Cuando evaluamos el peso molecular después del tratamiento, encontramos que el peso se igualó entre todos los grupos, incluidos el del hígado, plasma, riñón y orina de rata con LRA. Este experimento sugiere que la glicosilación es una modificación presente en la proteína secretada (Figura 4A, B, C).

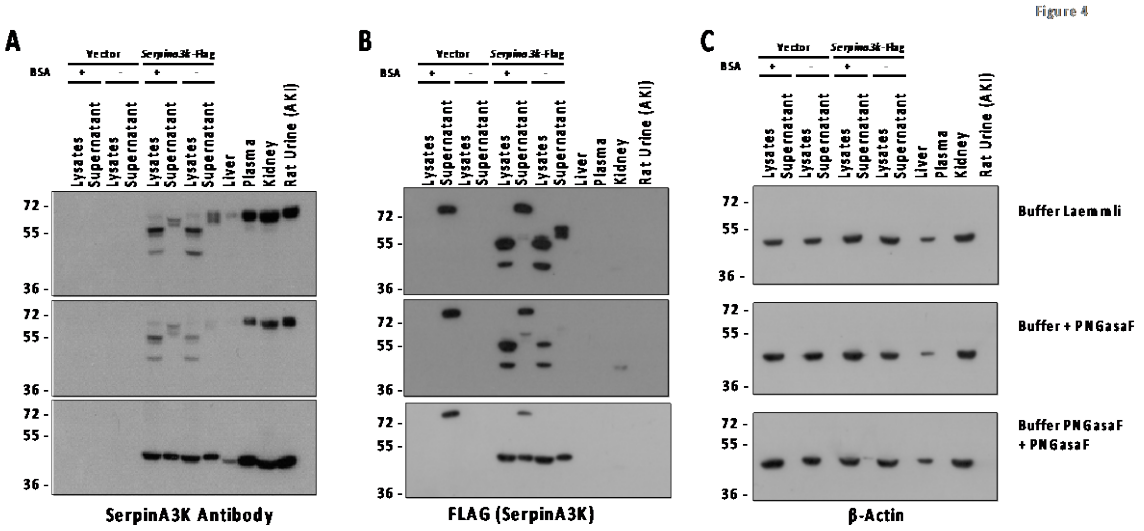

Figura 4. Glicosilación de la serpinA3K. A) WB del tratamiento con PNGasaF usando el anticuerpo contra serpinA3K. B) WB del tratamiento con PNGasaF usando el anticuerpo contra FLAG. C) WB del tratamiento con PNGasaF usando el anticuerpo contra β-actina.

Otra forma de inducir estrés celular fue exponer a las células a dosis crecientes de peróxido de hidrogeno y como se observa en la Figura 5, hubo un aumento en la secreción de serpinA3K de manera dosis dependiente (Figura 5).

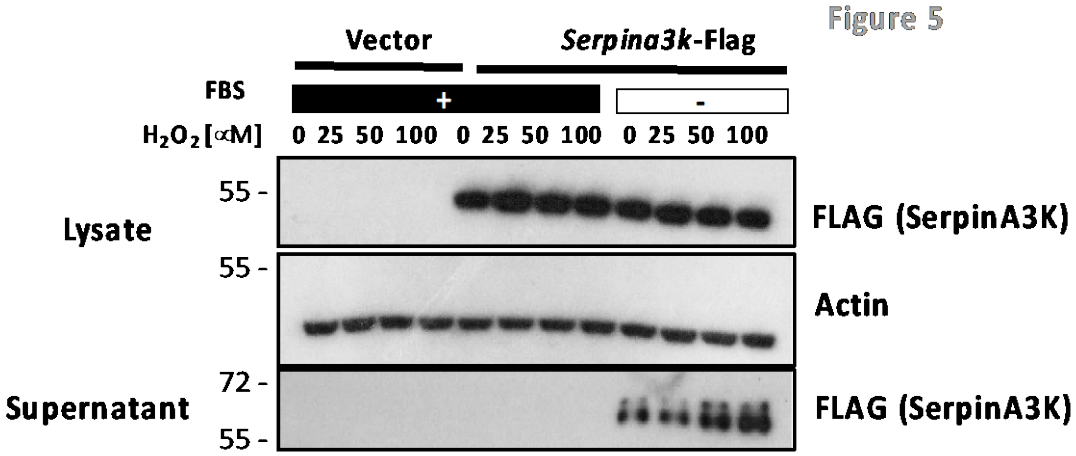

Figura 5. Secreción in vitro de serpinA3 en respuesta a estrés oxidante. WB de curva de diferente concentración de peroxido de hidrogeno (H_2O_2) para estimular la secreción de serpinA3K. Lisado celular y sobrenadante a las 24hrs del estímulo.

Finalmente, determinamos si se encontraban niveles anormales de serpinA3K en la orina de pacientes con LRA. Se incluyeron once pacientes, cinco (45.5%) de los cuales eran mujeres y seis (55.5%) hombres, con una edad promedio de 56.8 ± 4.4 años. El nivel medio de creatinina sérica basal fue de 0.8 ± 0.1 mg/dL y aumentó a 3.0 ± 0.4 mg/dl en el momento del diagnóstico de LRA. La severidad de la LRA clasificada como AKIN 1, 2 o 3 fue 27.3, 36.1 y 36.4%, respectivamente. Como se muestra en la Figura 6A, los pacientes con LRA exhibieron un aumento significativo en los niveles séricos de creatinina y de serpinA3K en la orina (Figura 6B). La serpinA3K no se detectó en la orina de voluntarios sanos.

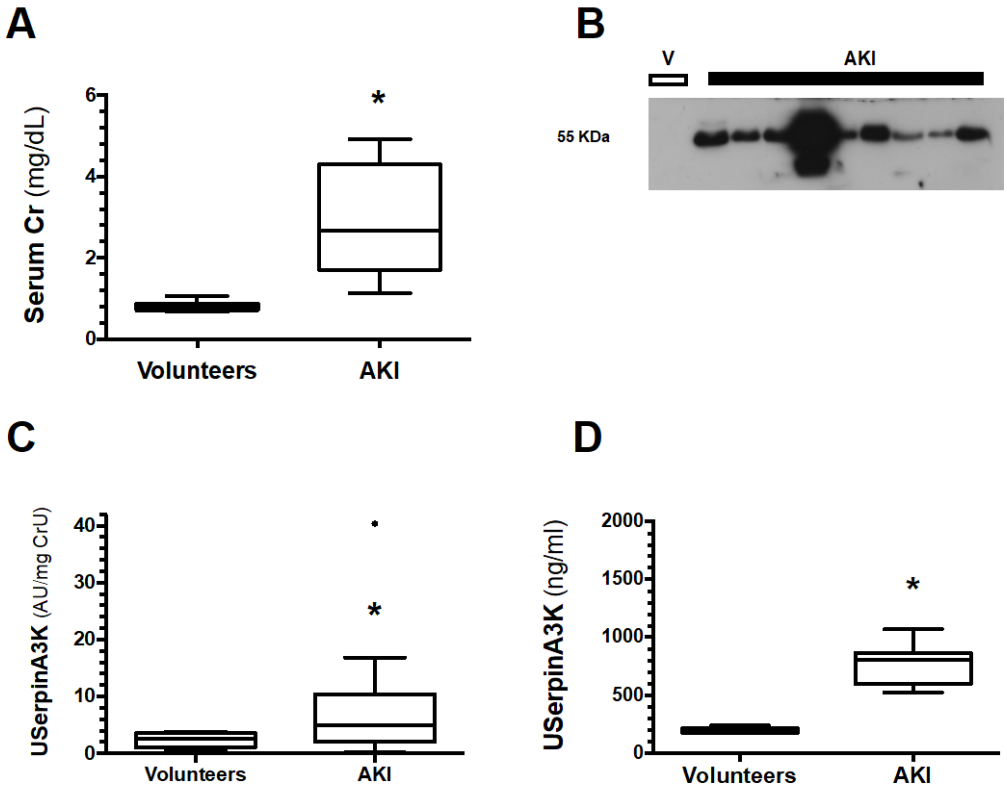

Figura 6. La serpinA3K urinaria aumenta significativamente en pacientes diagnosticados de LRA. A) Creatinina sérica. B) WB de serpinA3K representativa. C) Niveles de serpinA3K en orina corregidos por CrU. D) Niveles de ELISA de serpinA3K en orina. Los datos se representan como el diagrama de caja y bigotes de Tukey. * p <0,001 frente a voluntarios sanos.

DISCUSIÓN

Encontramos que el modelo de IR+UNx fue capaz de inducir LRA, además que aceleró la transición a ERC. La ERC se caracterizó por la caída del FSR, la disminución de la depuración de creatinina y el aumento de la creatinina sérica, así como un aumento progresivo de la proteinuria.

Los cambios que se presentaron de forma temprana fue el aumento del estrés oxidante que se mantuvo durante todo el seguimiento, así como una

disminución de la metilación global en corteza renal. Estos mecanismos deben estudiarse a mayor detalle, ya que podrían ser los responsables de la transición a ERC.

Este modelo nos permitirá estudiar las alteraciones epigenéticas que acompañan la transición de la LRA a ERC, así como el estudio de todos los mecanismos temporales involucrados en dicha transición, al acelerar este proceso.

En el presente estudio evaluamos si la serpinA3K urinaria podría ser también un biomarcador oportuno de LRA. Encontramos una elevación significativa de los niveles de serpinA3K en orina tan pronto como a las 3 h después de inducir la isquemia en la rata y esta mayor cantidad de serpina urinaria se mantuvo elevada hasta las 48 h después de la isquemia. Por el contrario, la elevación de la creatinina sérica y la aparición de proteinuria no se observaron hasta las 9 y 18 h posteriores a la isquemia, respectivamente. Cuando evaluamos los diferentes grados de LRA, hubo un aumento proporcional de los niveles de serpinA3K proporcionalmente a la gravedad de la lesión renal inducida. Se encontraron resultados similares cuando se evaluaron los niveles de RNAm de serpinA3K renal (datos no mostrados). Estos resultados sugieren que los niveles de serpinA3K en orina pueden ser una herramienta para la detección y estratificación temprana de LRA.

También demostramos la capacidad de las células tubulares para secretar serpinA3K bajo estrés celular sugiere que esta proteína, al igual que en otros tejidos, pudiera promover un efecto antioxidante y antiinflamatorio de las células tubulares adyacentes. La secreción de serpinA3K, se vio acompañada de un aumento de peso molecular y los resultados muestran que la glicosilación, es una modificación necesaria para la secreción de serpinA3K.

Este estudio en células en cultivo, animales y humanos muestra que, en condiciones fisiopatológicas, la serpinaA3 es secretada, muy probablemente para contrarrestar el daño oxidante e inflamatorio que ocurren después de estrés celular.

Este trabajo, deja la puerta abierta para evaluar el efecto de la serpinA3K en el riñón, frente a distintos escenarios fisiopatológicos, así como, la evaluación de la glicosilación como mecanismo de secreción frente a situaciones adversas. Además, queda pendiente la evaluación en un número mayor de pacientes para su función como biomarcador de LRA.

Debido a que se sabe que la serpina A3K es capaz de inhibir vías pro-inflamatorias como VEGF, TNF-α e ICAM (98, 99), previniendo efectos deletéreos de los procesos inflamatorios exacerbados (99-100) y conociendo que la LRA genera un proceso inflamatorio activo, decidimos evaluar que ocurría en las horas posteriores al episodio de isquemia bilateral. Encontramos que estos animales tenían presencia de serpina A3K de forma temprana a las 3 h pos-isquemia y permaneció elevada hasta las 120 h de reperfusión; mientras que la creatinina sérica y la proteinuria aparecieron de forma tardía (9 y 18h respectivamente) (Figura 5).

Al evaluar en animales con distintas severidades de LRA, vimos que la presencia de serpina A3K urinaria se reflejó desde los 30 min de isquemia y fue aumentando proporcionalmente al aumento de la severidad de daño, dejado de manifiesto la capacidad de esta proteína para estratificar el daño inducido por la LRA.

En los últimos años el aumento de los pacientes con ERC a nivel mundial ha aumentado de forma alarmante, aunado al reciente reconocimiento de la LRA como

factor de riesgo independiente para el desarrollo de ERC, que si no es tratado adecuadamente puede promover el desarrollo de enfermedad renal crónica terminal (ERCT), lo que, además, genera altos costos para los sistemas de salud y aumenta el riesgo de muerte en los pacientes. Es por ello por lo que resulta imprescindible encontrar biomarcadores que permitan identificar de forma temprana el desarrollo o transición de ERC, para promover que los tratamientos se den de forma oportunidad y prevenir el deterioro de la función renal.

El papel de la serpina A3K en fisiopatologías ha sido estudiada en modelos de daño en cornea y retina, pero no se conoce su función en la fisiopatología renal. Aunque, se ha encontrado que esta proteína ejerce actividades anti- inflamatorias, anti-angiogénicas y antioxidantes en la córnea y la retina, no se conoce si estos procesos son regulados de está misma manera en el riñón. Sin embargo, estos procesos antes mencionados, juegan un papel clave en la progresión y transición a ERC, por lo que se podría sugerir su posible función en esta patología.

Los resultados del presente trabajo apoyan a que la serpina A3K urinaria es un biomarcador temprano y eficaz para la detección de estos procesos, y con un panorama para en un futuro ser utilizado en pacientes.

7.2 Manuscrito 2: La deficiencia de sirtuina 7 reduce la inflamación y el daño tubular inducidos por un episodio de lesión renal aguda

Después de 24 h de la cirugía falsa de IRB renal, no se registraron diferencias significativas en el peso corporal entre los grupos (Figura 1A). El peso del riñón derecho y del izquierdo fueron significativamente mayores en los grupos WT+IRB y HT+IRB, curiosamente este efecto no se observó en el grupo KO-Sirt7+ IR (Figuras 1B-C), incluso cuando fueron normalizados por el peso corporal (Figuras 1D-E). Estos hallazgos sugieren que la IRB renal indujo inflamación renal en ratones WT y HT, que no se observó en ratones KO-Sirt7.

La LRA inducida por IRB se evidenció por la reducción significativa de la TFG evaluada por el monitor de fluorescencia y la inyección de FITC-sinistrina. Todos los grupos sometidos a IR bilateral mostraron un descenso significativo de la función renal (Figura 1F) Por lo tanto, la deficiencia de Sirt7 no tuvo impacto en la disfunción renal inducida por IR renal.

Figure 1

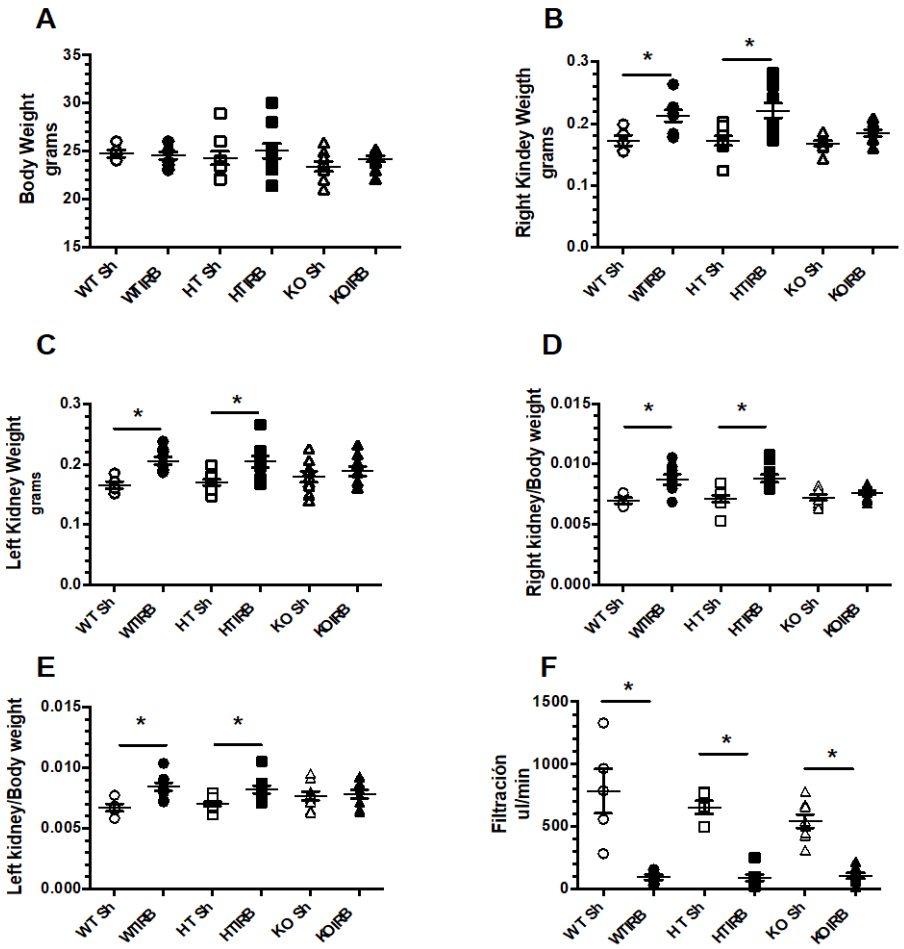

*Figura1.Efecto de la depleción de Sirt7 en la respuesta a LRA. A) Peso corporal, B)Peso riñón derecho, C) Peso riñón izquierdo, D) Peso riñón derecho corregido por peso corporal, E) Peso riñón izquierdo corregido por peso corporal, F)Tasa de filtrado glomerular. Circulo blanco WT Sh, Circulo negro WT IRB, Cuadrado blanco HT Sh, Cuadrado negro HT IRB, Triángulo blanco KO Sh, Triángulo negro KO IRB. n=5-10 por grupo. * p<0.05 vs. respectivo grupo marcado.*

La deficiencia de Sirt7 evitó el daño tubular

La albúmina urinaria y los biomarcadores de daño renal se evaluaron mediante ELISA y Western blot, respectivamente. Se observó un aumento significativo de la albuminuria en los grupos WT+IRB y HT+IRB, sin embargo, el incremento de la albuminuria en los grupos KO + IR fue de menor magnitud y no se encontró una diferencia significativa (Figura 2A).

Figure 2

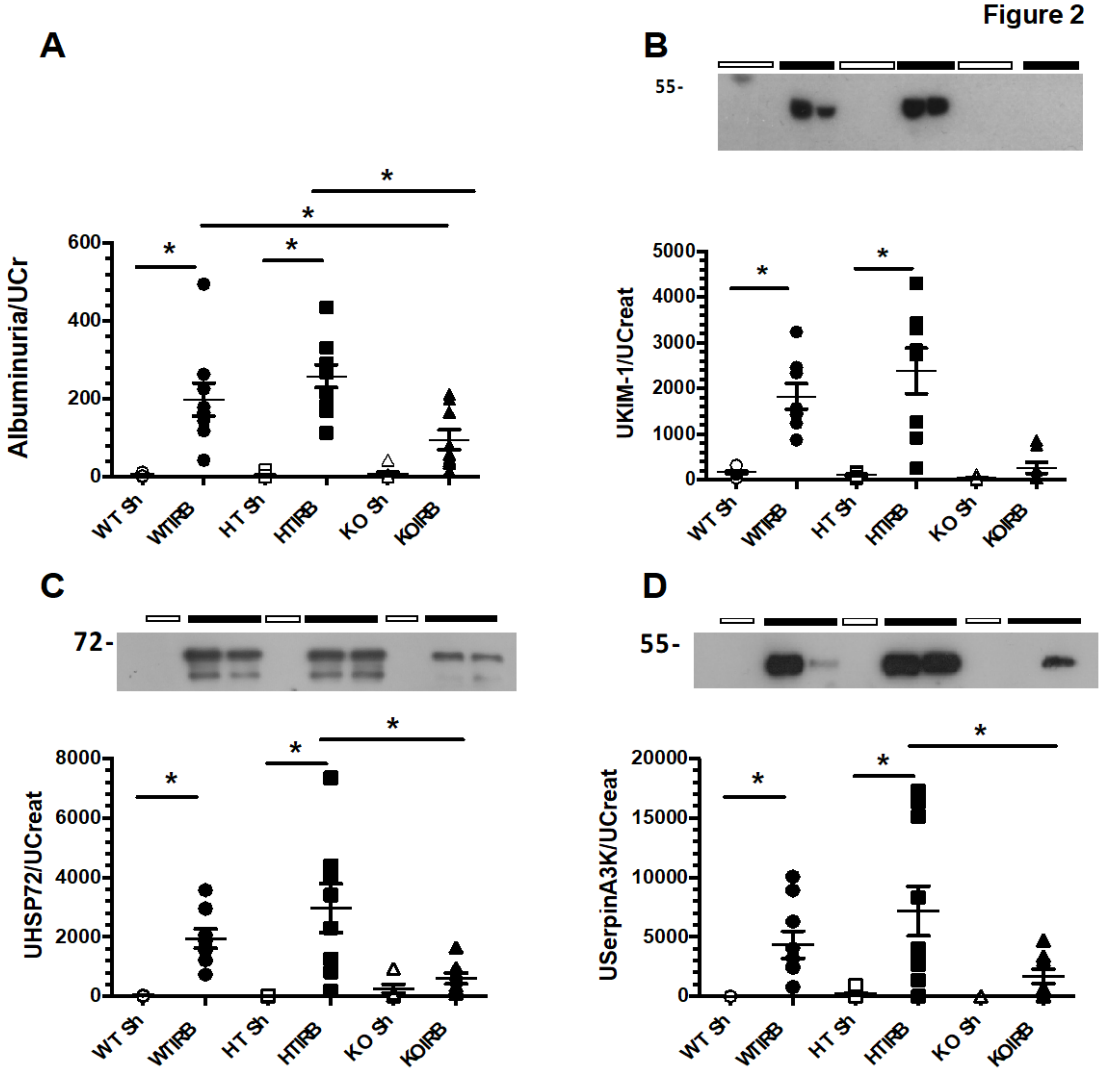

*Figura 2. La deficiencia de Sirt7 previno el daño renal . A)Relación Albuminuria/ Creatinina Urinaria(UCr), B) Relación UKIM-1/ UCr C) Relación UHSP72/ UCr, D) Relación USerpinA3/ UCr. Circulo blanco WT Sh, Circulo negro WT IRB, Cuadrado blanco HT Sh, Cuadrado negro HT IRB, Triángulo blanco KO Sh, Triángulo negro KO IRB. n=5-10 por grupo. * p<0.05 vs. respectivo grupo marcado.*

Se evaluaron los biomarcadores urinarios de lesión renal, KIM1, HSP72 y SerpinaA3K, los dos últimos previamente descritos por nuestro grupo (10-11). Estos biomarcadores se incrementaron significativamente en los grupos WT+IRB y HT + IRB (Figura 2B-2D), sin embargo, a pesar de que los grupos KO+IR exhibieron disfunción renal, no hubo elevación significativa en estos biomarcadores de lesión

renal. Todos estos resultados juntos muestran que la deficiencia de Sirt7 se asoció con una menor inflamación renal y menor lesión tubular.

La ausencia de Sir7 no se asoció con cambio en la expresión de Sirt1 y Sirt3

Evaluamos los niveles de RNAm y de proteína para Sirt7 en los animales para corroborar la deficiencia de esta proteína. Encontramos como era esperado, la desaparición total del RNAm y proteína de Sirt7 en los animales KO. En el caso de los animales WT, encontramos que la isquemia renal tendió a aumentar Sir7, sin embargo, la diferencia no fue estadísticamente significativa. (Figuras 3A-B). Para estudiar si Sirt1 y Sirt3 tenían una respuesta frente a la deficiencia de Sirt7, evaluamos los niveles de RNAm y de proteína. Encontramos una disminución significativa en los niveles de RNAm de Sirt1 (Figura 3C), sin embargo, no encontramos cambios a nivel de proteína (Figura 3D). Para el caso de Sirt3, no encontramos diferencias en los grupos estudiados (Figuras 3E-F).

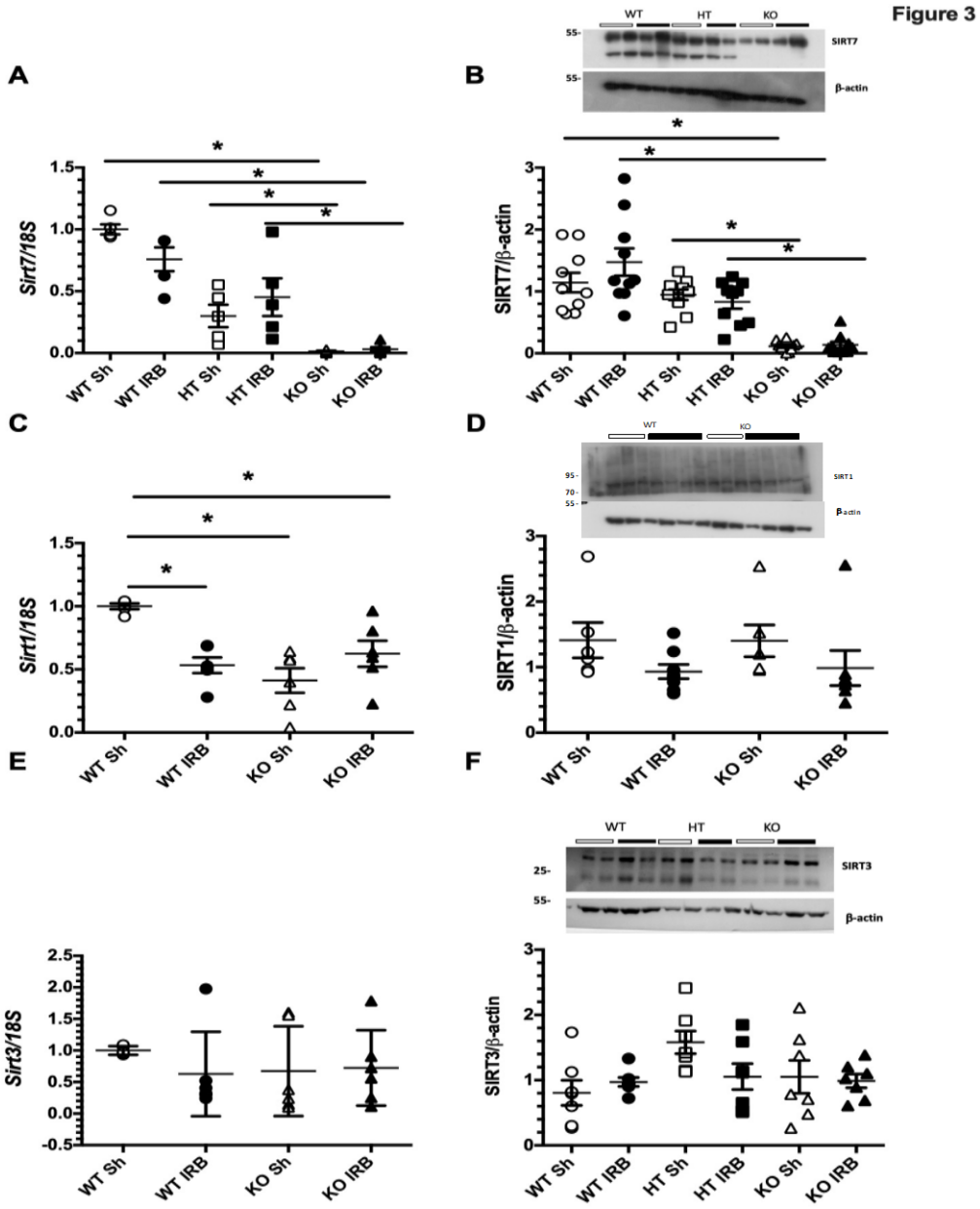

*Figura 3. Niveles de Sirt7, Sirt1 y Sirt3. A)Niveles de RNAm de Sirt7, B) Niveles de proteína de Sirt7 C) Niveles de RNAm de Sirt1, D) Niveles de proteína de Sirt1, E) Niveles de RNAm de Sirt3 D) Niveles de proteína de SirT3. Circulo blanco WT Sh, Circulo negro WT IRB, Cuadrado blanco HT Sh, Cuadrado negro HT IRB, Triángulo blanco KO Sh, Triángulo negro KO IRB. n=5-10 por grupo. * p<0.05 vs. respectivo grupo marcado*

Evaluación de vías antioxidantes y de respuesta a hipoxia.

Observamos que en los animales WT y HT después de un episodio de LRA, hubo un aumento significativo de peróxidos urinarios, que es un marcador de estrés oxidante (Figura 4A). Estos hallazgos correlacionaron con la disminución en los niveles de RNAm de catalasa y esto se previno de manera significativa en los animales KO+IRB en comparación con el grupo WT+IRB (Figura 4B). Aunado a este resultado, encontramos un aumento significativo del factor antioxidante Nfe2l2, que codifica para el factor Nrf2, en el grupo KO+IRB(Figura 4C). En Sod2 no encontramos diferencias significativas (Figura 4D).

Al evaluar los niveles de RNAm de HIF-1α datos no mostrados) no encontramos cambios, sin embargo, existe evidencia que sugiere que SIRT7 puede degradar a HIF-1α al interactuar con la proteína (78), por ello sería interesante evaluar los niveles de la proteína de HIF-1α.

Figura 4

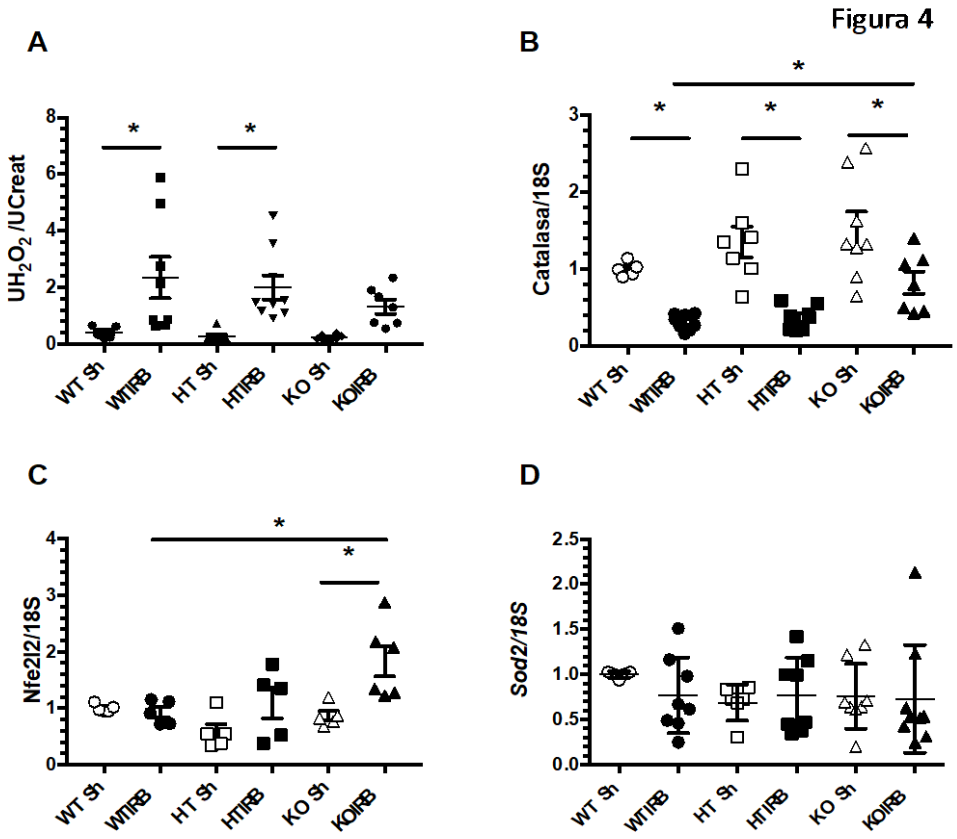

*Figura 4. Estrés oxidante y enzimas antioxidantes. A)Peróxidos de Hidrogeno urinarios, B) Niveles de RNAm de Catalasa. C) Niveles de RNAm Nfe2l2, D) Niveles de RNAm de Sod2. Circulo blanco WT Sh, Circulo negro WT IRB, Cuadrado blanco HT Sh, Cuadrado negro HT IRB, Triángulo blanco KO Sh, Triángulo negro KO IRB. n=5-10 por grupo. * p<0.05 vs. respectivo grupo marcado*

La deficiencia de Sirt7 promovió la inhibición de vías pro-inflamatorias y activó a TGFβ.

Se realizó la evaluación de los niveles de RNAm de Il6, Tnfa, Mcp-1, Tgfb y Il10. Observamos que en los grupos WT+IRB y HT+IRB los niveles de RNAm de Il6, Tnfa Mcp1y Il10 fueron significativamente mayores que su grupo control (Figura 5A-

C, E). De manera interesante, los animales KO se protegieron de la elevación de los niveles de RNAm de las moléculas proinflamatorias, y por el contrario presentaron una elevación significativa en los niveles de RNAm del gen Tgfb, lo que no se observó en los animales WT o HT (Figura 5D). Para el caso de Il10, no se encontró elevada en los ratones KO+IR, en contraste con los animales WT+IR y HT+IR. Este dato resulto interesante, ya que típicamente se considera a IL-10 como una citocina anti-inflamatoria, sin embargo, la evidencia acumulada demuestra que la expresión anormal de IL-10, ya sea transitoria o prolongada, así como las interacciones con otros factores de crecimiento como respuesta a diversos estímulos, está relacionada con la aparición y progresión de una variedad de trastornos renales. Además, el aumento de las concentraciones de IL-10 en suero predice la albuminuria y se correlaciona con la gravedad de la nefropatía diabética (103).

Figura 5

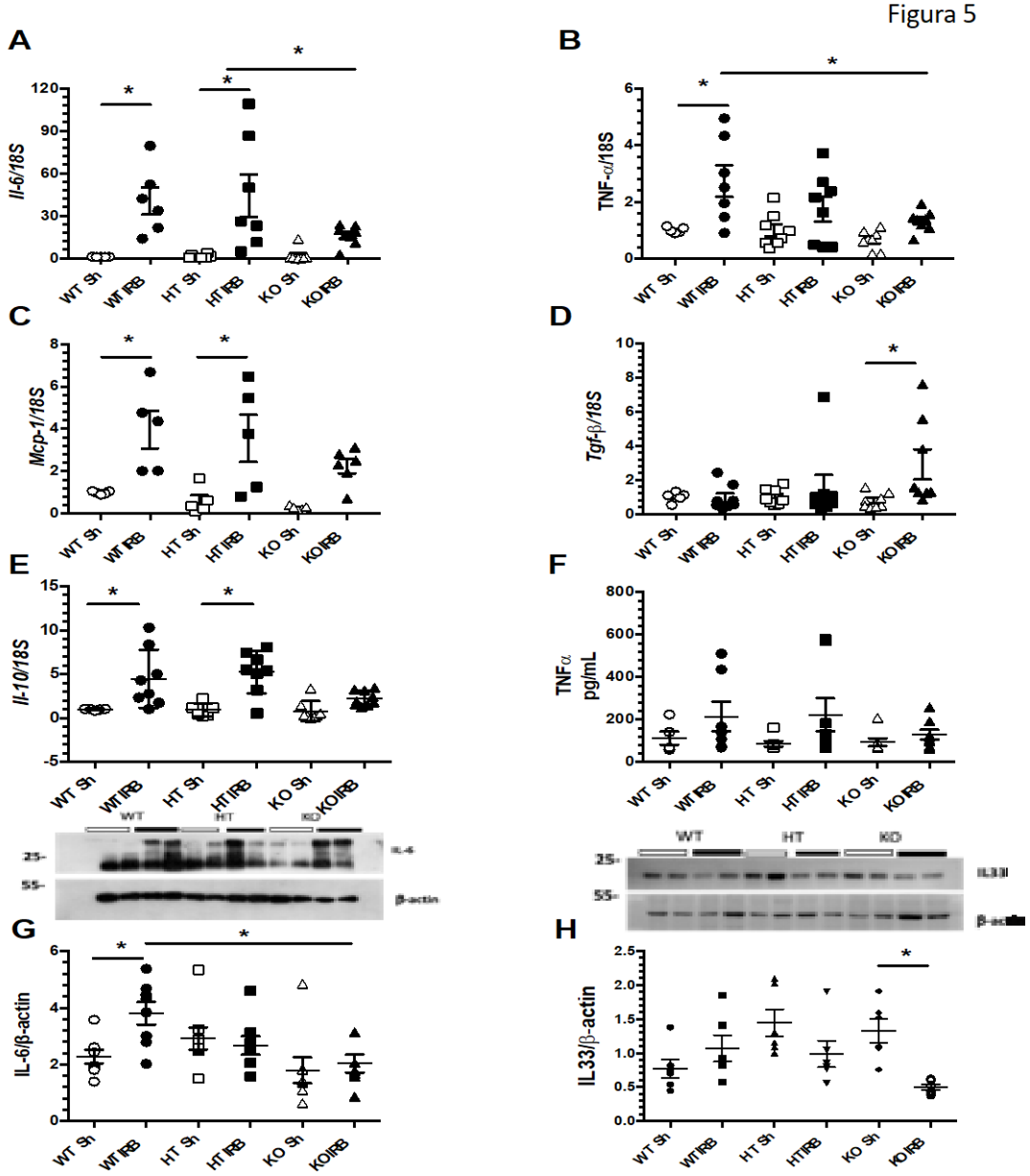

*Figura 5. Niveles de citocinas inflamatorias. A)Niveles de RNAm de Il6, B) Niveles de RNAm de Tnfa. C) Niveles de RNAm de Mcp1, D) Niveles de RNAm de Tgfb, E) Niveles de RNAm de Il10 D) Niveles de proteína de Tnfα por ELISA, E) Niveles de proteína de IL-6 F) Niveles de proteína de IL33. Circulo blanco WT Sh, Circulo negro WT IRB, Cuadrado blanco HT Sh, Cuadrado negro HT IRB, Triángulo blanco KO Sh, Triángulo negro KO IRB. n=5-10 por grupo. * p<0.05 vs. respectivo grupo marcado*

Mediante Western Blot evaluamos los niveles de IL-6 en tejido. En concordancia con los hallazgos encontrados con los niveles de RNAm, los niveles de proteína se elevaron en los animales WT con respecto a su grupo control, mientras que esta elevación se previno parcialmente en los animales KO (Figura 5G). En el caso de

IL-33 una citocina que funciona como alarmina durante la respuesta inflamatoria, se encontró significativamente menor en los animales KO (Figura 5H).

Además, evaluamos los niveles plasmáticos de TNF-α en donde vimos una tendencia a elevarse en los animales WT y HT con IRB, comparados con sus grupos control, mientras que en los animales KO los niveles plasmáticos de TNF-α se mantuvieron similares a su grupo control (Figura 5B).

Sir7 en la infiltración de células inflamatorias después de la IRB

Para hacer la evaluación del infiltrado de células inflamatorias, realizamos un análisis de citometría de flujo. En la Figura 6A se muestra la metodología empleada para hacer la elección de cada tipo celular usando a CD45 como marcador de células hematopoyéticas. Para el análisis de macrófagos se utilizó el marcador CD11b y para las subpoblaciones M1 y M2 se uso la expresión de F4/80 (M1 lowF4/80 y M2 high F4/80, respectivamente) (Figura 6B). En el caso de las células T se uso la subunidad b del receptor de células T (TCRb), así como, CD4 y CD8 para los subtipos de células T (Figura 5C).

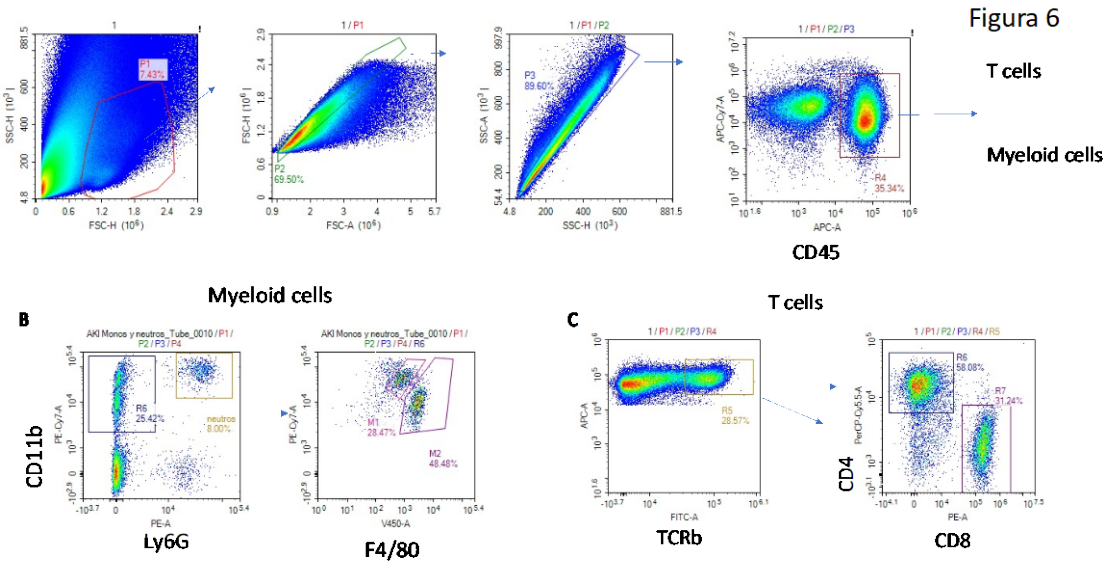

Figura 6. Gating para evaluación en citometría de flujo. Células hematopoyéticas (CD45). Células mieloides (CD11b+/Ly6G-). Macrófagos M1(F4/80low) y M2 (F4/80high). Células T (TCRb+), linfocitos CD4+ y linfocitos CD8+.

Encontramos, de acuerdo con los hallazgos en los niveles de citocinas inflamatorias, un aumento en la infiltración de leucocitos posterior a la IRB en el grupo WT, mientras que, esta infiltración fue mucho menor en los animales KO+ IRB p=0.588 (Figura 7A). Al evaluar las subpoblaciones M1 y M2 de macrófagos, encontramos una tendencia a mayor infiltración de M1 en los animales WT+IRB, que fue ligeramente menor en los animales KO+IRB, pero sin diferencias significativas (Figure 7B). De manera interesante, observamos un aumento significativo en la infiltración de M2 en los animales WT después de la LRA, que no fue observada en los animales KO (Figure 7C). En la infiltración de células T totales vimos un aumento significativo en el grupo WT+IRB y este cambio no se encontró en el grupo KO+IRB (Figura 7D). No encontramos diferencias en las subpoblaciones de células T, CD4 y CD8 (Figura 7E-F).

Figura 7

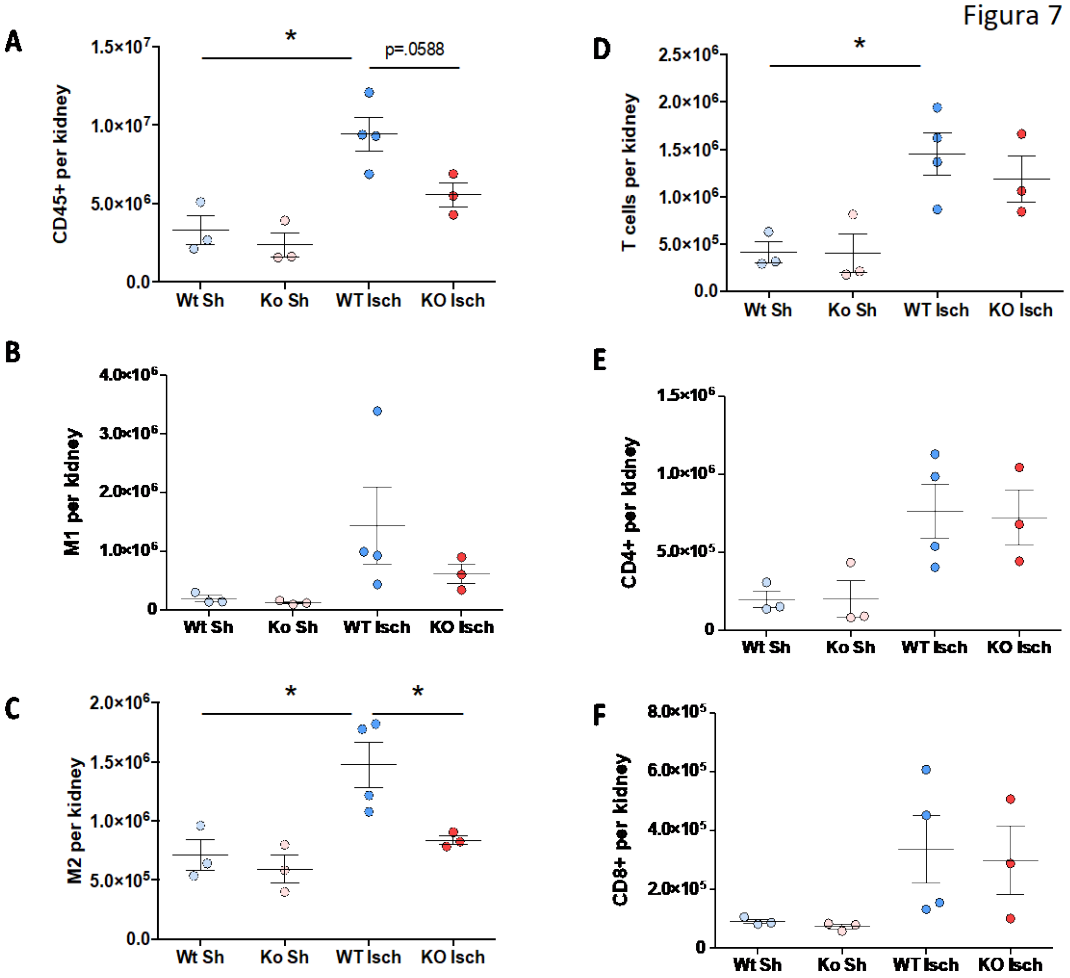

*Figura 7. Infiltración de células T y macrófagos. A)Células hematopoyéticas (CD45+) por riñón, B) Macrófagos M1 por riñón. C) Macrófagos M2 por riñón, D) Células T (TCRb+) por riñón, E) Células CD4+ por riñón D) Células CD8+ por riñón. Circulo azul claro WT Sh, Circulo rosa WT IRB, , Circulo azul oscuro KO Sh, Circulo rojo KO IRB. n=5-10 por grupo. * p<0.05 vs. respectivo grupo marcado.*

DISCUSIÓN

Encontramos que la deficiencia de SIRT7 atenuó el daño por isquemia/reperfusión renal, lo cual fue evidenciado por la menor excreción de proteínas y de biomarcadores urinarios de daño renal Hsp72, KIM-1 y serpinaA3 (56, 61, 81). Al mismo tiempo, se registró un menor aumento del peso renal. Lo anterior sugiere fuertemente que la deficiencia de Sirt7 se asocia con menor inflamación. Acorde con estos resultados, Miyasato, Y *et. al.* en 2018, encontraron que la deficiencia de Sirt7 en un modelo de daño renal inducido por cisplatino, previno el aumento de NGAL(80). No obstante que encontramos menor daño tubular, la deficiencia de Sirt7 no previno la disfunción renal (TFG) inducida por la isquemia/reperfusión. Estos resultados sugieren que la Sirt7 no reguló a los factores vasoconstrictores que se inducen tras un episodio de LRA.

Los datos de protección de daño tubular se asociaron con una menor inflamación renal, ya que los animales KO no tuvieron aumento del peso renal en comparación con los WT+IRB. Además, encontramos que los animales KO presentaron menor elevación de moléculas pro-inflamatorias como IL6, TNFα y MCP-1. Estudios recientes, llevados a cabo con endotelio pulmonar, han demostrado que la deficiencia de Sirt7 protege frente a procesos inflamatorios mediados por lipopolisacaridos (LPS). Más aún, esta protección se asoció con el aumento en la expresión TGF$-\beta$ 1 y sus genes blancos, permitiendo la transición endotelio-mesénquima y promoviendo la reparación (85). En el caso de los modelos de isquemia-reperfusión renal se ha estudiado, que la activación de TGF$-\beta$1 se produce como consecuencia directa de la hipoxia, la señalización de la angiotensina II y la pérdida de la integridad de la matriz extracelular (MEC). Por lo tanto, se

considera que TGF−β1 regula al alza la síntesis de componentes de la matriz extracelular como la fibronectina y el colágeno IV, proporcionando una base para la restauración del epitelial en el túbulo en regeneración. TGF−β1 también regula la proliferación y diferenciación de células tubulares epiteliales. Esta respuesta se apaga rápidamente en respuesta a la recuperación del riñón (86). En este estudio encontramos que la deficiencia de la Sirt7 promovió el aumento de TGF−β 1 como posible molécula antiinflamatoria. Además, se ha encontrado que la Sirt7 pudiera ser un modulador de la translocación al núcleo de NFkB y posterior activación por fosforilación (86), sin embargo, no queda claro en qué contexto patológico ocurre esto. Sobuz, S. et al. demostraron recientemente que la Sirt7 interactúa con una pequeña GTPasa, antígeno nuclear relacionado con Ras (Ran), promoviendo su desacetilación en K37 y con lo cual, la exportación nuclear de NFkB se inhibió en células deficientes en Sirt7 que expresaban K37R-Ran (mutante que imita la desacetilación). Estos datos sugieren que Sirt7 es una lisina desacetilasa que se dirige al residuo K37 de Ran al modular la exportación nuclear de p65(86). Por otro lado, este mecanismo puede estar relacionado con la acetilación de la subunidad RelA en la Lys310, que promueve la activación de NFkB y la posterior respuesta pro-apoptótica dependiente de NFkB (89). Aunque este mecanismo solo se ha visto como una marca reconocida por Sirt1 y Sirt2 (90), hay evidencia que sugiere que pueden existir mecanismos en paralelo que pueden modular la activación de NFkB mediado por Sirt7.

La protección en la elevación de citocinas pro-inflamatorias en los animales KO+IRB se asoció con una menor infiltración de células CD45, en particular de los macrófagos M1 y M2. Aunado a esto, este grupo presentó menor estrés oxidante y una menor reducción de la enzima antioxidante catalasa. Además, los animales

deficientes de Sirt7 presentaron una elevación significativa en los niveles de RNAm de Nfe2l2. Este factor regula la respuesta antioxidante y estudios previos han demostrado que la inducción farmacológica de Nrf2 puede promover protección renal en modelos de IR (91, 92). Sin embargo, existen pocos reportes que asocien de manera directa a Sirt7 como regulador directo de Nrf2, una de las posibles explicaciones podría ser la relación que existe entre la Sirt7 con la respuesta a estrés inducida por hipoxia, ya que, se ha demostrado que la Sirt7 puede interactuar con la proteína HIF-1α y HIF-2α y enviar ambas proteínas a degradación (79). Por lo que, sería interesante analizar los niveles de HIF-1α y HIF-2α, ya que estas proteínas a su vez son reguladas por factores antioxidantes como Nrf2 al unirse a los elementos de respuesta en dichos genes (93).

Debido a que NFκB está involucrado con enfermedades inflamatorias y metabólicas, existe un interés considerable en si la inhibición de Sirt7 podría ser útil para tratar estas enfermedades, así como el cáncer. Sin embargo, se requieren más estudios para lograr entender el papel en la regulación de esta sirtuina, ya que, la deficiencia de Sirt7 también se ha relacionado con la generación de fibrosis en el corazón de animales envejecidos, lo que se acompañó de inflamación y apoptosis de los cardiomiocitos al inducir la producción TGF−β 1(82-83). Por ello, es importante entender el papel de esta proteína en diversos tejidos y en edades diferentes que pudieran arrojar resultados mas sólidos y menos contradictorios.

Finalmente, uno de los posibles mecanismos de renoprotección en los ratones deficientes de Sirt7 era que se diera una sobreexpresión compensatoria de otras sirtuinas como, Sirt1 y Sirt3, previamente descritas como reguladores del proceso inflamatorio frente a episodios de LRA (74, 76). De manera interesante no

encontramos diferencias en los niveles de estas dos sirtuinas, lo que sugiere que el efecto es mediado por la deficiencia de Sirt7 y las vías que regula .

En conclusión, este estudio nos permitió analizar el papel de SIRT7 en la LRA, en donde encontramos que la deficiencia de Sirt7 previno el daño tubular, la inflamación y el estrés oxidante posterior a la IRB. En este punto no podemos descartar su participación en la viabilidad celular, proceso que podría modularse al regular otras vías como p53 y AKT, que deben ser analizadas. Por otro lado, queda pendiente evaluar su posible participación en la transición a ERC, así como la respuesta en animales envejecidos frente al episodio de LRA.

8. CONCLUSIÓN

En conjunto estos resultados permitieron conocer los puntos temporales de las alteraciones renales y posibles blancos terapéuticos para el tratamiento del daño renal. Estos datos se pueden trasladar a la práctica clínica, en pacientes que puedan desarrollar ERC por episodios de LRA o por obesidad, permitiendo prevenir o disminuir la progresión a ERC. Además, permitió el descubrimiento de la serpinA3K como biomarcador temprano, no solo del desarrollo de ERC, sino también para la detección de LRA y sus diferentes niveles de gravedad, que actualmente están en vías de validación en pacientes.

Por otro lado encontramos, que las modificaciones epigenéticas como la metilación del promotor de Vegfa y la inhibición de la Sirtuna7, pueden ser posibles blancos terapéuticos que deben ser evaluados para la prevención del desarrollo de ERC.

En conjunto, todos estos datos contribuyen de manera importante al conocimiento de la fisiopatología renal, abren vías de estudio y posibilidades de diagnóstico oportuno.

9. PERSPECTIVAS

1. Analizar el papel de Hif1a y Vegfa como posibles blancos terapéuticos en la transición de LRA a ERC.
2. Evaluar mecanismos de desmetilación activa en la transición a ERC.
3. Usando a los ratones transgénicos deficientes de serpinaA3K, analizar su función en la fisiopatología renal.
4. Analizar a la serpinA3K como biomarcador en la respuesta al tratamiento de los pacientes con NL, así como en los pacientes con nefropatía diabética.
5. En los ratones transgénicos deficientes de Sirt7, evaluar los niveles de la proteína HIF-1a y Vegfa como gen blanco y evaluar si la respuesta a la LRA es diferente en animales viejos respecto a los jóvenes, así como su participación en la transición a ERC.
6. Por otro lado, se sabe que existen diferencias importantes en la respuesta al daño renal dependientes del sexo de los animales, por ello seria interesante analizar el efecto de la deficiencia de sirt7 en hembras.

10. REFERENCIAS

1. Boron Walter F. (2015). *Medical Physiology*, 2nd Ed. Edinburgh, Scotland, Elservier Saunders,
2. Hall JE, Guyton AC. (2011). Tratado de Fisiología Médica, 12va Ed. Edinburgh, Scotland, Elservier Saunders.
3. Colín, R. D., & Saavedra, J. L. M. (2005). *Fisiología Medica: Rene Drucker Colín*. El manual moderno.
4. Zuk, A., & Bonventre, J. V. (2016). Acute Kidney Injury. *Annual review of medicine*, *67*, 293–307.
5. Bonventre, J. V, & Yang, L. (2011). Cellular pathophysiology of ischemic acute kidney injury. The Journal of Clinical Investigation, 121(11), 4210–21.
6. Susantitaphong, P., Cruz, D. N., Cerda, J., Abulfaraj, M., Alqahtani, F., Koulouridis, I., Jaber, B. L., & Acute Kidney Injury Advisory Group of the American Society of Nephrology (2013). World incidence of AKI: a meta-analysis. Clinical journal of the American Society of Nephrology : CJASN, 8(9), 1482–1493.
7. Kelly K. J. (2006). Acute renal failure: much more than a kidney disease. *Seminars in nephrology*, *26*(2), 105–113.
8. Makris, K., & Spanou, L. (2016). Acute Kidney Injury: Definition, Pathophysiology and Clinical Phenotypes. *The Clinical biochemist. Reviews*, *37*(2), 85–98.
9. Lameire, N., Levin, A., Kellum, J. A., Cheung, M., Jadoul, M., Winkelmayer, W. C., & Stevens, P. E. (2021). Harmonizing Acute and Chronic Kidney

Disease Definition and Classification : report of a Kidney Disease : Improving Global Outcomes (KDIGO) Consensus Conference, (July), 1–29.

10. Gonsalez, S. R., Cortês, A. L., Silva, R., Lowe, J., Prieto, M. C., & Silva Lara, L. D. (2019). Acute kidney injury overview: From basic findings to new prevention and therapy strategies. *Pharmacology & therapeutics*, *200*, 1–12.
11. Wasung, M. E., Chawla, L. S., & Madero, M. (2015). Biomarkers of renal function , which and when ? *Clinica Chimica Acta*, *438*(1), 350–357.
12. Bonventre J. V. (2003). Dedifferentiation and proliferation of surviving epithelial cells in acute renal failure. *Journal of the American Society of Nephrology : JASN*, *14 Suppl 1*, S55–S61.
13. Lech, M., Gröbmayr, R., Ryu, M., Lorenz, G., Hartter, I., Mulay, S. R., Susanti, H. E., Kobayashi, K. S., Flavell, R. A., & Anders, H. J. (2014). Macrophage phenotype controls long-term AKI outcomes--kidney regeneration versus atrophy. *Journal of the American Society of Nephrology : JASN*, *25*(2), 292–304).
14. Lee, S., Huen, S., Nishio, H., Nishio, S., Lee, H. K., Choi, B. S., Ruhrberg, C., & Cantley, L. G. (2011). Distinct macrophage phenotypes contribute to kidney injury and repair. *Journal of the American Society of Nephrology : JASN*, *22*(2), 317–326.
15. Zhang, M. Z., Yao, B., Yang, S., Jiang, L., Wang, S., Fan, X., Yin, H., Wong, K., Miyazawa, T., Chen, J., Chang, I., Singh, A., & Harris, R. C. (2012). CSF-1 signaling mediates recovery from acute kidney injury. *The Journal of clinical investigation*, *122*(12), 4519–4532.

16. Chawla, L. S., Amdur, R. L., Amodeo, S., Kimmel, P. L., & Palant, C. E. (2011). The severity of acute kidney injury predicts progression to chronic kidney disease. *Kidney international*, *79*(12), 1361–1369.
17. Ferenbach, D. A., & Bonventre, J. V. (2015). Mechanisms of maladaptive repair after AKI leading to accelerated kidney ageing and CKD. Nature Reviews. Nephrology, 11(5), 264–276.
18. Rodríguez-Romo, R., Benítez, K., Barrera-Chimal, J., Pérez-Villalva, R., Gómez, A., Aguilar-León, D., Rangel-Santiago, J. F., Huerta, S., Gamba, G., Uribe, N., & Bobadilla, N. A. (2016). AT1 receptor antagonism before ischemia prevents the transition of acute kidney injury to chronic kidney disease. *Kidney international*, *89*(2), 363–373.
19. Kramann, R., Wongboonsin, J., Chang-Panesso, M., Machado, F. G., & Humphreys, B. D. (2017). Gli1^{+} Pericyte Loss Induces Capillary Rarefaction and Proximal Tubular Injury. *Journal of the American Society of Nephrology : JASN*, *28*(3), 776–784.
20. Yang, L., Besschetnova, T. Y., Brooks, C. R., Shah, J. V., & Bonventre, J. V. (2010). Epithelial cell cycle arrest in G2/M mediates kidney fibrosis after injury. *Nature medicine*, *16*(5), 535–143.
21. Lima-Posada, I., Portas-Cortés, C., Pérez-Villalva, R., Fontana, F., Rodríguez-Romo, R., Prieto, R., Sánchez-Navarro, A., Rodríguez-González, G. L., Gamba, G., Zambrano, E., & Bobadilla, N. A. (2017). Gender Differences in the Acute Kidney Injury to Chronic Kidney Disease Transition. *Scientific reports*, *7*(1), 12270.
22. Humphreys, B. D., Lin, S. L., Kobayashi, A., Hudson, T. E., Nowlin, B. T., Bonventre, J. V., Valerius, M. T., McMahon, A. P., & Duffield, J. S. (2010).

Fate tracing reveals the pericyte and not epithelial origin of myofibroblasts in kidney fibrosis. *The American journal of pathology*, *176*(1), 85–97.

23. Kirita, Y., Wu, H., Uchimura, K., Wilson, P. C., & Humphreys, B. D. (2020). Cell profiling of mouse acute kidney injury reveals conserved cellular responses to injury. *Proceedings of the National Academy of Sciences of the United States of America*, *117*(27), 15874–15883.
24. Iwano, M., Plieth, D., Danoff, T. M., Xue, C., Okada, H., & Neilson, E. G. (2002). Evidence that fibroblasts derive from epithelium during tissue fibrosis. *The Journal of clinical investigation*, *110*(3), 341–350.
25. Moll, S., Ebeling, M., Weibel, F., Farina, A., Araujo Del Rosario, A., Hoflack, J. C., Pomposiello, S., & Prunotto, M. (2013). Epithelial cells as active player in fibrosis: findings from an in vitro model. *PloS one*, *8*(2), e56575.
26. Barrera-Chimal, J., Pérez-Villalva, R., Rodríguez-Romo, R., Reyna, J., Uribe, N., Gamba, G., & Bobadilla, N. A. (2013). Spironolactone prevents chronic kidney disease caused by ischemic acute kidney injury. *Kidney international*, *83*(1), 93–103.
27. Hörbelt, M., Lee, S. Y., Mang, H. E., Knipe, N. L., Sado, Y., Kribben, A., & Sutton, T. A. (2007). Acute and chronic microvascular alterations in a mouse model of ischemic acute kidney injury. *American journal of physiology. Renal physiology*, *293*(3), F688–F695.
28. Basile, D. P., Donohoe, D., Roethe, K., & Osborn, J. L. (2001). Renal ischemic injury results in permanent damage to peritubular capillaries and influences long-term function. *American journal of physiology. Renal physiology*, *281*(5), F887–F899.

29. Basile, D. P., Donohoe, D. L., Roethe, K., & Mattson, D. L. (2003). Chronic renal hypoxia after acute ischemic injury: effects of L-arginine on hypoxia and secondary damage. *American journal of physiology. Renal physiology*, *284*(2), F338–F348.

30. Kramann, R., Tanaka, M., & Humphreys, B. D. (2014). Fluorescence microangiography for quantitative assessment of peritubular capillary changes after AKI in mice. *Journal of the American Society of Nephrology : JASN*, *25*(9), 1924–1931.

31. Li, L., Kang, H., Zhang, Q., D'Agati, V. D., Al-Awqati, Q., & Lin, F. (2019). FoxO3 activation in hypoxic tubules prevents chronic kidney disease. *The Journal of clinical investigation*, *129*(6), 2374–2389.

32. Shu, S., Zhu, J., Liu, Z., Tang, C., Cai, J., & Dong, Z. (2018). Endoplasmic reticulum stress is activated in post-ischemic kidneys to promote chronic kidney disease. *EBioMedicine*, *37*, 269–280.

33. Chawla, L. S., Eggers, P. W., Star, R. A., & Kimmel, P. L. (2014). Acute kidney injury and chronic kidney disease as interconnected syndromes. *The New England journal of medicine*, *371*(1), 58–66.

34. Conger, J. D., Robinette, J. B., & Hammond, W. S. (1991). Differences in vascular reactivity in models of ischemic acute renal failure. *Kidney international*, *39*(6), 1087–1097.

35. Sesso, R. (1996) Late diagnosis of chronic renal failure and mortality on maintenance dialysis. Nephrology Dialysis Transplantation, 11(12), 2417-2420.

36. Neyra, J. A., & Chawla, L. S. (2021). Acute Kidney Disease to Chronic Kidney Disease. *Critical Care Clinics*, *37*(2), 453–474.

37. Isakova, T., Nickolas, T. L., Denburg, M., Yarlagadda, S., Weiner, D. E., Gutiérrez, O. M., Bansal, V., Rosas, S. E., Nigwekar, S., Yee, J., & Kramer, H. (2017). KDOQI US Commentary on the 2017 KDIGO Clinical Practice Guideline Update for the Diagnosis, Evaluation, Prevention, and Treatment of Chronic Kidney Disease-Mineral and Bone Disorder (CKD-MBD). *American journal of kidney diseases : the official journal of the National Kidney Foundation*, *70*(6), 737–751.

38. Grgic, I., Campanholle, G., Bijol, V., Wang, C., Sabbisetti, V. S., Ichimura, T., Humphreys, B. D., & Bonventre, J. V. (2012). Targeted proximal tubule injury triggers interstitial fibrosis and glomerulosclerosis. *Kidney international*, *82*(2), 172–183.

39. Basu, R. K., Hubchak, S., Hayashida, T., Runyan, C. E., Schumacker, P. T., & Schnaper, H. W. (2011). Interdependence of HIF-1α and TGF-β/Smad3 signaling in normoxic and hypoxic renal epithelial cell collagen expression. *American journal of physiology. Renal physiology*, *300*(4), F898–F905.

40. Bechtel, W., McGoohan, S., Zeisberg, E. M., Müller, G. A., Kalbacher, H., Salant, D. J., Müller, C. A., Kalluri, R., & Zeisberg, M. (2010). Methylation determines fibroblast activation and fibrogenesis in the kidney. *Nature medicine*, *16*(5), 544–550.

41. Xiao, L., Zhou, D., Tan, R. J., Fu, H., Zhou, L., Hou, F. F., & Liu, Y. (2016). Sustained Activation of Wnt/β-Catenin Signaling Drives AKI to CKD

Progression. *Journal of the American Society of Nephrology : JASN*, *27*(6), 1727–1740.

42. Zhou, D., Tan, R. J., & Liu, Y. (2016). Sonic hedgehog signaling in kidney fibrosis: a master communicator. *Science China. Life sciences*, *59*(9), 920–929.
43. Boutet, A., De Frutos, C. A., Maxwell, P. H., Mayol, M. J., Romero, J., & Nieto, M. A. (2006). Snail activation disrupts tissue homeostasis and induces fibrosis in the adult kidney. *The EMBO journal*, *25*(23), 5603–5613.
44. Tan, R. Z., Zhong, X., Li, J. C., Zhang, Y. W., Yan, Y., Liao, Y., Wen, D., Diao, H., Wang, L., & Shen, H. C. (2019). An optimized 5/6 nephrectomy mouse model based on unilateral kidney ligation and its application in renal fibrosis research. *Renal failure*, *41*(1), 555–566.
45. Becker, G. J., & Hewitson, T. D. (2013). Animal models of chronic kidney disease: useful but not perfect. *Nephrology, dialysis, transplantation : official publication of the European Dialysis and Transplant Association - European Renal Association*, *28*(10), 2432–2438.
46. Engin, A. (2017). Obesity and Lipotoxicity. Advances in Experimental Medicine and Biology (Vol. 960).
47. Wang, Y. C., McPherson, K., Marsh, T., Gortmaker, S. L., & Brown, M. (2011). Health and economic burden of the projected obesity trends in the USA and the UK. The Lancet, 378(9793), 815–825.
48. Garofalo, C., Borrelli, S., Minutolo, R., Chiodini, P., De Nicola, L., & Conte, G. (2017). A systematic review and meta-analysis suggests obesity predicts onset of chronic kidney disease in the general population. Kidney International, 91(5), 1224–1235.

49. ENSANUT. (2016). Informe final de resultados medio camino. Encuesta Nacional de Salud y Nutrición Medio Camino 2016, 2016, 47–50.
50. Dias, R. S. C., Calado, I. L., De Alencar, J. D., Hortegal, E. V., Santos, E. J. F., De Araújo Brito, D. J., Filho, N. S. (2018). Abdominal obesity and reduction of glomerular filtration. Revista Da Associacao Medica Brasileira, 64(4), 346–353.
51. Lakkis, J. I., & Weir, M. R. (2018). Obesity and Kidney Disease. Progress in Cardiovascular Diseases, 61(2), 157–167.
52. Brison, D. W. (2017). Definition, diagnosis, and classification of Diabetes and its complications. WHO. Ameliorating Mental Disability: Questioning Retardation.
53. Rhee, C. M., Ahmadi, S. F., & Kalantar-Zadeh, K. (2016). The dual roles of obesity in chronic kidney disease: A review of the current literature. Current Opinion in Nephrology and Hypertension, 25(3), 208–216.
54. Muskiet, M. H., Smits, M. M., Morsink, L. M., & Diamant, M. (2014). The gut-renal axis: do incretin-based agents confer renoprotection in diabetes?. *Nature reviews. Nephrology*, *10*(2), 88–103.
55. Soni, S. S., Cruz, D., Bobek, I., Chionh, C. Y., Nalesso, F., Lentini, P., de Cal, M., Corradi, V., Virzi, G., & Ronco, C. (2010). NGAL: a biomarker of acute kidney injury and other systemic conditions. *International urology and nephrology*, *42*(1), 141–150.
56. Vaidya, V. S., Ramirez, V., Ichimura, T., Bobadilla, N. A., & Bonventre, J. V. (2006). Urinary kidney injury molecule-1: a sensitive quantitative biomarker

for early detection of kidney tubular injury. *American journal of physiology. Renal physiology*, *290*(2), F517–F529.

57. Liangos, O., Perianayagam, M. C., Vaidya, V. S., Han, W. K., Wald, R., Tighiouart, H., MacKinnon, R. W., Li, L., Balakrishnan, V. S., Pereira, B. J., Bonventre, J. V., & Jaber, B. L. (2007). Urinary N-acetyl-beta-(D)-glucosaminidase activity and kidney injury molecule-1 level are associated with adverse outcomes in acute renal failure. *Journal of the American Society of Nephrology : JASN*, *18*(3), 904–912.
58. Parikh, C. R., Abraham, E., Ancukiewicz, M., & Edelstein, C. L. (2005). Urine IL-18 is an early diagnostic marker for acute kidney injury and predicts mortality in the intensive care unit. *Journal of the American Society of Nephrology : JASN*, *16*(10), 3046–3052.
59. Portilla, D., Dent, C., Sugaya, T., Nagothu, K. K., Kundi, I., Moore, P., Noiri, E., & Devarajan, P. (2008). Liver fatty acid-binding protein as a biomarker of acute kidney injury after cardiac surgery. *Kidney international*, *73*(4), 465–472.
60. Kashani, K., Al-Khafaji, A., Ardiles, T., Artigas, A., Bagshaw, S. M., Bell, M., Bihorac, A., Birkhahn, R., Cely, C. M., Chawla, L. S., Davison, D. L., Feldkamp, T., Forni, L. G., Gong, M. N., Gunnerson, K. J., Haase, M., Hackett, J., Honore, P. M., Hoste, E. A., Joannes-Boyau, O., … Kellum, J. A. (2013). Discovery and validation of cell cycle arrest biomarkers in human acute kidney injury. *Critical care (London, England)*, *17*(1), R25.
61. Barrera-Chimal, J., Pérez-Villalva, R., Cortés-González, C., Ojeda-Cervantes, M., Gamba, G., Morales-Buenrostro, L. E., & Bobadilla, N. A.

(2011). Hsp72 is an early and sensitive biomarker to detect acute kidney injury. *EMBO molecular medicine*, *3*(1), 5–20.

62. Morales-Buenrostro, L. E., Salas-Nolasco, O. I., Barrera-Chimal, J., Casas-Aparicio, G., Irizar-Santana, S., Pérez-Villalva, R., & Bobadilla, N. A. (2014). Hsp72 is a novel biomarker to predict acute kidney injury in critically ill patients. *PloS one*, *9*(10), e109407.
63. Devarajan, P. (2010). The Use of Targeted Biomarkers for Chronic Kidney Disease. *Advances in Chronic Kidney Disease*, *17*(6), 469–479.
64. Wong, M. G., & Pollock, C. A. (2014). Biomarkers in kidney fibrosis: are they useful? *Kidney International Supplements*, *4*(1), 79–83.
65. Lee, S. B., Kanasaki, K., & Kalluri, R. (2009). Circulating TGF-beta1 as a reliable biomarker for chronic kidney disease progression in the African-American population. *Kidney international*, *76*(1), 10–12.
66. Tang, C., & Dong, Z. (2015). Epigenetic regulation in acute kidney injury: new light in a dark area. Kidney International, 88(4), 665–668.
67. Rodríguez-Romo, R., Berman, N., Gómez, A., & Bobadilla, N. A. (2015). Epigenetic regulation in the acute kidney injury to chronic kidney disease transition. *Nephrology (Carlton, Vic.)*, *20*(10), 736–743.
68. Huang, N., Tan, L., Xue, Z., Cang, J., & Wang, H. (2012). Reduction of DNA hydroxymethylation in the mouse kidney insulted by ischemia reperfusion. *Biochemical and biophysical research communications*, *422*(4), 697–702.
69. Pang, M., Kothapally, J., Mao, H., Tolbert, E., Ponnusamy, M., Chin, Y. E., & Zhuang, S. (2009). Inhibition of histone deacetylase activity attenuates renal fibroblast activation and interstitial fibrosis in obstructive

nephropathy. *American journal of physiology. Renal physiology*, *297*(4), F996–F1005.

70. Naito, M., Zager, R. A., & Bomsztyk, K. (2009). BRG1 increases transcription of proinflammatory genes in renal ischemia. *Journal of the American Society of Nephrology : JASN*, *20*(8), 1787–1796.
71. Blank, M. F., & Grummt, I. (2017). The seven faces of SIRT7. *Transcription*, *8*(2), 67–74.
72. Kitada, M., Kume, S., & Koya, D. (2014). Role of sirtuins in kidney disease. *Current opinion in nephrology and hypertension*, *23*(1), 75–79.
73. Wang, H., Liu, S., Liu, S., Wei, W., Zhou, X., Lin, F., Wang, J., Chen, J., Zhang, G., & Pang, Y. (2017). Enhanced expression and phosphorylation of Sirt7 activates smad2 and ERK signaling and promotes the cardiac fibrosis differentiation upon angiotensin-II stimulation. *PloS one*, *12*(6), e0178530.
74. Raji-Amirhasani, A., Khaksari, M., Darvishzadeh Mahani, F., & Hajializadeh, Z. (2021). Activators of SIRT1 in the kidney and protective effects of SIRT1 during acute kidney injury (AKI) (effect of SIRT1 activators on acute kidney injury). *Clinical and experimental nephrology*, 10.1007/s10157-021-02057-0. Advance online publication.
75. Gao, Z., Chen, X., Fan, Y., Zhu, K., Shi, M., & Ding, G. (2020). Sirt6 attenuates hypoxia-induced tubular epithelial cell injury via targeting G2/M phase arrest. *Journal of cellular physiology*, *235*(4), 3463–3473.
76. Shen, H., Holliday, M., Sheikh-Hamad, D., Li, Q., Tong, Q., Hamad, C. D., & Pan, J. S. (2021). Sirtuin-3 mediates sex differences in kidney ischemia-reperfusion injury. *Translational research : the journal of laboratory and clinical medicine*, *235*, 15–31.

77. Li, W., Yang, Y., Li, Y., Zhao, Y., & Jiang, H. (2019). Sirt5 Attenuates Cisplatin-Induced Acute Kidney Injury through Regulation of Nrf2/HO-1 and Bcl-2. *BioMed research international*, *2019*, 4745132.

78. Kiran, S., Anwar, T., Kiran, M., & Ramakrishna, G. (2015). Sirtuin 7 in cell proliferation, stress and disease: Rise of the Seventh Sirtuin!. *Cellular signalling*, *27*(3), 673–682.

79. Hubbi, M. E., Hu, H., Kshitiz, Gilkes, D. M., & Semenza, G. L. (2013). Sirtuin-7 inhibits the activity of hypoxia-inducible factors. *The Journal of biological chemistry*, *288*(29), 20768–20775.

80. Miyasato, Y., (2018). Sirtuin 7 Deficiency Ameliorates Cisplatin-induced Acute Kidney Injury Through Regulation of the Inflammatory Response. Scientific Reports, 8(1), 1–14.

81. Sánchez-Navarro, A., Mejía-Vilet, J. M., Pérez-Villalva, R., Carrillo-Pérez, D. L., Marquina-Castillo, B., Gamba, G., & Bobadilla, N. A. (2019). SerpinA3 in the Early Recognition of Acute Kidney Injury to Chronic Kidney Disease (CKD) transition in the rat and its Potentiality in the Recognition of Patients with CKD. *Scientific reports*, *9*(1), 10350.

82. Vakhrusheva, O., Smolka, C., Gajawada, P., Kostin, S., Boettger, T., Kubin, T., Bober, E. (2008). Sirt7 increases stress resistance of cardiomyocytes and prevents apoptosis and inflammatory cardiomyopathy in mice. *Circulation Research*, *102*(6), 703–710.

83. Araki, S., Izumiya, Y., Rokutanda, T., Ianni, A., Hanatani, S., Kimura, Y., Ogawa, H. (2015). Sirt7 Contributes to Myocardial Tissue Repair by Maintaining Transforming Growth Factor-β Signaling Pathway CLINICAL PERSPECTIVE. *Circulation*, *132*(12), 1081–1093.

84. Shin, J., He, M., Liu, Y., Paredes, S., Villanova, L., Brown, K., … Chen, D. (2013). SIRT7 represses myc activity to suppress er stress and prevent fatty liver disease. *Cell Reports*, *5*(3), 654–665.

85. Docherty, N. G., Pérez-Barriocanal, F., Balboa, N. E., & López-Novoa, J. M. (2002). Transforming growth factor-beta1 (TGF-beta1): a potential recovery signal in the post-ischemic kidney. *Renal failure*, *24*(4), 391–406.

86. Sobuz, S. U., Sato, Y., Yoshizawa, T., Karim, F., Ono, K., Sawa, T., Miyamoto, Y., Oka, M., & Yamagata, K. (2019). SIRT7 regulates the nuclear export of NF-κB p65 by deacetylating Ran. *Biochimica et biophysica acta. Molecular cell research*, *1866*(9), 1355–1367.

87. Malek, M., & Nematbakhsh, M. (2015). Renal ischemia/reperfusion injury; from pathophysiology to treatment. *Journal of renal injury prevention*, *4*(2), 20–27.

88. Benchabane, M., Saint-Jore-Dupas, C., Bardor, M., Faye, L., Michaud, D., & Gomord, V. (2009). Targeting and post-translational processing of human alpha1-antichymotrypsin in BY-2 tobacco cultured cells. *Plant biotechnology journal*, *7*(2), 146–160.

89. Lanzillotta, A., Sarnico, I., Ingrassia, R., Boroni, F., Branca, C., Benarese, M., Faraco, G., Blasi, F., Chiarugi, A., Spano, P., & Pizzi, M. (2010). The acetylation of RelA in Lys310 dictates the NF-κB-dependent response in post-ischemic injury. *Cell death & disease*, *1*(11), e96.

90. Rothgiesser, K. M., Erener, S., Waibel, S., Lüscher, B. & Hottiger, M. O. (2010). SIRT2 regulates NF-κB dependent gene expression through deacetylation of p65 Lys310. J. Cell Sci. 123, 4251–4258

91. Zhao, H., Qiu, Y., Wu, Y., Sun, H., & Gao, S. (2021). Protective Effects of GYY4137 on Renal Ischaemia/Reperfusion Injury through Nrf2-Mediated Antioxidant Defence. *Kidney & blood pressure research*, 1–9. Advance online publication.
92. Su, Y., Wang, Y., Liu, M., & Chen, H. (2021). Hydrogen sulfide attenuates renal I/R-induced activation of the inflammatory response and apoptosis via regulating Nrf2-mediated NLRP3 signaling pathway inhibition. *Molecular medicine reports*, *24*(1), 518.
93. Lacher, S. E., Levings, D. C., Freeman, S., & Slattery, M. (2018). Identification of a functional antioxidant response element at the HIF1A locus. *Redox biology*, *19*, 401–411.
94. Shinagawa, M., Tamura, I., Maekawa, R., Sato, S., Shirafuta, Y., Mihara, Y., Okada-Matsumoto, M., Taketani, T., Asada, H., Tamura, H., & Sugino, N. (2019). C/EBPβ regulates Vegf gene expression in granulosa cells undergoing luteinization during ovulation in female rats. *Scientific reports*, *9*(1), 714.
95. Valdes-Quezada, C., Arriaga-Canon, C., Fonseca-Guzmán, Y., Guerrero, G., & Recillas-Targa, F. (2013). CTCF demarcates chicken embryonic α-globin gene autonomous silencing and contributes to adult stage-specific gene expression. *Epigenetics*, *8*(8), 827–838.
96. Dell, R. B., Holleran, S., & Ramakrishnan, R. (2002). Sample size determination. *ILAR journal*, *43*(4), 207–213.
97. Castro-Rodríguez, D. C., Reyes-Castro, L. A., Vega, C. C., Rodríguez-González, G. L., Yáñez-Fernández, J., & Zambrano, E. (2020). Leuconostoc

mesenteroides subsp. mesenteroides SD23 Prevents Metabolic Dysfunction Associated with High-Fat Diet-Induced Obesity in Male Mice. *Probiotics and antimicrobial proteins*, *12*(2), 505–516.

98. Liu, X., Lin, Z., Zhou, T., Zong, R., He, H., Liu, Z., Ma, J. X., Liu, Z., & Zhou, Y. (2011). Anti-angiogenic and anti-inflammatory effects of SERPINA3K on corneal injury. *PloS one*, *6*(1), e16712.

99. Zhang, B., Hu, Y., & Ma, J. xing. (2009). Anti-inflammatory and antioxidant effects of SERPINA3K in the retina. Investigative Ophthalmology and Visual Science, 50(8), 3943–3952.

100. Hu, J., Zhang, Z., Xie, H., Chen, L., Zhou, Y., Chen, W., & Liu, Z. (2013). Serine protease inhibitor A3K protects rabbit corneal endothelium from barrier function disruption induced by TNF-alpha. Investigative Ophthalmology and Visual Science, 54(8), 5400–5407.

101. García-Ortuño, L. E., & Bobadilla, N. A. (2018). Integrative View of the Mechanisms that Induce Acute Kidney Injury and its Transition to Chronic Kidney Disease. Revista de investigacion clinica; organo del Hospital de Enfermedades de la Nutricion, 70(6), 261–268.

102. Li, C., Wen, A., Shen, B., Lu, J., Huang, Y., & Chang, Y. (2011). FastCloning: a highly simplified, purification-free, sequence- and ligation-independent PCR cloning method. BMC biotechnology, 11, 92.

103. Sinuani, I., Beberashvili, I., Averbukh, Z., & Sandbank, J. (2013). Role of IL-10 in the progression of kidney disease. World journal of transplantation, 3(4), 91–98.

11. OTROS ARTICULOS PUBLICADOS

A continuación se presentan otros artículos en los que participe durante mi estancia en el laboratorio de la Dra. Bobadilla.

11.1 ARTÍCULO 5 **https://pubmed.ncbi.nlm.nih.gov/28947737/**

11.2 ARTÍCULO 6 **https://pubmed.ncbi.nlm.nih.gov/31608674/**

11.3 ARTÍCULO 7 **https://pubmed.ncbi.nlm.nih.gov/33682442/**

SCIENTIFIC REPORTS

OPEN

Gender Differences in the Acute Kidney Injury to Chronic Kidney Disease Transition

Received: 10 April 2017
Accepted: 27 July 2017
Published online: 25 September 2017

Ixchel Lima-Posada[1,2], Cinthya Portas-Cortés[1,2], Rosalba Pérez-Villalva[1,2], Francesco Fontana[1,2], Roxana Rodríguez-Romo[1,2], Rodrigo Prieto[1,2], Andrea Sánchez-Navarro[1,2], Guadalupe L. Rodríguez-González[3], Gerardo Gamba[1,2], Elena Zambrano[3] & Norma A. Bobadilla[1,2]

This study evaluated if there is a sexual dimorphism in the acute kidney injury (AKI) to chronic kidney disease (CKD) transition and the time-course of the potential mechanisms involved in the dimorphic response. Female and male rats were divided into sham-operated or underwent 45-min renal ischemia (F + IR, and M + IR). All groups were studied at 24-h and 1, 2, 3, or 4-months post-ischemia. Additionally, oophorectomized rats were divided into sham or IR groups. After 24-h, AKI extent was simllar in females and males, but female rats exhibited less oxidative stress and increased renal GSH content. After 4-months and despite similar AKI, the M + IR group developed CKD characterized by proteinuria, tubulointerstitial fibrosis, glomerular hypertrophy, increased oxidative stress and a reduction in HIF1α and VEGF from the 1st-month and persisting throughout the time-course studied. Interestingly, the F + IR group did not develop CKD due to lesser oxidative stress and increased eNOS, TGFβ and HIF1α mRNA levels from the 1st-month after IR. Whereas, oophorectomized rats did develop CKD. We found a sexual dimorphic response in the AKI to CKD transition. Early antioxidant defense and higher TGFβ, HIF1α and eNOS were among the renoprotective mechanisms that the F + IR group demonstrated.

Renal ischemia/reperfusion injury (IRI) is a major cause of acute kidney injury (AKI) in patients hospitalized with native or transplanted kidneys[1,2]. It affects 15% of hospitalized patients, and the highest incidence is found in patients in the intensive care unit, with up to 60% of patients affected[2–4]. Ischemic AKI is provoked by a reduction in renal blood flow (RBF)[3,5], producing endothelial and tubular epithelial injury[6–8]. Consequently, peritubular capillary perfusion is also reduced, which favors the harm of S2 and S3 segments of the proximal tubule due to the large number of mitochondria in these sections. Therefore, this segment is highly susceptible to oxygen tension changes, with the Na^+/K^+ ATPase as one of most affected enzymes. Likewise, a reduction in ATP produces uncoupling of the respiratory chain and the subsequent formation of free radicals that favor the detachment of epithelial cells and death by apoptosis or necrosis[9,10].

Although the tubular epithelium can recover from lethal or sublethal cell damage, cellular processes in endothelial and tubular cells may not fully recover, thereby conditioning the development of progressive renal dysfunction[11].

In the last two decades, the incidence of CKD has increased more than three times, and according to the World Health Organization (WHO), it will be one of the three leading causes of death and disability worldwide by 2020[12]. This will certainly impact health systems around the world. CKD is characterized by progressive loss of nephrons and renal function, in which tubule-interstitial fibrosis plays an important role[13,14]. Accumulated evidence during the last decade from epidemiological and experimental observations have revealed that AKI is an important risk factor for the development of CKD and may also promote the CKD transition to end stage renal disease (ESRD)[8,14–17]. However, few studies have addressed the mechanisms of AKI transition to CKD. Several theories have tried to explain how an episode of AKI leads to renal function and structure injury over time. These theories include repeated cycles of damage and repair[18], rarefaction of peritubular capillaries with the subsequent development of chronic hypoxia[7,19,20], and activation of signaling pathways such as hypoxia inducible

[1]Molecular Physiology Unit, Instituto de Investigaciones Biomédicas, Universidad Nacional Autónoma de México, Mexico City, Mexico. [2]Departament of Nephrology, Instituto Nacional de Ciencias Médicas y Nutrición Salvador Zubirán, Mexico City, Mexico. [3]Departament of Reproductive Biology, Instituto Nacional de Ciencias Médicas y Nutrición Salvador Zubirán, Mexico City, Mexico. Correspondence and requests for materials should be addressed to N.A.B. (email: nab@biomedicas.unam.mx)

factor (HIF1), pro-fibrotic and pro-inflammatory cytokines[21,22]. In addition, although it is essential that the tubular cells proliferate to restore normal tubular structure, studies suggest that epithelial cells of the renal tubules also play a critical role in the development of tubulointerstitial fibrosis by inducing an arrest in the cell cycle, causing disproportionate tubular proliferation, TGFβ generation, and epigenetic modifications[23–26].

Moreover, there is a growing evidence that the pathogenesis, clinical features and prognosis of cardiovascular and renal diseases is completely different between men and women, which makes sense since the physiology of women is different from men. In this sense, one of the largest meta-analysis to assess gender differences in the progression of renal diseases included 11,000 patients referred from 60 different studies and showed that women demonstrate lower progression compared to men in different renal diseases, such as polycystic kidney disease, IgA nephropathy, membranous glomerulonephritis and CKD[27]. In support of this meta-analysis, two recent studies showed that the progression to CKD is worse in men than in women[28,29]. Likewise, the PREVEND cohort revealed that age, albuminuria, body mass index and blood glucose levels in men are risk factors that exacerbate the progression to ESRD at a greater magnitude than in women[30].

In this study, we evaluated whether there is a sexual dimorphism in the AKI to CKD transition, the time-course of functional and structural alterations in both genders, the effect of oophorectomy on this transition, and the mechanisms responsible for gender differences.

Results

Our first target was focused on assessing the severity IRI in male and female rats. The AKI was induced by 45 min of ischemia and compared with the control groups. These groups were studied 24-h after IR. The M + IR and F + IR groups developed AKI, characterized by a significant reduction in creatinine clearance (Fig. 1A), and renal blood flow (Fig. 1B), together with a significant increase in proteinuria (Fig. 1C). The urinary excretion of hydrogen peroxide (UH_2O_2V) increased 4-fold in the M + IR group compared to its control group, interestingly, in the F + IR group, the UH_2O_2V remained unaltered (Fig. 1D). Previously our group showed that the urinary heat shock protein 72 kDa levels (UHsp72) is a sensitive and early biomarker of AKI, capable of stratifying the intensity of epithelial tubular damage[31]. As shown in Fig. 1E and F, the female control group showed almost no UHsp72. In contrast, the F + IR group showed a significant increase in UHsp72 (upper WB). Similar levels of Hsp72 were found in the M + IR and F + IR groups (lower WB and densitometric analysis). This similar degree of IRI was confirmed by the histopathologic analysis as is shown in the representative PAS-stained kidney slices and in the quantification of injured tubules (Fig. 1G–H). These results indicate that IRI caused structural and functional alterations of the same magnitude in male and female rats, except in UH_2O_2V. The dimorphic response observed in the UH_2O_2V was further analyzed by measuring glutathione levels (GSH) into the kidney (Fig. 2). In renal cortex, GSH content was similar in control and the F + IR groups. In contrast, the M + IR group displayed a significant reduction by 60% in the GSH levels compared to both control groups. (Fig. 2A). In renal medulla, GSH content was similar in both control groups, whereas the F + IR group exhibited greater GSH content by t-test ($p = 0.01$) but it not reach statistical difference by ANOVA. In contrast, the M + IR group exhibited lesser GSH levels compared to F + IR group (Fig. 2B). The GSSG levels in the renal cortex, a subrogate metabolite of GSH oxidation, we only observed a trend to increase in the M + IR group (Fig. 2C). Whereas in the renal medulla, GSSG levels were greater in the F + IR group (Fig. 2D). These findings indicate that despite similar IRI female rats had a greater ability to generate GSH.

Our second target was focused on assessing the time-course of AKI to CKD transition in female and male rats. As we previously reported[23,26,32], an ischemic episode in male rats induced a progressive increase in proteinuria from 17.2 ± 1.4 (1^{st}-month) to 169.2 ± 26.2 mg/dL (4^{th}-month) and it was evident since the 2^{nd}-month (Fig. 3A). The temporal course of renal function corrected by body weight was similar among the groups and did not alter by IRI (Fig. 3B). In contrast, an early increase in UH_2O_2V was observed in the M + IR group (1^{st}-month) that remained elevated during the time-course of the study when it was compared to its control group by t-test (Fig. 3C), but only significant by ANOVA at the 1^{st} and 4^{th}-month compared with F + IR group. Despite the same initial IRI, the F + IR group did not develop neither proteinuria nor elevation of UH_2O_2V (Fig. 3A,C).

At the end of the experimental period (4-months), both female groups exhibited a lesser body weight than male, due to the well-known biological sex difference in size and body weight. In the M + IR group there was a slight reduction that was associated with the AKI to CKD transition that exhibited the male rats, but not the females (Fig. 3D). No differences in the mean arterial pressure among the studied groups were observed (Fig. 3E). The M + IR and F + IR groups did not exhibit changes in RBF, although it was significantly higher in male than in female groups (Fig. 3F), this difference was not observed when RBF was corrected by the body weight (data not shown).

In accord with our findings at functional level, after the 4^{th}-month, the F + IR group showed almost no renal structural alterations compared to the M + IR group. The representative microphotomicrograph from a F + IR rat (Fig. 4A) contrast with a M + IR rat microphotomicrograph (Fig. 4B), wherein the presence of a large percentage of tubulointerstitial fibrosis-affected area is clearly visible. The morphometric analysis of the time-course of tubulointerstitial fibrosis showed that 4-months post-ischemia, the F + IR (Fig. 4C) and the M + IR groups (Fig. 4D) showed a significant increase in fibrosis, however the degree of damage was much greater in males than in females, 38% vs. 12%, respectively ($p < 0.05$). Tubular dilataion and glomerular hypertrophy was not observed in the F + IR (Fig. 4E and G, respectively). Alterations that were do present in the M + IR group (Fig. 4F and H). Supplemental Fig. 1 shows the time-course of glomerular diameter distribution in male control group (top panel) compared with the M + IR (middle panel) and F + IR groups (lower panel). After one month, the control group exhibited a normal distribution, in which about 50% of glomeruli was found in the size range of 101–125 μm (Supplemental Fig. 1A). After 2, 3 or 4-months, in the control male group, the glomerular size increased that was in accord with the rats grow-up, so the largest percentage of glomeruli diameter was found between 126 to 150 μm and the distribution looks like a bell-shaped (Supplemental Figure 1B, C and D, respectively). In contrast, in

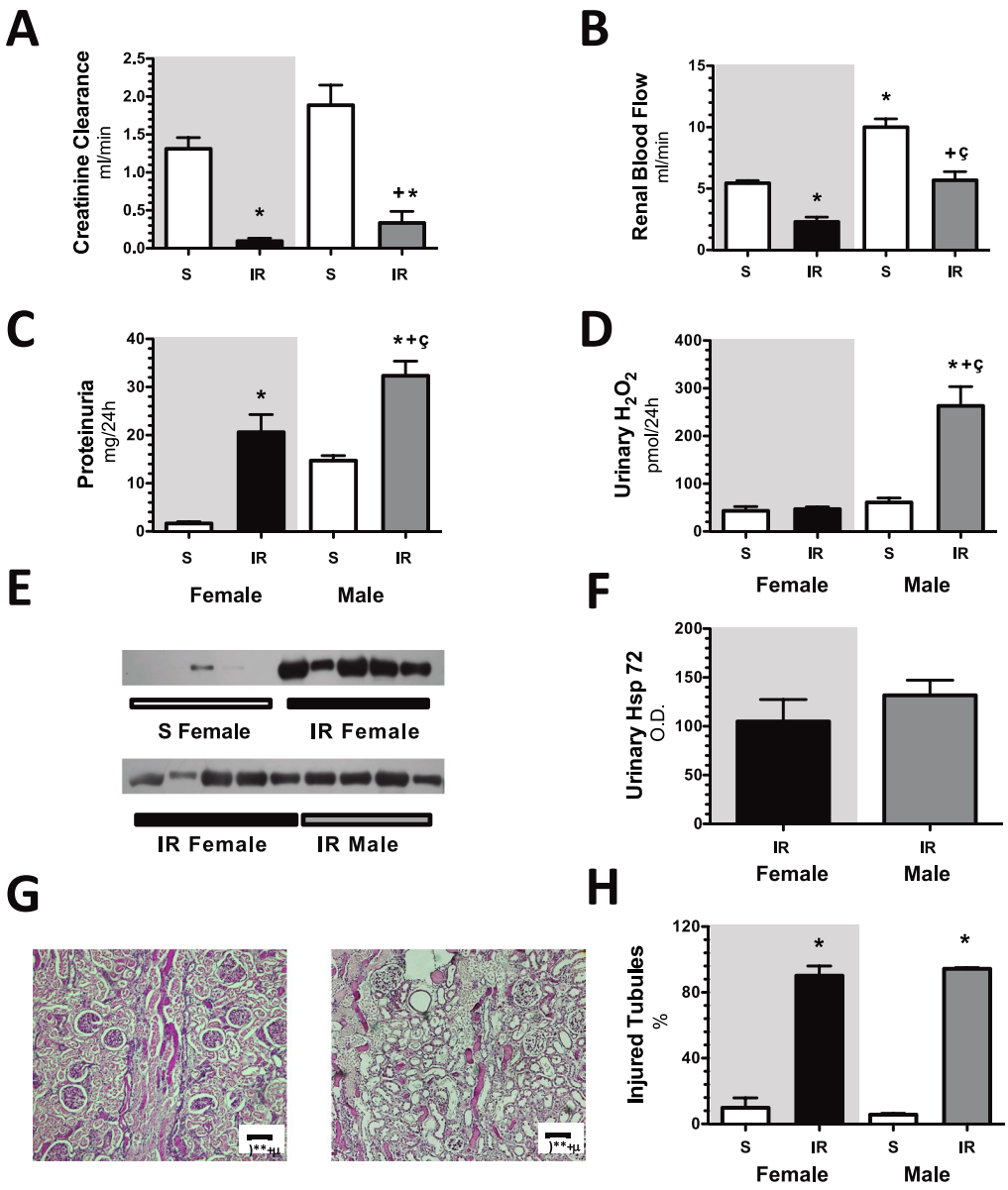

Figure 1. Renal injury induced by ischemia/reperfusion after 24-h in both female and male rats. (**A**) Creatinine clearance, (**B**) renal blood flow, (**C**) proteinuria, (**D**) Urinary H_2O_2 excretion, (**E**) Urinary Hsp72 levels by Western blot (n = 4–5 per group). (**F**) Densitometric analysis of Hsp72 levels, (**G**) a representative image of a periodic acid–Schiff (PAS) stained kidney slides from a female rat underwent IR (left), and an IR male rat (right), (**H**) percentage of injured tubules. Female groups are in a gray background in which sham female is represented by white bars and IR female group in black bars. Following by sham male in white bars and IR male group in gray bars. Control groups were formed at least n = 5, and IR Female or Male = at least 6. Data are shown as mean ± SE. *$p < 0.05$ vs, Sham female group, $^{+}p < 0.05$ vs. sham male group, and $^{ç}p < 0.05$ vs. F + IR group.

the M + IR group there was a significant increase in the proportion of glomeruli in higher ranks to 176 μ (12%, Supplemental Figure 1H). This is in clear contrast to rats belonging to the control group, which had less than 2% in this range and none glomerulus in the range between 201–225 μm. The F + IR group had a distribution pattern like the control group (Supplemental Figures 1I–1L).

The results presented in Figs 3 and 4 and Supplemental Fig. 1 clearly show that the M + IR group developed progressive CKD, this complication was not observed in the F + IR group, despite the same AKI degree induced at the beginning of the study.

To dissect the renoprotective role of female sexual hormones in the long-term renoprotection observed, female rats were oophorectomized. Figure 5A shows that in oophorectomized rats one month after, estradiol levels were reduced by 55% compared with the control group, and this group of rats won more body weight than the female control rats. Although the creatinine clearance was greater in Oop group than S group the difference by ANOVA was not significant (Fig. 5C) and when the creatinine clearance was corrected by body weight, similar

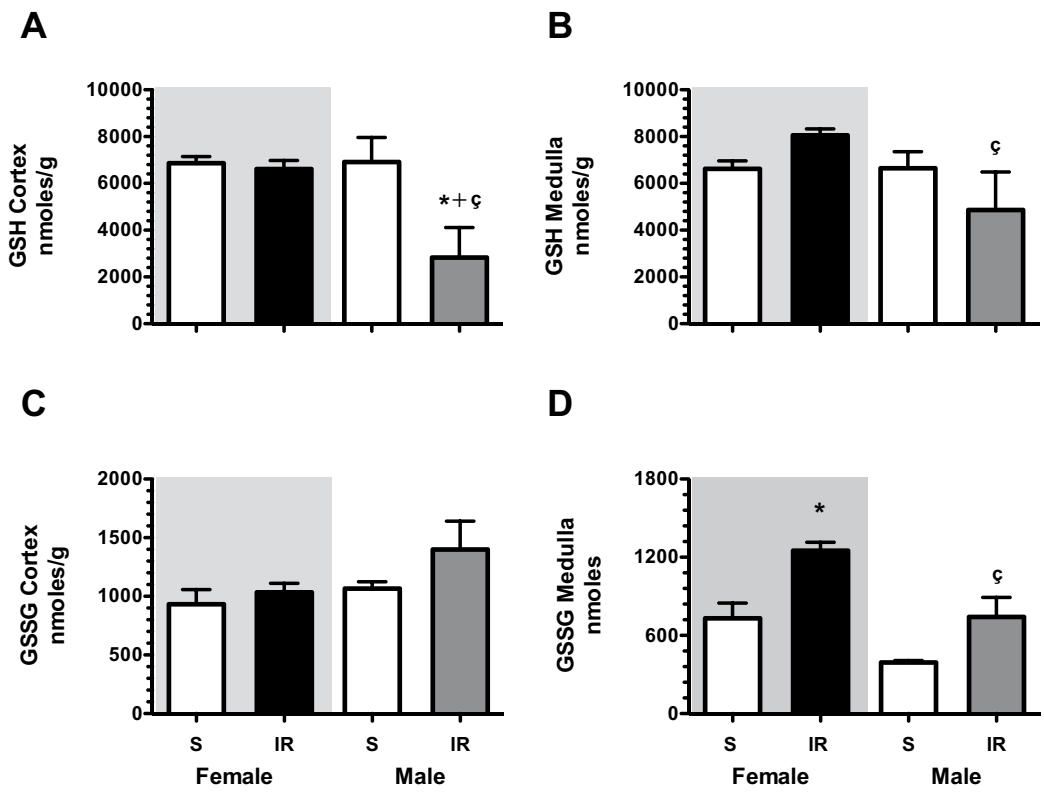

Figure 2. The IR renal injury induced a dimorphic GSH and GSSG kidney content response. (**A**) Cortex GSH levels, (**B**) Medulla GSH levels, (**C**) Cortex GSSG levels, (**D**) Medulla GSSG levels. Female groups are in a gray background in which Sham female is represented by white bars and IR female group in black bars. Following by sham male in white bars and IR male group in gray bars. The GSH and GSSG kidney content was evaluated 24-h post-ischemia. Control groups were formed by n = 4, whereas F + IR and M + IR groups included n = 6. Data are shown as mean ± SE. *$p < 0.05$ vs, Sham female group, $^{+}p < 0.05$ vs. sham male group, and $^{ç}p < 0.05$ vs. F + IR group.

results were observed (0.53 ± 0.07 vs. 0.66 ± 0.08 ml/min/100 g BW, p = NS). One month after, one half of these rats underwent IR and the other half, sham surgery. After 24-h, proteinuria was much greater in Oop + IR than in the F + IR group, (Fig. 5B). The IRI was also evidenced by the reduction in creatinine clearance and renal blood flow in both groups (Fig. 5C and D, respectively). Then, the time-course of AKI to CKD was analyzed. Urinary protein excretion progressively increased in the Oop + IR group since the 3rd-month post-ischemia (Fig. 5E), being a pretty like the M + IR group comportment. Similarly, oxidative stress in the Oop + IR group was higher than F + IR group since the 2nd- month (p = 0.05), reaching a statistically significant difference in the 3rd and 4th-months (Fig. 5F). These results suggest that female sexual hormones play a crucial role in avoiding the AKI to CKD transition.

In order to know the mechanisms responsible in the renoprotection observed in female rats, we evaluated the mRNA levels of several signal pathways involved in the pathophysiology of CKD. The endothelial nitric oxide synthase (eNOS) mRNA levels were significantly increased in the F + IR group at 1st and 3rd-months after IRI compared to sham group. In contrast, mRNA levels of eNOS remained unaltered in the M + IR groups, but were significantly different than those observed in F + IR groups (Fig. 6A). There were not changes in catalase mRNA levels among the groups, except for the 1st-month in M + IR, in which a significant reduction was observed compared to F + IR group (Fig. 6B). We also found a significant increase in hypoxia-inducible factor (HIF1α) mRNA levels in the F + IR group at the 2nd and 3rd-month post-ischemia, contrasting with the behavior in the M + IR group that was significantly smaller than the corresponding F + IR groups and different from S male group at 4th-month (Fig. 6C). Although, the VEGF mRNA levels were similar during the time-course of the study in the F + IR and M + IR groups (Fig. 6D), the VEGF protein levels towards to be lower in M + IR group during the follow-up, but a significant difference was only found at the fourth month (Fig. 6E-F), Finally, the mRNA levels of anti- inflammatory cytokines and vasoactive receptors were evaluated. There was a significant increase in TGF-β mRNA levels in the F + IR group, since the 1st-month post-ischemia and this effect was not seen in the M + IR groups (Fig. 7A). Similarly, there was a trend to increase of interleukin-10 mRNA levels in the F + IR groups (Fig. 7B). No differences were found in the mRNA levels of vasoactive factors (Fig. 7C,E and F), except in ET_B receptor in which the values tended to be lesser in male groups (Fig. 7D).

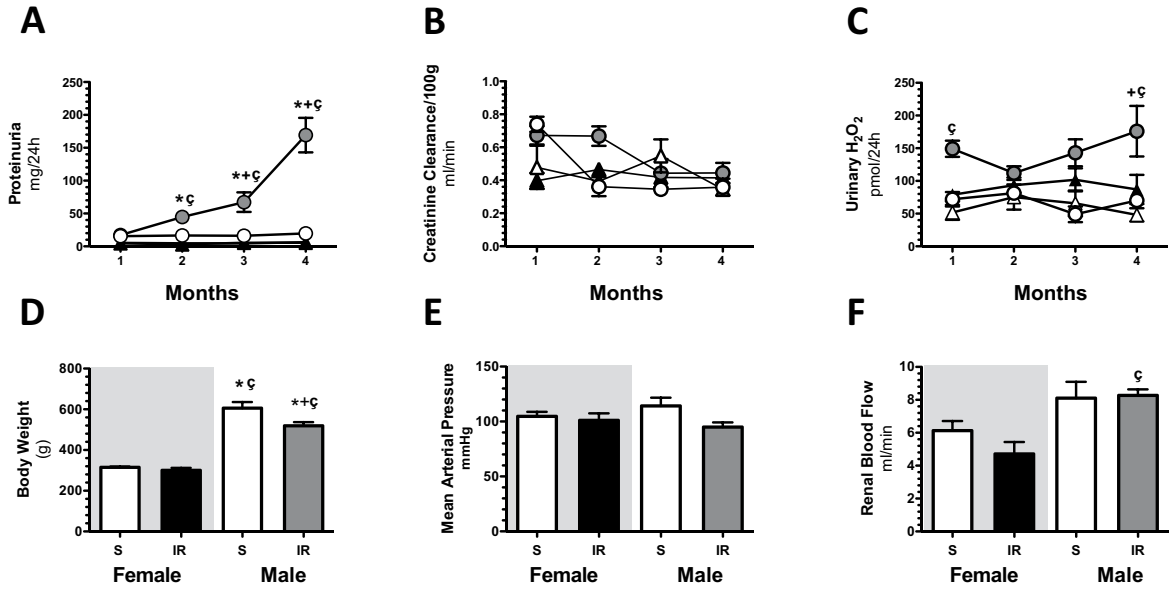

Figure 3. The AKI to CKD transition is prevented in female rats. Every 30-days (**A**) Urinary protein excretion, (**B**) creatinine clearance and (**C**) Urinary H_2O_2 excretion were measured. White triangles represent Sham female (n = at least 7), black triangles represent IR female (n = at least 10), white circles represent Sham male (n = at least 4) and gray circles represent IR male group (n = at least 4). After 4 months, (**D**) body weight, (**E**) mean arterial pressure, and (**F**) renal blood flow were recorded. Sham Female or Male (n = at least 4) and IR Female or Male groups (n = at least 7). Female groups are in a gray background in which sham is represented by white bars and F + IR group in black bars, following by Sham male in white bars and M + IR group in gray bars. Data are shown as mean ± SE. *$p < 0.05$ vs, Sham female group, $^{+}p < 0.05$ vs. Sham male group, and $^{ç}p < 0.05$ vs. F + IR group.

Discussion

In this study, we show that after 24-h that of inducing renal injury by 45 min of renal bilateral ischemia, female and male rats exhibited a similar extent of IRI, but after 4 months of the initial IRI, the M + IR group, but not the F + IR group, exhibited clear signs of CKD, characterized by proteinuria, increased oxidative stress and structural changes such as: glomerular hypertrophy and tubulointerstitial fibrosis. These findings provide evidence to support that the F + IR group were protected from the development of CKD, even though they had a similar degree of initial AKI (Fig. 1). Moreover, when the female rats were oophorectomized, this group exhibited proteinuria and oxidative stress as the M + IR group. These results indicate that sexual dimorphism observed can be attributed to sex hormones, since, the oophorectomy generated a similar behavior of the AKI to CKD transition in female rats to that observed in male rats.

Several studies have shown that renal response to different pathological processes is different between males and females animals and it has also been observed in humans. Specifically, it has been reported that renal disease in males is associated with faster progression independently of differences in blood pressure[29,33–42]. When it comes from ischemia/reperfusion the observations are not consistent. Studies conducted in Wistar rats have found that functional and structural injuries induced by ischemia/reperfusion are worsen in the male than female[43–46], similar between female and male[47,48], or even worsen in female than male rats[49,50], and these results differ to that occurs in mice in which the females are more resistant to IR injury[39]. Using renal function (creatinine clearance and renal blood flow), and tubular injury markers (proteinuria, injured tubules %, and urinary excretion of Hsp72), we found, that after 24-h of renal bilateral ischemia, female and male rats displayed the same magnitude of IRI. Therefore, sexual dimorphism in IRI after 24-h was not observed, except in the oxidative stress, because the F + IR did not exhibit elevation of UH_2O_2V, as was observed in the M + IR group (Fig. 1D). This finding on oxidative stress was further explored in the renal tissue by measuring renal GSH content. The M + IR indeed exhibited a significant reduction in renal GSH, an effect that was not observed in the F + IR group (Fig. 2A), despite the extensive tubular proximal injury (Fig. 1). These results indicate that female hormones seems to maintain the GSH content in extreme conditions and they also are able to protect for their powerful antioxidant activity, as has been previously demonstrated[51]. Although female exhibited a lesser oxidative stress than male rats, it was not enough to reduce IR injury, because several players take place into AKI pathophysiology, mainly: 1) enhanced vasoconstriction, due to an imbalance in the release of vasoconstrictor and vasodilator factors; 2) endothelial cell injury, that promotes activation and transmigration of leucocytes which are able to produce cytokines and a pro-inflammatory state; 3) and epithelial cell injury by also contributing to the inflammation through releasing chemotactic cytokines, and by the loss of the tubular integrity that provokes a reduction in the survival pathways[8].

The CKD progression after IRI was observed in the M + IR group accordingly with our previous studies[23,26,32], but interestingly, female rats did not develop CKD.

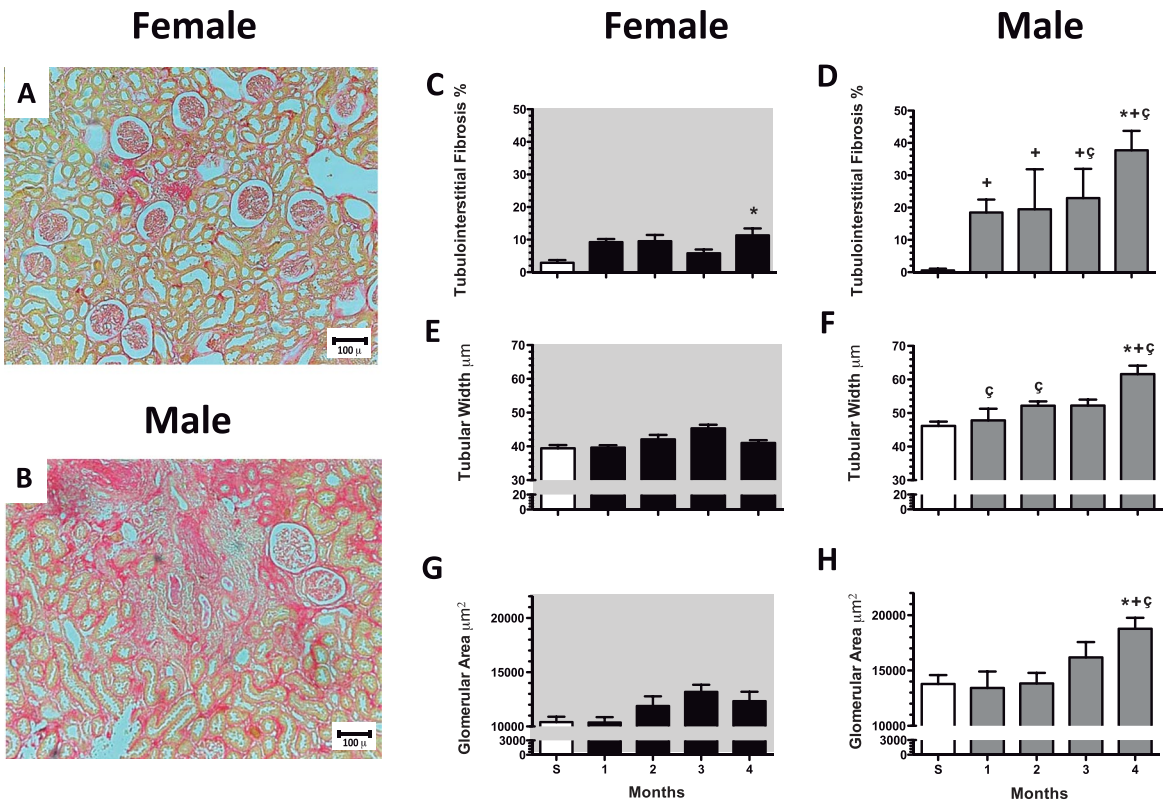

Figure 4. CKD induced by an AKI episode was associated with glomerular and tubulointerstitial injury in males but prevented in females. Representative light microphotographs of kidney slides stained with Sirius red from (**A**) female IR rat an (**B**) male IR rat after 4-months of IR injury (Magnification ×100). Temporal course of tubulointerstitial fibrosis in (**C**) female (white bar represents sham and black bars IR groups) and in (**D**) male groups (white bar represents sham and gray bars IR groups). Temporal course of tubular dilation (μm) in (**E**) female and in (**F**) male groups. Temporal course of Glomerular area (μm²) in (**G**) female and in (**H**) male groups. All parameters were determined at 1, 2, 3 and 4-months in both F + IR and M + IR groups and at 4-months in female and male sham groups in at least 4 rats per group. Data are shown as mean ± SE. *$p < 0.05$ vs, Sham female group, $^{+}p < 0.05$ vs. sham male group, and $^{ç}p < 0.05$ vs. F + IR group.

Among the potential mechanisms regulated by sex hormones are: changes in renal hemodynamics, and altered vasoactive factors release, transcription factors, pro-fibrotic and pro-inflammatory cytokines[52]. Moreover, female hormones may influence the defense in response to pathophysiological events by its antioxidant property[49,53]. The antioxidant effect of estrogen is mediated by the hydroxyl group at the C3 position of the A ring of the steroid molecule and has been reported that ouabain, an inhibitor of Na^+/K^+ ATPase blocks these protective effects, suggesting that the antioxidant effect helps to maintain the function of this pump reducing the accumulation of intracellular sodium[54]. In fact, our study of the time-course of UH_2O_2V in the AKI to CKD transition, showed that oxidative stress was higher in the M + IR than in the F + IR group, an effect that was seen in a very early phase post-ischemia and remained along the study (Figs 1D, 2A, and 3C). The lower oxidative stress in female rats exposed to IRI, was not seen when the rats were oophorectomized (Fig. 5F). However, a limitation of the present study is that it cannot exclude that the present observations are characteristic of Wistar rats only. A broader study would be beneficial.

Endothelial dysfunction is caused by reduced levels of nitric oxide (NO) derived from the endothelium. It has been reported that renal diseases are associated with reduced NO synthesis provoked by the reduced eNOS expression or activity[55]. We found that during the AKI to CKD transition, the M + IR group have similar eNOS mRNA levels throughout the study. In contrast, them were significantly increased in the F + IR group very early after IRI. These results indicate that female rats besides having better antioxidant response, also may generate more NO, which was associated with the disease prevention.

Under conditions of low oxygen tension, HIF1α plays an essential role in regulating several of its target genes to mediate actions on: cell proliferation, angiogenesis, apoptosis, etc.[56]. HIF1α regulates angiogenesis by increasing the expression of VEGF. During the AKI to CKD transition there is a chronic hypoxia and a reduction in the peritubular capillaries[19,57]. These findings suggest that HIF1α signaling may be affected during this transition. In fact, we observed that the greatest damage in the M + IR group was associated with a significant reduction in HIF1α and VEGF protein levels. Whereas a dimorphic response was observed in the F + IR group, because HIF1α mRNA levels was enhanced after IRI since the 1st-month, reaching statistical difference by ANOVA after the 2nd-month. These results suggest that another mechanism by which female rats did not progress to CKD is

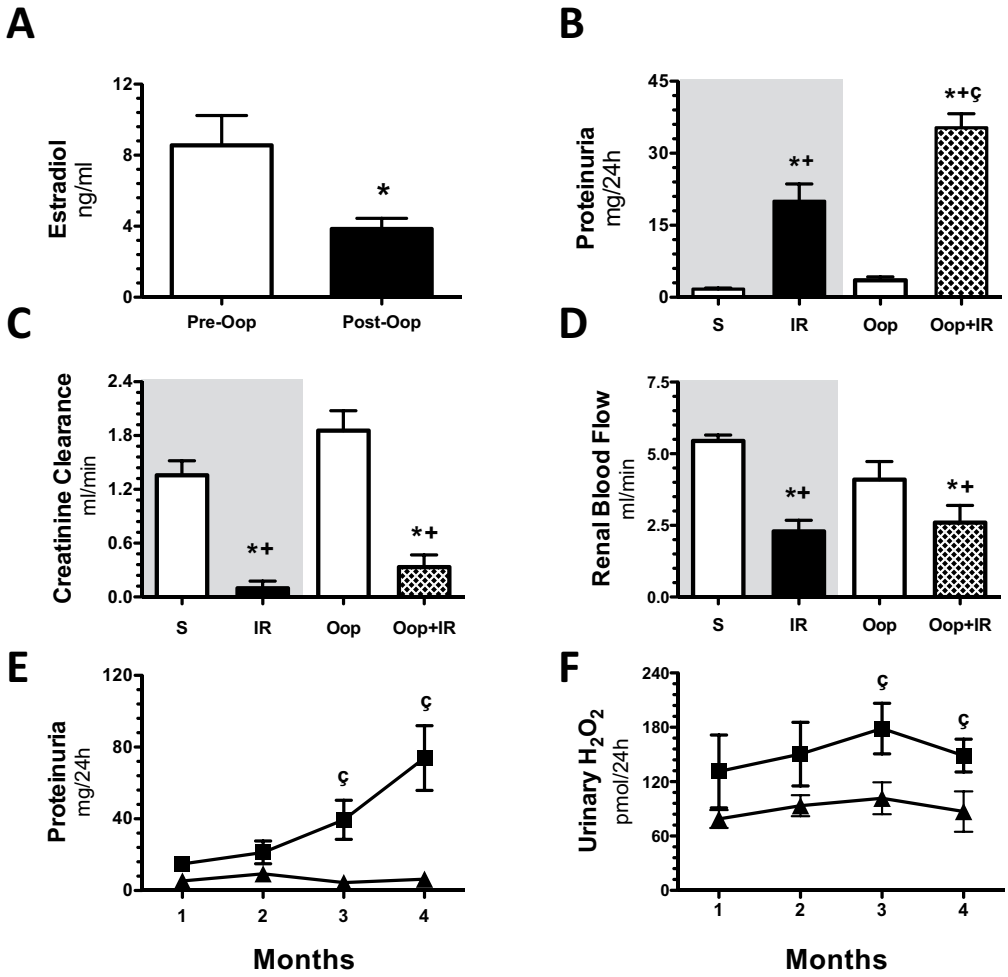

Figure 5. The depletion of estrogens is associated with AKI to CKD transition in female rats. (**A**) Estradiol levels before oophorectomy (Pre-Op) is represented in white bars (n = 24) and 1-month after oophorectomy (Post-Op) in black bars (n = 24). Then, oophrorectomized rats (Oop) were underwent to sham surgery or bilateral renal ischemia of 45 min (Oop + IR) and studied 24-h or 1 to 4-months. In (**B**) proteinuria, (**C**) creatinine clearance, and (**D**) renal blood flow evaluated 24-h post-ischemia. Both female groups without oophorectomy are in a gray background in which sham (S) is represented by white bars and IR female group (IR) in black bars, following by the sham oophorectomized group (Op) in white bars and the ophrorectomized underwent IR group (Oop + IR) in pattern bars. For the long-time experiment, (**E**) urinary protein excretion, and (**F**) Urinary H_2O_2 excretion were measured every 30 days during the follow-up. Black triangles represent IR female (n = at least 8), black squares represent IR + Oop (n = at least 4). Data are shown as mean ± SE. *$p < 0.05$ vs. sham female group, $^{+}p < 0.05$ vs. Op, $^{ç}p < 0.05$ vs. F + IR group.

mediated by its ability to increase HIF1α since early stages after IRI, which in turn could help to prevent vascular rarefaction, chronic hypoxia and renal fibrosis.

In addition to this, it has been observed that estrogens have anti-fibrotic and anti-apoptotic properties in the cardiomyocytes[58]. Also, it has been reported that administration of 17-beta estradiol to hypertensive oophorectomized rats attenuates glomerulosclerosis and tubulointerstitial fibrosis[59] while, in rats with type II diabetes, this hormone protects podocytes by increasing estrogen receptor beta[35]. This effect on podocytes, apparently is mediated by stabilizing the cytoskeleton of these cells[60]. On contrary, it has been postulated that testosterone has fibrotic and apoptotic properties through increasing TNFα signaling[37]. Accordingly, with this evidence, the M + IR group developed glomerular hypertrophy and tubule-interstitial fibrosis after IRI and the female rats do not. Surprisingly, the time-course of TGF-β mRNA levels after the ischemic insult showed a clearly dimorphic response. In the F + IR, TGF-β mRNA levels were significantly increased, since the 1st- month and remained elevated along the study, whereas in the M + IR group this anti-inflammatory response did not occur. Similarly, interleukin-10 only trend to increase in the F + IR groups. Although several studies have revealed the fundamental role of TGF-β in renal fibrosis[61], has also been observed that the use of antibodies against TGF-β in models of diabetic nephropathy[62], or in puromycin aminonucleoside induced nephropathy[63] worsen proteinuria. In fact, Wang W *et al*. showed that TGF-β can relieve the inflammation through Smad7[64]. Given the significant tubulointerstitial fibrosis in male rats compared with females, we believe that the early elevation of this cytokine in female

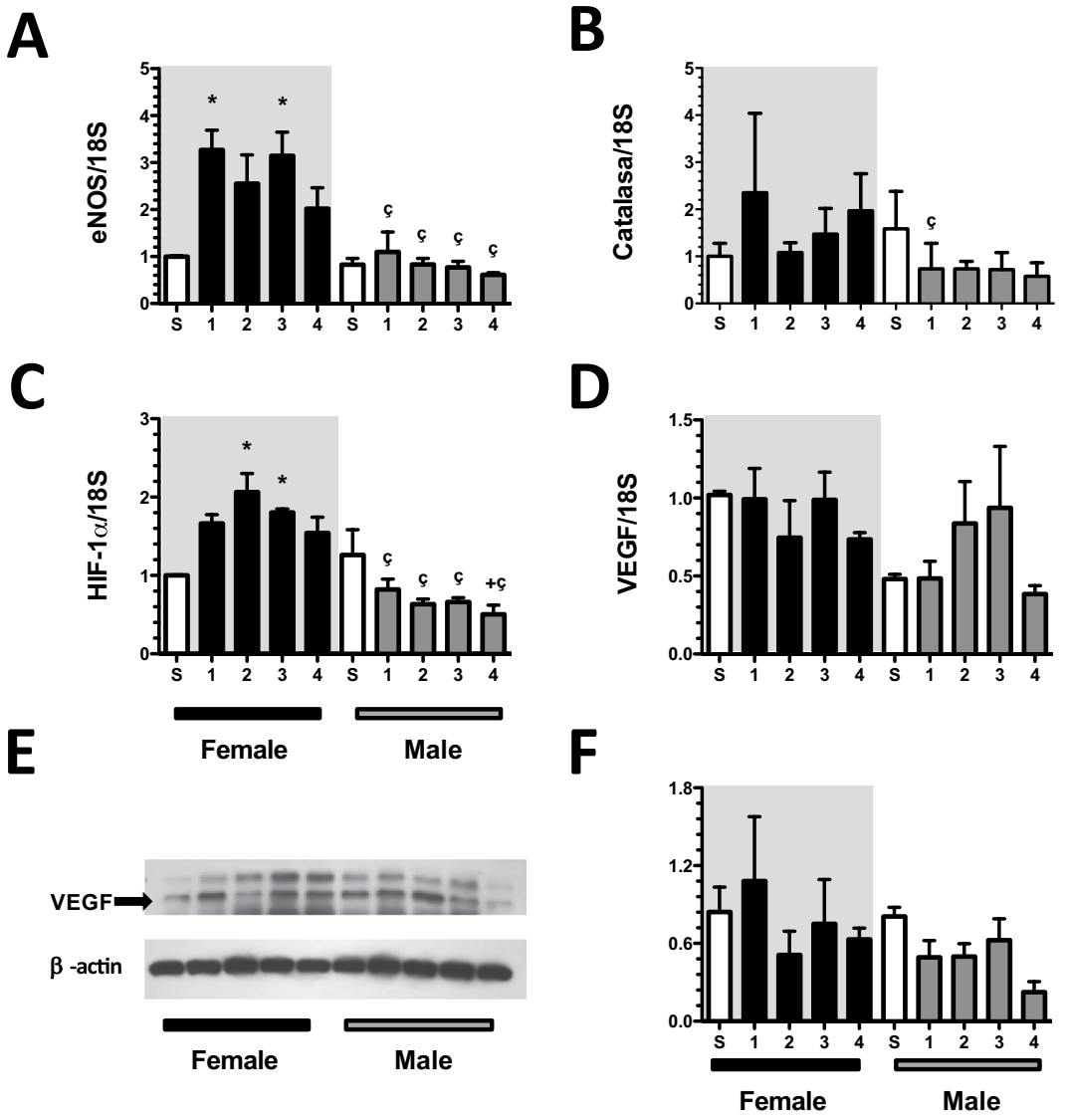

Figure 6. Dimorphic response of some mediators involved in the AKI to CKD transition. (**A**) eNOS mRNA levels, (**B**) catalase mRNA levels, (**C**) HIF1α mRNA levels, (**D**) VEGF mRNA levels, (**E**) Representative autoradioghraphies of VEGF and β-actin Western Blot analysis, and (**F**) VEGF protein levels. Female groups are in a gray background, in which sham is represented by white bars and F + IR group in black bars, following by sham male in white bars and M + IR group in gray bars. The mRNA levels were determined at least by duplicate (n = at least 4 per group). Data are shown as mean ± SE. *$p < 0.05$ vs, Sham female group, $^{+}p < 0.05$ vs. sham male group, and $^{ç}p < 0.05$ vs. F + IR group.

rats, could be exerting a renoprotector effect. In support of this, Klempt *et al*. reported that TGF-β is induced after cerebral ischemia and this rise was associated with post-axial repair[65]. Furthermore, it has been reported that TGF-β anti-inflammatory properties are mediated by promoting polarization of anti-inflammatory Th2 macrophages in cerebral malaria[66]. Therefore, the increment in TGF-β mRNA levels in early stages after ischemia observed in the F + IR group is another beneficial mechanism that females install after the IRI.

In summary, there is a sexual dimorphism in the AKI to CKD transition and the renoprotection observed in the F + IR group was lost with the oophorectomy: These results strongly suggest that female sex hormones are responsible of the renoprotection observed. Within the renoprotective mechanisms that installed females after IRI are: best antioxidant and anti-inflammatory defense, as well as higher HIF1α and eNOS mRNA levels.

Methods

All experiments involving animals were conducted in accordance with NIH Guide for the Care and Use of Laboratory Animals and with the Mexican Federal Regulation for animal reproduction, care, and experimentation (NOM-062-ZOO-2001). The study was approved by the Animal Care and Use Committees: Comité para el cuidado y uso de animales de laboratorio, Instituto de Investigaciones Biomédicas and for Comité de investigación en animales, Instituto Nacional de Ciencias Médicas y Nutrición.

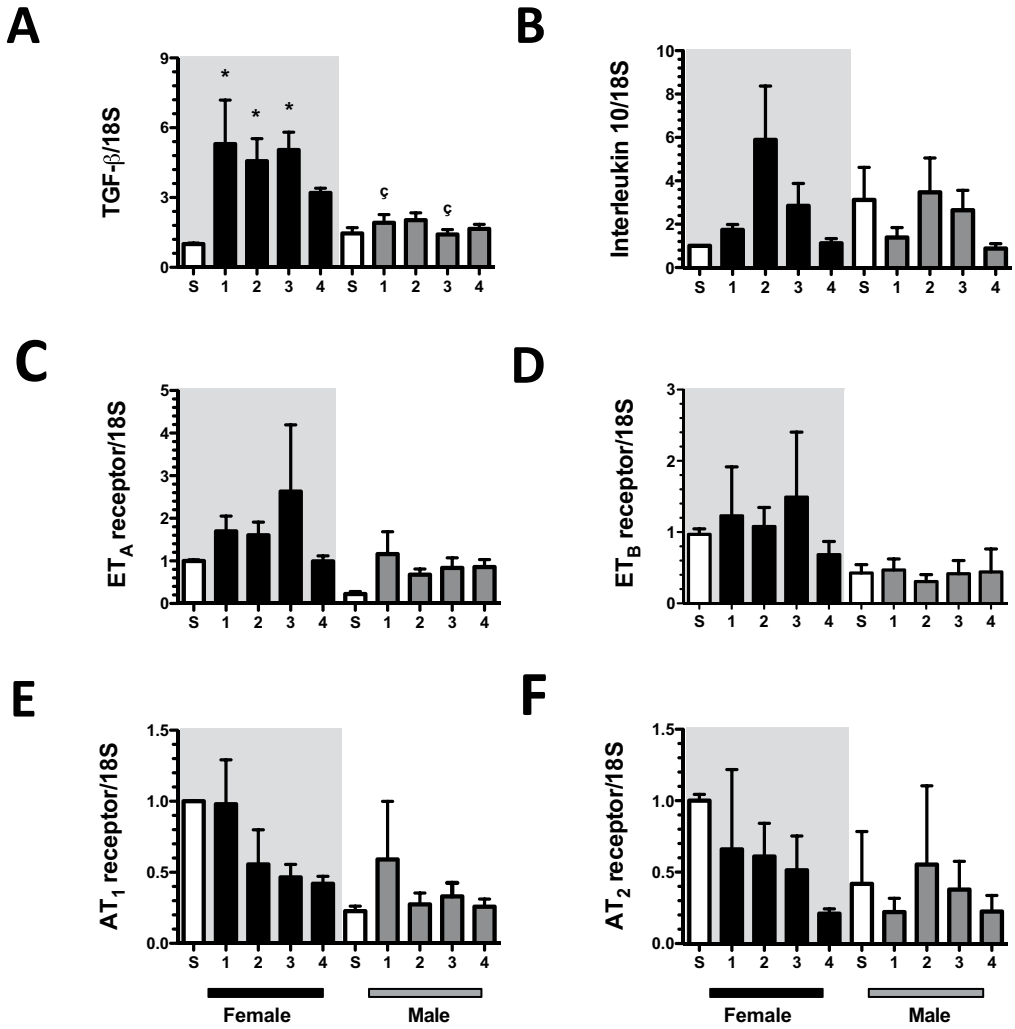

Figure 7. Anti-inflammatory and vasoactive pathways mRNA levels in the dimorphism found in the progression of CKD induced by AKI. (**A**) TGF-β mRNA levels, (**B**) Interleukin 10 mRNA levels, (**C**) ET_A receptor mRNA levels, (**D**) ET_B receptor mRNA levels, (**E**) AT_1 receptor mRNA levels, (**F**) AT_2 receptor mRNA levels. Female groups are in a gray background, in which sham is represented by white bars and F + IR group in black bars, following by sham male in white bars and M + IR group in gray bars. Groups included at least 4 rats per group. Data are shown as mean ± SE. *$p < 0.05$ vs, Sham female group, $^{+}p < 0.05$ vs. sham male group, and $^{ç}p < 0.05$ vs. F + IR group.

Experimental Protocol 1. Thirty-nine female (250–280 g) and thirty-nine (290–310 g) male Wistar rats were included and divided into seven groups: Two groups of control animals underwent sham surgery that were studied and sacrificed at 24-h (5 females and 5 males) and at 4-months (4 females and 4 males); and 5-groups who underwent bilateral renal ischemia for 45 min and were studied at 24-h (6 females and 6 males) and at 1 (5 females and 5 males), 2 (6 females and 6 males), 3 (5 females and 5 males), or 4-months post-ischemia (8 females and 8 males), F + IR and M + IR, respectively. The bilateral renal ischemia in the female rats was performed during the estrogenic phase. This phase was evaluated by vaginal smear, briefly cyclicity was recorded following examination of vaginal smears for the proportions of leucocytes, epithelial cells and cornified cells in the smear. The smears were assessed and cycles identified as described previously[67].

Experimental Protocol 2. Fifty-five female Wistar rats were oophorectomized at 70 days of age and allowed to evolve 1-month until estrogen levels decreased and were divided into 7-groups: two groups of control animals underwent sham surgery that were studied and sacrificed at 24-h (n = 8) and at 4-months (n = 9); and five groups who underwent bilateral renal ischemia for 45 min and were studied at 24-h (n = 8), and at 1 (n = 8), 2 (n = 6), 3 (n = 8), or 4-months post-ischemia (n = 8).

Ischemia/reperfusion model. Rats were anesthetized with an intra-peritoneal injection of sodium pentobarbital (30 mg/kg) and placed on a heating pad to maintain core body temperature at 37 °C. Renal pedicles were isolated, and bilateral renal ischemia was induced using a non-traumatic clamp on each renal artery for 45 min.

Reperfusion was achieved by release of the clips and confirmed by return of oxygenated blood to the kidney. The muscle and the skin were closed with 3-0 vicryl and silk sutures, respectively. For sham surgery, laparotomy and renal pedicle dissection, without clamping, was performed in anesthetized rats.

Bilateral Oophorectomy. The animals were anesthetized by intraperitoneal injection of sodium pentobarbital at a dose of 30 mg/Kg and were placed in a heating bed. Double dorsolateral incision was performed and the oviducts were ligated and removed; then, the abdominal wall and skin were sutured. After surgery, the animals remained in the heating bed until their anesthesia recovery. One month after, rats underwent to bilateral renal ischemia (45 min) and studied either, 24-h or 4-months after.

Functional Studies. At the end of the experimental period, rats were anesthetized with sodium pentobarbital (30 mg/kg) and placed on a homoeothermic table. The femoral arteries were catheterized with polyethylene tubing (PE-50). The mean arterial pressure (MAP) was monitored with a pressure transducer (model p23 db, Gould) and recorded on a polygraph (Grass Instruments, Quincy, MA). An ultrasound transit-time flow probe (transonic flowprobe, New York, NY) was placed around the left artery and filled with ultrasonic coupling gel (HR Lubricating Jelly, Carter-Wallace, New York, NY) to record the renal blood flow (Transonic flowmeter, New York, NY). Blood samples were taken at the end of the study.

Biochemical Studies. Proteinuria was determined monthly from 24-h urine collections using the turbidimetric method with trichloroacetic acid (TCA) throughout the monthly follow-up in all studied groups.

Urine and serum creatinine concentrations were measured with Quantichrom creatinine assay kit (DICT-500), and renal creatinine clearance was calculated.

Serum estradiol concentrations were determined by radioimmune analysis using a commercial rat kit, (DPC Coat-a-count, TKE21, Diagnostic Products, CA, USA).

Light microscopy analysis. For the light microscopy, the left kidney was perfused through the femoral catheter with PBS and then 4% neutral buffered formalin, and perfusion was continued until fixation was completed, maintaining the MAP that each rat had during the experiment. Renal tissue was paraffin embedded, 3 μm sections were stained with periodic acid Schiff (PAS) or Sirius red. For the acute study, ten subcortical fields (magnification ×100) were recorded from each kidney slide using a digital camera incorporated in a Nikon Light microscope. The injured tubules were analyzed blindly. Tubular damage was characterized by a loss of brush border, lumen dilation, and detachment from basement membrane. In each microphotograph, injured tubules were counted, and the results were expressed as the average of fields observed. For the chronic study, the glomerular diameter and area was measured in at least 50 glomeruli per rat, as we previously reported[23]. For this purpose, ten to fifteen images of different renal cortex fields were recorded (magnification ×100). In another ten images (magnification ×400), tubular width was measured in at least 100 tubules. Tubulointerstitial fibrosis consisted in extra cellular matrix expansion with collagen deposition together with distortion and collapse of the tubules; fibrosis was evidenced by red coloration in Sirus red stained slides. The degree of tubulo-interstitial fibrosis was measured by morphometry in five to eight subcortical fields (magnification ×400). The affected area was delimited and the percentage of tubulo-interstitial fibrosis was calculated by dividing the fibrotic area by the total field area, excluding the glomerular area. All the analyses were performed blinded.

Urinary hydrogen peroxide assay. The amount of hydrogen peroxide (H_2O_2) in urine was determined with an Amplex Red Hydrogen Peroxide/Peroxidase Assay Kit (Invitrogen, Eugene, OR) according to the manufacturer's instructions.

Glutathione (GSH) and glutathione disulfide (GSSG) levels. *Tissue Preparation.* The right kidney was excised and separated into renal cortex and medulla. The sections were maintained in ice-cold saline solution (0.9% NaCl). A 10% whole homogenate was prepared in ice-cold homogenization buffer [154 mM KCl, 5 mM diethylenetriaminepentaacetic acid (DTPA), and 0.1 M potassium phosphate (KPi) buffer, pH 6.8]. Immediately after, one volume of cold acid buffer consisting of 40 mM HCl, 10 mM DTPA, 20 mM ascorbic acid, and 10% trichloroacetic acid (TCA) was added to one volume of homogenate. The suspension was centrifuged at 14,000 rpm and the resulting supernatant solution was maintained at −70 °C for at least 4 weeks.

O-phthalaldehyde assay (*OPA*) *Assay Procedure.* The following solutions were required to perform the OPA assay: redox quenching buffer (RQB) (20 mM HCl, 5 mM DTPA, 10 mM ascorbic acid); 5% TCA in RQB (TCA–RQB); 7.5 mM N-ethylmaleimide (NEM) in RQB; 1.0 M KPi buffer (pH 7.0); 0.1 M KPi buffer (pH 6.9); 100 mM dithionite (DT; sodium hydrosulfite) in RQB; 5.0 mg/ml OPA in methanol. DT and OPA solutions were prepared immediately before use. Standards were prepared as follows: 0.1 mM GSSG in TCA–RQB; 0.1 mM GSH in TCA–RQB. The trace levels of GSSG were removed by treating 1.0 ml of a 1.0 mM solution of GSH in TCA–RQB with 25 mg of zinc dust. The assays consisted of paired samples labeled A and B. Sample A was the background consisting of non-glutathione-dependent fluorescence that was subtracted from the paired sample B. From GSSG 1 mM stock, 20 μl was taken and 980 μl of TCA-RQB was added to make the standard curve. OPA-derived fluorescence was measured at 365-nm excitation (slit width 5 nm) and 430-nm emission (slit width 20 nm)[68].

eNOS, catalase, HIF1α, VEGF, ETA, ETB, AT1, AT2, TGF-β, and IL-10 mRNA levels. The right kidney was removed and quickly frozen. The total renal cortex RNA was isolated from the kidneys using the TRIzol method (Invitrogen, Carlsbad, CA) and checked for integrity using 1% agarose gel electrophoresis. To avoid DNA contamination, total RNA samples were treated with DNAase (DNAase I; Invitrogen). Reverse transcription (RT) was carried out with 1 μg of total RNA and 200 U of Moloney murine leukemia virus reverse

transcriptase (Invitrogen). The mRNA levels eNOS, catalase, HIF1α, VEGF, ET_A, ET_B, AT_1, AT_2, TGF- β and IL-10 were quantified by real-time PCR on an ABI Prism 7300 Sequence Detection System (TaqMan, ABI, Foster City, CA). Primers and probes were ordered as follows: eNOS (Rn02132634_s1), catalase (Rn00560930_m1), HIF1α, (Rn0057756_m1), VEGF (Rn01511602_m1), ET_A (Rn00561137_m1), ET_B (Rn00569139_m1), AT_1 (Rn00561409_s1), AT_2 (Rn00560677_s1), TGF-β (Rn00572010_m1), and IL-10 (Rn99999012_m1). As an endogenous control, eukaryotic 18S rRNA (predesigned assay reagent Applied by ABI, external run, Rn03928990_g1) was used. The relative quantification of each gene expression was performed with the comparative threshold cycle (Ct) method.

Renal VEGF protein levels. VEGF protein levels were detected by Western blot, using 30 μg of protein in 8.5% SDS-PAGE electrophoresis gel and electroblotted. The membranes were incubated with mouse anti-VEGF antibody (1:1000, ThermoScientific) overnight. Next, the membranes were incubated with a secondary antibody and HRP-conjugated anti-mouse IgG (1:5000, Santa Cruz Biotechnology). The proteins were detected with an enhanced chemiluminescence kit (Millipore) and by radiography. All Western blot analyses were performed within the linear range of protein loads and antibody use. The bands were scanned for densitometric analysis using the UVP EC3 Imaging System and the UVP VisionWorks LS Image acquisition and Analysis Software.

Urinary Hsp72 levels. Urinary Hsp72 levels were detected by Western blot, each urine was diluted 1:10 in 0.9% saline solution, and 10 μL of each dilution was loaded and resolved by 8.5% SDS-PAGE electrophoresis and electroblotted. The membranes were incubated with mouse anti-Hsp72 antibody (ENZO Life Sciences, 1:5000 dilution) for 2-h and then incubated with a secondary antibody, HRP-conjugated goat anti-mouse IgG (1:5000, Santa Cruz Biotechnology). The proteins were detected using a commercial chemiluminiscence kit (Millipore).

Statistical analysis. The results are presented as the mean ± SE. The differences among the four studied groups at 24-h and 4-months were assessed by ANOVA using the Bonferroni correction for multiple comparisons. All comparisons passed the normality test. The differences in the ranks of glomerular diameters among the groups were evaluated by contingency analysis, and the differences were assessed using the chi-squared test with the Yates correction. Statistical significance was defined when the p value was <0.05.

The data generated during and/or analyzed during the current study are available from the corresponding author on reasonable request.

References

1. Kelly, K. J. Acute renal failure: much more than a kidney disease. *Semin. Nephrol.* **26**, 105–113 (2006).
2. Zappitelli, M. Epidemiology and diagnosis of acute kidney injury. *Semin. Nephrol.* **28**, 436–446 (2008).
3. Friedewald, J. J. & Rabb, H. Inflammatory cells in ischemic acute renal failure. *Kidney Int.* **66**, 486–491 (2004).
4. Lafrance, J. P. & Miller, D. R. Acute kidney injury associates with increased long-term mortality. *J. Am. Soc. Nephrol.* **21**, 345–352 (2010).
5. Go, A. S. *et al*. The assessment, serial evaluation, and subsequent sequelae of acute kidney injury (ASSESS-AKI) study: design and methods. *BMC. Nephrol.* **11**, 22 (2010).
6. Basile, D. P. The endothelial cell in ischemic acute kidney injury: implications for acute and chronic function. *Kidney Int.* **72**, 151–156 (2007).
7. Basile, D. P. *et al*. Impaired endothelial proliferation and mesenchymal transition contribute to vascular rarefaction following acute kidney injury. *Am. J. Physiol Renal Physiol* **300**, F721–F733 (2011).
8. Bonventre, J. V. & Yang, L. Cellular pathophysiology of ischemic acute kidney injury. *J. Clin. Invest* **121**, 4210–4221 (2011).
9. Le, D. M., Legrand, M., Payen, D. & Ince, C. The role of the microcirculation in acute kidney injury. *Curr. Opin. Crit Care* **15**, 503–508 (2009).
10. Molitoris, B. A., Dahl, R. & Geerdes, A. Cytoskeleton disruption and apical redistribution of proximal tubule Na(+)-K(+)-ATPase during ischemia. *Am. J. Physiol* **263**, F488–F495 (1992).
11. Bedford, M., Farmer, C., Levin, A., Ali, T. & Stevens, P. Acute kidney injury and CKD: chicken or egg? *Am. J. Kidney Dis.* **59**, 485–491 (2012).
12. Lozano, R. *et al*. Global and regional mortality from 235 causes of death for 20 age groups in 1990 and 2010: a systematic analysis for the Global Burden of Disease Study 2010. *Lancet* **380**, 2095–2128 (2012).
13. Ferenbach, D. A. & Bonventre, J. V. Mechanisms of maladaptive repair after AKI leading to accelerated kidney ageing and CKD. *Nat. Rev. Nephrol.* **11**, 264–276 (2015).
14. Chawla, L. S., Eggers, P. W., Star, R. A. & Kimmel, P. L. Acute kidney injury and chronic kidney disease as interconnected syndromes. *N. Engl. J. Med.* **371**, 58–66 (2014).
15. Block, C. A. & Schoolwerth, A. C. Acute renal failure: outcomes and risk of chronic kidney disease. *Minerva Urol. Nefrol.* **59**, 327–335 (2007).
16. Hsu, C. Y. *et al*. The risk of acute renal failure in patients with chronic kidney disease. *Kidney Int.* **74**, 101–107 (2008).
17. Venkatachalam, M. A. *et al*. Acute kidney injury: a springboard for progression in chronic kidney disease. *Am. J. Physiol Renal Physiol* (2010).
18. Lewington, A. J., Cerda, J. & Mehta, R. L. Raising awareness of acute kidney injury: a global perspective of a silent killer. *Kidney Int.* **84**, 457–467 (2013).
19. Basile, D. P. Rarefaction of peritubular capillaries following ischemic acute renal failure: a potential factor predisposing to progressive nephropathy. *Curr. Opin. Nephrol. Hypertens.* **13**, 1–7 (2004).
20. Horbelt, M. *et al*. Acute and chronic microvascular alterations in a mouse model of ischemic acute kidney injury. *Am. J. Physiol Renal Physiol* **293**, F688–F695 (2007).
21. Chen, J. *et al*. EGFR signaling promotes TGFbeta-dependent renal fibrosis. *J. Am. Soc. Nephrol.* **23**, 215–224 (2012).
22. Tanaka, S., Tanaka, T. & Nangaku, M. Hypoxia and Dysregulated Angiogenesis in Kidney Disease. *Kidney Dis (Basel).* **1**, 80–89 doi:10.1159/000381515 (2015).
23. Rodriguez-Romo, R. *et al*. AT1 receptor antagonism before ischemia prevents the transition of acute kidney injury to chronic kidney disease. *Kidney Int* **89**, 363–373, doi:10.1038/ki.2015.320 (2016).
24. Bechtel, W. *et al*. Methylation determines fibroblast activation and fibrogenesis in the kidney. *Nat. Med.* **16**, 544–550 (2010).
25. Yang, L., Besschetnova, T. Y., Brooks, C. R., Shah, J. V. & Bonventre, J. V. Epithelial cell cycle arrest in G2/M mediates kidney fibrosis after injury. *Nat. Med.* **16**, 535–543, 531p (2010).

26. Barrera-Chimal, J. *et al*. Spironolactone prevents chronic kidney disease caused by ischemic acute kidney injury. *Kidney Int.* **83**, 93–103 (2013).
27. Neugarten, J., Acharya, A. & Silbiger, S. R. Effect of gender on the progression of nondiabetic renal disease: a meta-analysis. *J.Am. Soc.Nephrol.* **11**, 319–329 (2000).
28. Evans, M. *et al*. The natural history of chronic renal failure: results from an unselected, population-based, inception cohort in Sweden. *Am. J. Kidney Dis.* **46**, 863–870 (2005).
29. Eriksen, B. O. & Ingebretsen, O. C. The progression of chronic kidney disease: a 10-year population-based study of the effects of gender and age. *Kidney Int.* **69**, 375–382 (2006).
30. Verhave, J. C. *et al*. Cardiovascular risk factors are differently associated with urinary albumin excretion in men and women. *J. Am. Soc. Nephrol.* **14**, 1330–1335 (2003).
31. Barrera-Chimal, J. *et al*. Hsp72 is an early and sensitive biomarker to detect acute kidney injury. *EMBO Mol. Med.* **3**, 5–20 (2011).
32. Barrera-Chimal, J. *et al*. Mild ischemic Injury Leads to Long-Term Alterations in the Kidney: Amelioration by Spironolactone Administration. *Int. J. Biol. Sci.* **11**, 892–900 (2015).
33. Cattran, D. C. *et al*. The impact of sex in primary glomerulonephritis. *Nephrol Dial Transplant* **23**, 2247–2253, doi:10.1093/ndt/gfm919 (2008).
34. Attia, D. M. *et al*. Male gender increases sensitivity to renal injury in response to cholesterol loading. *Am. J. Physiol Renal Physiol* **284**, F718–F726 (2003).
35. Catanuto, P. *et al*. 17 beta-estradiol and tamoxifen upregulate estrogen receptor beta expression and control podocyte signaling pathways in a model of type 2 diabetes. *Kidney Int.* **75**, 1194–1201 (2009).
36. Erdely, A., Greenfeld, Z., Wagner, L. & Baylis, C. Sexual dimorphism in the aging kidney: Effects on injury and nitric oxide system. *Kidney Int.* **63**, 1021–1026 (2003).
37. Metcalfe, P. D. *et al*. Testosterone exacerbates obstructive renal injury by stimulating TNF-alpha production and increasing proapoptotic and profibrotic signaling. *Am. J. Physiol Endocrinol. Metab* **294**, E435–E443 (2008).
38. Muller, V. *et al*. Sexual dimorphism in renal ischemia-reperfusion injury in rats: possible role of endothelin. *Kidney Int.* **62**, 1364–1371 (2002).
39. Park, K. M., Kim, J. I., Ahn, Y., Bonventre, A. J. & Bonventre, J. V. Testosterone is responsible for enhanced susceptibility of males to ischemic renal injury. *J. Biol. Chem.* **279**, 52282–52292 (2004).
40. Pechere-Bertschi, A. & Burnier, M. Gonadal steroids, salt-sensitivity and renal function. *Curr Opin Nephrol Hypertens* **16**, 16–21, doi:10.1097/MNH.0b013e328011d7f6 (2007).
41. Robert, R. *et al*. Gender difference and sex hormone production in rodent renal ischemia reperfusion injury and repair. *J. Inflamm. (Lond)* **8**, 14 (2011).
42. Verhagen, A. M., Attia, D. M., Koomans, H. A. & Joles, J. A. Male gender increases sensitivity to proteinuria induced by mild NOS inhibition in rats: role of sex hormones. *Am. J. Physiol Renal Physiol* **279**, F664–F670 (2000).
43. Fekete, A. *et al*. Sex differences in heat shock protein 72 expression and localization in rats following renal ischemia-reperfusion injury. *Am. J. Physiol Renal Physiol* **291**, F806–F811 (2006).
44. Bazzano, T., Restel, T. I., Porfirio, L. C., Souza, A. S. & Silva, I. S. Renal biomarkers of male and female Wistar rats (Rattus norvegicus) undergoing renal ischemia and reperfusion. *Acta Cir Bras* **30**, 277–288, doi:10.1590/S0102-865020150040000007 (2015).
45. Fekete, A. *et al*. Sex differences in the alterations of Na(+), K(+)-ATPase following ischaemia-reperfusion injury in the rat kidney. *J Physiol* **555**, 471–480, doi:10.1113/jphysiol.2003.054825 (2004).
46. Moslemi, F. *et al*. Effect of angiotensin II type 1 receptor blockade on kidney ischemia/reperfusion; a gender-related difference. *J Renal Inj Prev* **5**, 140–143, doi:10.15171/jrip.2016.29 (2016).
47. Takayama, J. *et al*. Actinonin, a meprin inhibitor, protects ischemic acute kidney injury in male but not in female rats. *Eur J Pharmacol* **581**, 157–163, doi:10.1016/j.ejphar.2007.11.044 (2008).
48. Afyouni, N. E. *et al*. Preventive Role of Endothelin Antagonist on Kidney Ischemia: Reperfusion Injury in Male and Female Rats. *Int J Prev Med* **6**, 128, doi:10.4103/2008-7802.172549 (2015).
49. Iran-Nejad, A., Nematbakhsh, M., Eshraghi-Jazi, F. & Talebi, A. Preventive role of estradiol on kidney injury induced by renal ischemia-reperfusion in male and female rats. *Int J. Prev. Med* **6**, 22 (2015).
50. Aryamanesh, S., Ebrahimi, S. M., Abotaleb, N., Nobakht, M. & Rahimi-Moghaddam, P. Role of endogenous vitamin E in renal ischemic preconditioning process: differences between male and female rats. *Iran Biomed J* **16**, 44–51 (2012).
51. Giergiel, M., Lopucki, M., Stachowicz, N. & Kankofer, M. The influence of age and gender on antioxidant enzyme activities in humans and laboratory animals. *Aging Clin Exp Res* **24**, 561–569, doi:10.3275/8587 (2012).
52. Silbiger, S. R. & Neugarten, J. The impact of gender on the progression of chronic renal disease. *Am. J. Kidney Dis.* **25**, 515–533 (1995).
53. Singh, A. P., Singh, N. & Singh Bedi, P. M. Estrogen attenuates renal IRI through PPAR-gamma agonism in rats. *J Surg Res* **203**, 324–330, doi:10.1016/j.jss.2016.02.038 (2016).
54. Sugishita, K., Li, F., Su, Z. & Barry, W. H. Anti-oxidant effects of estrogen reduce [Ca2+]i during metabolic inhibition. *J Mol Cell Cardiol.* **35**, 331–336 (2003).
55. Ji, H. *et al*. Sex differences in renal injury and nitric oxide production in renal wrap hypertension. *Am. J. Physiol Heart Circ. Physiol* **288**, H43–H47 (2005).
56. Shoji, K., Tanaka, T. & Nangaku, M. Role of hypoxia in progressive chronic kidney disease and implications for therapy. *Curr. Opin. Nephrol. Hypertens.* **23**, 161–168 (2014).
57. Tanaka, S., Tanaka, T. & Nangaku, M. Hypoxia as a key player in the AKI-to-CKD transition. *Am J Physiol Renal Physiol* **307**, F1187–1195, doi:10.1152/ajprenal.00425.2014 (2014).
58. Fliegner, D. *et al*. Female sex and estrogen receptor-beta attenuate cardiac remodeling and apoptosis in pressure overload. *Am J Physiol Regul Integr Comp Physiol* **298**, R1597–1606, doi:10.1152/ajpregu.00825.2009 (2010).
59. Maric, C., Sandberg, K. & Hinojosa-Laborde, C. Glomerulosclerosis and tubulointerstitial fibrosis are attenuated with 17beta-estradiol in the aging Dahl salt sensitive rat. *J. Am. Soc. Nephrol.* **15**, 1546–1556 (2004).
60. Catanuto, P. *et al*. *In vivo* 17beta-estradiol treatment contributes to podocyte actin stabilization in female db/db mice. *Endocrinology* **153**, 5888–5895 (2012).
61. Meng, X. M., Nikolic-Paterson, D. J. & Lan, H. Y. TGF-beta: the master regulator of fibrosis. *Nat Rev Nephrol* **12**, 325–338, doi:10.1038/nrneph.2016.48 (2016).
62. Ziyadeh, F. N. *et al*. Long-term prevention of renal insufficiency, excess matrix gene expression, and glomerular mesangial matrix expansion by treatment with monoclonal antitransforming growth factor-beta antibody in db/db diabetic mice. *Proc. Natl. Acad. Sci. USA* **97**, 8015–8020 (2000).
63. Ma, L.-J. *et al*. Divergent effects of low versus high dose anti-TGF-Î² antibody in puromycin aminonucleoside nephropathy in rats. *Kidney International* **65**(1), 106–115 (2004).
64. Wang, W. *et al*. Signaling mechanism of TGF-beta1 in prevention of renal inflammation: role of Smad7. *J Am Soc Nephrol* **16**, 1371–1383, doi:10.1681/ASN.2004121070 (2005).
65. Klempt, N. D. *et al*. Hypoxia-ischemia induces transforming growth factor beta 1 mRNA in the infant rat brain. *Brain Res Mol Brain Res* **13**, 93–101 (1992).

66. Hunt, N. H. & Grau, G. E. Cytokines: accelerators and brakes in the pathogenesis of cerebral malaria. *Trends Immunol* **24**, 491–499 (2003).
67. Rosa, E. S. A., Guimaraes, M. A., Padmanabhan, V. & Lara, H. E. Prepubertal administration of estradiol valerate disrupts cyclicity and leads to cystic ovarian morphology during adult life in the rat: role of sympathetic innervation. *Endocrinology* **144**, 4289–4297, doi:10.1210/en.2003-0146 (2003).
68. Senft, A. P., Dalton, T. P. & Shertzer, H. G. Determining glutathione and glutathione disulfide using the fluorescence probe o-phthalaldehyde. *Anal Biochem* **280**, 80–86, doi:10.1006/abio.2000.4498 (2000).

Acknowledgements

The results presented in this paper have not been published previously in whole or in part, except as an abstract presented at the World Congress of Nephrology 2017 (Mexico City, Mexico). This project was supported by grants from the Mexican Council of Science and Technology (CONACyT) (235855, 235964 and 272390 to NAB) and from the National University of Mexico (IN223915 to NAB). This study was performed in partial fulfillment of the requirements for the PhD degree in the Biochemical Sciences of ILP at Universidad Nacional Autónoma de México and was supported by a scholarship from CONACyT-Mexico. We are grateful to Dr. Mariela Contreras for her helping with the animal care.

Author Contributions

I.L.P., E.Z. and N.A.B.: conceived and design the study. I.L.P., C.P.C., R.P.V., F.F., R.R.R., R.P., and G.R.G.: performed the experiments, C.P.C. and N.A.B.: histopathological analysis. I.L.P. and A.S.N.: Oxidative stress analysis. I.L.P., E.Z. and N.A.B.: analyzed the data. N.A.B. and G.G.: contributed reagents or analysis tools. I.L.P., G.G. and N.A.B.: wrote the article.

Additional Information

Supplementary information accompanies this paper at doi:10.1038/s41598-017-09630-2

Competing Interests: The authors declare that they have no competing interests.

Publisher's note: Springer Nature remains neutral with regard to jurisdictional claims in published maps and institutional affiliations.

Am J Physiol Renal Physiol 317: F1637–F1648, 2019.
First published October 14, 2019; doi:10.1152/ajprenal.00356.2019.

RESEARCH ARTICLE

Resilience to acute kidney injury in offspring of maternal protein restriction

Luis Enrique García-Ortuño,[1,2,3] Jonatan Barrera-Chimal,[1,4] Rosalba Pérez-Villalva,[1,2] Juan Antonio Ortega-Trejo,[1,2] Emma Luna-Bolaños,[1,2] Ixchel Lima-Posada,[1,2] Andrea Sánchez-Navarro,[1,2] Luis Reyes-Castro,[5] Gerardo Gamba,[1,2,6] Elena Zambrano,[5] and Norma A. Bobadilla[1,2]

[1]*Molecular Physiology Unit, Instituto de Investigaciones Biomédicas, Universidad Nacional Autónoma de México, Mexico City, Mexico;* [2]*Department of Nephrology, Instituto Nacional de Ciencias Médicas y Nutrición Salvador Zubirán, Mexico City, Mexico;* [3]*Department of Pathology, Facultad de Medicina Veterinaria y Zootecnia, Universidad Nacional Autónoma de México, Mexico City, Mexico;* [4]*Translational Medicine Unit, Instituto Nacional de Cardiología Ignacio Chávez, Mexico City, Mexico;* [5]*Reproductive Biology, Instituto Nacional de Ciencias Médicas y Nutrición Salvador Zubirán, Mexico City, Mexico; and* [6]*Tecnológico de Monterrey, Escuela de Medicina y Ciencias de la Salud, Monterrey, New Lion, Mexico*

Submitted 29 July 2019; accepted in final form 4 October 2019

García-Ortuño LE, Barrera-Chimal J, Pérez-Villalva R, Ortega-Trejo JA, Luna-Bolaños E, Lima-Posada I, Sánchez-Navarro A, Reyes-Castro L, Gamba G, Zambrano E, Bobadilla NA. Resilience to acute kidney injury in offspring of maternal protein restriction. *Am J Physiol Renal Physiol* 317: F1637–F1648, 2019. First published October 14, 2019; doi:10.1152/ajprenal.00356.2019.—Protein restriction (PR) during pregnancy induces morphofunctional alterations related to deficient nephrogenesis. We studied the renal functional and morphological significance of PR during pregnancy and/or lactation in adult male rat offspring and the repercussions on acute kidney injury (AKI) severity. Female rats were randomly assigned to the following groups: control diet during pregnancy and lactation (CC), control diet during pregnancy and PR diet during lactation (CR), PR during pregnancy and control diet during lactation (RC), and PR during pregnancy and lactation (RR). Three months after birth, at least 12 male offspring of each group randomly underwent either bilateral renal ischemia for 45 min [ischemia-reperfusion (IR)] or sham surgery. Thus, eight groups were studied 24 h after reperfusion: CC, CC + IR, CR, CR + IR, RC, RC + IR, RR, and RR + IR. Under basal conditions, the CR, RC, and RR groups exhibited a significant reduction in nephron number that was associated with a reduction in renal blood flow. Glomerular hyperfiltration was present as a compensatory mechanism to maintain normal renal function. mRNA levels of several vasoactive, antioxidant, and anti-inflammatory molecules were decreased. After IR, renal function was similarly reduced in all of the studied groups. Although all of the offspring from maternal PR exhibited renal injury, the magnitude was lower in the RC and RR groups, which were associated with faster renal blood flow recovery, differential vasoactive factors, and hypoxia-inducible factor-1α signaling. Our results show that the offspring from maternal PR are resilient to AKI induced by IR that was associated with reduced tubular injury and a differential hemodynamic response.

hypoxia-inducible factor-1α; nephron number; renal blood flow; vasoactive factors

INTRODUCTION

Evidence in animals and in humans has shown that alterations in the uterine environment during pregnancy have an impact on the development of vertebrate organisms (55, 62). In particular, it has been shown that protein restriction (PR) during pregnancy in rats produces renal morphofunctional alterations, characterized mainly by a decrease in nephron number and number of well-differentiated glomeruli in the offspring (9, 26, 35, 36, 60, 63, 68). In addition, there are ultrastructural changes, such as thickening of the glomerular basement membrane, disorganization of the fenestrated endothelium, and degeneration of podocyte pedicels (58). Although the influence of maternal PR (MPR) during gestation and/or lactation in offspring has been extensively studied in pathologies that include metabolic syndrome (37), glucose metabolism (14), and reproductive physiology (67), among others, little is known about its impact on renal function and against a renal injury hit during adulthood. Moreover, in the rat, nephrogenesis continues up to 10 days after birth, and the impact of the lactation period on renal physiology has not been explored.

The physiological consequences of a reduced number of nephrons in humans were first proposed by Brenner et al. (11) in 1988. After that, it was demonstrated that the reduction of nephrons, whether acquired or congenital, is associated with hypertrophy, hyperfiltration, and glomerular hypertension (32, 45). All of these alterations are observed in the early phase of life as compensatory mechanisms to fight against nephron number reduction and to maintain normal renal function. In the long term, however, they can favor an accelerated, progressive loss of nephrons that leads to chronic kidney disease and cardiovascular injury (31). Nonetheless, the impact of low birth nephron number on how the kidney deals with sudden renal pathological situations that may occur during adulthood remains largely unexplored.

Acute kidney injury (AKI) is a public health concern, and its clinical importance is due to its high morbidity and mortality rates (47). AKI affects 13.3 million people and contributes to ~1.7 million deaths per year (28). The pathophysiological mechanisms by which AKI occurs are complex and involve several factors, such as hypoxia (56), the establishment of an inflammatory process, and the production of reactive oxygen species (39, 46), which are the main mediators that injure the renal epithelium and endothelium (7, 21, 27, 33, 34, 52, 57).

Although the mechanisms by which MPR induces alterations in nephrogenesis and the long-term consequences of low

Address for reprint requests and other correspondence: N. A. Bobadilla, Unidad de Fisiología Molecular, Vasco de Quiroga No. 15, Tlalpan, Mexico City 14080, Mexico (e-mail: nab@iibiomedicas.unam.mx).

nephron numbers at birth have been established, to our knowledge, it has not yet been explored how this could impact the renal response to an AKI episode induced by ischemia-reperfusion (IR). With the consideration of the high worldwide prevalence of both malnutrition and AKI, in the present study, we decided to evaluate the effect of MPR during pregnancy and/or lactation on the severity of ischemic AKI in male offspring.

METHODS

All experiments involving animals were conducted in accordance with the National Institutes of Health *Guide for the Care and Use of Laboratory Animals* and with the Mexican Federal Regulation for animal reproduction, care, and experimentation (NOM-062-ZOO-2001). The study was approved by the Animal Care and Use Committee of the Instituto Nacional de Ciencias Médicas y Nutrición Salvador Zubirán (Mexico City, Mexico).

MPR model. Twelve female Wistar rats (age: 10–12 wk) were obtained from our animal facility. Rats were kept under controlled 12:12-h light-dark cycles at 21–22°C. Before being bred, female rats were maintained on a standard diet. Female rats were mated with male breeders (16 wk of age) until the day on which spermatozoa were present in the vaginal smear and was designated *day 0* of conception. Only female rats that were pregnant within 5 days of introduction of male rats were retained in the study. Pregnant rats were transferred to individual cages and randomly allocated to be fed either a 20% casein (control diet) or a 10% casein isocaloric diet (restricted diet) during the gestation. In the lactation period, the control diet-fed mother group was divided again into two subgroups: one-half continued to be fed with the control diet (CC group; $n = 3$) and the other half was fed with a restricted diet (CR group; $n = 3$). The restricted diet-fed mother group was also divided into two subgroups: one-half was fed a control diet (RC group; $n = 3$) and the other half was fed a restricted diet (RR group; $n = 3$). All litters studied were adjusted to 10 pups. Control and restricted diets were prepared in our laboratory following the American Institute of Nutrition's recommendation to supplement low-protein diets with L-cystine (Sigma). The components are shown in Table 1, and each diet was provided in the form of flat biscuits, as we have previously reported (66). Food and water were available ad libitum. The offspring were weaned at *postnatal day 21*, and only male offspring were studied and fed a commercial diet during all of their life. Male offspring were allocated to the following groups: CC ($n = 12$), CR ($n = 12$), RC ($n = 12$), and RR ($n = 12$). In turn, each offspring group was subdivided into two groups: one-half underwent IR injury (CC + IR, CR + IR, RC + IR, and RR + IR groups) and the other half underwent sham surgery (CC, CR, RC, and RR groups). Surgeries were induced at 12–14 wk of age.

Renal injury induced by IR in offspring. Rats were anesthetized with an intraperitoneal injection of pentobarbital sodium (30 mg/kg) and placed on a heating pad to maintain body temperature at 37°C. A laparotomy was performed to access the retroperitoneum and to dissect the renal vascular hilum to interrupt blood flow to the kidney by placing a nontraumatic vascular clamp in each renal hilum for 45 min. Ischemia was verified visually by changes in kidney color. Reperfusion was achieved by release of the clamps. Animals were sutured from the abdominal wall with 3-0 Vicryl (muscle) and 3-0 silk (skin). The same procedure was performed in the sham-operated groups with the exception of the placement of the vascular clamp in the renal hilum. After recovery, rats were placed in metabolic cages with free access to water for 16–18 h for urine collection. Urinary protein excretion was determined from the urine collections after the surgery using the turbidimetric method with trichloroacetic acid.

Table 1. *Composition of the two isocaloric diets*

Components	Control Diet, %	Restricted Diet, %
Casein	20	10
Cystine	0.3	0.15
Choline	0.165	0.165
Vitamin mix	1	1
Mineral mix	5	5
Cellulose	5	5
Corn oil	5	5
Carbohydrates		
Corn starch	31.76	37.34
Dextrose	31.76	37.34
kcal/g Diet	4	4

Renal functional measurements. Twenty-four hours after surgery, rats were anesthetized again with pentobarbital sodium (30 mg/kg) and placed on a homeothermic table. The femoral arteries were catheterized with polyethylene tubing (PE-50). Mean arterial pressure (MAP) was monitored with a pressure transducer (model P23DB, Gould) and recorded on a polygraph (Grass Instrument, Quincy, MA). To record renal blood flow (RBF), the left kidney artery was dissected, and an ultrasound transit-time flow probe filled with ultrasonic coupling gel (Transonic Flow Probe, Transonic, New York, NY) was placed around the artery (HR Lubricating Jelly, Carter-Wallace, New York, NY). At the end of the experiment, a blood sample was taken from the femoral artery. Urine and serum creatinine concentrations were measured with the QuantiChrom creatinine assay kit (DICT-500, BioAssay Systems) following the manufacturer's instructions. Renal creatinine clearance (CrCl) was calculated according to the following formula: $CrCl = (U \times V)/P$, where U is the creatinine concentration in the urine, V is the urine flow rate, and P is the plasma creatinine concentration. The filtration fraction was estimated as the ratio of CrCL and renal plasma flow.

Urinary biomarkers of ischemic renal injury. Urinary heat shock protein 72 (HSP72) and urinary kidney injury molecule-1 (KIM-1) levels were detected by Western blot analysis. Briefly, each urine sample was diluted 1:10 in 0.9% saline solution, and 10 μL of each dilution was loaded and resolved by 8.5% SDS-PAGE and electroblotted onto PVDF membranes. Membranes were incubated overnight at 4°C with mouse HSP72 antibody (1:5,000 dilution, Enzo Life Sciences) or KIM-1 antibody (1:1,000 dilution, Biorbyt) and then incubated with secondary antibody, namely, horseradish peroxidase-conjugated goat anti-mouse IgG for HSP72 (1:5,000, Santa Cruz Biotechnology) and horseradish peroxidase-conjugated goat anti-rabbit IgG for KIM-1 (1:15,000, Biorbyt), at room temperature for 90 min. Proteins were detected using a commercial chemiluminescence kit (Millipore).

Light microscopy analysis. Once the physiological parameters were recorded, the left kidney was perfused through the femoral catheter with 0.9% NaCl and then with 4% neutral-buffered formalin, and perfusion was continued until fixation was completed. Renal tissue was embedded in paraffin, and 3-μm sections were stained with periodic acid-Schiff. Twelve cortical fields (magnification: ×100) were recorded from each kidney slide using a digital camera incorporated in a Nikon light microscope. Nephron number was estimated by glomerular counting in 10,000-μm^2 field. The glomerular area was measured in at least 10 glomeruli/rat from the microphotographs with the help of Eclipse Net software, as we have previously reported (41, 48). In each microphotograph, injured tubules were counted. Tubular damage was characterized by loss of the brush border, lumen dilation, and detachment of epithelial tubular cells from the basement membrane. All analyses were blinded.

Gene expression analysis. The right kidney was removed and quickly frozen. Total renal cortex RNA was isolated from the kidneys using the TRIzol method (Invitrogen, Carlsbad, CA), and RNA integrity was checked by 1% agarose gel electrophoresis. Reverse transcription was carried out with 1 μg total RNA and 200 units Moloney murine leukemia virus reverse transcriptase (Invitrogen). mRNA levels of the angiotensin II type 1 (AT_1) receptor, endothelin,

endothelin type A (ET_A) receptor, endothelin type B (ET_B) receptor, endothelial nitric oxide synthase (eNOS), catalase, glutathione, peroxidase, SOD1, hypoxia-inducible factor (HIF)-1α, IL-6, TNF-α, and VEGF were quantified by real-time PCR on an ABI Prism 7300 Sequence Detection System (TaqMan, Applied Biosystems, Foster City, CA). Probes were ordered as the following kits: AT_1 receptor, Rn00561409_S1; prepro-endothelin-1, Rn00561129_m1; ET_A receptor, Rn00561129_m1; ET_B receptor, Rn00569139_m1; eNOS, Rn02132634_s1; catalase, Rn00560930_m1; glutathione peroxidase (Gpx), Rn00577994_g1; SOD1, Rn00566938_m1; HIF-1α, Rn00577560_m1; IL-6, Rn01410330_m1; TNF-α, Rn99999017_m1; and VEGF, Rn01511601_m1. 18S mRNA levels were used to normalize the data.

Statistics. Results are presented as means ± SE. Data were analyzed by one-way ANOVA, and differences among the groups were determined by the Bonferroni post hoc test for multiple comparisons. Basal parameters in all of the groups, tubular injury, and percent differences between each experimental group and the control group were determined by Dunnett's multiple-comparisons post hoc test. Differences in the distribution of the glomerular areas were evaluated by contingency analysis, and differences were assessed using a χ^2-test with the Yates correction. Differences were considered statistically significant at $P < 0.05$.

RESULTS

Effect of MPR on kidney physiology and glomerular number of offspring. First, we studied whether MPR modifies basal renal function parameters in rat male offspring at 12–16 wk of age. A similar body weight was observed among the groups [CC group: 295 ± 13.8 g, CR group: 302 ± 9.1 g, RC group: 307 ± 16.6 g, and RR group: 299 ± 13.9 g, P = not significant (NS)] as well as in kidney weight (CC group: 1.32 ± 0.09 g, CR group: 1.30 ± 0.05 g, RC group: 1.39 ± 0.05 g, and RR group: 1.31 ± 0.04 g, P = NS). No significant differences in MAP (Fig. 1*A*) or proteinuria (Fig. 1*B*) in the offspring of any of the studied groups were recorded. Interestingly, the CR, RC, and RR groups exhibited a significant decrease in the number of nephrons compared with the control group of 11.2%, 15.7%, and 16.2%, respectively (Fig. 1*C*). In addition, there was a significant reduction of RBF in all of the offspring from protein-restricted mothers compared with the control group (Fig. 1*D*). Nevertheless, CrCl remained within normal values in all of the studied groups (Fig. 1*E*). It is interesting to note that the reduction of nephrons in the MPR groups induced a state of glomerular hyperfiltration that was revealed by an increased renal filtration fraction (Fig. 1*F*), which might explain the normal renal function.

Vasoactive, antioxidant, and inflammatory factors in mRNA levels. mRNA levels of the AT_1 receptor, prepro-endothelin-1, ET_A receptor, and ET_B receptor are shown in Fig. 2. A significant decrease in AT_1 receptor, prepro-endothelin-1, and their receptors was detected in all of the offspring from protein-restricted mothers compared with the control group, except for ET_B receptor mRNA levels in the CR group.

mRNA levels of eNOS, HIF-1α, antioxidant enzymes, and proinflammatory cytokines are shown in Fig. 3. eNOS mRNA levels were similar among the studied groups (Fig. 3*A*). A significant reduction in mRNA levels of GPx, catalase, and HIF-1α was found in all offspring from protein-restricted mothers (Fig. 3, *B–D*, respectively). Although IL-6 mRNA levels remained unchanged among the studied groups (Fig. 3*E*), we observed a statistically significant reduction in TNF-α mRNA levels in male rat offspring from protein-restricted mothers compared with the control group (Fig. 3*F*).

Influence of MPR on AKI severity in offspring. Once the effect of MPR on the basal renal function of the offspring was characterized, we evaluated the impact of the lower nephron number induced by MPR on the severity of an AKI episode. The renal injury induced by renal bilateral ischemia in the studied groups is represented as the percent change relative to the basal value of their respective control groups.

After 24 h of reperfusion, offspring from maternal unrestricted rats showed characteristic renal injury, as we have previously reported (6, 30, 48, 49), that is, a significant increase in proteinuria and a decrease in RBF and CrCl, together with renal inflammation, denoted by a significant increase in kidney weight (Fig. 4, *A–D*). Although all offspring from

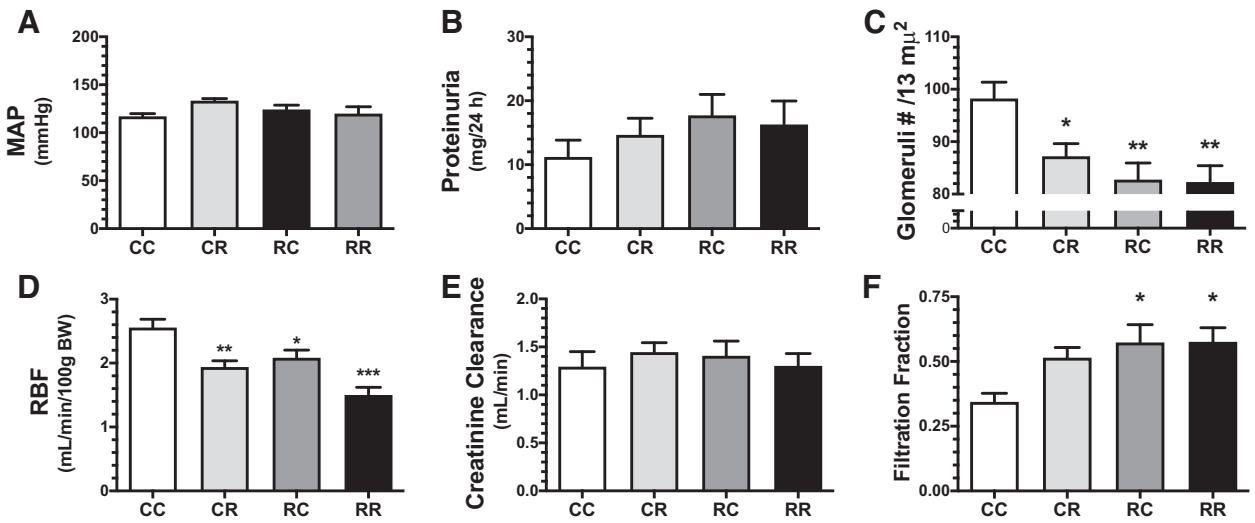

Fig. 1. Renal physiological parameters and glomerular number in offspring from control diet-fed mothers (CC group) or mothers with protein restriction during lactation (CR group), gestation (RC group), or both (RR group). *A*−*F*: mean arterial pressure (MAP; *A*), proteinuria (*B*), glomeruli number (*C*), renal blood flow (RBF; *D*), creatinine clearance (*E*), and filtration fraction (*F*). BW, body weight. Data are shown as means ± SE, n = at least 6 rats/group. *$P < 0.05$, **$P < 0.01$, and ***$P < 0.001$ vs. the CC group.

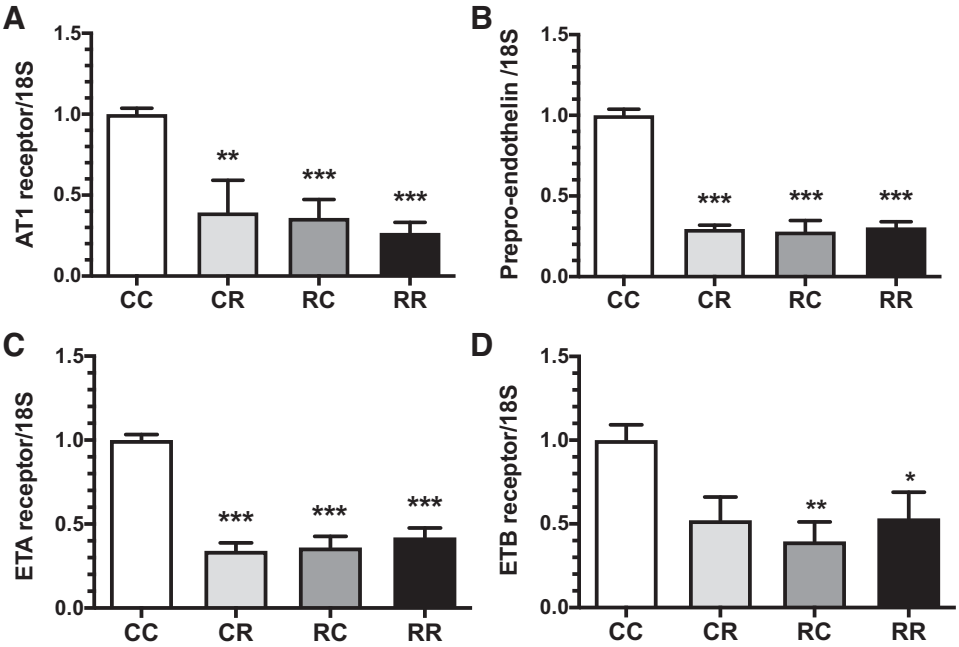

Fig. 2. mRNA levels of vasoactive molecules in kidney tissue of offspring from control diet-fed mothers (CC group) or mothers with protein restriction during lactation (CR group), gestation (RC group), or both (RR group). *A*−*D*: angiotensin II type 1 (AT1) receptor (*A*), prepro-endothelin (*B*), endothelin type A (ET_A) receptor (*C*), and endothelin type B (ET_B) receptor (*D*). Data are shown as means ± SE, n = at least 4 rats/group. *$P < 0.05$, **$P < 0.01$, and ***$P < 0.001$ vs. the CC group.

protein-restricted mothers exhibited proteinuria, renal dysfunction, and renal inflammation, the magnitude of the changes in proteinuria and kidney weight was significantly lower in the RC + IR and RR + IR groups compared with the control group (Fig. 4, *A*, *B*, and *D*). Proteinuria increased significantly in all groups compared against their respective control groups, except for the RR + IR group (Fig. 4*A*). CrCl decreased in a similar way in all of the studied groups (Fig. 4*B*); in other words, the strength of renal dysfunction induced by IR was similar in all of the studied groups. Interestingly, the renal hypoperfusion induced by IR was not observed in all MPR groups when compared against their respective control groups (Fig. 4*C*). The increase in renal weight was lower in the RR + IR group (Fig. 4*D*). In addition, the filtration fraction was calculated as a ratio of glomerular filtration rate to RBF after the ischemic insult, and no statistical differences among the groups were observed: 0.020 ± 0.010 for the CC + IR group, 0.012 ± 0.003 for the CR + IR group, 0.014 ± 0.0036 for the RC + IR group, and 0.022 ± 0.012 for the RR + IR group (P = NS). The improvement in RBF, recorded just 24 h after renal ischemia in MPR offspring, was not evidenced in the

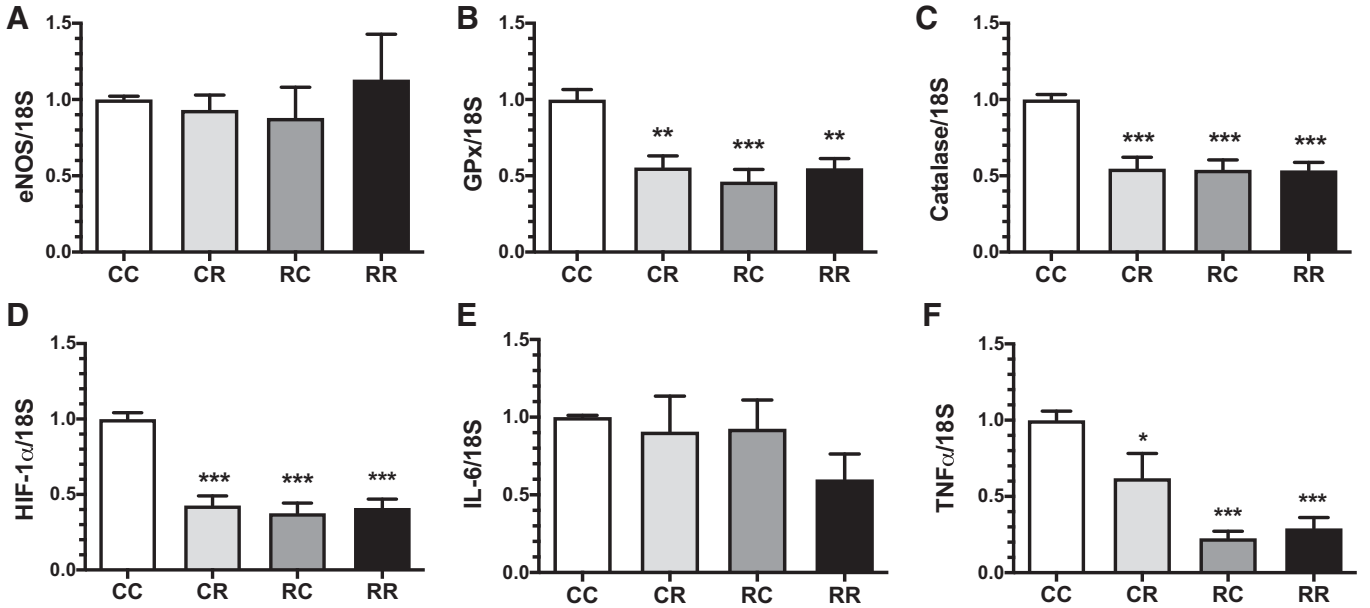

Fig. 3. mRNA levels of anti-inflammatory and antioxidant molecules in kidney tissue of offspring from control diet-fed mothers (CC group) or mothers with protein restriction during lactation (CR group), gestation (RC group), or both (RR group). *A*−*F*: endothelial nitric oxide synthase (eNOS; *A*), glutathione peroxidase (Gpx; *B*), catalase (*C*), hypoxia-inducible factor (HIF)-1α (*D*), IL-6 (*E*), and TNF-α (*F*). Data are shown as means ± SE, n = at least 6 rats/group. *$P < 0.05$, **$P < 0.01$, and ***$P < 0.001$ vs. the CC group.

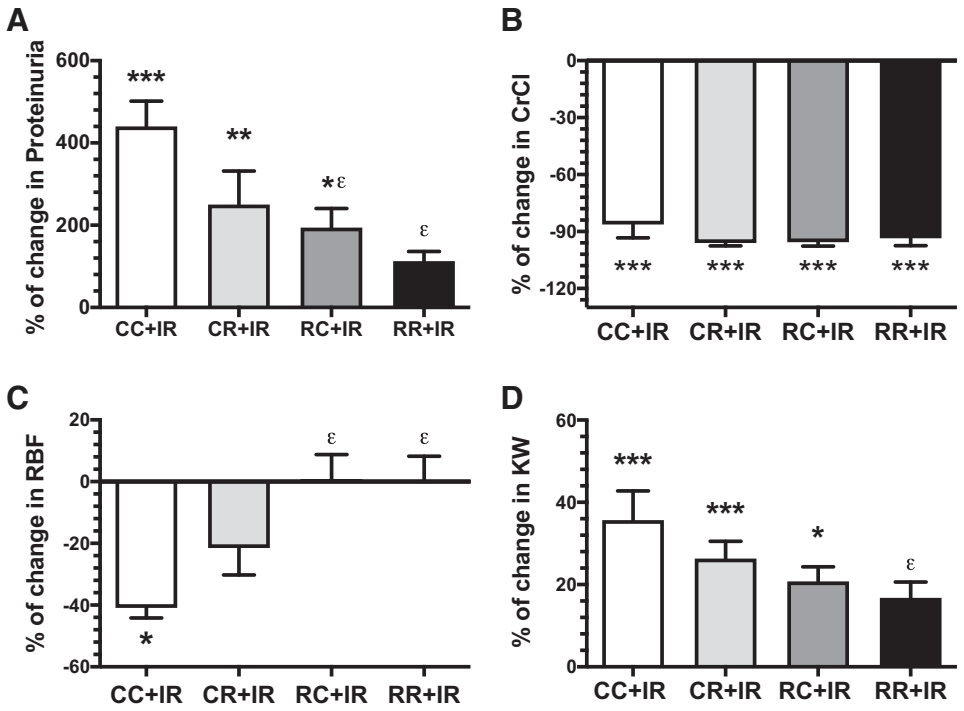

Fig. 4. Severity of acute renal injury induced by ischemia-reperfusion (IR) in offspring from control diet-fed mothers (CC group) or mothers with protein restriction during lactation (CR group), gestation (RC group), or both (RR group). *A*−*D*: proteinuria (*A*), creatinine clearance (CrCl; *B*), renal blood flow (RBF; *C*), and kidney weight (KW; *D*). Data are shown as means ± SE of the percentage of change based on the control group (without ischemia); n = at least 6 rats/group. $^{*}P < 0.05$, $^{**}P < 0.01$, and $^{***}P < 0.001$ vs. control of each group; $^{\varepsilon}P < 0.05$ vs. the CC + IR group.

filtration fraction; perhaps CrCl reflects the renal function along 24 h after ischemia.

Tubular epithelial injury induced by IR in offspring with MPR. The tubular epithelium injury induced by IR was evaluated by histopathological analysis and quantification of sensitive urinary biomarkers (HSP72 and KIM-1). To determine the percentage of tubular damage, periodic acid-Schiff-stained sections of the kidney were analyzed. Figure 5 shows representative microphotographs of renal tissue from the control group (Fig. 5*A*), CC + IR group (Fig. 5*B*), and MPR groups

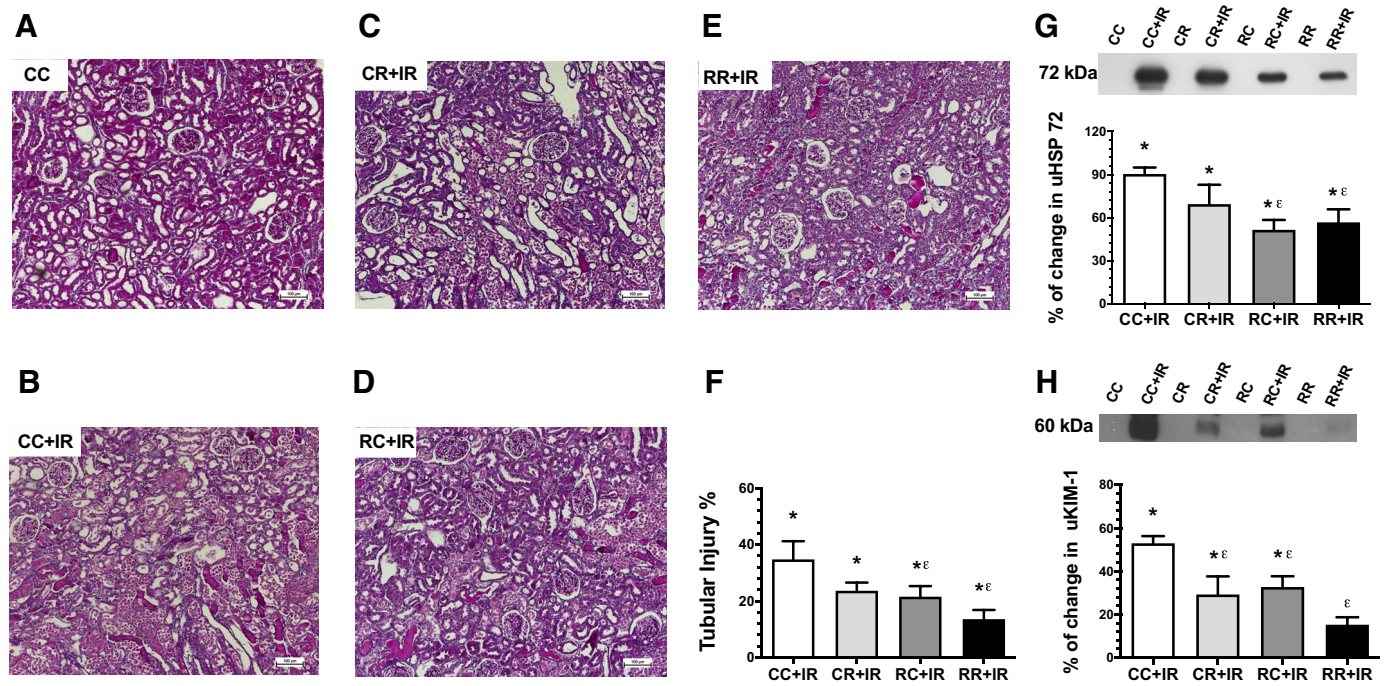

Fig. 5. Tubular epithelial injury induced by ischemia-reperfusion (IR) in offspring from control diet-fed mothers (CC group) or mothers with protein restriction during lactation (CR group), gestation (RC group), or both (RR group). *A*–*E*: representative images of kidney histological sections stained with periodic acid-Schiff. Magnification: ×100. *A*: CC group; *B*: CC + IR group; *C*: CR + IR group; *D*: RC + IR group; *E*: RR + IR group. *F*−*H*: percentage of tubular injury (*F*), urinary heat shock protein 72 (uHSP72) levels by Western blot analysis (*G*), and urinary kidney injury molecule-1 (uKIM-1) levels by Western blot analysis (*H*). *G* and *H*, *top*: representative blots; *bottom*: densitometric analyses. Data are shown as means ± SE of the percentage of change based on the control group (without ischemia); n = at least 5 rats/group. $^{*}P < 0.05$ vs. control of each group; $^{\varepsilon}P < 0.05$ vs. the CC + IR group.

that underwent ischemia (CR + IR, RC + IR, and RR + IR group; Fig. 5, *C–E*, respectively). Tubular injury was characterized by cell death, epithelial cell detachment toward the lumen of the tubule, and the presence of tubular casts. Consistent with our observations at the physiological level, the RC + IR and RR + IR groups showed a significantly lower percentage of tubular injury compared with the CC + IR group (Fig. 5*F*). Urinary HSP72 and KIM-1 was undetectable in all of the sham-operated groups. Urinary HSP72 levels increased significantly in all groups after IR-induced injury; however, the increase in the RC + IR and RR + IR groups was significantly lower than that observed in the CC + IR group (Fig. 5*G*). A similar behavior was observed for urinary levels of KIM-1, except for the RR + IR group, which despite its increase, was not significantly different compared with its respective sham-operated group. In all of the rats from protein-restricted mothers, the increase in urinary KIM-1 was significantly lower compared with the CC + IR group (Fig. 5*H*).

Influence of IR in the area of glomerular tufts in offspring with MPR. In previous studies from our laboratory using the model of cyclosporine nephrotoxicity, in which renal vasoconstriction is the main player, glomerular constriction was demonstrated by the reduction in glomerular diameter (41), whereas glomerular hypertrophy was evidenced by the increment in glomerular diameter (48). In the present study, we evaluated glomerular contraction by measuring the area of glomerular tufts in offspring with MPR. Figure 6*A* shows a histogram of glomerular tuft areas for the CC group, in which a Gaussian distribution was observed. In contrast, in the CC + IR group, there was a decrease in the proportion of glomeruli of normal and greater areas corresponding to the intervals of 5,001–7,000 and 7,001–9,000 μm^2, which showed values of 15.9% and 3.9%, respectively, unlike the CC group, which presented percentages of 41.8% and 23.5%, respectively (Fig. 6, *A* and *B*). Consequently, there was a significant increase in the percentage of glomeruli with smaller areas of 3,001–5,000

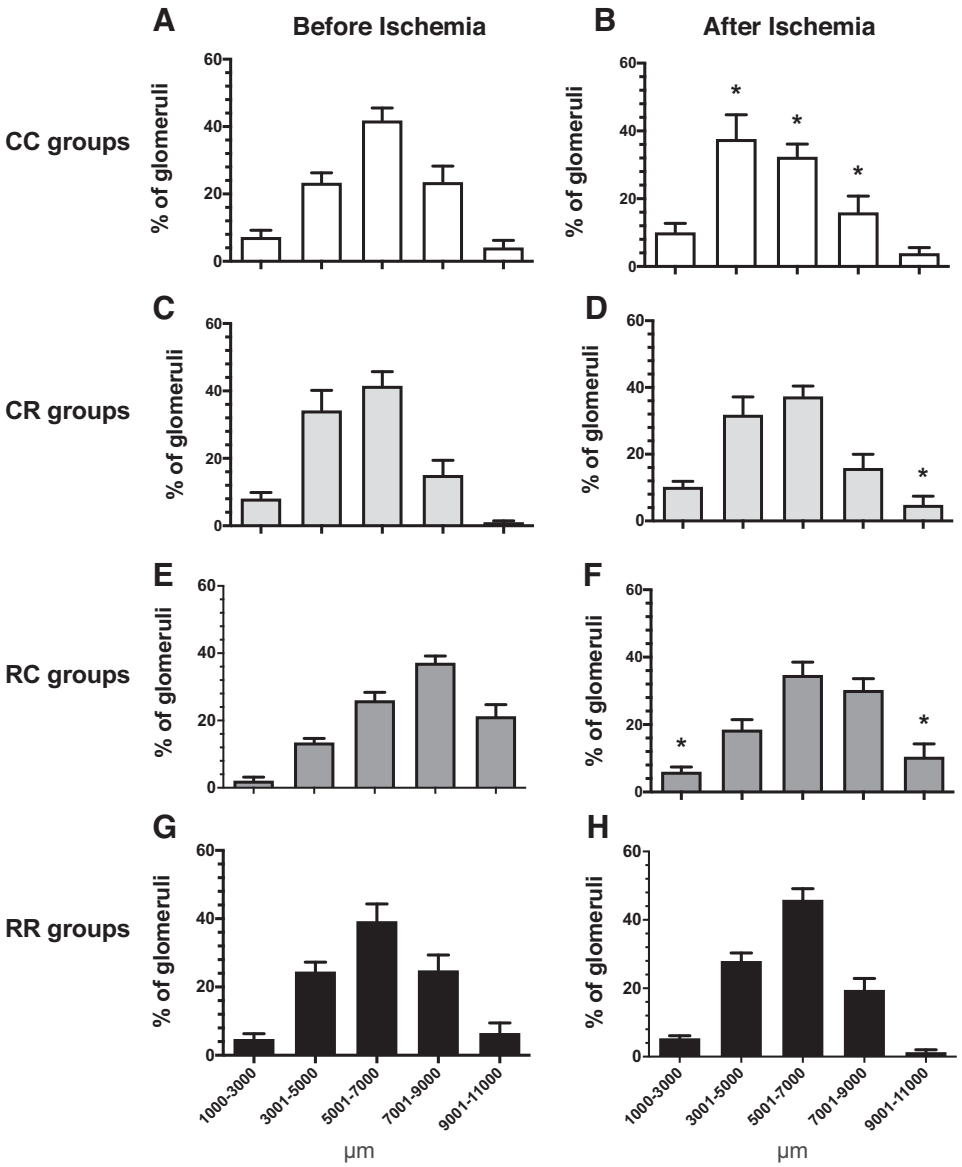

Fig. 6. Influence of acute kidney injury induced by ischemia-reperfusion (IR) in the glomerular tuft area of offspring from control diet-fed mothers (CC group) or mothers with protein restriction during lactation (CR group), gestation (RC group), or both (RR group). *A*, *C*, *E*, and *G*: CC, CR, RC, and RR groups, respectively, before IR. *B*, *D*, *F*, and *H*: CC + IR, CR + IR, RC + IR, and RR + IR groups, respectively, after IR. Data are shown as means ± SE; n = at least 6 rats/group. *$P <$ 0.05 vs. rats without ischemia for each group and interval.

μm^2 (37.6%) with respect to the control group (23.3%). These results suggest that after IR, the control group exhibited glomerular hypoperfusion. Interestingly, the offspring of protein-restricted mothers (Fig. 6, *D*, *F*, and *H*) showed no relevant alterations in glomerular distribution with respect to their own sham-operated group (Fig. 6, *C*, *E*, and *G*), indicating that these animals have a better adaptation to damage by IR and in accord with the early RBF recovery observed in these groups.

mRNA levels of vasoactive, antioxidant, and inflammatory factors after AKI in male rat offspring from protein-restricted mothers. The renal injury induced by IR was associated with a significant reduction in the AT_1 receptor in the CC + IR group (−80%) that was expressed as the percent change relative to its respective sham-operated group (CC group), whereas in the offspring of protein-restricted mothers, the reduction was significantly less than in the CC + IR group at ~40% (Fig. 7*A*). The percent change in mRNA levels of prepro-endothelin-1 (Fig. 7*B*) was not different among the studied groups. In contrast, ET_A receptor mRNA levels increased significantly in the offspring of MPR groups with respect to their respective sham-operated groups, except for the RR + IR group. This effect was not observed in the CC + IR group (Fig. 7*C*). ET_B receptor mRNA levels decreased significantly in the CC + IR group. In the rest of the groups, this reduction was not significant (Fig. 7*D*).

eNOS mRNA levels were not altered in any studied group (Fig. 8*A*). In the CC + IR group, GPx mRNA levels decreased by 68.7% with respect to its sham-operated group (CC group); this marked decrease was not observed in the rest of the rats from MPR groups (Fig. 8*B*). Similarly, SOD1 mRNA levels were significantly reduced in the CC + IR and CR + IR groups and to a lesser extent in the RR + IR group (Fig. 8*C*). Catalase mRNA levels were significantly reduced in all studied groups by the same magnitude (Fig. 8*D*). IL-6 mRNA levels increased significantly in all groups compared with their respective sham-operated groups (Fig. 8*E*). TNF-α mRNA levels increased significantly in all MPR groups but not in the CC + IR group (Fig. 8*F*).

mRNA levels of HIF-1α and its target gene VEGF were analyzed, as is shown in Fig. 9. In the CC + IR group, a significant decrease in HIF-1α mRNA levels was observed. Whereas the experimental groups exhibited the opposite behavior, HIF-1α mRNA levels increased significantly in all offspring from MPR groups (Fig. 9*A*). The impact of this difference was evidenced in VEGF mRNA levels, which were significantly reduced in the CC + IR group, an effect that was not seen in the CR + IR, RC + IR, and RR + IR groups (Fig. 9*B*).

DISCUSSION

The present study was designed to assess the impact of an AKI episode in male rat offspring derived from protein-restricted mothers during gestation and/or lactation. Before the induction of renal injury, it was essential to understand the basal renal physiology of all of the studied offspring groups. First, we confirmed a significant reduction in nephron number in all of the male rat offspring from protein-restricted mothers during gestation, as has been previously reported (8, 16, 19, 24, 25, 32, 42). In all these studies, however, the influence of PR during lactation was not evaluated. Our study is the first to address this issue, finding that the RC and RR groups exhibited a greater reduction in nephron number compared with the CR group, suggesting that MPR, during gestation, affects more nephrogenesis than lactation. The importance of nephron number at birth is based on growing evidence in humans and animals, which emphasizes that the lower the nephron number, the higher the risk of kidney and cardiovascular diseases in adult life (8, 16, 19, 25, 32, 42, 45, 61).

A particularly interesting finding was the significant reduction in RBF in the offspring from protein-restricted mothers, which could result from the reduced nephron number. This finding has also been recently reported in a murine model with

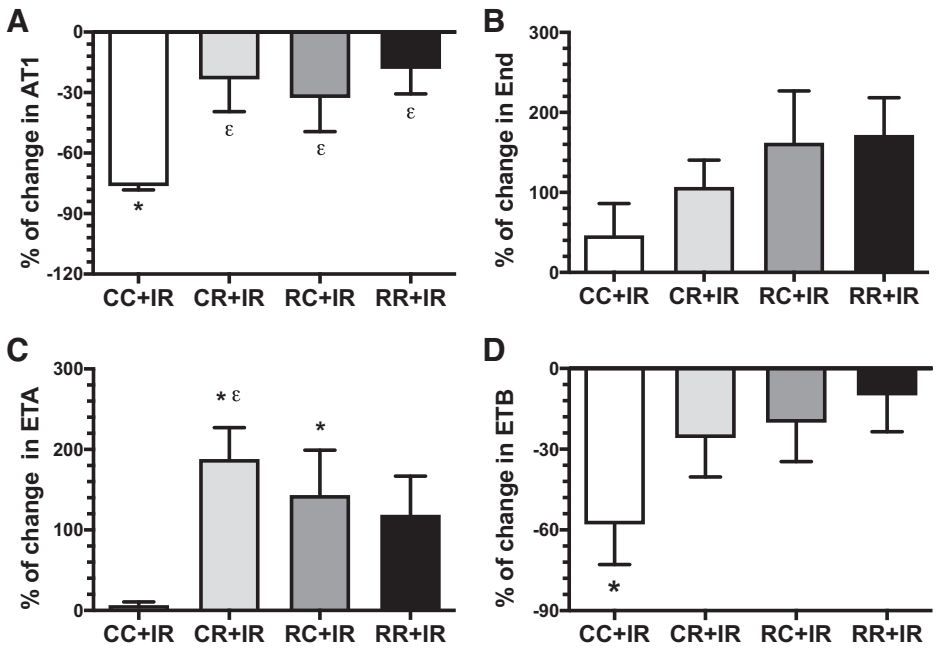

Fig. 7. mRNA levels of vasoactive molecules in kidney tissue of offspring from control diet-fed mothers (CC group) or mothers with protein restriction during lactation (CR group), gestation (RC group), or both (RR group) after acute renal injury induced by ischemia-reperfusion (IR). *A*−*D*: angiotensin II type 1 (AT_1) receptor (*A*), prepro-endothelin (End; *B*), endothelin type A (ET_A) receptor (*C*), and endothelin type B (ET_B) receptor (*D*). Data are shown as means ± SE of the percentage of change based on the control group (without ischemia); n = at least 5 rats/group. $^*P < 0.05$ vs. control of each group; $^\varepsilon P < 0.05$ vs. the CC + IR group.

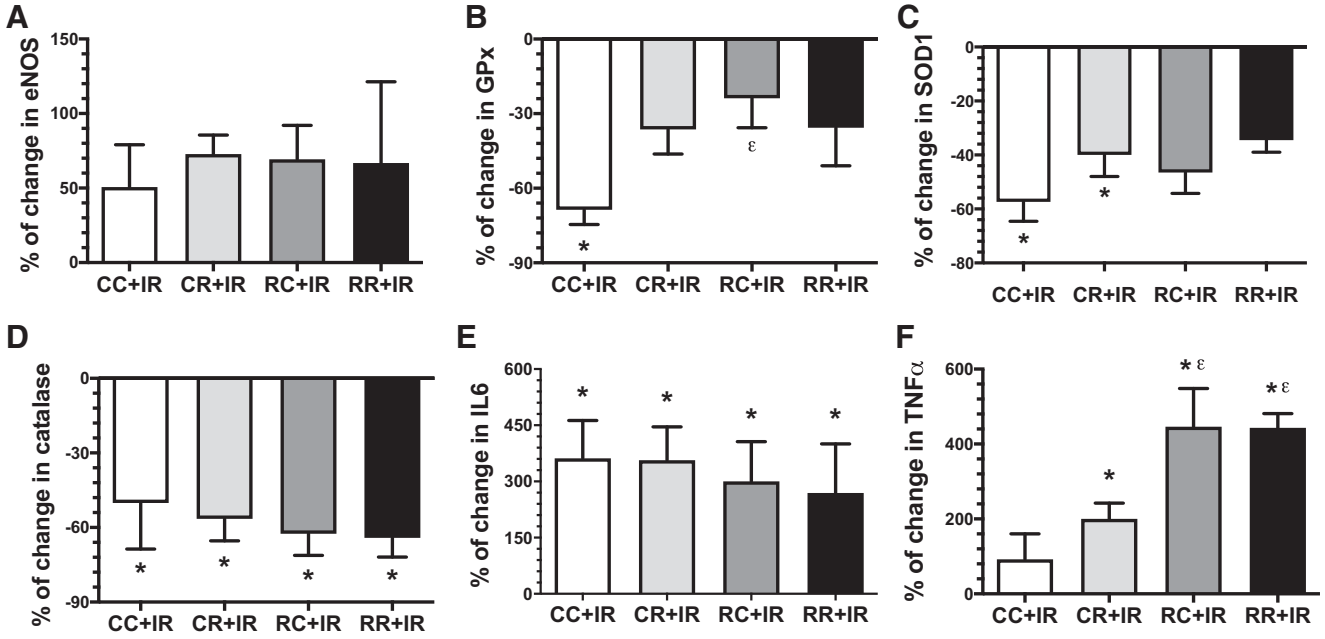

Fig. 8. mRNA levels of anti-inflammatory and antioxidant molecules in kidney tissue of offspring from control diet-fed mothers (CC group) or mothers with protein restriction during lactation (CR group), gestation (RC group), or both (RR group) after acute renal injury induced by ischemia-reperfusion (IR). *A*−*F*: endothelial nitric oxide synthase (eNOS; *A*), glutathione peroxidase (GPx; *B*), SOD1 (*C*), catalase (*D*), IL-6 (*E*), and TNF-α (*F*). Data are shown as means ± SE of the percentage of change based on the control group (without ischemia); n = at least 5 rats/group. $^{*}P < 0.05$ vs. control of each group; $^{\varepsilon}P < 0.05$ vs. the CC + IR group.

caloric restriction and PR and was associated with endothelial dysfunction and reduced vascular density (1, 5). Despite the lack of alterations in MAP, proteinuria, or CrCl, the greater filtration fraction in the experimental groups suggested a hyperfiltration state that allowed for the maintenance of renal function within normal parameters. This glomerular hyperfiltration has been reported as a deleterious hemodynamic mechanism that leads to progressive loss of nephrons in adult life (20, 22, 31, 32, 45).

RBF regulation is complex, and it is determined by the vascular tone of pre- and postglomerular arterioles, which are finely controlled by several vasoactive factors (12). In the present study, we explored main vasoactive factor mRNA levels (eNOS, prepro-endothelin-1 and its receptors, and AT_1 receptor), antioxidant enzymes (catalase, SOD1, and GPx), and proinflammatory molecules (TNF-α and IL-6). In support of our results, Woods et al. (63) have shown that maternal restriction induces a significant reduction in renal renin concentration and renal tissue angiotensin II levels in newborn pups. Thus, a consistent result in this study was that all offspring from MPR groups exhibited a significant decrease in mRNA levels of most of the studied molecules. This could be explained by the theory of the "thrifty phenotype," proposed by Hales and Barker (17), which has been demonstrated in human fetuses under malnutrition during pregnancy, where metabolic adaptations occur as a strategy to survive and save energy expenditure (43, 44). It is increasingly evident that the response to fetal malnutrition drives not only the selective preservation of essential organs for life but also induces advantageous metabolic adaptations for postnatal survival. Therefore, the thrifty phenotype is not only thrifty with respect to prenatal life but also in the efficient conservation of all nutritional and metabolic resources after birth. The poorly fed mother provides the fetus with a nutritional environment in which it will be born and will have to adapt to survive in the best way. This is a process that leads to postnatal metabolism adapted to survival in conditions where poor nutrition is in place. Similar observations have been made regarding exposure to cold. The offspring of sheep exposed to cold during pregnancy are, during delivery, better adapted to respond to adverse cold

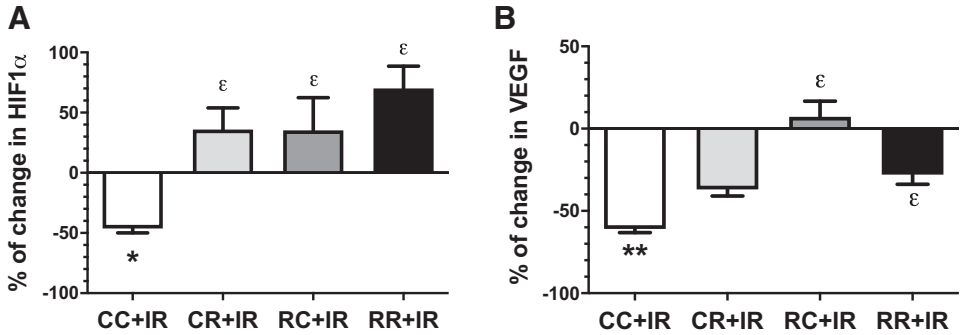

Fig. 9. Signaling of hypoxia-inducible factor (HIF)-1α in kidney tissue of offspring from control diet-fed mothers (CC group) or mothers with protein restriction during lactation (CR group), gestation (RC group), or both (RR group) after acute renal injury induced by ischemia-reperfusion (IR). HIF-1α (*A*) and VEGF (*B*) mRNA levels are shown. Data are shown as means ± SE of the percentage of change based on the control group (without ischemia); n = at least 5 rats/group. $^{*}P < 0.05$ and $^{**}P < 0.01$ vs. control of each group; $^{\varepsilon}P < 0.05$ vs. the CC + IR group.

conditions after birth (4, 15). However, we cannot exclude the possibility that lesser mRNA levels of the molecules studied could result from the lesser number of nephrons observed in offspring from protein-restricted mothers.

Originally, we hypothesized that due to the known reduction in nephron number of offspring from protein-restricted mothers, there would be more susceptibility to a second challenge, such as kidney damage induced by IR. However, we observed the opposite; although the offspring of MPR groups presented renal dysfunction similar to the control group, the structural damage induced by IR was minor, particularly in the RC + IR and RR + IR groups compared with the CC + IR group. These results were also confirmed by lower proteinuria, lower levels of kidney injury biomarkers (urinary HSP72 and urinary KIM-1), and less inflammation (renal weight). These data suggest that PR during gestation has a deeper impact on kidney development and adaptation than those observed with PR during lactation.

Here, we propose that offspring from protein-restricted mothers during pregnancy or pregnancy and lactation are resilient compared with the control group. Resilience can be considered as the ability of an organism to adapt adequately after exposure to some adverse or stressful circumstances (2, 10). According to our results, a first explanation of the lower severity of AKI is that these animals had a better ability to recover RBF, which was not only evident in the direct measurement of RBF but also structurally. Therefore, after renal IR, there was a reduction in the glomerular tuft diameter in the CC + IR group, indicating glomerular vasoconstriction and renal hypoperfusion, an effect that was not observed in the experimental groups after 24 h of renal ischemia (Fig. 6). This faster recovery of RBF in the offspring of MPR groups makes an important difference, because renal perfusion and oxygenation play a central role in the installation and extent of AKI (7, 34, 40, 57, 69).

We explored some mechanisms that may influence the lower severity of AKI observed in the progeny of protein-restricted mothers. The ischemic injury in the control group (CC + IR group) was associated with a significant reduction in AT_1 receptor and ET_B receptor mRNA levels compared with the control sham-operated group. In contrast, these effects were not observed in the offspring of MPR groups; instead, there was a significant increase in ET_A receptor mRNA levels. This differential pattern, found in vasoactive molecule mRNA levels, promoted faster RBF recovery, which was different from the control group. However, studies of renal hemodynamics by micropuncture would be helpful for evaluating the afferent and efferent resistances and their contribution to RBF under these MPR conditions.

Acute renal injury induced by IR is characterized by a persistent state of hypoxia that contributes to the pathophysiological mechanisms of tubular and endothelial damage (3). The kidneys, and particularly the renal tubules, are highly demanding of oxygen, which makes them vulnerable to hypoxia (53). One of the cellular responses to hypoxia corresponds to the induction of HIF-1α, which is a master transcription factor that, when activated by hypoxia, induces a variety of adaptive responses, including the expression of genes that control the release of oxygen, vascularization, and glucose metabolism (erythropoietin, VEGF, and glucose transporter 1, among others). These genes are in charge of restoring homeostasis and stimulating erythropoiesis, angiogenesis, anaerobic glycolysis, and other reparative processes (3, 38, 50, 51, 56). Therefore, HIF-1α induction has a key role during the repair process and has a protective effect in AKI (38, 56). In the present study, we explored HIF-1α as one of the potential mechanisms responsible for the reduced AKI severity observed in the RC + IR and RR + IR groups. We found that HIF-1α has a clear differential response to renal ischemia in the offspring of MPR groups compared with the control group (CC + IR group). In fact, there was a significant decrease in HIF-1α mRNA levels in the CC + IR group, which was not observed in the RC + IR, CR + IR, and RR + IR groups. To confirm HIF-1α signaling activation, we measured VEGF mRNA as one of its target genes and by its implication in AKI. The VEGF response matches with our results in HIF-1α, since there was a significant decrease in VEGF in the CC + IR group that was not observed in the offspring of MPR groups. These results suggest that the enhanced HIF-1α signaling after renal injury in the offspring of MPR groups might be another mechanism by which these groups were protected from ischemic injury. In support of this hypothesis, different studies have demonstrated that the increase in HIF-1α levels confers renoprotection against ischemic AKI. HIF-1α stabilization through inhibition of prolyl hydroxylases has shown an attenuation of renal damage induced by IR, associated with lower apoptosis, less infiltration of macrophages and vascular adhesion molecules, as well as an increase in the regulation of HIF target genes (23, 59, 64). Similar results were found in a model of renal damage induced by cisplatin (65). Conversely, when siRNA was used against HIF-1α (13) or when HIF-1 and HIF-2 knockout mice were studied, the renal damage was exacerbated (18). In addition to this, it is also known that the activation of HIF during the reperfusion phase is a key factor in the regeneration of the proximal tubular epithelium, promoting the expression of tissue repair genes (13). Moreover, it was recently demonstrated that under hypoxia conditions, the activation of HIF-1 and inhibition of prolyl hydroxylase proteins can activate the forkhead box O3 transcription factor, conferring renal protection by modulating the oxidative stress response, autophagy, cell metabolism, apoptosis, and cell differentiation (29).

Reactive oxygen species play an important role in mediating renal IR injury (46, 54). SOD1 and GPx mRNA levels that protect against oxidative damage were decreased after renal IR, but the decrement in both enzymes was minor in the MPR groups. Thus, the antioxidant defense could be an additional factor to explain the lower renal damage in these groups.

Regarding IL-6 mRNA levels, there was a significant increase that occurred in all of the groups and without differences among them; however, for TNF-α mRNA levels, the increase was only significant in the RC and RR groups. This is an unexpected result, since these groups exhibited less renal damage; however, other inflammatory mediators might participate.

In summary, under basal conditions, MPR negatively impacts nephrogenesis, inducing a smaller number of nephrons at birth. The remaining nephrons compensatively respond through glomerular hyperfiltration that maintains kidney function. Another important finding of this study was the decrease in most of the mRNA levels studied, which suggests that MPR during pregnancy, lactation, or both induces a thrifty phenotype in the offspring.

After renal injury induced by IR, rats from the MPR groups, and particularly the RC + IR and RR + IR groups, had lower renal damage, which could be attributed to the early recovery of RBF. The cause of this response could not be elucidated, but the changes in the pattern of vasoactive mRNA compared with the control group could contribute to faster RBF recovery. These results open a new line of research for studying the multifactorial mechanisms that are involved in the differential response exhibited by offspring of protein-restricted mothers.

This study highlights the alterations that an adverse intrauterine environment can induce in the renal physiology of the offspring. Specifically, we show that MPR, during pregnancy and/or lactation, resulted in a reduction in nephron number in the offspring, which exhibited renal resilience, allowing an efficient response to an ischemic insult during adulthood. However, this response could be different in the long term, which merits further investigation.

ACKNOWLEDGMENTS

We are grateful to Dr. Mariela Contreras for aid with the animal care.

The results presented in this paper have not been previously published in whole or in part, except as an abstract presented at the American Society of Nephrology Kidney Week Meeting 2018 (San Diego, CA).

GRANTS

This work was supported by Mexican Council of Science and Technology (CONACyT) Grants A1-S-8715, 235855, and 272390 (to N. A. Bobadilla) and by National University of Mexico Grants IN223915, IN201619, and 00000000030015 (to N. A. Bobadilla). This study was performed in partial fulfillment of the requirements for the PhD degree of L. E. García-Ortuño, a doctoral student from Programa de Doctorado en Ciencias Biomédicas, Universidad Nacional Autónoma de México (UNAM), and was supported by a fellowship from the Programa de Apoyos para la Superación del Personal Académico de la UNAM-DGAPA.

DISCLOSURES

No conflicts of interest, financial or otherwise, are declared by the authors.

AUTHOR CONTRIBUTIONS

N.A.B. conceived and designed research; L.E.G.-O., J.B.-C., R.P.-V., J.A.O.-T., E.L.-B., I.L.-P., A.S.-N., and L.R.-C. performed experiments; L.E.G.-O., E.L.-B., and N.A.B. analyzed data; L.E.G.-O., J.A.O.-T., G.G., E.Z., and N.A.B. interpreted results of experiments; N.A.B. prepared figures; N.A.B. drafted manuscript; L.E.G.-O., G.G., E.Z., and N.A.B. edited and revised manuscript; L.E.G.-O., J.B.-C., R.P.-V., J.A.O.-T., E.L.-B., I.L.-P., A.S.-N., L.R.-C., G.G., E.Z., and N.A.B. approved final version of manuscript.

REFERENCES

1. **Abdulmahdi W, Rabadi MM, Jules E, Marghani Y, Marji N, Leung J, Zhang F, Siani A, Siskind T, Vedovino K, Chowdhury N, Sekulic M, Ratliff BB.** Kidney dysfunction in the low-birth weight murine adult: implications of oxidative stress. *Am J Physiol Renal Physiol* 315: F583–F594, 2018. doi:10.1152/ajprenal.00164.2018.
2. **Aburn G, Gott M, Hoare K.** What is resilience? An integrative review of the empirical literature. *J Adv Nurs* 72: 980–1000, 2016. doi:10.1111/jan.12888.
3. **Andringa KK, Agarwal A.** Role of hypoxia-inducible factors in acute kidney injury. *Nephron Clin Pract* 127: 70–74, 2014. doi:10.1159/000363669.
4. **Bagby SP.** Maternal nutrition, low nephron number, and hypertension in later life: pathways of nutritional programming. *J Nutr* 137: 1066–1072, 2007. doi:10.1093/jn/137.4.1066.
5. **Barnett C, Nnoli O, Abdulmahdi W, Nesi L, Shen M, Zullo JA, Payne DL, Azar T, Dwivedi P, Syed K, Gromis J, Lipphardt M, Jules E, Maranda EL, Patel A, Rabadi MM, Ratliff BB.** Low birth weight is associated with impaired murine kidney development and function. *Pediatr Res* 82: 340–348, 2017. doi:10.1038/pr.2017.53.
6. **Barrera-Chimal J, Pérez-Villalva R, Cortés-González C, Ojeda-Cervantes M, Gamba G, Morales-Buenrostro LE, Bobadilla NA.** Hsp72 is an early and sensitive biomarker to detect acute kidney injury. *EMBO Mol Med* 3: 5–20, 2011. doi:10.1002/emmm.201000105.
7. **Bonventre JV, Yang L.** Cellular pathophysiology of ischemic acute kidney injury. *J Clin Invest* 121: 4210–4221, 2011. doi:10.1172/JCI45161.
8. **Boubred F, Buffat C, Feuerstein JM, Daniel L, Tsimaratos M, Oliver C, Lelièvre-Pégorier M, Simeoni U.** Effects of early postnatal hypernutrition on nephron number and long-term renal function and structure in rats. *Am J Physiol Renal Physiol* 293: F1944–F1949, 2007. doi:10.1152/ajprenal.00141.2007.
9. **Boubred F, Daniel L, Buffat C, Tsimaratos M, Oliver C, Lelièvre-Pégorier M, Simeoni U.** The magnitude of nephron number reduction mediates intrauterine growth-restriction-induced long term chronic renal disease in the rat. A comparative study in two experimental models. *J Transl Med* 14: 331, 2016. doi:10.1186/s12967-016-1086-3.
10. **Bowes L, Jaffee SR.** Biology, genes, and resilience: toward a multidisciplinary approach. *Trauma Violence Abuse* 14: 195–208, 2013. doi:10.1177/1524838013487807.
11. **Brenner BM, Garcia DL, Anderson S.** Glomeruli and blood pressure. Less of one, more the other? *Am J Hypertens* 1: 335–347, 1988. doi:10.1093/ajh/1.4.335.
12. **Burke M, Pabbidi MR, Farley J, Roman RJ.** Molecular mechanisms of renal blood flow autoregulation. *Curr Vasc Pharmacol* 12: 845–858, 2014. doi:10.2174/15701611113116660149.
13. **Conde E, Alegre L, Blanco-Sánchez I, Sáenz-Morales D, Aguado-Fraile E, Ponte B, Ramos E, Sáiz A, Jiménez C, Ordoñez A, López-Cabrera M, del Peso L, de Landázuri MO, Liaño F, Selgas R, Sanchez-Tomero JA, García-Bermejo ML.** Hypoxia inducible factor 1-alpha (HIF-1 alpha) is induced during reperfusion after renal ischemia and is critical for proximal tubule cell survival. *PLoS One* 7: e33258, 2012. doi:10.1371/journal.pone.0033258.
14. **Fagundes AT, Moura EG, Passos MC, Oliveira E, Toste FP, Bonomo IT, Trevenzoli IH, Garcia RM, Lisboa PC.** Maternal low-protein diet during lactation programmes body composition and glucose homeostasis in the adult rat offspring. *Br J Nutr* 98: 922–928, 2007. doi:10.1017/S0007114507750924.
15. **Godfrey KM, Forrester T, Barker DJ, Jackson AA, Landman JP, Hall JS, Cox V, Osmond C.** Maternal nutritional status in pregnancy and blood pressure in childhood. *Br J Obstet Gynaecol* 101: 398–403, 1994. doi:10.1111/j.1471-0528.1994.tb11911.x.
16. **Gross ML, Amann K, Ritz E.** Nephron number and renal risk in hypertension and diabetes. *J Am Soc Nephrol* 16, *Suppl* 1: S27–S29, 2005. doi:10.1681/ASN.2004110967.
17. **Hales CN, Barker DJ.** The thrifty phenotype hypothesis. *Br Med Bull* 60: 5–20, 2001. doi:10.1093/bmb/60.1.5.
18. **Hill P, Shukla D, Tran MG, Aragones J, Cook HT, Carmeliet P, Maxwell PH.** Inhibition of hypoxia inducible factor hydroxylases protects against renal ischemia-reperfusion injury. *J Am Soc Nephrol* 19: 39–46, 2008. doi:10.1681/ASN.2006090998.
19. **Hoy WE, Hughson MD, Bertram JF, Douglas-Denton R, Amann K.** Nephron number, hypertension, renal disease, and renal failure. *J Am Soc Nephrol* 16: 2557–2564, 2005. doi:10.1681/ASN.2005020172.
20. **Hughson MD, Puelles VG, Hoy WE, Douglas-Denton RN, Mott SA, Bertram JF.** Hypertension, glomerular hypertrophy and nephrosclerosis: the effect of race. *Nephrol Dial Transplant* 29: 1399–1409, 2014. doi:10.1093/ndt/gft480.
21. **Kanagasundaram NS.** Pathophysiology of ischaemic acute kidney injury. *Ann Clin Biochem* 52: 193–205, 2015. doi:10.1177/0004563214556820.
22. **Kanzaki G, Tsuboi N, Haruhara K, Koike K, Ogura M, Shimizu A, Yokoo T.** Factors associated with a vicious cycle involving a low nephron number, hypertension and chronic kidney disease. *Hypertens Res* 38: 633–641, 2015. doi:10.1038/hr.2015.67.
23. **Kapitsinou PP, Jaffe J, Michael M, Swan CE, Duffy KJ, Erickson-Miller CL, Haase VH.** Preischemic targeting of HIF prolyl hydroxylation inhibits fibrosis associated with acute kidney injury. *Am J Physiol Renal Physiol* 302: F1172–F1179, 2012. doi:10.1152/ajprenal.00667.2011.
24. **Kawazoe N, Eto T, Abe I, Takishita S, Ueno M, Kobayashi K, Uezono K, Muratani H, Kimura Y, Tomita Y, et al.** Long-term prognosis of malignant hypertension; difference between underlying diseases such as essential hypertension and chronic glomerulonephritis. *Clin Nephrol* 29: 53–57, 1988.

25. **Keller G, Zimmer G, Mall G, Ritz E, Amann K.** Nephron number in patients with primary hypertension. *N Engl J Med* 348: 101–108, 2003. doi:10.1056/NEJMoa020549.
26. **Kett MM, Denton KM.** Renal programming: cause for concern? *Am J Physiol Regul Integr Comp Physiol* 300: R791–R803, 2011. doi:10.1152/ajpregu.00791.2010.
27. **Lee SA, Noel S, Sadasivam M, Hamad ARA, Rabb H.** Role of immune cells in acute kidney injury and repair. *Nephron* 137: 282–286, 2017. doi:10.1159/000477181.
28. **Lewington AJ, Cerdá J, Mehta RL.** Raising awareness of acute kidney injury: a global perspective of a silent killer. *Kidney Int* 84: 457–467, 2013. doi:10.1038/ki.2013.153.
29. **Li L, Kang H, Zhang Q, D'Agati VD, Al-Awqati Q, Lin F.** FoxO3 activation in hypoxic tubules prevents chronic kidney disease. *J Clin Invest* 129: 2374–2389, 2019. doi:10.1172/JCI122256.
30. **Lima-Posada I, Portas-Cortés C, Pérez-Villalva R, Fontana F, Rodríguez-Romo R, Prieto R, Sánchez-Navarro A, Rodríguez-González GL, Gamba G, Zambrano E, Bobadilla NA.** Gender differences in the acute kidney injury to chronic kidney disease transition. *Sci Rep* 7: 12270, 2017. doi:10.1038/s41598-017-09630-2.
31. **Luyckx VA, Brenner BM.** Birth weight, malnutrition and kidney-associated outcomes--a global concern. *Nat Rev Nephrol* 11: 135–149, 2015. doi:10.1038/nrneph.2014.251.
32. **Luyckx VA, Brenner BM.** The clinical importance of nephron mass. *J Am Soc Nephrol* 21: 898–910, 2010. doi:10.1681/ASN.2009121248.
33. **Malek M, Nematbakhsh M.** Renal ischemia/reperfusion injury; from pathophysiology to treatment. *J Renal Inj Prev* 4: 20–27, 2015.
34. **Maringer K, Sims-Lucas S.** The multifaceted role of the renal microvasculature during acute kidney injury. *Pediatr Nephrol* 31: 1231–1240, 2016. doi:10.1007/s00467-015-3231-2.
35. **Mesquita FF, Gontijo JA, Boer PA.** Expression of renin-angiotensin system signalling compounds in maternal protein-restricted rats: effect on renal sodium excretion and blood pressure. *Nephrol Dial Transplant* 25: 380–388, 2010. doi:10.1093/ndt/gfp505.
36. **Mesquita FF, Gontijo JA, Boer PA.** Maternal undernutrition and the offspring kidney: from fetal to adult life. *Braz J Med Biol Res* 43: 1010–1018, 2010. doi:10.1590/S0100-879X2010007500113.
37. **Moretto VL, Ballen MO, Gonçalves TS, Kawashita NH, Stoppiglia LF, Veloso RV, Latorraca MQ, Martins MS, Gomes-da-Silva MH.** Low-protein diet during lactation and maternal metabolism in rats. *ISRN Obstet Gynecol* 2011: 1, 2011. doi:10.5402/2011/876502.
38. **Nangaku M, Rosenberger C, Heyman SN, Eckardt KU.** Regulation of hypoxia-inducible factor in kidney disease. *Clin Exp Pharmacol Physiol* 40: 148–157, 2013. doi:10.1111/1440-1681.12005.
39. **Okamura DM, Pennathur S.** The balance of powers: redox regulation of fibrogenic pathways in kidney injury. *Redox Biol* 6: 495–504, 2015. doi:10.1016/j.redox.2015.09.039.
40. **Ou J, Ou Z, Ackerman AW, Oldham KT, Pritchard KA Jr.** Inhibition of heat shock protein 90 (hsp90) in proliferating endothelial cells uncouples endothelial nitric oxide synthase activity. *Free Radic Biol Med* 34: 269–276, 2003. doi:10.1016/S0891-5849(02)01299-6.
41. **Pérez-Rojas JM, Derive S, Blanco JA, Cruz C, Martínez de la Maza L, Gamba G, Bobadilla NA.** Renocortical mRNA expression of vasoactive factors during spironolactone protective effect in chronic cyclosporine nephrotoxicity. *Am J Physiol Renal Physiol* 289: F1020–F1030, 2005. doi:10.1152/ajprenal.00166.2005.
42. **Pires KM, Aguila MB, Mandarim-de-Lacerda CA.** Early renal structure alteration in rat offspring from dams fed low protein diet. *Life Sci* 79: 2128–2134, 2006. doi:10.1016/j.lfs.2006.07.006.
43. **Prentice AM.** Nutrition and chronic disease: lessons from the developing and developed world. *Nestle Nutr Inst Workshop Ser* 78: 155–160, 2014. doi:10.1159/000354957.
44. **Prentice AM, Rayco-Solon P, Moore SE.** Insights from the developing world: thrifty genotypes and thrifty phenotypes. *Proc Nutr Soc* 64: 153–161, 2005. doi:10.1079/PNS2005421.
45. **Puelles VG, Hoy WE, Hughson MD, Diouf B, Douglas-Denton RN, Bertram JF.** Glomerular number and size variability and risk for kidney disease. *Curr Opin Nephrol Hypertens* 20: 7–15, 2011. doi:10.1097/MNH.0b013e3283410a7d.
46. **Ratliff BB, Abdulmahdi W, Pawar R, Wolin MS.** Oxidant mechanisms in renal injury and disease. *Antioxid Redox Signal* 25: 119–146, 2016. doi:10.1089/ars.2016.6665.
47. **Rewa O, Bagshaw SM.** Acute kidney injury-epidemiology, outcomes and economics. *Nat Rev Nephrol* 10: 193–207, 2014. doi:10.1038/nrneph.2013.282.
48. **Rodríguez-Romo R, Benítez K, Barrera-Chimal J, Pérez-Villalva R, Gómez A, Aguilar-León D, Rangel-Santiago JF, Huerta S, Gamba G, Uribe N, Bobadilla NA.** AT1 receptor antagonism before ischemia prevents the transition of acute kidney injury to chronic kidney disease. *Kidney Int* 89: 363–373, 2016. doi:10.1038/ki.2015.320.
49. **Sánchez-Pozos K, Barrera-Chimal J, Garzón-Muvdi J, Pérez-Villalva R, Rodríguez-Romo R, Cruz C, Gamba G, Bobadilla NA.** Recovery from ischemic acute kidney injury by spironolactone administration. *Nephrol Dial Transplant* 27: 3160–3169, 2012. doi:10.1093/ndt/gfs014.
50. **Semenza GL.** HIF-1: mediator of physiological and pathophysiological responses to hypoxia. *J Appl Physiol (1985)* 88: 1474–1480, 2000. doi:10.1152/jappl.2000.88.4.1474.
51. **Sethi K, Rao K, Bolton D, Patel O, Ischia J.** Targeting HIF-1α to prevent renal ischemia-reperfusion injury: does it work? *Int J Cell Biol* 2018: 1, 2018. doi:10.1155/2018/9852791.
52. **Sharfuddin AA, Molitoris BA.** Pathophysiology of ischemic acute kidney injury. *Nat Rev Nephrol* 7: 189–200, 2011. doi:10.1038/nrneph.2011.16.
53. **Shu S, Wang Y, Zheng M, Liu Z, Cai J, Tang C, Dong Z.** Hypoxia and hypoxia-inducible factors in kidney injury and repair. *Cells* 8: 207, 2019. doi:10.3390/cells8030207.
54. **Sureshbabu A, Ryter SW, Choi ME.** Oxidative stress and autophagy: crucial modulators of kidney injury. *Redox Biol* 4: 208–214, 2015. doi:10.1016/j.redox.2015.01.001.
55. **Sutton EF, Gilmore LA, Dunger DB, Heijmans BT, Hivert MF, Ling C, Martinez JA, Ozanne SE, Simmons RA, Szyf M, Waterland RA, Redman LM, Ravussin E.** Developmental programming: state-of-the-science and future directions-Summary from a Pennington Biomedical symposium. *Obesity (Silver Spring)* 24: 1018–1026, 2016. doi:10.1002/oby.21487.
56. **Tanaka S, Tanaka T, Nangaku M.** Hypoxia and dysregulated angiogenesis in kidney disease. *Kidney Dis (Basel)* 1: 80–89, 2015. doi:10.1159/000381515.
57. **Tögel F, Westenfelder C.** Recent advances in the understanding of acute kidney injury. *F1000Prime Rep* 6: 83, 2014. doi:10.12703/P6-83.
58. **Villar-Martini VC, Carvalho JJ, Neves MF, Aguila MB, Mandarim-de-Lacerda CA.** Hypertension and kidney alterations in rat offspring from low protein pregnancies. *J Hypertens Suppl* 27, *Suppl* 6: S47–S51, 2009. doi:10.1097/01.hjh.0000358838.71675.5e.
59. **Wang Z, Schley G, Türkoglu G, Burzlaff N, Amann KU, Willam C, Eckardt KU, Bernhardt WM.** The protective effect of prolyl-hydroxylase inhibition against renal ischaemia requires application prior to ischaemia but is superior to EPO treatment. *Nephrol Dial Transplant* 27: 929–936, 2012. doi:10.1093/ndt/gfr379.
60. **Welham SJ, Wade A, Woolf AS.** Protein restriction in pregnancy is associated with increased apoptosis of mesenchymal cells at the start of rat metanephrogenesis. *Kidney Int* 61: 1231–1242, 2002. doi:10.1046/j.1523-1755.2002.00264.x.
61. **Wlodek ME, Westcott K, Siebel AL, Owens JA, Moritz KM.** Growth restriction before or after birth reduces nephron number and increases blood pressure in male rats. *Kidney Int* 74: 187–195, 2008. doi:10.1038/ki.2008.153.
62. **Wood-Bradley RJ, Barrand S, Giot A, Armitage JA.** Understanding the role of maternal diet on kidney development; an opportunity to improve cardiovascular and renal health for future generations. *Nutrients* 7: 1881–1905, 2015. doi:10.3390/nu7031881.
63. **Woods LL, Ingelfinger JR, Nyengaard JR, Rasch R.** Maternal protein restriction suppresses the newborn renin-angiotensin system and programs adult hypertension in rats. *Pediatr Res* 49: 460–467, 2001. doi:10.1203/00006450-200104000-00005.
64. **Wu MJ, Wen MC, Chiu YT, Chiou YY, Shu KH, Tang MJ.** Rapamycin attenuates unilateral ureteral obstruction-induced renal fibrosis. *Kidney Int* 69: 2029–2036, 2006. doi:10.1038/sj.ki.5000161.
65. **Yang Y, Yu X, Zhang Y, Ding G, Zhu C, Huang S, Jia Z, Zhang A.** Hypoxia-inducible factor prolyl hydroxylase inhibitor roxadustat (FG-4592) protects against cisplatin-induced acute kidney injury. *Clin Sci (Lond)* 132: 825–838, 2018. doi:10.1042/CS20171625.
66. **Zambrano E, Martínez-Samayoa PM, Bautista CJ, Deás M, Guillén L, Rodríguez-González GL, Guzmán C, Larrea F, Nathanielsz PW.** Sex differences in transgenerational alterations of growth and metabolism in progeny (F2) of female offspring (F1) of rats fed a low protein diet during pregnancy and lactation. *J Physiol* 566: 225–236, 2005. doi:10.1113/jphysiol.2005.086462.

67. **Zambrano E, Rodríguez-González GL, Guzmán C, García-Becerra R, Boeck L, Díaz L, Menjivar M, Larrea F, Nathanielsz PW.** A maternal low protein diet during pregnancy and lactation in the rat impairs male reproductive development. *J Physiol* 563: 275–284, 2005. doi:10.1113/jphysiol.2004.078543.

68. **Zeman FJ.** Effects of maternal protein restriction on the kidney of the newborn young of rats. *J Nutr* 94: 111–116, 1968. doi:10.1093/jn/94.2.111.

69. **Zuk A, Bonventre JV.** Acute kidney injury. *Annu Rev Med* 67: 293–307, 2016. doi:10.1146/annurev-med-050214-013407.

Am J Physiol Renal Physiol 320: F734–F747, 2021.
First published March 8, 2021; doi:10.1152/ajprenal.00575.2020

american physiological society

AMERICAN JOURNAL OF PHYSIOLOGY
RENAL PHYSIOLOGY

RESEARCH ARTICLE

Mechanisms of Renal Electrolyte Transport and Ion Channel Regulation in Honor of Dr. Gerhard Giebisch

Role of KLHL3 and dietary K^+ in regulating KS-WNK1 expression

Mauricio Ostrosky-Frid,[1,2] María Chávez-Canales,[3] Jinwei Zhang,[4] Olena Andrukhova,[5]† Eduardo R. Argaiz,[1] Fernando Lerdo-de-Tejada,[3] Adrian Murillo-de-Ozores,[6,7] Andrea Sanchez-Navarro,[1,7] Lorena Rojas-Vega,[7] Norma A. Bobadilla,[1,7] Norma Vazquez,[1] María Castañeda-Bueno,[7] Dario R. Alessi,[5] and Gerardo Gamba[1,2,7]

[1]*Molecular Physiology Unit, Instituto de Investigaciones Biomédicas, Universidad Nacional Autónoma de México, Mexico City, Mexico;* [2]*PECEM (MD/PhD), Facultad de Medicina, Universidad Nacional Autónoma de México, Mexico City, Mexico;* [3]*Unidad de Investigación UNAM-INC, Instituto Nacional de Cardiología Ignacio Chávez and Instituto de Investigaciones Biomédicas, Universidad Nacional Autónoma de México, Mexico City, Mexico;* [4]*Institute of Biomedical and Clinical Sciences, Medical School, College of Medicine and Health, University of Exeter, Hatherly Laboratories, Exeter, United Kingdom;* [5]*MRC Protein Phosphorylation and Ubiquitylation Unit, College of Life Sciences, University of Dundee, Dundee, United Kingdom;* [6]*Facultad de Medicina, Universidad Nacional Autónoma de México, Mexico City, Mexico; and* [7]*Department of Nephrology and Mineral Metabolism, Instituto Nacional de Ciencias Médicas y Nutrición Salvador Zubirán, Mexico City, Mexico*

Abstract

The physiological role of the shorter isoform of with no lysine kinase (WNK)1 that is exclusively expressed in the kidney (KS-WNK1), with particular abundance in the distal convoluted tubule, remains elusive. KS-WNK1, despite lacking the kinase domain, is nevertheless capable of stimulating the NaCl cotransporter, apparently through activation of WNK4. It has recently been shown that a less severe form of familial hyperkalemic hypertension featuring only hyperkalemia is caused by missense mutations in the WNK1 acidic domain that preferentially affect cullin 3 (CUL3)-Kelch-like protein 3 (KLHL3) E3-induced degradation of KS-WNK1 rather than that of full-length WNK1. Here, we show that full-length WNK1 is indeed less impacted by the CUL3-KLHL3 E3 ligase complex compared with KS-WNK1. We demonstrated that the unique 30-amino acid NH_2-terminal fragment of KS-WNK1 is essential for its activating effect on the NaCl cotransporter and recognition by KLHL3. We identified specific amino acid residues in this region critical for the functional effect of KS-WNK1 and KLHL3 sensitivity. To further explore this, we generated KLHL3-R528H knockin mice that mimic human mutations causing familial hyperkalemic hypertension. These mice revealed that the KLHL3 mutation specifically increased expression of KS-WNK1 in the kidney. We also observed that in wild-type mice, the expression of KS-WNK1 was only detectable after exposure to a low-K^+ diet. These findings provide new insights into the regulation and function of KS-WNK1 by the CUL3-KLHL3 complex in the distal convoluted tubule and indicate that this pathway is regulated by dietary K^+ levels.

NEW & NOTEWORTHY In this work, we demonstrated that the kidney-specific isoform of with no lysine kinase 1 (KS-WNK1) in the kidney is modulated by dietary K^+ and activity of the ubiquitin ligase protein Kelch-like protein 3. We analyzed the role of different amino acid residues of KS-WNK1 in its activity against the NaCl cotransporter and sensitivity to Kelch-like protein 3.

distal convoluted tubule; hypertension; salt transport; STE20/SPS1-related proline-alanine-rich protein kinase; with no lysine kinase 4

INTRODUCTION

Familial hyperkalemic hypertension (FHHt) encompasses a spectrum of diseases that are mainly the consequence of overactivity of the renal thiazide-sensitive NaCl cotransporter (NCC) of the distal convoluted tubule (DCT) (1). NCC activity is modulated by with no lysine kinase (WNK)1 and WNK4, whose half-life is, in turn, regulated by the cullin–RING E3 ligase complex containing Kelch-like protein 3 (KLHL3) and cullin 3 (CUL3) proteins. The severity of FHHt depends on which one of these genes is affected and is defined by age of diagnosis, K^+ levels, blood pressure levels, and percentage of affected individuals with hypertension before the age of 18 yr old. The more severe disease presentation is due to exon 9 deletion of CUL3, followed by dominant or recessive mutations in KLHL3 (2, 3). These mutations impair the ubiquitylation

† Deceased 3 October 2017.
Correspondence: G. Gamba (gamba@iibiomedicas.unam.mx).
Submitted 27 October 2020 / Revised 3 March 2021 / Accepted 3 March 2021

and degradation of WNK kinases in the DCT. Less severe is FHHt due to missense mutations in the acidic motif of WNK4, which constitutes the recognition site for KLHL3 (4, 5) and thus abrogate only WNK4 ubiquitylation (6). Finally, the mildest form of FHHt is due to intronic deletions in the *WNK1* gene that apparently result in ectopic expression of the full-length catalytic isoform of this kinase (known as L-WNK1) in the DCT (7). Louis-Dit-Picard et al. (8) have recently described, however, an even milder form of FHHt. In this work, humans and mice with heterozygous mutations in the acidic domain of WNK1 display an inherited phenotype with hyperkalemia, hyperchloremia, and metabolic acidosis, but without arterial hypertension, that is nevertheless accompanied by low renin expression levels, suggesting a mild volume expansion that is, however, not enough to produce hypertension.

The major product of the *WNK1* gene in the kidney is a shorter isoform known as kidney-specific WNK1 (KS-WNK1) (9–11). This isoform is transcribed from an alternative promoter located between exons 4 and 4a that lacks the kinase domain and contains a unique 30-amino acid residues sequence encoded by exon 4a. Despite lacking a kinase domain, recent evidence suggests that KS-WNK1 may function as an activator of NCC. First, in *Xenopus laevis* oocytes, we have shown that KS-WNK1 is able to induce phosphorylation and activation of NCC by interacting with other WNKs and reducing its sensitivity to Cl^-. For instance, in the presence of KS-WNK1, WNK4 is active at higher levels of intracellular Cl^- concentration, increasing the activity of the intermediate kinase, STE20/SPS1-related proline-alanine-rich protein kinase (SPAK), toward NCC (12). Second, it has been observed that under conditions in which NCC activity is expected to be increased, like in response to low dietary K^+, conglomerations of WNKs, known as WNK bodies, are formed in DCT cells, and their formation requires the presence of KS-WNK1 (13, 14), also supporting that KS-WNK1 is associated with activation of NCC. Third, Louis-Dit-Picard et al. (8) suggested that the FHHt phenotype observed in patients with mutations in the acidic domain of WNK1 is likely due to increased protein expression of KS-WNK1 in DCT cells because it was observed that the sensitivity of KS-WNK1 to the CUL3-KLHL3 E3 ligase complex is several times higher than that of L-WNK1 and, thus, mutations of the acidic motif in WNK1 seem to preferentially protect KS-WNK1 from ubiquitylation by the CUL3-KLHL3 E3 ligase complex.

Given that both KS-WNK1 and L-WNK1 contain the acidic motif involved in KLHL3 binding, the different sensitivity to CUL3-KLHL3 E3 ligase complex-mediated degradation is surprising. Our goal in the present study was to analyze and characterize the effect of the CUL3-KLHL3 E3 ligase complex on KS-WNK1 and to define the protein domains responsible for the difference in sensitivity. In addition, we began to explore the physiological stimuli that regulate KS-WNK1 protein expression levels by modulating its targeting to degradation by the CUL3-KLHL3 E3 complex.

METHODS

Generation of KLHL3$^{+/R528H}$ Mice

KLHL3$^{+/R528H}$ knockin mice were generated through homologous recombination strategies by TaconicArtemis (https://www.taconic.com/). For vector construction, mouse genomic fragments (obtained from the C57BL/6J RPCIB-731 BAC library) and selected features (such as desired point mutation, recombination sites, and selection markers, as provided in Supplemental Fig. S1; see https:/doi.org/10.6084/m9.figshare.13721791) were assembled into the targeting vector.

The linearized vector was transfected into the TaconicArtemis C57BL/N Tac embryonic stem (ES) cell line. Homologous recombinant clones were isolated using positive (PuroR) and negative [thymidine kinase (TK)] selection. Specific ES clones were selected by Southern blot analysis of genomic DNA. Blastocysts were isolated from the uterus of pregnant BALB/c females at *day postcoitum 3.5* and injected with 10–15 targeted C57BL/6NTac ES cells. After recovery, eight injected blastocysts were transferred to each uterine horn of 2.5 days postcoitum, pseudopregnant Naval Medical Research Institute (NMRI) females. Chimerism was measured in chimeras (G_0) by coat color contribution of ES cells to the BALB/c host (black/white). Highly chimeric mice were bred to C57BL/6-Tg(CAG-Flpe)2 Arte females for elimination of the puromycin resistance cassette. This produced mice that constitutively express mutated KLHL3 protein. The remaining FRT recombination site in these mice is located in a nonconserved region of the genome. Primers 6560_31 (5′-CACTGTGTTCTGCCTTTCAGG-3′) and 6560_32 (5′-CAGACCAAGACCAGAGAGAAGG-3′) were used to confirm the presence of the R528H mutation by PCR amplification and product sequencing.

For genotyping analysis, genomic DNA was extracted from tail biopsies and analyzed by PCR. *Primer 1* (5′-GATACCCACTGGCATTTGG-3′) and *primer 2* (5′-GGTAAGGGCAGCATTACTGG-3′) were used to detect wild-type and knockin alleles. The wild-type allele generates a 308-bp product, whereas the knockin allele generates a 383-bp product. The latter product is larger due to the presence of the FRT site and flanking region that remains in an intronic region following Flp-mediated excision of the puromycin selection cassette.

Generation of KLHL3$^{R528H/R528H}$/KS-WNK1$^{-/-}$ Mice

KS-WNK1$^{-/-}$ mice were a kind gift from Hadchouel (15) (INSERM Paris), and the generation and genotyping have been described in the supporting information of the cited article.

Mice were crossed with of *KLHL3*$^{+/R528H}$ to produce the desired genotypes: wild type, *KLHL3*$^{R528H/R528H}$, *KS-WNK1*$^{-/-}$, and *KLHL3*$^{R528H/R528H}$/*KS-WNK1*$^{-/-}$. Male mice were used for experimental purposes.

Low-K^+ Diet Experiments

Wild-type and *KLHL3*$^{+/R528H}$ mice were placed on normal (1% K^+) or K^+-deficient diets (0.0% K^+) for 4 days. The OpenStandard diet with no added K^+ (D16120202) was purchased from Research Diets and used as the K^+-deficient diet. The normal-K^+ diet was prepared by adding KCl. By the end of the 4-day period, mice were euthanized under isoflurane anesthesia, and kidney samples were collected.

Western Blot Analysis of Mouse Kidney Proteins

Kidney lysates were prepared with lysis buffer containing 50 mM Tris-HCl (pH 7.5), 1 mM EGTA, 1 mM EDTA, 50 mM sodium fluoride, 5 mM sodium pyrophosphate, 1 mM

sodium orthovanadate, 1% (w/v) Nonidet P-40, 0.27 M sucrose, 0.1% (v/v) 2-mercaptoethanol, and protease inhibitors (1 tablet per 50 mL). Lysates (20 μg) in SDS sample buffer were subjected to electrophoresis on polyacrylamide gels and transferred to nitrocellulose membranes. Membranes were incubated for 30 min with Tris-buffered saline-Tween 20 (TBS-T) containing 5% (w/v) skim milk. Membranes were then immunoblotted in 5% (w/v) skim milk in TBS-T with the indicated primary antibodies overnight at 4°C. Sheep antibodies were used at a concentration of 1–2 μg/mL. The incubation with phospho-specific sheep antibodies was performed with the addition of 10 μg/mL of the dephospho-peptide antigen used to raise the antibody. Blots were then washed six times with TBS-T and incubated for 1 h at room temperature with secondary horseradish peroxidase (HRP)-conjugated antibodies diluted 5,000-fold in 5% (w/v) skim milk in TBS-T. After the washing steps were repeated, the signal was detected with an enhanced chemiluminescence reagent. Immunoblots were developed using a film automatic processor (SRX-101, Konica Minolta Medical), and films were scanned with 600-dpi resolution on a scanner (PowerLook 1000, UMAX).

For the detection of KS-WNK1, kidney tissue was homogenized in lysis buffer containing 250 mM sucrose, 10 mM triethanolamine, 1× protease inhibitors (Roche), 50 mM sodium fluoride, 10 mM sodium pyrophosphate, and 1 mM sodium orthovanadate.

Protein samples were subjected to polyacrylamide gel electrophoresis and then transferred to PVDF membranes for 2 h at 10 mV. Membranes were blocked for 2 h in 10% nonfat dry milk dissolved in TBS-T solution (2 mM Tris-HCl, 150 mM NaCl, and 0.2% Tween 20, pH 7.5).

Membranes were incubated overnight with the indicated antibodies diluted in 5% nonfat dry milk in TBS-T, followed by incubation for 1 h at room temperature with HRP-conjugated secondary antibodies diluted in 5% nonfat dry milk in TBS-T. After the incubation, membranes were washed six times for 10 min with TBS-T. For signal detection by chemiluminescence, Luminata Forte Western HRP substrate (Merck Millipore) was used, and LI-COR equipment was used to perform the reading.

The following antibodies were used. Rabbit anti-WNK4 (1:4,000) was a gift from David Ellison (Oregon Health & Science University) (16). For WNK1 detection, we used commercially available rabbit anti-WNK1 antibody from Bethyl Laboratories (1:1,000, A301-515A, pan-WNK1). The following antibodies were raised in the sheep and affinity purified on the appropriate antigen by the Division of Signal Transduction Therapy Unit of the University of Dundee: WNK4 total antibody (S064B, second bleed, raised against residues 1,221–1,243 of human WNK4), NCC phospho-Thr^{60} antibody (S995B, residues 54–66 of human NCC phosphorylated at Thr^{60}, RTFGYNpTIDVVPT), NCC total antibody (S965B, residues 906–925 of human NCC, CHTKRFEDM-IAPFRLNDGFKD), SPAK NH_2-terminal antibody (S668D, raised against residues 2–76 of mouse SPAK), oxidative stress response-1 (OSR1) mouse antibody (S149C, residues 389–408 of mouse OSR1, SAHLPQPAGQMPTQPAQVSL), SPAK/OSR1 (S motif) phospho-Ser^{373}/Ser^{325} antibody [S670B, raised against residues 367–379 of human SPAK, RRVPGS(S)GHLHKT, which is highly similar to residues 319–331 of human OSR1, in which the sequence is RRVPGS(S)GRLHKT]. α-Epithelial Na^+ channel (ENaC) antibody was kindly provided by Land (17); p44/42 MAPK (Erk1/2) antibody (3062) was purchased from Cell Signaling Technology. Secondary antibodies coupled to HRP used for immunoblot analysis were obtained from Pierce. All antibodies used and their corresponding validation studies are cited in Supplemental Table S1; see https://doi.org/10.6084/m9.figshare.13721797).

Immunofluorescent Staining of Mouse Kidney Sections

Harvested mouse kidneys were immersion fixed in fresh 4% (w/v) formaldehyde-PBS (pH 6.9) for 16 h at 37°C, washed three times in PBS, and stored at 4°C until paraffin embedded. Sections (5 μm) were deparaffinized in Histoclear (National Diagnostics) and rehydrated in graded methanol steps. An antigen retrieval step was performed with R-Universal buffer in the 2100 antigen retriever for a single heat-pressure cycle (Aptum Biologics). Sections were permeabilized with 0.05% (v/v) Triton X-100-PBS for 20 min and blocked for 1 h at 37°C with 2% (v/v) donkey serum in 0.05% (v/v) Triton X-100-PBS. Primary antibodies were incubated overnight for 16 h at 4°C at the following concentrations diluted in 1% (v/v) donkey serum in 0.05% (v/v) Triton X-100-PBS: 2 μg/mL for total SPAK and phospho-SPAK S373 and anti-α-ENaC (Novus Biologicals, 1:500). Phospho-specific antibodies included the addition of 10 μg/mL of the nonphosphopeptide used to raise the antibody per 2 μg/mL of antibody used. Negative controls omitted the primary antibody and were processed in parallel. Slides were then washed for 20 min in 0.05% (v/v) Triton X-100-PBS and incubated in secondary antibody for 1 h at 37°C. Preabsorbed donkey IgG-conjugated Alexa Fluor 488, 633, and 647 secondary antibodies (Life Technologies/Abcam) were used at 1:200 diluted in 1% (v/v) donkey serum in 0.05% (v/v) Triton X-100-PBS for immunofluorescent labeling. Slides were washed as above, counterstained using Sytox orange nucleic acid stain (S11368, Life Technologies), mounted using Prolong gold antifade (P36930, Life Technologies), and shielded from light.

Mutagenesis and Constructs

Rat NCC, human WNK4-Flag, human L-WNK1-Δ11-c-Myc, and human KS-WNK1-Δ11-c-Myc have been previously described (12, 18, 19). KS-WNK1-Δ4a, KS-WNK1-2CxS (KS-2CxS), KS-WNK1-6CxS (KS-6CxS), KS-WNK1-5Q (KS-5Q), KS-WNK1-V11A, KS-WNK1-F12A, KS-WNK1-V13A, KS-WNK1-I14A, and KS-WNK1-I15A were made from KS-WNK1-Δ11 using the QuikChange mutagenesis system (Stratagene). All modifications were confirmed by DNA sequencing. cRNA was made from linearized cDNA using the T7 RNA polymerase mMESSAGE kit (Ambion). The KLHL3-Flag clone was a gift from Richard P. Lifton (Rockefeller University). The open reading frame was subcloned into a pGEMHE vector.

Functional Expression of NCC

Oocytes were extracted in clusters from adult female *X. laevis* frogs anesthetized by submerging them in 0.17% Tricaine. Oocytes were incubated with collagenase type 2 (3 mg/mL) eluted in Ca^{2+}-free ND-96 (96 mM NaCl, 2 mM KCl, 1.0 mM $MgCl_2$, and 5 mM HEPES, pH 7.4) for 1.5 h, washed three times with Ca^{2+}-free ND-96, and incubated again with collagenase type 2 for 1.5 h. Oocytes were washed with ND-

96 solution (96.0 mM NaCl, 2.0 mM KCl, 1.8 mM $CaCl_2$, 1.0 mM $MgCl_2$, and 5.0 mM HEPES, pH 7.4) three times and incubated overnight at 16°C.

Oocytes were injected with 20 ng of each of the indicated cRNAs and then incubated at 16°C for 48 h in ND-96 before protein extraction for Western blot analysis or 72 h before transport experiments. MG132 (100 μM) was added to the media 16 h before protein extraction in the described cases.

Consent for the Performance of Animal Experiments

The use of *X. laevis* oocytes as well as wild-type and transgenic mice were approved by Institutional Animal Care and Use Committee of the Instituto Nacional de Ciencias Medicas y Nutricion Salvador Zubiran and in accordance with regulations set by the Universities of Cambridge and Dundee and the United Kingdom Home Office. Only male mice at 12–16 wk old were used.

Western Blot Analysis of *X. laevis* Oocyte Proteins

Twenty oocytes per experimental group were collected, and samples were extracted using 5 μL/oocyte of lysis buffer containing 50 mM Tris-HCl (pH 7.5), 1 mM EGTA, 1 mM EDTA, 50 mM sodium fluoride, 10 mM sodium pyrophosphate, 1 mM sodium orthovanadate, 1% (w/v) Nonidet P-40, 0.27 M sucrose, and protease inhibitors (Complete tablets, Roche).

Western blots were performed as described above. The antibody concentrations used were anti-Flag 1:5,000 (Sigma), anti-Myc 1:1,000 (Sigma), and anti-actin 1:2,500 (Santa Cruz Biotechnology). Densitometric analysis was performed using ImageStudioLite software.

Transport Assays

NCC activity was evaluated using the radioactive tracer $^{22}Na^+$ (Perkin Elmer Life Sciences). Oocytes were injected as previously described; 72 h later, 15 oocytes per group were incubated at room temperature for 30 min in Cl^--free ND-96 medium [containing (in mM) 96 sodium isethionate, 2 potassium gluconate, 1.8 calcium gluconate, 1 magnesium gluconate, and 5 HEPES, pH 7.4] containing 1 mM ouabain, 100 μM amiloride, and 100 μM bumetanide in the presence or absence of 100 μM trichlormethiazide. Oocytes were transferred to K^+-free uptake medium [containing (in mM) 40 NaCl, 56 NMDG-Cl, 1.8 $CaCl_2$, 1 $MgCl_2$, and 5 HEPES, pH 7.4] with ouabain, amiloride, and bumetanide with or without trichlormethiazide and with 0.5 μCi of $^{22}Na^+$ for 60 min at 32°C. Oocytes were washed five times in an ice-cold radioactive-free medium and placed in individual tubes with 1% SDS. After lysis scintillation counting, liquid (ecolume, MP Biomedicals) was added.

Statistical Analysis

In experiments with $n \geq 3$, statistical significance was calculated with one-way ANOVA with multiple comparisons using GraphPad Prism 8.4.3. Significance was defined as $P \leq 0.05$. Results are presented as means ± SEM.

RESULTS

Generation and Characterization of a New Strain of KLHL3 Knockin Mice

KLHL3 knockin mice carrying the FHHt mutation R528H that prevents binding to WNK kinases (20, 21) were generated by TaconicArtemis (http://www.taconic.com/wmspage.cfm?parm1=1453).

Phenotypic characterization under basal conditions showed that the mice displayed the expected FHHt-like phenotype with hyperkalemia, metabolic acidosis, and hyperchloremia (Table 1). The abundance and phosphorylation of relevant renal transporters and regulatory proteins were also studied. As previously reported for a $KLHL3^{+/R528H}$ strain generated by Susa and collaborators (22), higher WNK4 and NCC expression levels as well as higher NCC (Thr^{60}) and SPAK (Ser^{373}) phosphorylation levels were observed in $KLHL3^{+/R528H}$ mice compared with wild-type mice. These differences were more dramatic in $KLHL3^{R528H/R528H}$ mice (Fig. 1). In homozygotes, SPAK and OSR1 expression levels were also higher than in wild-type mice. Additionally, in contrast to what was reported by Susa et al., a clear decrease in the abundance of the full-length and cleaved forms of α-ENaC was observed in both $KLHL3^{+/R528H}$ and $KLHL3^{R528H/R528H}$ mice made for this study. This finding was corroborated by immunofluorescent staining of kidney sections (Fig. 2). Finally, in sections stained with SPAK and phospho-SPAK (Ser^{373}) antibodies, a punctate signal was observed in the cytoplasm of some cortical tubular cells of $KLHL3^{+/R528H}$ and $KLHL3^{R528H/R528H}$ mice that contrasted with the apical signal observed in wild-type mice. In the medullary portion, an apical expression pattern was observed in some tubules of wild-type and mutant mice, and this signal intensity was higher in mutant mice.

KS-WNK1 Is Highly Sensitive to CUL3-KLHL3 E3 Ligase Complex-Mediated Degradation in Vivo

To analyze the effect of the KLHL3-R528H mutation on WNK1 expression, we used an antibody directed against a COOH-termi-

Table 1. *Serum electrolytes of wild-type, $KLHL3^{+/R528H}$, and $KLHL3^{R528H/R528H}$ mice*

	$KLHL3^{+/+}$	$KLHL3^{+/R528H}$	$KLHL3^{R528H/R528H}$
Na^+, mM	146.6 ± 1.06 (n = 17)	147.3 ± 0.45 (n = 28)	148.5 ± 0.77 (n = 16)
K^+, mM	4.63 ± 0.09 (n = 18)	5.40 ± 0.1 (n = 28)*	5.56 ± 0.13 (n = 16)*
Cl^-, mM	115.3 ± 1.46 (n = 17)	123.8 ± 1.94 (n = 24)*	123.3 ± 2.03 (n = 14)*
Ca^{2+}, mM	2.21 ± 0.05 (n = 4)	2.28 ± 0.05 (n = 5)	2.36 ± 0.09 (n = 5)
pH	7.32 ± 0.03 (n = 6)	ND	7.18 ± 0.03 (n = 3)*

Data are means ± SE; n represents the number of mice included in the analyses. KLHL3, Kelch-like protein 3. *$P < 0.05$ versus wild-type mice.

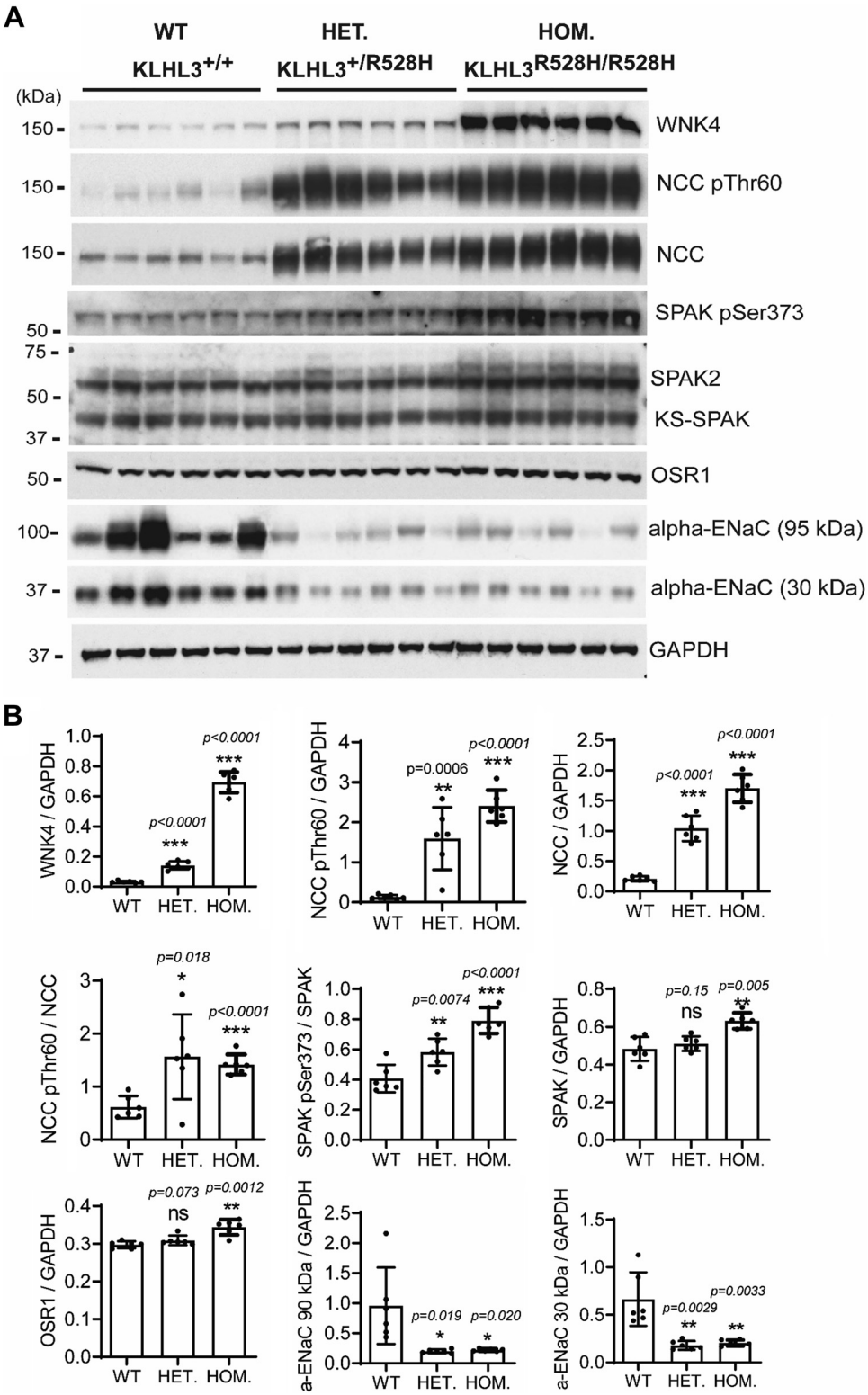

Figure 1. Kelch-like protein 3 (*KLHL3*)$^{+/R528H}$ and *KLHL3*$^{R528H/R528H}$ mice display the expected changes in the expression and phosphorylation levels of components of the with no lysine kinase 4 (WNK4)-STE20/SPS1-related proline-alanine-rich protein kinase (SPAK)/oxidative stress response-1 (OSR1)-NaCl cotransporter (NCC) pathway. *A*: total kidney extracts from wild-type (WT), *KLHL3*$^{+/R528H}$ [heterozygous (HET)] and *KLHL3*$^{R528H/R528H}$ [homozygous (HOM)] mice were subjected to Western blot analysis with the indicated antibodies. Each sample was derived from a separate littermate animal. *B*: band intensities were quantified using ImageJ, and the results are presented relative to the expression of GAPDH. Increased expression of NCC and WNK4 as well as increased phosphorylation of SPAK (Ser^{373}) and NCC (Thr^{60}) were observed in *KLHL3*$^{+/R528H}$ mice. Such differences were more dramatic in *KLHL3*$^{R528H/R528H}$ mice, in which an increase in the expression of SPAK and OSR1 was also observed. ENaC, epithelial Na^+ channel; ns, not significant.

nal epitope of the protein that can recognize both L-WNK1 and KS-WNK1 (pan-WNK1 antibody). Given that several bands were observed in the blots performed with this antibody, in order to identify the band corresponding to KS-WNK1, we included in these experiments lysates from KS-WNK1 knockout mice [*KS-WNK1*$^{-/-}$, a kind gift of Hadchouel (15), INSERM Paris] and *KLHL3*$^{R528H/R528H}$; *KS-WNK1*$^{-/-}$ double mutants.

Interestingly, we observed no band at the expected size for KS-WNK1 in wild-type mice, but a robust band of this size was observed in *KLHL3*$^{R528H/R528H}$ mice (Fig. 3). Its absence in

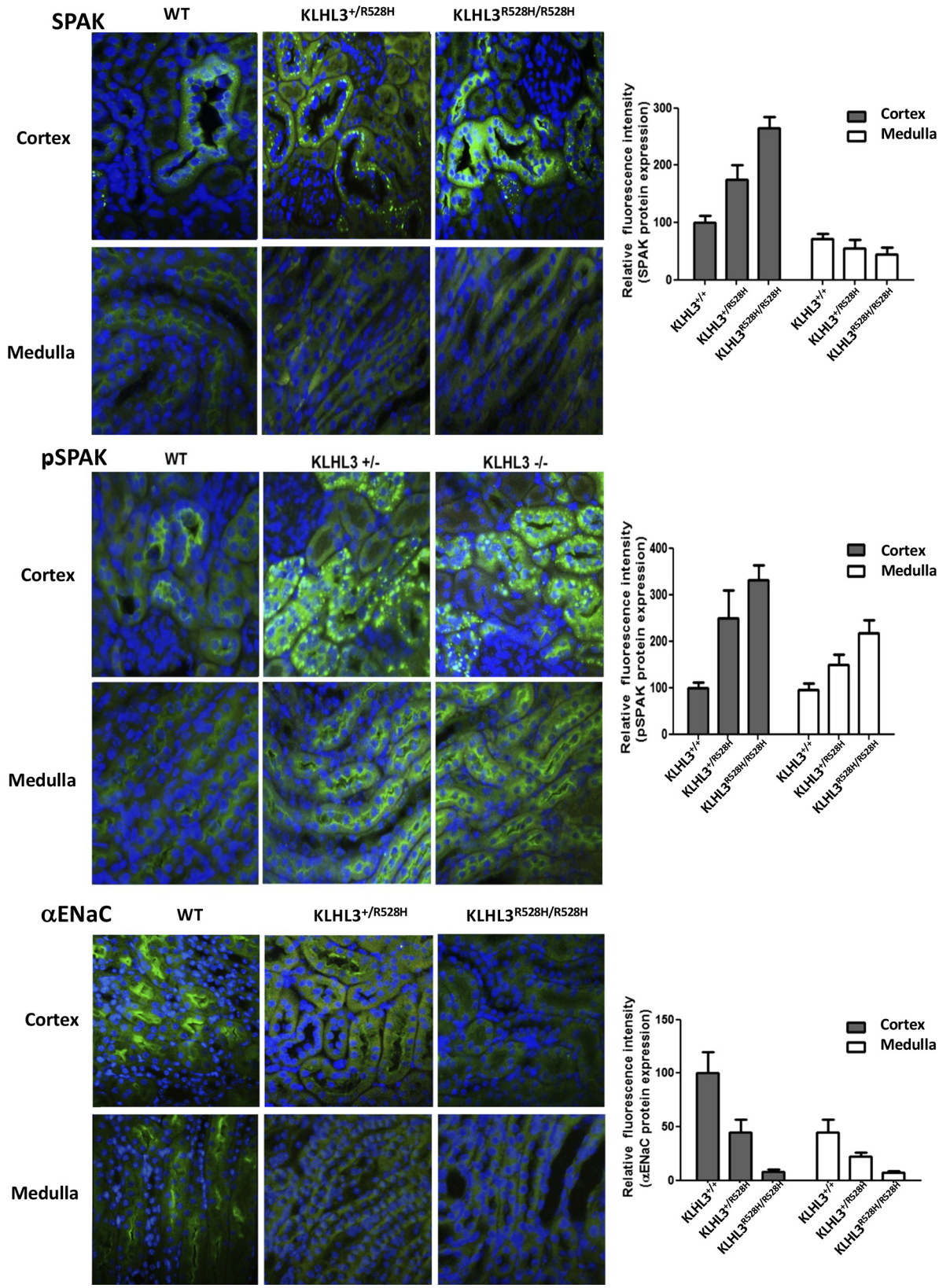

Figure 2. Immunofluorescent staining of kidney sections was performed. The primary antibodies used are indicated. Representative images from cortical and medullary regions are shown. Fluorescence intensity was quantified using ImageJ, and the results are presented in the corresponding bar graphs. ENaC, epithelial Na^+ channel; KLHL3, Kelch-like protein 3; pSPAK, phospho-SPAK; SPAK, STE20/SPS1-related proline-alanine-rich protein kinase; WNK1, with no lysine kinase 1.

double-mutant mice confirmed that indeed this band corresponds to KS-WNK1. These observations suggest that the KS-WNK1 protein expression level is very low (undetectable by Western blot) in kidneys from wild-type mice under basal conditions, which is striking given the high KS-WNK1 mRNA levels that have been reported for renal tissue (11). This observation supports, as suggested by Luis-Dit-Picard et al. (8), that KS-WNK1 is highly sensitive to CUL3-KLHL3 E3-mediated degradation, given the large upregulation observed in *KLHL3*$^{R528H/R528H}$ mice in which WNK-KLHL3 binding is impaired.

Finally, a band of higher molecular weight that may correspond to L-WNK1 was observed with the pan-WNK1 antibody, whose intensity was similar in all genotypes. We cannot rule out, however, that this may be a nonspecific band. WNK4 expression in the kidneys from wild-type and *KS-WNK1*$^{-/-}$ mice was similar, whereas, as expected, it was increased in *KLHL3*$^{R528H/R528H}$ mice and double-mutant mice.

Knockout of KS-WNK1 Does Not Prevent the FHHt Phenotype of KLHL3$^{R528H/R528H}$ Mice

Given the striking KS-WNK1 protein upregulation that we observed in *KLHL3*$^{R528H/R528H}$ mice, we decided to evaluate whether this upregulation is implicated in the pathogenesis of FHHt. Thus, we studied the phenotype of *KLHL3*$^{R528H/R528H}$; *KS-WNK1*$^{-/-}$ mice and compared it with the phenotype of *KLHL3*$^{R528H/R528H}$ mice. We observed that double-knockout mice have an FHHt phenotype with serum K^+, Cl^-, HCO_3^-, and pH levels similar to those observed in *KLHL3*$^{R528H/R528H}$ mice (Table 2). Thus, KS-WNK1 upregulation does not seem to play a central role in the pathogenesis of FHHt. In further experiments, administration of diets with altered content of K^+ and Na^+ may help to uncover phenotypic differences. However, this was out of the scope of this work.

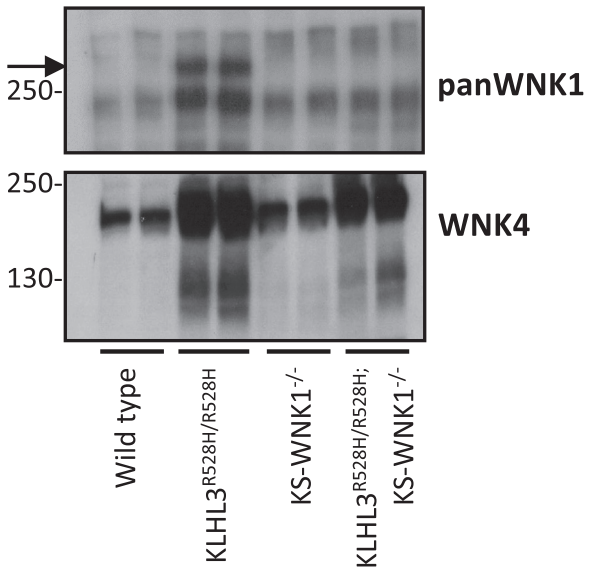

Figure 3. Kidney-specific with no lysine kinase (WNK)1 (KS-WNK1) protein levels are undetectable in kidney tissue of wild-type mice but are high in mice in which cullin 3-Kelch-like protein 3 (KLHL3) E3-mediated degradation is prevented. Total kidney lysates from *KLHL3*$^{R528H/R528H}$ mice, *KS-WNK1*$^{-/-}$ mice, and double mutants (*KLHL3*$^{R528H/R528H}$; *KS-WNK1*$^{-/-}$ mice) were analyzed by Western blot to assess the expression of WNK1 isoforms (as measured by the pan-WNK1 antibody). The robust band observed in *KLHL3*$^{R528H/R528H}$ mice (arrow) that was absent in wild-type mice corresponds to KS-WNK1, as corroborated by its absence in the double mutants. The WNK4 blot is presented at the *bottom*. The expected increase in WNK4 expression was observed in *KLHL3*$^{R528H/R528H}$ samples and in *KLHL3*$^{R528H/R528H}$; *KS-WNK1*$^{-/-}$ mice.

KS-WNK1 and L-WNK1 Exhibit Different Sensitivity to CUL3-KLHL3 E3-Mediated Degradation

Our preliminary data, published in Louis-Dit-Picard et al. (8), showed that KS-WNK1 is heterologously expressed in *X. laevis* oocytes and in human embryonic kidney (HEK)-293 cells is readily degraded when coexpressed with KLHL3. In contrast, L-WNK1 is resistant to such degradation. To further explore this phenomenon, we began by analyzing the effect of KLHL3 coexpression on KS-WNK1 and L-WNK1-mediated activation of NCC. We microinjected *X. laevis* oocytes with NCC cRNA in the absence or presence of L-WNK1 or KS-WNK1 cRNA with or without KLHL3 cRNA. Three days later, thiazide-sensitive tracer Na^+ uptake was assessed. As we have previously shown (12), both KS-WNK1 and L-WNK1 were able to increase the activity of NCC, despite the fact that KS-WNK1 has no kinase domain (Fig. 4*A*). Our previous work supported that the effect of KS-WNK1 on NCC is likely due to an interaction of KS-WNK1 with an endogenous WNK kinase, since the presence of KS-WNK1 increased the phosphorylation of SPAK and NCC, and the effect was prevented by the specific WNK inhibitor WNK463 (12). Consistent with our preliminary observations (8), the effect of KS-WNK1 on NCC was completely prevented by coinjection with KLHL3 cRNA, whereas the effect of L-WNK1 on NCC was not.

We then analyzed the effect of KLHL3 expression on L-WNK1, KS-WNK1, WNK3, and WNK4 abundances. This effect has been previously described. However, no study has compared the effect of KLHL3 on all these WNK isoforms in parallel (4, 5, 21). Figure 4*B* shows a representative image of such analysis. Oocytes were injected with each WNK cRNA alone or coinjected with KLHL3 cRNA. L-WNK1, KS-WNK1, and WNK3 expression was assessed with anti-c-myc antibodies and WNK4 and KLHL3 with anti-Flag antibodies. Consistent with the results shown in Fig. 4*A*, the presence of KLHL3 had little to no effect on the L-WNK1 expression level, whereas the expression of KS-WNK1 in the presence of KLHL3 was completely abrogated. In addition, we observed that WNK3 and WNK4 exhibited high sensitivity to CUL3-KLHL3 E3-mediated degradation. Thus, according to the densitometric analysis (Fig. 4*C*), it appears that at least in *X. laevis* oocytes the sensitivity of L-WNK1 to the effect of the CUL3-KLHL3 E3 complex was significantly lower than that observed for the other WNKs. A similar observation has also been reported in HEK-293 cells by Louis-Dit-Picard et al. (8).

The Unique KS-WNK1 Segment Encoded by Exon 4a Is Involved in the Sensitivity to the CUL3-KLHL3 E3 Ligase Complex

L-WNK1 and KS-WNK1 have different NH_2-terminal portions but are identical from the beginning of the segment encoded by exon 5 until the end of the protein. Thus, they

Table 2. *Serum electrolytes of wild-type, KLHL3$^{R528H/R528H}$, KS-WNK1$^{-/-}$, and double-mutant mice*

	KLHL3$^{+/+}$; KS-WNK1$^{+/+}$	KLHL3$^{R528H/R528H}$; KS-WNK1$^{+/+}$	KLHL3$^{+/+}$; KS-WNK1$^{-/-}$	KLHL3$^{R528H/R528H}$; KS-WNK1$^{-/-}$
Na^+, mM	151 ± 0.56 (n = 6)	152 ± 0.56 (n = 6)	150 ± 0.61 (n = 6)	153 ± 0.58 (n = 6)
K^+, mM	4.5 ± 0.16 (n = 6)	5.1 ± 0.10 (n = 6)*	4.7 ± 0.12 (n = 6)	5.0 ± 0.12 (n = 6)*
Cl^-, mM	118 ± 0.61 (n = 6)	123 ± 0.22 (n = 6)*	118 ± 0.53 (n = 6)	122 ± 0.40 (n = 6)*
Ca^{2+}, mM	4.2 ± 0.3 (n = 6)	4.5 ± 0.06 (n = 6)	4.2 ± 0.12 (n = 6)	4.3 ± 0.04 (n = 6)
pH	7.3 ± 0.03 (n = 6)	7.2 ± 0.01 (n = 6)	7.3 ± 0.02 (n = 6)	7.2 ± 0.01 (n = 6)
HCO_3^-, mM	20 ± 0.76 (n = 6)	14 ± 0.42 (n = 6)*	17 ± 0.36 (n = 6)	15 ± 0.52 (n = 6)*

Data are means ± SE; n represents the number of mice included in the analyses. KLHL3, Kelch-like protein 3; WNK1, with no lysine kinase 1. *$P < 0.05$ versus wild-type mice.

both contain the acidic motif (EPEEPEADQHQ) that mediates interactions with KLHL3 (Supplemental Fig. S2; see https://doi.org/10.6084/m9.figshare.13721794).

The first 30-amino acid residues of KS-WNK1 are unique to this isoform because they are encoded by exon 4a, which is not included in the L-WNK1 transcript. Exon 4a is highly conserved across evolution since its amino acid sequence is almost identical from coelacanths to humans (13), suggesting that it plays a key role in species that have evolved a renal tubule. This segment has been shown to be key for the formation of KS-WNK1-dependent WNK bodies (13). Thus, to evaluate its effect on KS-WNK1 activity and CUL3-KLHL3 E3-mediated degradation, we generated the KS-WNK1-Δ4a clone that lacks this fragment. We assessed its ability to activate NCC and its sensitivity to degradation promoted by CUL3-KLHL3 E3. As previously described (12), the absence of the 4a fragment prevents the positive effect of KS-WNK1 on NCC activity (Fig. 5*A*). Interestingly, this modification prevented KS-WNK1 functionality and also prevented its degradation, as demonstrated by the representative blot shown in Fig. 5*B* and the densitometric analysis shown in Fig. 5*C*. We observed a mild protective effect of the proteasome inhibitor MG132 against CUL3-KLHL3-RING-induced degradation of KS-WNK1, suggesting that other pathways may also be involved in degradation (Fig. 5*B*).

The Cysteines in Region 4a Are Important for KS-WNK1 Function but Not for Its CUL3-KLHL3 E3-Mediated Degradation

Boyd-Shiwarski et al. (13) have previously analyzed the degree of conservation of individual residues within the 4a segment and have identified a cluster of conserved cysteines and a cluster of conserved hydrophobic residues (Fig. 6*A*). Mutagenic analysis led them to conclude that these clusters, which they termed the "cysteine-rich hydrophobic motif," are key for the formation of KS-WNK1-dependent WNK bodies. Thus, we decided to evaluate their role on KS-WNK1-dependent NCC activation and sensitivity to CUL3-KLHL3 E3-induced degradation.

We first decided to analyze the role of conserved cysteines. For this purpose, we generated a clone with the six conserved cysteines mutated to serine (KS-6CxS mutant) and a clone in which only the outer two cysteines were mutated to serine (KS-2CxS mutant; Fig. 6*A*). According to the data by Boyd-Shiwarski et al. (13), the KS-6CxS mutation prevents the formation of WNK bodies, but the KS-2CxS mutation only partially does so.

We injected oocytes with NCC and wild-type KS-WNK1 or mutants KS-6CxS or KS-2CxS and treated them with or without MG132 to evaluate their function and degradation. We observed that the ability of the KS-6CxS mutant to activate NCC was completely abrogated, whereas that of the KS-2CxS mutant was only partially impaired (Fig. 6*B*). Regarding CUL3-KLHL3 E3-mediated degradation, we observed that both mutants were degraded in the presence of KLHL3, suggesting that, although the whole exon 4a seems to be important in conferring sensitivity to CUL3-KLHL3 E3-mediated degradation, the cysteine residues are not involved (Fig. 6, *C* and *D*).

The Cluster of Hydrophobic Residues in the 4a Segment of KS-WNK1 Are Key for NCC Activation and Confers KS-WNK1 Sensitivity to CUL3-KLHL3 E3-Mediated Degradation

We next analyzed the role of the cluster of hydrophobic residues on KS-WNK1 ability to activate NCC and on its sensitivity to CUL3-KLHL3 E3-mediated degradation. This cluster includes the five hydrophobic amino acid residues between the positions 11 and 15 (valine, phenylalanine, valine, isoleucine, and isoleucine; Fig. 6*A*). We generated a clone in which these five residues were mutated to glutamine (KS-5Q mutant). We decided to mutate these residues to glutamine given that Boyd-Shiwarski et al. (13) used this strategy to substitute the hydrophobic residues for hydrophilic ones and showed that these mutations prevented WNK body formation. Thus, we evaluated if the same mutations can also affect kidney-specific function and KLHL3-induced degradation. We observed that the ability of this mutant to activate NCC was completely impaired (Fig. 7*A*). Interestingly, however, we observed that this mutant was insensitive to CUL3-KLHL3 E3-induced degradation (Fig. 7, *B* and *C*).

Valine 11 and Valine 13 of KS-WNK1 Are Relevant for Its CUL3-KLHL3 E3-Mediated Degradation

To evaluate the role of individual residues within the hydrophobic cluster on KS-WNK1 activity and degradation, we generated the five single residue mutants and studied them in the oocyte system as performed for the other mutants. For the individual mutants, we decided to mutate each of the hydrophobic amino acid residues to alanine to explore whether the sole absence of the hydrophobic lateral chain is sufficient to produce these effects. We observed that the V11A mutant was unable to activate NCC and that this function was significantly reduced for the V13A mutant. For

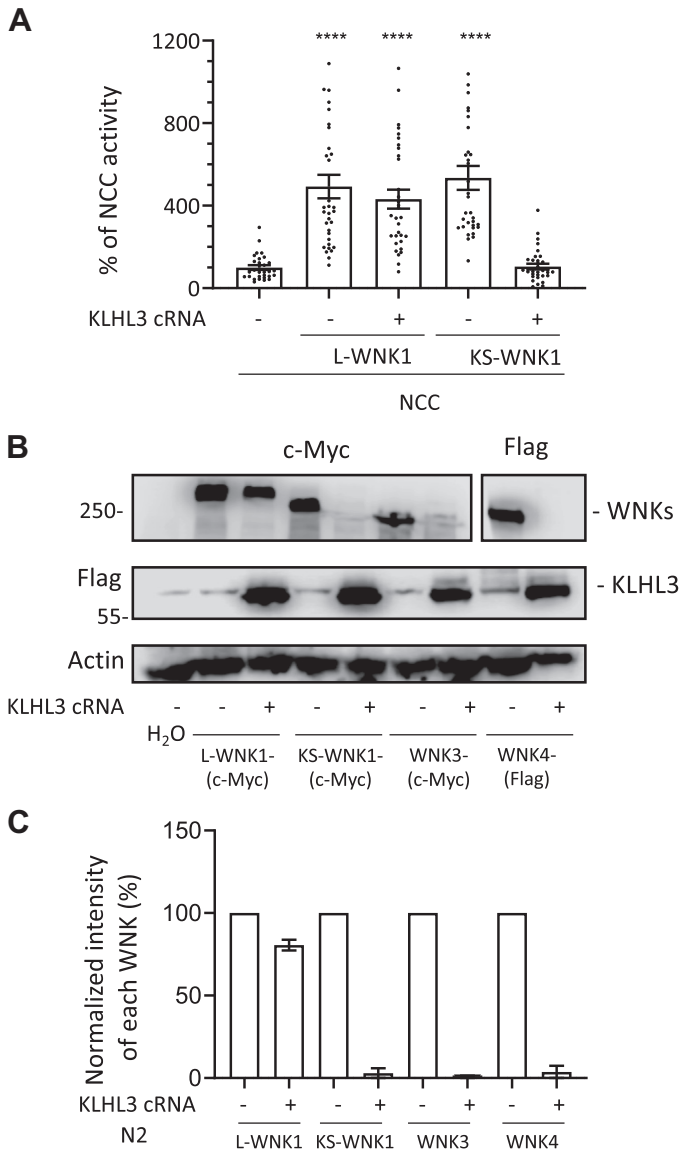

Figure 4. Kidney-specific with no lysine kinase (WNK)1 (KS-WNK1), WNK3, and WNK4, but not full-length WNK1 (L-WNK1), are degraded when coexpressed with Kelch-like protein 3 (KLHL3) in oocytes. *A*: thiazide-sensitive $^{22}Na^+$ uptake was assessed in *Xenopus laevis* oocytes injected with the indicated cRNAs. Uptake values observed in the control group (NCC only) were set to 100%, and the other groups were normalized accordingly. While both L-WNK1 and KS-WNK1 increased Na^+ uptake, KLHL3 coexpression prevented NaCl cotransporter (NCC) activation by KS-WNK1 but not by L-WNK1. Dots represent uptake values for individual oocytes. At least three independent experiments were performed with >10 oocytes per group (****$P < 0.0001$ vs. NCC; three points outside graphic limits). *B*: representative Western blots showing the effect of KLHL3 coexpression on L-WNK1, KS-WNK1, WNK3, and WNK4 levels. Oocytes were injected with cRNAs encoding for c-Myc-tagged L-WNK1, KS-WNK1, or WNK3 or Flag-tagged WNK4 with or without Flag-tagged KLHL3. All kinases except L-WNK1 were degraded in the presence of KLHL3. *C*: densitometric analysis of the Western blots presented in *B*. Two independent experiments were performed with similar results. c-Myc-tagged L-WNK1, KS-WNK1, or WNK3 or Flag-tagged WNK4 were normalized to 100% and compared with those observed in groups expressing KLHL3.

the remaining three mutants, this function was only slightly reduced (Fig. 8*A*). CUL3-KLHL3 E3-mediated degradation was impaired for the V11A and V13A mutants (Fig. 8, *B* and *C*), suggesting that these residues may participate in conferring the sensitivity to CUL3-KLHL3E3-mediated degradation.

KS-WNK1 Protein Expression Is Upregulated in Kidneys of Mice Maintained on Low-K^+ Diet

Ishizawa et al. (23) recently showed that phosphorylation of KLHL3 in a residue located within the substrate-binding domain is upregulated in mice that are maintained on a low-K^+ diet. This reduces CUL3-KLHL3 E3-targeted degradation

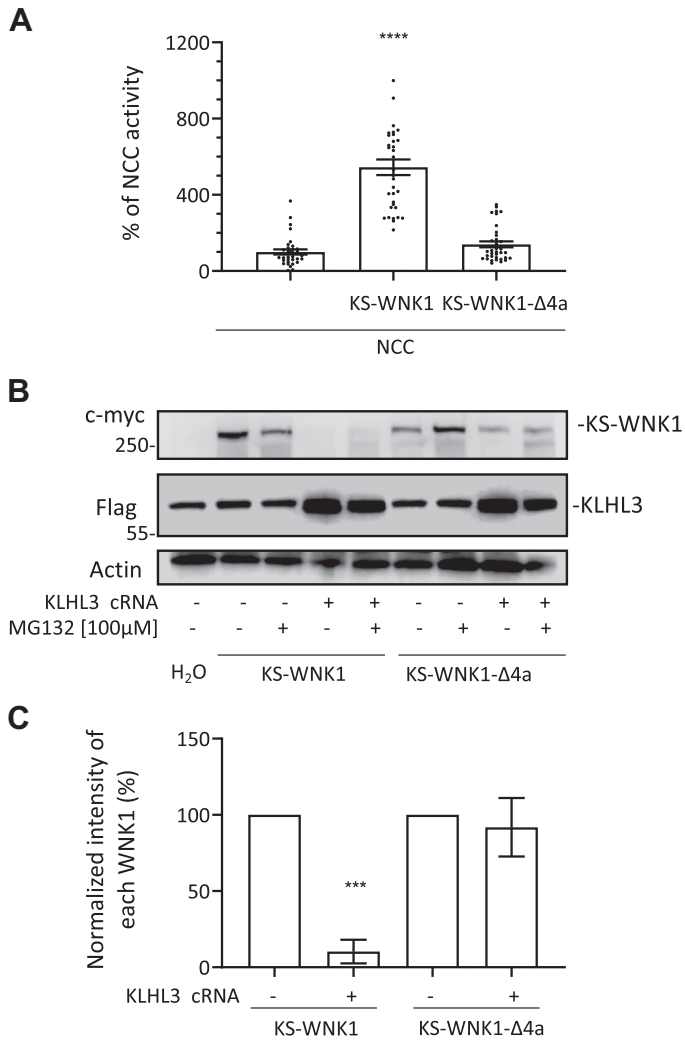

Figure 5. The segment encoded by exon 4a in kidney-specific with no lysine kinase 1 (KS-WNK1) is needed to activate NaCl cotransporter (NCC) and to be targeted for degradation by cullin-3 (CUL3)–Kelch-like protein 3 (KLHL3) E3. *A*: thiazide-sensitive Na^+ uptake of NCC cRNA-injected oocytes was set to 100%, and uptake values of additional groups were normalized accordingly. KS-WNK1 coexpression increased NCC activity, but the KS-WNK1-Δ4a mutant failed to activate (n = 3 transport assays, ****$P < 0.0001$ vs. NCC; one point outside graphic limits). *B*: representative Western blots showing KS-WNK1 and KS-WNK1-Δ4a expression in the absence or presence of KLHL3. CUL3-KLHL3 E3-induced degradation of KS-WNK1 is observed regardless of proteosome inhibition, whereas KS-WNK1-Δ4a is expressed but resistant to CUL3-KLHL3 E3-induced degradation. *C*: densitometric analysis of the Western blots presented in *B*. Results from four different experiments were included. Expression of KS-WNK1 or KS-WNK1-Δ4a in the absence of KLHL3 were arbitrarily set to 100% and compared with expression levels observed in the presence of KLHL3 (n = 4 Western blots, ***$P > 0.001$ vs. control without KLHL3).

AJP-Renal Physiol • doi:10.1152/ajprenal.00575.2020 • www.ajprenal.org

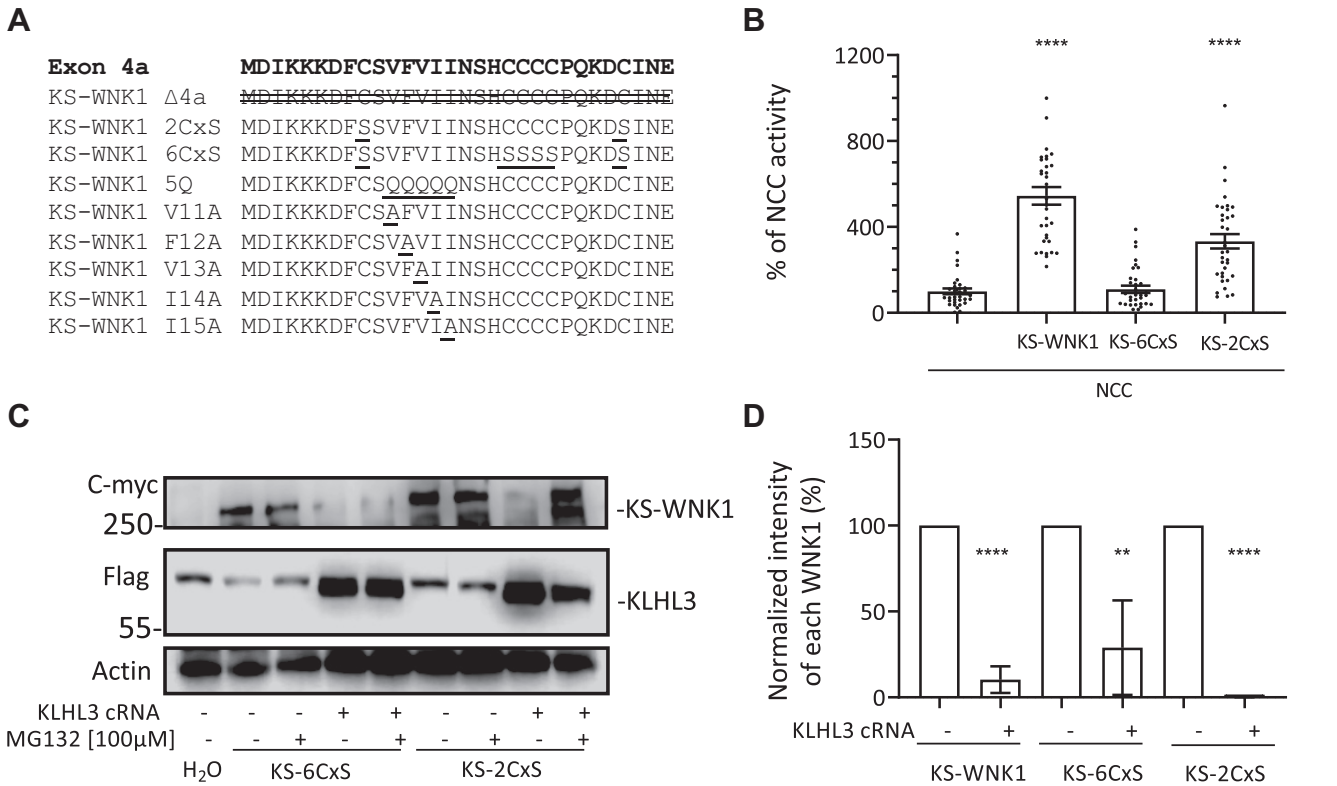

Figure 6. Mutation of the six conserved cysteines encoded in exon 4a impairs the ability of kidney-specific with no lysine kinase 1 (KS-WNK1) to activate NaCl cotransporter (NCC) but does not prevent cullin-3 (CUL3)-Kelch-like protein 3 (KLHL3) E3-induced degradation. *A*: amino acid sequence encoded by exon 4a. Different KS-WNK1 mutants were generated for this work with variations in the sequence of this region. The modifications introduced in each mutant are indicated. *B*: NCC was coexpressed in oocytes with KS-WNK1, KS-6CxS (in which all six cysteines were mutated to serine), or KS-2CxS (in which the two peripheral cysteines were mutated to serine). Thiazide-sensitive Na^+ uptake of NCC-expressing oocytes was set to 100% and compared with all other groups, which were normalized accordingly. KS-WNK1-6CxS did not activate NCC, whereas KS-WNK1-2CxS did activate NCC, albeit at a lower level than wild-type KS-WNK1 ($n = 3$ transport assays, $^{****}P < 0.0001$ vs. NCC; 3 points outside graphic limits). *C*: representative Western blots showing the expression of KS-WNK1-6CxS and KS-WNK1-2CxS. Both mutant proteins are targeted for degradation by CUL3-KLHL3 E3, whereas treatment with MG132 could prevent KS-WNK1-2CxS degradation. *D*: compiled results of densitometric analysis from at least two different Western blot experiments like that presented in (*B*). Expression levels of KS-WNK1, KS-WNK1-6CxS, and KS-WNK1-2CxS in the absence of KLHL3 were normalized to 100% and compared with groups expressing KLHL3 ($n = 2-4$ Western blots, $^{**}P < 0.01$ and $^{****}P < 0.0001$ vs. control without KLHL3).

of WNK4. Thus, to evaluate whether K^+ restriction is a possible physiological stimuli for induction of KS-WNK1 expression, wild-type, and *KLHL3*$^{+/R528H}$ mice were placed on low-K^+ diet for 7 days and then euthanized for renal tissue collection. Kidney lysates were prepared and analyzed by Western blot analysis with pan-WNK1 and WNK4 antibodies (Fig. 9).

The band corresponding to KS-WNK1 was only barely observed in samples from *KLHL3*$^{+/R528H}$ mice (Fig. 9), in contrast to what we previously observed with *KLHL3*$^{R528H/R528H}$ mouse samples (Fig. 3). This suggests that the residual activity of the CUL3-KLHL3 E3 complex present in heterozygous mice is sufficient to almost entirely degrade KS-WNK1. A more robust band was observed in samples from wild-type and *KLHL3*$^{+/R528H}$ mice maintained on the low-K^+ diet, showing that indeed KS-WNK1 expression is induced under conditions of dietary K^+ restriction. WNK4 upregulation was also observed, as previously reported (23).

DISCUSSION

In the present study, we show that KS-WNK1 is more sensitive to CUL3-KLHL3 E3-mediated degradation than L-WNK1, and we began to explore the elements of their primary sequence that are responsible for this difference. Given that the known binding site for KLHL3 in WNK kinases is the acidic motif, the observation is puzzling as both proteins present the exact same binding site. Interestingly, we observed that removal of the unique sequence of KS-WNK1 encoded by exon 4a decreases its sensitivity to CUL3–KLHL3 E3-mediated degradation. This shows that targeting by KLHL3 of the COOH-terminal segment of WNK1 (comprising the sequence encoded from exon 5 until the end that includes the acidic motif) is not efficient unless this 30-amino acid residue segment is present. We also showed that this segment is critical for the ability of KS-WNK1 to activate NCC. Other works also support the key role of exon 4a for KS-WNK1 function. For instance, Argaiz et al. (12) showed that the ability of KS-WNK1 to activate NCC by promoting WNK4 phosphorylation is impaired by the removal of this segment, although KS-WNK1 binding to WNK4 was not affected, and Boyd-Shiwarski et al. (13) showed that exon 4a is necessary for the KS-WNK1-dependent formation of WNK bodies.

Interestingly, the analysis of the effects of mutation of certain conserved residues within exon 4a showed that some of

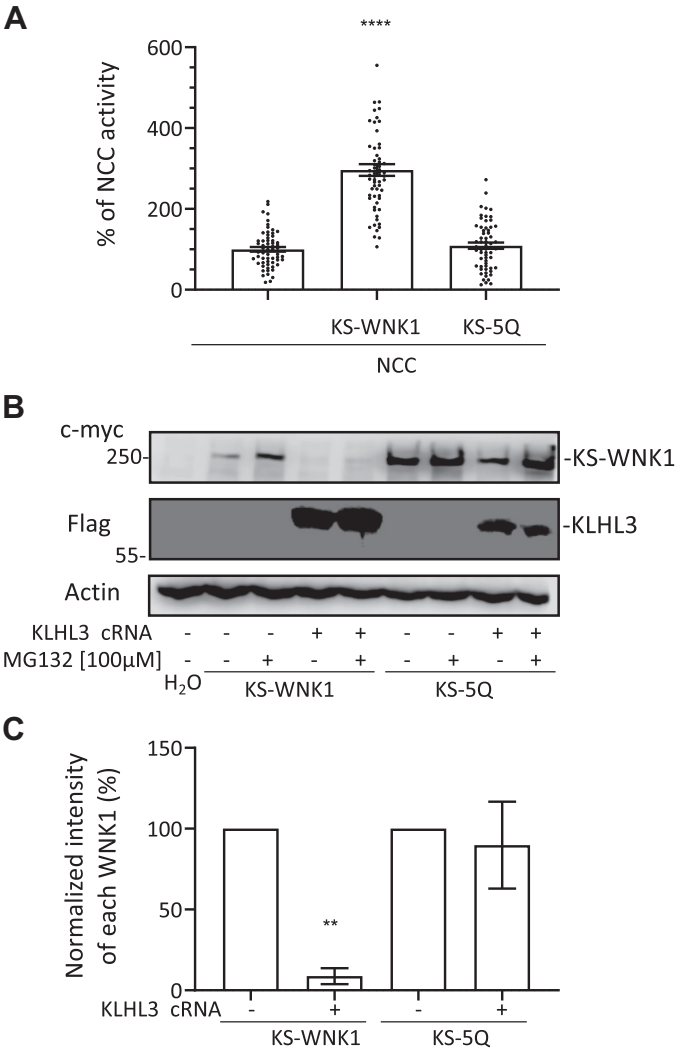

Figure 7. Mutation of the five conserved hydrophobic residues encoded in exon 4a impairs the ability of kidney-specific with no lysine kinase 1 (KS-WNK1) to activate NaCl cotransporter (NCC) and prevent cullin-3-Kelch-like protein 3 (KLHL3) E3-induced degradation. *A*: NCC was coexpressed in oocytes with KS-WNK1 or KS-5Q (in which all five hydrophobic residues were mutated to glutamine), and thiazide-sensitive Na^+ uptake was assessed. Uptake levels observed for NCC-expressing oocytes were normalized to 100% and compared with those observed for groups expressing KS-WNK1 and KS-5Q. The strong activation of NCC induced by KS-WNK1 was not observed in the KS-5Q mutant ($n = 5$ transport assays, $^{****}P < 0.0001$ vs. NCC; 2 points outside graphic limits). *B*: representative Western blots showing the expression of KS-WNK1 and KS-5Q. KS-WNK1 was degraded in the presence of KLHL3, whereas KS-5Q was not degraded. Treatment with MG132 increased KS-5Q expression, probably by impairing degradation even more. *C*: compiled results of densitometric analysis from three different experiments like that presented in *B*. Expression levels of KS-WNK1 and KS-5Q in the absence of KLHL3 were normalized to 100% and compared with those observed in groups expressing KLHL3 ($n = 3$ Western blots, $^{**}P < 0.01$ vs. control without KLHL3).

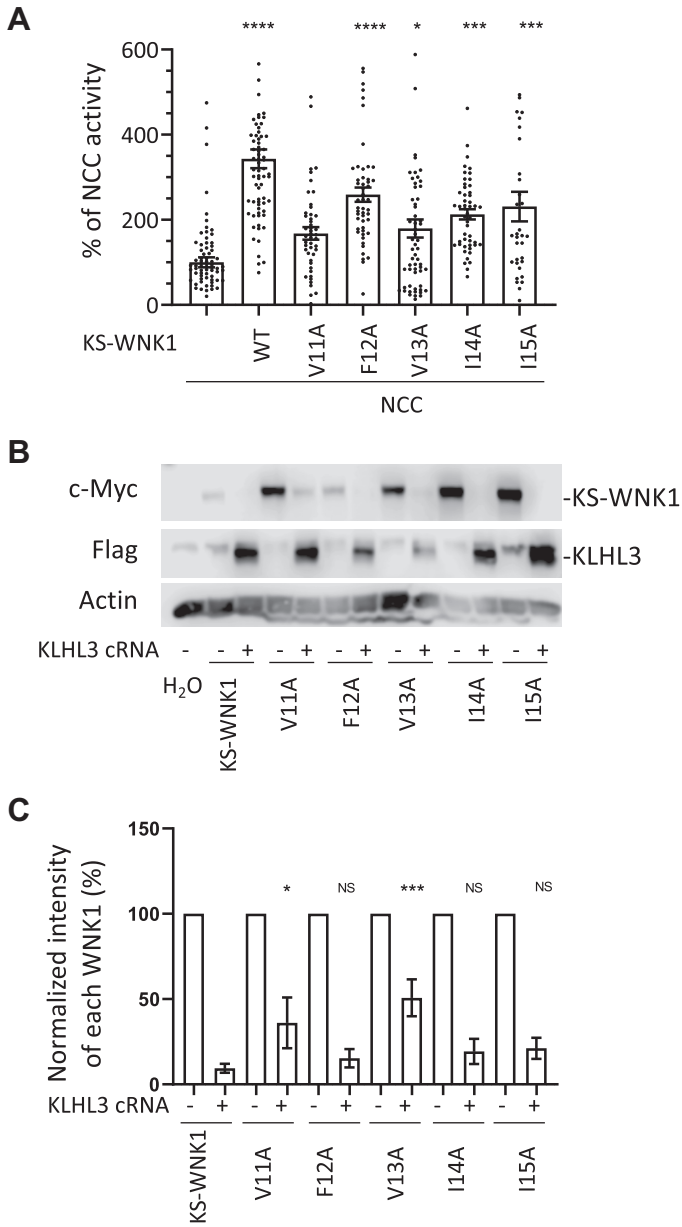

Figure 8. Mutation of valine 11 or valine 13 located in the hydrophobic motif of exon 4a impairs the ability of kidney-specific with no lysine kinase 1 (KS-WNK1) to activate NaCl cotransporter (NCC) and cullin-3-Kelch-like protein 3 (KLHL3) E3-induced degradation of KS-WNK1. *A*: NCC was coexpressed in oocytes with KS-WNK1 or with KS-WNK1 mutants containing one of the following single amino acid substitutions: V11A, F12A, V13A, I14A, or I15A. Uptake levels observed for NCC-expressing oocytes were normalized to 100% and compared with those observed for groups expressing KS-WNK1 mutants. All mutants except KS-WNK1-V11A were capable of activating NCC ($n = 3–5$ transport assays, $^{*}P < 0.05$, $^{***}P < 0.001$, and $^{****}P < 0.0001$ vs. NCC; 16 points outside graphic limits). *B*: representative Western blots showing the expression of KS-WNK1 and of each single-residue mutant in the absence or presence of KLHL3. Compared with wild-type (WT) KS-WNK1, there was significantly less degradation of the V11A and V13A mutants in the presence of KLHL3. Other mutants degraded similarly to the WT. *C*: compiled results of densitometric analysis from at least five different experiments like that presented in *B*. Expression levels of KS-WNK1 and single-residue mutants in the absence of KLHL3 were normalized to 100%. Degradation of single-residue mutants were compared with WT KS-WNK1 in the presence of KLHL3 ($n = 5–8$ Western blots, $^{*}P < 0.05$ and $^{***}P < 0.001$ vs. control with KLHL3).

these modifications alter KS-WNK1 ability to activate NCC, but not its targeting by KLHL3, whereas those that affect KLHL3 targeting also affect the ability to activate NCC. Thus, although the same segment is key to define the sensitivity to CUL3-KLHL3 E3 and the ability of KS-WNK1 to activate NCC, these properties can be dissociated, suggesting that they are not strictly dependent on one another.

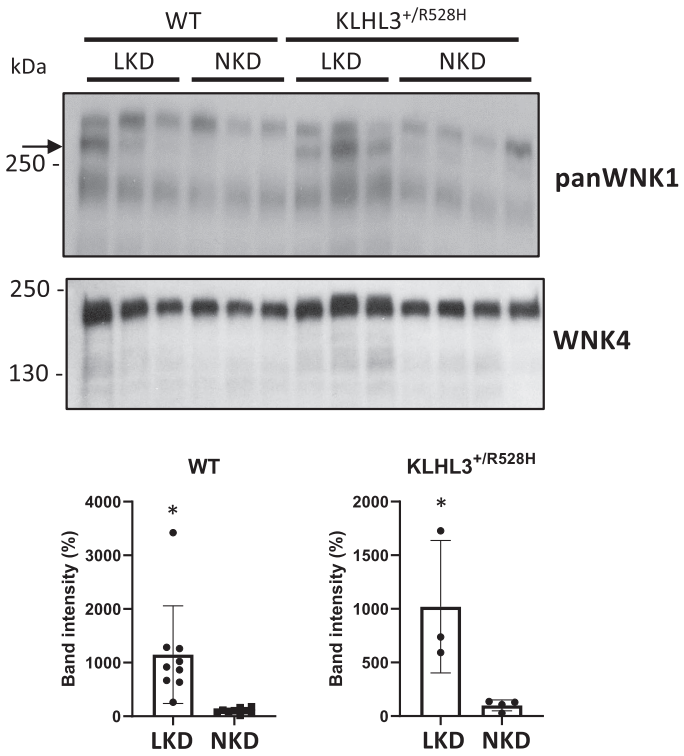

Figure 9. Renal kidney-specific with no lysine kinase 1 (KS-WNK1) expression is induced by a low-K^+ diet (LKD). Total kidney lysates from wild-type (WT) and Kelch-like protein 3 (KLHL3)$^{+/R528H}$ mice maintained on a normal-K^+ diet (NKD) or LKD were analyzed by Western blot to assess the expression of KS-WNK1. Compared with WT mice, moderately higher expression was observed in KLHL3$^{+/R528H}$ mice. In addition, a robust increase in KS-WNK1 expression was observed in WT mice but also in KLHL3$^{+/R528H}$ mice, suggesting that KLHL3-targeted degradation was further affected under this condition. Results of quantitation of the band corresponding to KS-WNK1 are shown at the *bottom*. Band intensity values of mice on a NKD were normalized to 100%. A WNK4 blot is also shown. The expected increase in WNK4 expression was observed in KLHL3$^{+/R528H}$ samples. Expression was further increased when mice were placed on a LKD, as previously reported (10). $n = 9$ for WT mice on the LKD and NKD, $n = 3$ for KLHL3$^{+/R528H}$ mice on the NKD, and $n = 4$ for KLHL3$^{+/R528H}$ mice on the LKD. *$P < 0.05$ versus the NKD. WNK1, with no lysine kinase 1.

Substitution of either one of two specific residues within the conserved hydrophobic motif in exon 4a was enough to prevent CUL3-KLHL3 E3-mediated degradation of KS-WNK1. The mechanisms underlying 4a segment's role on KS-WNK1 activity and sensitivity to targeting by KLHL3 remain as open questions for future studies. Possible mechanisms are, for example, that this segment may be involved in establishing key interactions or that perhaps it could be a determinant to achieve a specific conformational state of the protein.

Our data suggest that KS-WNK1 is also highly sensitive to CUL3-KLHL3 E3-mediated degradation in vivo. Vidal-Petiot et al. (11) reported that KS-WNK1 mRNA levels are high in the kidney (higher than L-WNK1 mRNA levels). Despite this, we were unable to detect KS-WNK1 protein in kidney lysates from wild-type mice by Western blot analysis. However, robust KS-WNK1 protein expression was detected in lysates from *KLHL3*$^{R528H/R528H}$ mice in which KLHL3-WNK binding is impaired. Thus, the low protein expression observed in wild-type mice may result from a high degradation rate of KS-WNK1. The physiological significance of this observation remains to be determined. Analogous biological phenomena have been described. For example, the ubiquitous transcription factor hypoxia-inducible factor-1α (HIF-1α) is normally undetectable at the protein level due to highly active proteasomal degradation that is dependent on the presence of O_2 (24). HIF-1α is marked for degradation by a cullin–RING E3 ligase complex in which the von Hippel-Lindau (VHL) tumor suppressor protein acts as the substrate recognition element. VHL can only recognize HIF-1α when it is hydroxylated at two proline residues, and hydroxylation is dependent on the activity of prolyl-hydroxylases that are activated in the presence of O_2. Thus, in conditions of hypoxia, hydroxylation is prevented and HIF-1α expression is rapidly induced, as well as expression of its target genes.

In the case of KS-WNK1, the physiological stimuli that can upregulate its expression remain to be elucidated. We show here, however, that one of these stimuli is dietary K^+ restriction. Ishizawa et al. (23) have shown that KLHL3 phosphorylation in the substrate recognition domain is induced by low-K^+ intake in mice. Thus, low-K^+-induced phosphorylation of KLHL3 may underlie the observed upregulation of KS-WNK1 in mice on a low-K^+ diet. This observation is in line with the fact that the formation of WNK bodies, which is induced by low-K^+ intake, requires the presence of KS-WNK1, suggesting that indeed the DCT response to low-K^+ intake involves KS-WNK1 upregulation due to KLHL3 inhibition by phosphorylation. This agrees with the observation that WNK bodies are present in KLHL3$^{R528H/R528H}$ mice (Fig. 2) but not in mice with FHHt caused by mutations in WNK4 (14).

The physiological role of KS-WNK1 is currently a very controversial issue. However, knowledge of the conditions in which KS-WNK1 protein is expressed in the DCT may help guide experiments to uncover this physiological role. In the present work, we show that despite the high KS-WNK1 protein upregulation observed in FHHt mice due to a mutation in KLHL3, KS-WNK1 is not essential to develop the FHHt phenotype. That is, WNK4 overexpression appears to be sufficient to produce the disease, consistent with prior results (25).

Different lines of evidence obtained from a diversity of transgenic mouse models suggest that the WNK1 isoform expressed in the DCT is KS-WNK1 and that L-WNK1 is not normally present (1). Absence of WNK4 expression completely impairs the phosphorylation and activity of NCC (26), demonstrating that WNK4 absence cannot be compensated by L-WNK1 activity. Additionally, in KLHL3$^{R528H/R528H}$ mice, expression of both L-WNK1 and WNK4 is increased but the FHHt phenotype is completely abrogated by elimination of WNK4, although L-WNK1 remains upregulated, strongly suggesting that L-WNK1 is not present in the DCT (25). Thomson et al. (14) have shown that, within the large WNK bodies observed in WNK4 knockout mice, no active WNK1 is present, as indicated by the lack of signal obtained with the pT-loop WNK antibody, supporting that the WNK1 product in the WNK bodies is KS-WNK1, not L-WNK1. Finally, it has been demonstrated that intronic *WNK1* deletions responsible for FHHt cause ectopic expression of L-WNK1 in the DCT (7), and this is the unique situation in which the absence of WNK4 does not result in NCC downregulation (18). Thus, given that L-WNK1 activity is less sensitive to inhibition by

Cl^- than WNK4 (27, 28) and less sensitive to CUL3-KLHL3 E3-induced degradation, as shown by this work, it is likely that ectopic expression of L-WNK1 promotes higher levels of NCC activity at any given value of intracellular Cl^- concentration and activity level of the CUL3-KLHL3 E3 complex. In this regard, it is noteworthy that *WNK1* intronic deletions cause FHHt even in the absence of WNK4 (18), supporting that if L-WNK1 is expressed in the DCT, the presence of WNK4 would be irrelevant. In future work, it would be interesting to establish how low-K^+ interferes with CUL3-KLHL3 E3-mediated degradation of KS-WNK1.

Finally, as mentioned in the INTRODUCTION, Louis-Dit-Picard et al. (8) have shown that humans and mice with heterozygous mutations in the acidic motif of WNK1 display a mild FHH phenotype that is easily corrected with thiazide treatment in both species. They also showed that the SPAK/OSR1-NCC pathway is upregulated in *WNK1*$^{+/delE631}$ mice. Thus, they proposed that NCC upregulation is the primary defect leading to the phenotypic alterations. Also, based on results from in vitro experiments, they proposed that the increased expression of KS-WNK1 in the DCT is largely responsible for NCC upregulation as KS-WNK1 abundance is preferentially affected by these mutations. The large WNK bodies observed in DCT cells of these mice also support this idea, as well as the in vitro and in vivo data presented in this work, showing that KS-WNK1 is very sensitive to CUL3-KLHL3 E3-induced degradation. However, as KS-WNK-1 activates NCC via WNK4, the effect of an increase in KS-WNK1 may be buffered by the amount of WNK4, causing only a mild activation of NCC. This activation is probably enough to cause slight hyperkalemia and volume retention but not enough to produce a rise in blood pressure.

In conclusion, our work shows, both in vivo and in vitro, that KS-WNK1 is highly sensitive to CUL3-KLHL3 E3-induced degradation, whereas L-WNK1 is much less sensitive. The high sensitivity of KS-WNK1 seems to be due to the presence of the unique segment encoded in exon 4a. This segment is also key for KS-WNK1 function and its ability to activate NCC. We propose that this exquisite sensibility of KS-WNK1 to targeting by KLHL3 may be relevant to achieve rapid induction of KS-WNK1 protein expression under certain conditions, one of which appears to be extracellular K^+ depletion. The mechanisms by which exon 4a affects the activity and sensitivity to degradation of KS-WNK1 and the role that KS-WNK1 upregulation plays under conditions of dietary K^+ deprivation remain to be explored.

ACKNOWLEDGMENTS

We thank Dr. Juliette Hadchouel for the kind gift of KS-WNK1 knockout colony and Hilda Sánchez for assistance.

GRANTS

This work was supported by National Institute of Diabetes and Digestive and Kidney Diseases Grant DK51496 (to G.G.), Grants 87794, 101720, and A1-S-8290 from Conacyt Mexico (to M.C-C., M.C-B., and G.G., respectively), Grants IA203620 and RA202718 from PAPIIT UNAM and Loreal L'Oréal-UNESCO-AMC-CONALMEX "For Women in Science, 2019" (to M.C-C.), and Grant IN201519 from PAPIIT UNAM (to G.G.). M.O-F. was supported by a scholarship from Conacyt-Mexico and is a graduate student in the PECEM MD/PhD program of the Universidad Nacional Autónoma de México. G.G. is the guarantor of the study. D.R.A. is supported by Medical Research Council Grant MC_UU_12016/2.

DISCLOSURES

No conflicts of interest, financial or otherwise, are declared by the authors.

AUTHOR CONTRIBUTIONS

M.O-F., M.C-C., J.Z., E.R.A., L.R-V., N.A.B., M.C-B., D.R.A., and G.G. conceived and designed research; M.O-F., N.V., M.C-B., J.Z., O.A., E.R.A., F.L.d-T., A.M.d-O., A.S-N., and L.R-V. performed experiments; M.O-F., M.C-C., J.Z., O.A., E.R.A., F.L.d-T., A.M.d-O., A.S-N., L.R-V., N.A.B., N.V., M.C-B., D.R.A., and G.G. analyzed data; M.O-F., M.C-C., M.C-C., J.Z., E.R.A., D.R.A., G.G., A.M.d-O., and A.S.N. interpreted results of experiments; M.O-F., M.C-B., J.Z., N.V., and G.G. prepared figures; M.O-F., M.C-C., M.C-B., and G.G. drafted manuscript; M.O-F., M.C-C., M.C-C., J.Z., E.R.A., A.M.d-O., A.S-N., L.R.V., N.A.B., D.R.A., and G.G. edited and revised manuscript; M.O-F., M.C-C., E.R.A., F.L.d-T., A.M.d-O., J.Z., A.S-N., L.R.V., N.A.B., N.V., M.C-B., D.R.A., and G.G. approved final version of manuscript.

REFERENCES

1. **Ostrosky-Frid M**, **Castaneda-Bueno M**, **Gamba G.** Regulation of the renal NaCl cotransporter by the WNK/SPAK pathway: lessons learned from genetically altered animals. *Am J Physiol Renal Physiol* 316: F146–F158, 2019. doi:10.1152/ajprenal.00288.2018.
2. **Boyden LM**, **Choi M**, **Choate KA**, **Nelson-Williams CJ**, **Farhi A**, **Toka HR**, et al**.** Mutations in kelch-like 3 and cullin 3 cause hypertension and electrolyte abnormalities. *Nature* 482: 98–102, 2012. doi:10.1038/nature10814.
3. **Louis-Dit-Picard H**, **Barc J**, **Trujillano D**, **Miserey-Lenkei S**, **Bouatia-Naji N**, **Pylypenko O**; **International Consortium for Blood Pressure (ICBP)**, et al**.** KLHL3 mutations cause familial hyperkalemic hypertension by impairing ion transport in the distal nephron. *Nat Genet* 44: 456–460, 2012 [Erratum in *Nat Genet* 44: 609, 2012]. doi:10.1038/ng.2218.
4. **Shibata S**, **Zhang J**, **Puthumana J**, **Stone KL**, **Lifton RP.** Kelch-like 3 and Cullin 3 regulate electrolyte homeostasis via ubiquitination and degradation of WNK4. *Proc Natl Acad Sci USA* 110: 7838–7843, 2013. doi:10.1073/pnas.1304592110.
5. **Wakabayashi M**, **Mori T**, **Isobe K**, **Sohara E**, **Susa K**, **Araki Y**, **Chiga M**, **Kikuchi E**, **Nomura N**, **Mori Y**, **Matsuo H**, **Murata T**, **Nomura S**, **Asano T**, **Kawaguchi H**, **Nonoyama S**, **Rai T**, **Sasaki S**, **Uchida S.** Impaired KLHL3-mediated ubiquitination of WNK4 causes human hypertension. *Cell Rep* 3: 858–868, 2013. doi:10.1016/j.celrep.2013.02.024.
6. **Lifton RP**, **Gharavi AG**, **Geller DS.** Molecular mechanisms of human hypertension. *Cell* 104: 545–556, 2001. doi:10.1016/s0092-8674(01)00241-0.
7. **Vidal-Petiot E**, **Elvira-Matelot E**, **Mutig K**, **Soukaseum C**, **Baudrie V**, **Wu S**, **Cheval L**, **Huc E**, **Cambillau M**, **Bachmann S**, **Doucet A**, **Jeunemaitre X**, **Hadchouel J.** WNK1-related Familial Hyperkalemic Hypertension results from an increased expression of L-WNK1 specifically in the distal nephron. *Proc Natl Acad Sci USA* 110: 14366–14371, 2013. doi:10.1073/pnas.1304230110.
8. **Louis-Dit-Picard H**, **Kouranti I**, **Rafael C**, **Loisel-Ferreira I**, **Chavez-Canales M**, **Abdel KW**, **Argaiz E**, **Baron S**, **Vacle S**, **Migeon T**, **Coleman R**, **Do Cruzeiro M**, **Hureaux M**, **Thurairajasingam N**, **Decramer S**, **Girerd X**, **O'Shaughnessy KM**, **Mulatero P**, **Roussey G**, **Tack I**, **Unwin RJ**, **Vargas-Poussou R**, **Staub O**, **Grimm PR**, **Welling PA**, **Gamba G**, **Clauser E**, **Hadchouel J**, **Jeunemaitre X.** Mutations affecting the conserved acidic WNK1 motif cause inherited hyperkalemic hyperchloremic acidosis. *J Clin Invest* 130: 6379–6394 2020. doi:10.1172/JCI94171.
9. **Delaloy C**, **Lu J**, **Houot AM**, **Disse-Nicodeme S**, **Gasc JM**, **Corvol P**, **Jeunemaitre X.** Multiple promoters in the WNK1 gene: one controls

expression of a kidney-specific kinase-defective isoform. *Mol Cell Biol* 23: 9208–9221, 2003. doi:10.1128/mcb.23.24.9208-9221.2003.

10. **O'Reilly M**, **Marshall E**, **Speirs HJ**, **Brown RW.** WNK1, a gene within a novel blood pressure control pathway, tissue-specifically generates radically different isoforms with and without a kinase domain. *J Am Soc Nephrol* 14: 2447–2456, 2003. doi:10.1097/01.asn.0000089830.97681.3b.
11. **Vidal-Petiot E**, **Cheval L**, **Faugeroux J**, **Malard T**, **Doucet A**, **Jeunemaitre X**, **Hadchouel J.** A new methodology for quantification of alternatively spliced exons reveals a highly tissue-specific expression pattern of WNK1 isoforms. *PLoS One* 7: e37751, 2012. doi:10.1371/journal.pone.0037751.
12. **Argaiz ER**, **Chavez-Canales M**, **Ostrosky-Frid M**, **Rodriguez-Gama A**, **Vazquez N**, **Gonzalez-Rodriguez X**, **Garcia-Valdes J**, **Hadchouel J**, **Ellison DH**, **Gamba G.** Kidney-specific WNK1 isoform (KS-WNK1) is a potent activator of WNK4 and NCC. *Am J Physiol Renal Physiol* 315: F734–F745, 2018. doi:10.1152/ajprenal.00145.2018.
13. **Boyd-Shiwarski CR**, **Shiwarski DJ**, **Roy A**, **Nkashama LJ**, **Namboodiri HN**, **Xie J**, **McClain KL**, **Marciszyn A**, **Kleyman TR**, **Tan RJ**, **Stolz DB**, **Puthenveedu MA**, **Huang CL**, **Subramanya AR.** Potassium-regulated distal tubule WNK bodies are kidney-specific WNK1 dependent. *Mol Biol Cell* 29: 499–509, 2018. doi:10.1091/mbc.E17-08-0529.
14. **Thomson MN**, **Cuevas CA**, **Bewarder TM**, **Dittmayer C**, **Miller LN**, **Si J**, **Cornelius RJ**, **Su XT**, **Yang CL**, **McCormick JA**, **Hadchouel J**, **Ellison DH**, **Bachmann S**, **Mutig K.** WNK bodies cluster WNK4 and SPAK/OSR1 to promote NCC activation in hypokalemia. *Am J Physiol Renal Physiol* 318: F216–F228, 2020. doi:10.1152/ajprenal.00232.2019.
15. **Hadchouel J**, **Soukaseum C**, **Busst C**, **Zhou XO**, **Baudrie V**, **Zurrer T**, **Cambillau M**, **Elghozi JL**, **Lifton RP**, **Loffing J**, **Jeunemaitre X.** Decreased ENaC expression compensates the increased NCC activity following inactivation of the kidney-specific isoform of WNK1 and prevents hypertension. *Proc Natl Acad Sci USA* 107: 18109–18114, 2010. doi:10.1073/pnas.1006128107.
16. **McCormick JA**, **Yang CL**, **Zhang C**, **Davidge B**, **Blankenstein KI**, **Terker AS**, **Yarbrough B**, **Meermeier NP**, **Park HJ**, **McCully B**, **West M**, **Borschewski A**, **Himmerkus N**, **Bleich M**, **Bachmann S**, **Mutig K**, **Argaiz ER**, **Gamba G**, **Singer JD**, **Ellison DH.** Hyperkalemic hypertension-associated cullin 3 promotes WNK signaling by degrading KLHL3. *J Clin Invest* 124: 4723–4736, 2014. doi:10.1172/JCI76126.
17. **Watt GB**, **Ismail NA**, **Caballero AG**, **Land SC**, **Wilson SM.** Epithelial Na(+) channel activity in human airway epithelial cells: the role of serum and glucocorticoid-inducible kinase 1. *Br J Pharmacol* 166: 1272–1289, 2012.
18. **Chavez-Canales M**, **Zhang C**, **Soukaseum C**, **Moreno E**, **Pacheco-Alvarez D**, **Vidal-Petiot E**, **Castaneda-Bueno M**, **Vazquez N**, **Rojas-Vega L**, **Meermeier NP**, **Rogers S**, **Jeunemaitre X**, **Yang CL**, **Ellison DH**, **Gamba G**, **Hadchouel J.** WNK-SPAK-NCC cascade revisited: WNK1 stimulates the activity of the Na-Cl cotransporter via SPAK, an effect antagonized by WNK4. *Hypertension* 64: 1047–1053, 2014. doi:10.1161/HYPERTENSIONAHA.114.04036.
19. **Gamba G**, **Miyanoshita A**, **Lombardi M**, **Lytton J**, **Lee WS**, **Hediger MA**, **Hebert SC.** Molecular cloning, primary structure and characterization of two members of the mammalian electroneutral sodium-(potassium)-chloride cotransporter family expressed in kidney. *J Biol Chem* 269: 17713–17722, 1994. doi:10.1016/S0021-9258(17)32499-7.
20. **Mori Y**, **Wakabayashi M**, **Mori T**, **Araki Y**, **Sohara E**, **Rai T**, **Sasaki S**, **Uchida S.** Decrease of WNK4 ubiquitination by disease-causing mutations of KLHL3 through different molecular mechanisms. *Biochem Biophys Res Commun* 439: 30–34, 2013. doi:10.1016/j.bbrc.2013.08.035.
21. **Ohta A**, **Schumacher FR**, **Mehellou Y**, **Johnson C**, **Knebel A**, **Macartney TJ**, **Wood NT**, **Alessi DR**, **Kurz T.** The CUL3-KLHL3 E3 ligase complex mutated in Gordon's hypertension syndrome interacts with and ubiquitylates WNK isoforms; disease-causing mutations in KLHL3 and WNK4 disrupt interaction. *Biochem J* 451: 111–122, 2013. doi:10.1042/BJ20121903.
22. **Susa K**, **Sohara E**, **Rai T**, **Zeniya M**, **Mori Y**, **Mori T**, **Chiga M**, **Nomura N**, **Nishida H**, **Takahashi D**, **Isobe K**, **Inoue Y**, **Takeishi K**, **Takeda N**, **Sasaki S**, **Uchida S.** Impaired degradation of WNK1 and WNK4 kinases causes PHAII in mutant KLHL3 knock-in mice. *Hum Mol Genet* 23: 5052–5060, 2014. doi:10.1093/hmg/ddu217.
23. **Ishizawa K**, **Xu N**, **Loffing J**, **Lifton RP**, **Fujita T**, **Uchida S**, **Shibata S.** Potassium depletion stimulates Na-Cl cotransporter via phosphorylation and inactivation of the ubiquitin ligase Kelch-like 3. *Biochem Biophys Res Commun* 480: 745–751, 2016. doi:10.1016/j.bbrc.2016.10.127.
24. **Semenza GL.** Hydroxylation of HIF-1: oxygen sensing at the molecular level. *Physiology (Bethesda)* 19: 176–182, 2004.
25. **Susa K**, **Sohara E**, **Takahashi D**, **Okado T**, **Rai T**, **Uchida S.** WNK4 is indispensable for the pathogenesis of pseudohypoaldosteronism type II caused by mutant KLHL3. *Biochem Biophys Res Commun* 491: 727–732, 2017. doi:10.1016/j.bbrc.2017.07.121.
26. **Castaneda-Bueno M**, **Cervantes-Perez LG**, **Vazquez N**, **Uribe N**, **Kantesaria S**, **Morla L**, **Bobadilla NA**, **Doucet A**, **Alessi DR**, **Gamba G.** Activation of the renal Na^+:Cl^- cotransporter by angiotensin II is a WNK4-dependent process. *Proc Natl Acad Sci USA* 109: 7929–7934, 2012. doi:10.1073/pnas.1200947109.
27. **Bazua-Valenti S**, **Chavez-Canales M**, **Rojas-Vega L**, **Gonzalez-Rodriguez X**, **Vazquez N**, **Rodriguez-Gama A**, **Argaiz ER**, **Melo Z**, **Plata C**, **Ellison DH**, **Garcia-Valdes J**, **Hadchouel J**, **Gamba G.** The effect of WNK4 on the Na^+-Cl^- cotransporter is modulated by intracellular chloride. *J Am Soc Nephrol* 26: 1781–1786, 2015. doi:10.1681/ASN.2014050470.
28. **Terker AS**, **Zhang C**, **Erspamer KJ**, **Gamba G**, **Yang CL**, **Ellison DH.** Unique chloride-sensing properties of WNK4 permit the distal nephron to modulate potassium homeostasis. *Kidney Int* 89: 127–134, 2016. doi:10.1038/ki.2015.289.